Establishing a Cost Effective Method to Quantify and Predict the Combustion Stability of Solid Rocket Motors using Pulse Tests

by

Charle Werner Rousseau

Dissertation presented in partial fulfilment of the requirements for the degree of Doctor of Chemical Engineering at Stellenbosch University

Department of Process Engineering
University of Stellenbosch
Private Bag X1, 7602 Matieland, South Africa

Promoter: Prof J.H. Knoetze

March 2011

Declaration

By submitting this dissertation electronically, I declare that the entirety of the work contained therein is my own, original work, and that I am the owner of the copyright thereof (unless to the extend explicitly otherwise stated) and that I have not previously in its entirety or in part submitted it for obtaining any qualification.

Signature: .....
C.W. Rousseau

Date: .....

Abstract

Establishing a Cost Effective Method to Quantify and Predict the Combustion Stability of Solid Rocket Motors using Pulse Tests

C.W. Rousseau

Department of Process Engineering
University of Stellenbosch
Private Bag X1, 7602 Matieland, South Africa

Dissertation: PhD

March 2011

Combustion instability (CI) has plagued the solid rocket motor (SRM) industry since its inception. It has often been misunderstood or ignored. This has often proven to be costly for the industry. Acoustic instability and pulsed instability in particular were the focus areas of this study. Acoustic instability is a complex interaction of acoustic waves in a combustor environment. This study develops a CI strategy for the South African SRM industry. A mathematical description of the problem, based on the latest research in the field of combustion instability is given. The mathematical tools to predict the stability of a solid rocket motor are discussed. Specific attention is given to the simplest case, namely that of a tubular grain solid rocket motor. Since the test motor is of this design, a complete and accurate description of its gain and loss mechanisms is vital. There has been substantial debate about which growth and loss mechanisms should be included. Much of this study focuses on these conflicting frameworks. Experimental devices were investigated. It is clear from literature that the T-Burner is the only device that is regarded as dependable in producing an admittance/response function for a propellant. A new method was developed to obtain an admittance/response function from a tubular grain motor that has been pulsed. Hardware and data acquisition schemes were developed to implement this methodology. A reusable test motor and pulsers were designed and manufactured. The tubular grain motor proved successful and allowed for multiple tests to be performed. The modular pulser design allowed for the desired pulse amplitude to be achieved. The data acquisition scheme was improved on through the course of the study, allowing for the maximum amount of data to be obtained. The predominant non-linear theories and linear theories have been investigated using this methodology. It addresses the lack of confidence in the predictive tools by allowing these different interpretations to be evaluated directly with experimental data in a way not done before. Contentious issues such as the inclusion or exclusion of certain linear terms can be investigated. Non-linear terms such as velocity coupling can be investigated and for the first time a practical way to measure velocity coupling has emerged. Investigating the different interpretations of triggering has shed new light on the triggering amplitude and the mechanisms responsible for the real or perceived triggering. This methodology is

independent of a linear framework and thus allows these frameworks to be evaluated. This method reduces cost as it allows up to the equivalent of 30 T-Burner tests to be replaced with a single test. In most cases man-hours and not material costs are the driving factor. The time taken to evaluate a large enough test matrix to provide enough data to predict the CI characteristics of motors can be quite substantial. The time taken to evaluate several propellants that are considered for a system in most cases is just not feasible. This method gives the SRM designer the opportunity to quickly and effectively obtain the data required.

Opsomming

Ontwikkeling van 'n Koste-Effektiewe Metode om die Verbrandings Stabiliteit van Vaste Dryfmiddel Vuurpylmotors te Bepaal en te Voorspel

("Establishing a Cost Effective Method to Quantify and Predict the Stability of Solid Rocket Motors using Pulse Tests")

C.W. Rousseau

Departement Process Ingenieurswese
Universiteit van Stellenbosch
Privaatsak X1, 7602 Matieland, Suid Afrika

Proefskrif: PhD

Maart 2011

Verbrandings-onstabiliteit veroorsaak probleme vir die vaste dryfmiddel vuurpylmotor (VDV) nywerheid sedert sy ontstaan. Die verskynsel is dikwels nie ten volle verstaan nie of dit is bloot geïgnoreer. Hierdie probleem het al dikwels tot groot onvoorsiene uitgawes gelei. Verbrandings-onstabiliteit as 'n kennisveld sluit die volgende onderwerpe in: L*, nie-akoestiese en akoestiese onstabiliteit. Akoestiese onstabiliteit en gepulseerde onstabiliteit was op gefokus gedurende hierdie studie. Akoestiese onstabiliteit ontstaan as gevolg van 'n komplekse interaksie tussen akoestiese golwe in 'n verbrandingsomgewing. Hierdie studie bevat 'n verbrandings-onstabiliteit strategie vir die Suid-Afrikaanse VDV nywerheid. 'n Breedvoerige wiskundige beskrywing van die probleem gegrond op die nuutste navorsing in die veld van verbrandings-onstabiliteit word gegee. Die wiskundige tegnieke wat gebruik word om die onstabiliteit van 'n vaste dryfmiddel vuurpylmotor te voorspel word bespreek. Spesifieke klem word geplaas op die eenvoudigste geval van so 'n motor, naamlik die silindriese grein VDV. Aangesien die eksperimentele motor so 'n motor is, is dit van kardinale belang dat 'n volledige en akkurate beskrywing van die wins en verlies meganismes gegee word. Daar is ernstige meningsverskille oor watter wins en verlies meganismes ingesluit moet word. Die ondersoek van die teenstrydige raamwerke was 'n fokuspunt van hierdie studie.

Eksperimentele tegnieke is ondersoek. Dit is duidelik vanuit die literatuur dat die T-Brander as die enigste betroubare apparaat vir die verkryging van 'n admittansie/respons funksie vir 'n dryfmiddel beskou word. 'n Nuwe metode is ontwikkel om 'n admittansie of respons funksie te verkry vanaf 'n silindriese grein motor wat 'n puls ondergaan het.

Die nodige hardeware en data data opnameskemas is ontwikkel om die metode te implementeer. 'n Toetsmotor en pulsers wat hergebruik kan word is ontwerp en vervaardig vir hierdie studie. Die silindriese grein motor is suksesvol gebruik en veelvoudige toetse kon uitgevoer word. Die modulêre pulser ontwerp het toegelaat dat die gewenste pulser amplitude bereik kan word. Die data data opnameskemas is deur die loop van die studie verbeter,

wat gelei het daartoe dat die maksimum aantal data verkry is. Die heersende nie-lineêre en lineêre teorië is op die proef gestel deur hierdie metodologie te gebruik. Dit spreek die gebrek aan vertroue in die hulpmiddels vir voorspellings aan deur dit moontlik te maak om op 'n nuwe wyse die verskillende interpretasies deur middel van eksperimentele data direk te evalueer. Omstrede sake soos die insluiting of uitsluiting van sekere lineêre terme kan hierdeur ondersoek word. Nie-lineêre terme soos die snelheidskoppelterm kan verder ondersoek word en vir die eerste keer op 'n praktiese wyse gemeet word. Deur die verskillende interpretasies van snellering te ondersoek, is nuwe insigte verkry oor hoe die afsettingsamplitude werk en die meganismes wat verantwoordelik is vir die werklike of waargenome snellering. Hierdie metodologie is onafhanklik van 'n lineêre raamwerk en laat dus toe dat hierdie raamwerke sonder partydigheid hersien kan word.

Die metode wat in die studie ontwikkel is verminder uitgawes, aangesien dit die ekwivalent van 30 T-Brander toetse vervang met 'n enkele toets. In die meeste gevalle is die oorwegende faktor die aantal werksure wat gespandeer is en nie die materiaalkoste nie. Om 'n toets matriks te evalueer wat voldoende is om die verbrandings-onstabiliteit van motors te voorspel kan aansienlike tyd in beslag neem. Die tyd wat benodig word om verskeie dryfmiddels te evalueer wat oorweeg word vir 'n opstelling is dikwels te veel om haalbaar te wees. Die metode wat hier bespreek word gee die VDV-ontwerper die geleentheid om vinnig en effektief die nodig data in die hande te kry.

Acknowledgements

I would like to express my sincere gratitude to the following people and organisations:

- Francois Steyn for the opportunity to work on this project and championing CI work in South Africa.
- Prof. J.H. Knoetze for his guidance, advice and willingness to have a conversation when the work was not progressing.
- Johan Rossouw for pyrotechnic and mechanical design of Pulsers.
- Mornê Josephs for experimental set up and safety procedures.
- Hein Dahms T2 Manager.
- Jacques Rousseau for proof reading and helpful input.
- Niel Goosen for helping translate the abstract.
- Francis Ballot for proof reading and finishing the translation of the abstract.
- Rheinmetall Denel Munition for sponsoring this work.
- Francois Marais for doing a final spot check.

Dedications

I would like to dedicate this thesis to my Family for all their support.
To all my friends that have had to listen to me babble on about my work for five years.

Contents

List of Figures

List of Tables

Nomenclature

Glossary

Al Aluminium

APC Ammonium Perchlorate

CFD Computational Fluid Dynamics

CI Combustion Instability

$CSAR$ Center for Simulation of Advanced Rockets

FEA Finite Element Analysis

FFT Fast Fourier Transform

HTPB Hydroxyl Terminated Polybutadiene

$NAWC$ Naval Air Warfare Center

$QSHOD$ The quasi-steady, homogeneous propellant, and one-dimensional combustion assumption

SiC Silicon Carbide

SPP Standard Performance Prediction

SRM Solid Rocket Motor

SSP Standard Stability Prediction

Symbols

A Parameter in the Two Parameter Solution

a Speed of sound $[m\ s^{-1}]$

A_b Admittance function for the burning surface

A_c Nozzle entrance area $[m^2]$

A_e Ejecta area $[m^2]$

A_n, B_n Defined by equation 3.6.23

A_N Nozzle entrance plane admittance $[m^2]$

Ar_n Defined by equation 4.3.3

A_s Inert surface admittance $[m^2]$

A_t Nozzle throat area $[m^2]$

R_{vc} Velocity coupling response

B Parameter in the Two Parameter Solution

$B_b^{(r)}$ Real part of the response function for boundary layer pumping

C Specific heat of the particles [J $mol^{-1}K^{-1}$]

$C_{ni}^{(1)}, C_{ni}^{(2)}$ Parameters Equation (3.6.29)

C_m Weight ratio particles to gas

C_p Specific heat at constant pressure [J $mol^{-1}K^{-1}$]

C_v Specific heat at constant volume [J $mol^{-1}K^{-1}$]

D Diameter [m]

$D_{ni}^{(1)}, D_{ni}^{(2)}$ Parameters Equation (3.6.29)

e Extension ratio L/(length of extended section)

E_m^2 Energy normalization function

F_n Forcing function of the n^{th} acoustic mode

$\mathbf{F}$ The Body Force place holder

f_b Fraction of nozzle blocked

f_c Non-linear functional arising from boundary conditions

h Non-linear functional arising from conservation equations

$I_{nij}^{(A)}, I_{ni}^{(B)}, I_{nij}^{(C)}$ Integrals defined by Equation (3.7.7)

e_e Oscillatory energy density $[J/m^3]$

J	Ratio of nozzle and throat area
k_n	Solutions to the eigen value propblem (3.6.18)
k_c	Complex wave number
k_m	Wave number for axial mode m, $n\pi R/L$
K_n	Restriction ratio, The ratio of burning surface area, S_b to nozzle throat area, A_t
L	Length of the motor [m]
L^*	Characteristic length: V/A_t
M	Mach Number
m	Mass flux rate [kg/s]
M_b	Mach number at the burning surface
M_N	Mach number at the at the nozzle inlet
n_b	Linear burn rate law exponent
$\mathbf{n}$	Outward Pointing unit normal vector
n	Mode number
$O()$	Refers to the order magnitude
P	Chamber pressure [MPa]
p'	Acoustic pressure [MPa]
Pr	The Prandtl number
p_a	Acoustic Pressure [MPa]
$\mathbf{R}$	Gas constant
R	Mean chamber radius [m]
r	Radial position
R_∞	The Limit amplitude of a T-Burner [MPa]
R_b	Response function for the burning surface
r_b	Burning Rate in mm a second [mm/s]
Re	The Reynolds Number
r_n	Amplitude of the n^{th} mode
R_{vc}	Velocity coupled response
S	Surface area [m^2]
s	Entropy [J kg^{-1} K^{-1}]
St	Strouhal number
T	Temperature in degrees Kelvin [K]
t	Time [s]
U	Mean flow velocity [m s^{-1}]
u	Gas velocity [m s^{-1}]
$\mathbf{u}$	Oscillatory velocity vector
$\mathbf{e}_r, \mathbf{e}_\theta, \mathbf{e}_z$	Unit vectors in the r, θ, and z direction 3.2
U_r, U_z	Mean flow velocity components [m s^{-1}]
V	Volume [m^3]
v	Velocity [m s^{-1}]
w	Reaction rate
X	The mass fraction of the particles in the gas
$\tilde{x}$	$\tilde{x} = \pi x/L$
Y_i	Species mass fraction
z	Axial position [m]

Greek and Latin Symbols

α	Growth or decay constants [s^{-1}]
β_c	Non-linear gas dynamics term arising from Culick's method
β_{DC}	Mean Pressure constant from equation 3.6.12
β_{sw}	Refers to the non-linear shock wave losses
δ	Ratio of the particle density the gas density ρ_p/ρ_{gas}
δ_d^2	Viscous dilation function

λ	Second Coefficient of Viscosity
E	Time averaged energy density
ε	The system amplitude
$\epsilon(t)$	Instantaneous pressure amplitude ratio$[p'/P_0]$
η	The Normalized variable $\eta = 1/\gamma \ln p$
γ	Ratio of specific heats
$\Im$	Refers to the real part of an equation
δ^2_{Re}	Inverse square root of the Reynolds number based on the radius or length
κ	The Thermal Diffusivity [w/mK]
ν	Kinematic viscosity $[m^2/s]$
μ	Viscosity $[pa \cdot s]$
η_n	Defined by equation 3.6.23
ω_n	Angular frequency of the n^{th} mode
Ω_d	Defined as $\Omega_d = \omega\tau_d$
Ω_t	Defined as $\Omega_t = \omega\tau_t$
$\phi(r)$	Function defined, Equation (3.4.13)
Φ_m	Pure Mode or Eigenfunction of the n^{th} Mode
ψ_n	Mode shape of the n^{th} mode
$\psi(r)$	Exponential argument, Equation (3.4.11)
Π	The Pi Theoerem defined by equation (B.4.11)
ρ	Density $[kg\ m^{-3}]$
τ_d	Defined as $\tau_d = \rho_{g/p} s d^2/18\mu$
τ_d	Particle relaxation time [s]
τ_t	Defined as $\tau_t = (3CPr/2C_p)\tau_d$
θ_n	Frequency shifting of the n^{th} mode
$\boldsymbol{\omega}_v$	Mean vorticity amplitude
$\boldsymbol{\omega}_n$	Three dimensional angular Frequency
ξ	A parameter O(1) that shows the relative importance of viscous dampening. Refered to as the penetration number. Equation (3.4.13)
$\langle\zeta\rangle$	Time averaged oscillatory energy

Subscripts

0	Indicates the quiescent chamber reference conditions
1	Initial prior to Disturbance
$*$	Dimensional quantity
atm	Refers to atmosphere
b	Refers to the Burning Surface
c	Refers to the motor chamber
ch	Refers to the pulser chamber gasses
d	Refers to decay of acoustic energy in the system
D_p	The diameter of the burning port [m]
g	Refers to growth acoustic decay in the system
gas	Refers to the gas
g/p	Refers to gas and particle mixture
l	Longitudinal modes
lim	Indicates the limiting amplitude is reached
N	Normal wave incidence
p	Refers to particles
$prop$	Refers to the propellant
r	Refers to the point at which the burst diaphragm ruptures
$(r), (i)$	Refers to the real and imaginary parts
Re	Reynolds number
b	Burning propellant surface
std	Predicted value

sw	Refers to the non-linear shockwave losses
t	Tangential modes
v	Refers to the connecting tube
y	Refers to the point the burst diaphragm starts to yield

Superscripts

(1)	Denotes first order accuracy
$'$	Denotes acoustic parameter
$\hat{(\ )}$	Acoustic (irrotational) part
$()^{(i)}$	Refers to the imaginary part of a function
$\overline{(\ )}$	Indicates the mean value
NL	Non-linear
$()^{(r)}$	Refers to the real part of a function
$\tilde{(\ )}$	Vortical (rotational) part
$*$	Non-Dimensional Quantity
$\langle\rangle$	Time averaged

Chapter 1

Overview of work

1.1 Introduction

Combustion instability(CI) has been a problem since the dawn of Solid Rocket Motors (SRMs) and all chemical propulsion systems. It has been recorded in all development programs in all countries including the United States, Canada, France, Russia, Italy etc. This problem has been the subject of intensive study. Many approaches and theoretical models have been developed and applied to explain and predict the phenomenon of combustion instability. Several different experimental procedures have been used to try and quantify this phenomenon and obtain data that can be used in a meaningful manner. Since the inception of the SRM industry, this phenomenon has cost the industry millions of dollars. Often the strategy is to attempt to eliminate instability in an *ad hoc* manner, often resulting in project delays and in extreme cases project cancellations. Instability has appeared in some of the most well known SRMs, such as the Standard Missile, Sidewinder, Harm, Trident, Hellfire and Minuteman (1). In the past, a large part of the problem was that the computational power that was available was not sufficient at the time to be able to apply theory as well as capture the relevant data during tests. The costs related to data capturing and computational costs have reduced significantly over the past 50 years. Combustion instability requires three resource intensive computations to be done simultaneously. Firstly, the program must be able to calculate the internal ballistics of a motor. The internal ballistics requires the complete characterisation of the propellant burn rate. Secondly, the burning of the propellant causes a change in the internal geometry and thus also changes the fundamental frequencies of the motor. Thus, it is necessary to perform a finite element analysis on an object that is changing rapidly. Lastly, the flow dynamics need to be modelled. This is further complicated by the changing internal geometry, mass addition from the wall and combustion. These three different fields of computational technology need to be integrated to model an SRM. Due to the time it would take to analyse the entire burn time of a motor, the analysis is generally limited to several specific time steps.

Therefore, in the absence of effective tools for predicting the possibility of combustion instability, SRM developers would apply different solution strategies to solve the problem retroactively if and when it did occur. These solutions include: changing the oxidizer, metal and the additive particles' sizes that can effect both the propellant response and particle dampening; modifying the internal motor geometry which can affect the nozzle dampening and the acoustic flow field and the velocity coupling; adding stability additives to modify the particulate dampening; addition of baffles and resonant rods; and adding a burning rate

catalyst that can lower the response. All these techniques have advantages and disadvantages, but all of them have an affect on the motor operating dynamics and, in general, affects the SRM performance adversely. Many rules of thumb exist, but are in many cases proprietary and are not available in the open literature (2).

The way combustion instability is solved is also strongly dependent on the mission requirements of the SRM. During the 60's and 70's aluminium particles were used extensively. This, seemingly, completely eliminated tangential mode instability and furthermore significantly damped longitudinal modes. However, it has become a prerequisite that SRMs (especially tactical motors) must be reduced-smoke motors. This requirement has made aluminium particles obsolete. Thus, tangential mode instability has again become a factor, especially as it produces a larger pressure shift than longitudinal modes (3). As a result more emphasis on propellant formulation and geometry is required in modern SRM design.

1.2 Overview of Combustion Instability

Combustion instability manifests itself in the following ways (4):

- Violent, high frequency pressure oscillations.
- Increased mean pressure (referred to as the DC pressure shift). This may exceed the design value for a motor;
- Increased heat transfer to metal parts that can lead to motor failure;
- Unexpected roll torques;
- Combustion efficiency deterioration;
- High level of thrust alteration. The oscillation may also modulate the thrust.

This section will describe combustion instability in its different forms. It will also describe all components that can dampen or add energy to the oscillations. In short, an analysis of combustion instability has to take the following physical features into account(5):

- Steady and Unsteady Combustion;
- Time Dependent Compressible Fluid Dynamics;
- Two Phase Flow;
- Vortex Shedding;
- Rotational Flow Effect;
- Vibration of Propellant and Motor Case;
- Turbulence;
- Unsteady Heat Transfer Effects;
- Non-linear Interaction of Processes;

There exist two kinds of combustion instability, namely acoustic and non-acoustic instability. Non-acoustic instability can take the form of chuffing which is the drop in pressure from normal operating pressure to near atmospheric pressure. This is referred to as L* instability (which is named L* as it refers to the fact that the characteristic length of the motor is a key parameter and is defined as the free volume divided by the nozzle throat area), the interaction between the bulk mode and the fluid dynamics, and finally, unsteady burning. Since motors are unstable for low values of L*, an SRM that experiences this kind of instability typically has a free chamber volume that is relatively low and operates at low pressure, which implies a large nozzle opening (large A_t). This makes it a problem essentially found in small motors with high propellant volumes and low operating pressures. Since few motors fall in this category it is rarely encountered in practice (6). The emphasis of this project will not be on this kind of instability and it will not be discussed further. The reader is referred to references (6–15) for additional information.

Acoustic instability is regarded as more important than non-acoustic instability and more extensive work has been done in this field. Acoustic instability is the attenuation or amplification of acoustic waves within a combustor. Acoustic instability is characterised by the growth of the acoustic amplitude to a limiting amplitude as shown in Figure 1.1. The acoustic wave is characterised by modal content that are multiples of the first mode with a fixed amplitude ratio. The growth is initially linear then proceeds to non-linear growth until non-linear loss mechanisms equal the growth terms resulting in a limiting amplitude. This growth is described mathematically by linear and non-linear terms that either adds or subtracts energy from the system resulting in the amplitude growing or decaying.

Such a system can either be linearly stable or linearly unstable. Linear instability is characterised only by the linear growth constant being positive with no second order driving terms required to result in a limiting amplitude. This is associated with inherent instability since the acoustic wave will grow to a limiting amplitude without requiring a pulse. In the case of linearly stable systems, a disturbance in the form of a pulse is required to initiate or trigger second order driving terms, causing a limiting amplitude to be reached. Many studies (16–19) have been done applying dynamical systems theory to predict the triggering amplitude required to initiate non-linear growth. Some researchers state that all motors that exhibit a limiting amplitude are also linearly unstable, that CI is always present and that there are no second order driving terms. The amplitude of these oscillations, however, is often not noticed as their values are the same order of magnitude as the transducer noise.These oscillations also grow too slowly to move into the non-linear region during the burn time (5; 20; 21). A pulse in this context moves the amplitude from linear growth to non-linear growth resulting in a limiting amplitude. Both these interpretations of combustion instability will be investigated, namely, that the motor is always linearly unstable and the interpretation that the motor is linearly stable and that second order driving terms are responsible for non-linear instability.

A large variety of interactions are possible to produce non-linear instability. They can be divided into either dampening or gain effects. There are several mechanisms that are considered in classical acoustic instability theory (1; 5):

- *Pressure Coupled Response*: This occurs when pressure oscillations couple with the combustion processes. In the analysis of this phenomenon it is assumed that the gas phase is Quasi-Steady (QS), the solid propellant is Homogeneous (H), and the combustion is One-Dimensional (OD). This is known the QSHOD Method. This was first introduced by Denison and Baum (22) and has been used by subsequent researchers

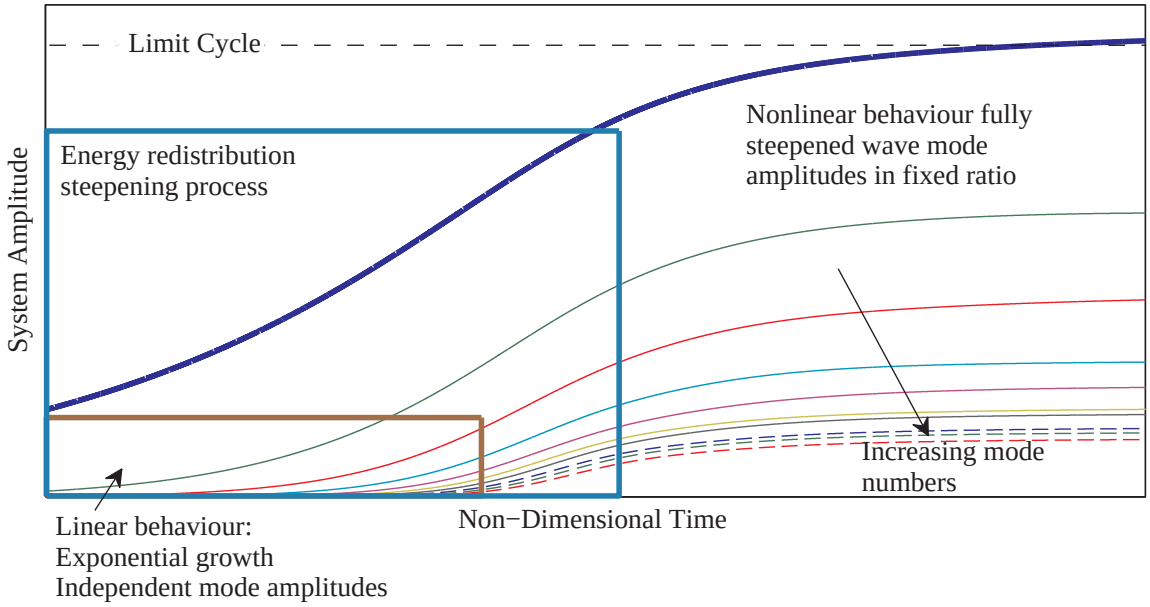

Figure 1.1: Non-linear evolution of Amplitude [Redrawn Flandro *el al.* (31)]

(23). Figure 1.2 shows a one dimensional representation of the combustion zone. As the pressure fluctuates, the zone between the solid propellant surface and flame is reduced. This compression increases the combustion rate. This in turn increases the heat generation and heat transfer and produces an unsteady heat wave. Energy is gained by the acoustic wave during this process and is called "pressure" coupling. No widely accepted model exists and the use of experimental data is required to predict the energy gains. To be able to predict the pressure coupled response it is necessary to determine the admittance/response function of the propellant. The T-Burner is the industry standard device for more than 50 years to obtain the response function. The T-Burner is, however, labour intensive and expensive to maintain. All other devices investigated have been shown to be too limited to use. A viable alternative is required in the tactical missile environment.

- *Velocity Coupling*: This refers to coupling between the acoustic velocity and combustion. The combustion process is very sensitive to flow parallel to the burning surface. The combustion process is sensitive to the magnitude and not the direction of the velocity. This makes it intrinsically non-linear and thus has often been used in an *ad hoc* manner as a second order driving term. Though it is accepted that this response may be a vital component in non-linear instability, there exists no explanation for the physical mechanism of this interaction. There is also no adequate way to measure the phenomenon. This *ad hoc* feature of predictive codes has become unpopular among researchers and has been abandoned by some.

- *Vortex Shedding*: This occurs when flow goes past edges which can cause unstable shear layers that can develop into vortices. These vortices remove energy from the flow fields, couple with an acoustic field and create local acoustic sources by impinging on the surface. Much work has been done on this phenomenon in the last 30 years. Figure 1.3 shows how vortices are generated due to irregularities or segmentation within the

SRM. Figure 1.4 shows actual vortices generated within an SRM. The pictures were taken in window tests. Parietal vortex shedding is when a vortex forms without being induced by edges or discontinuities. This phenomenon is usually associated with large SRMs such as Arian 5, but is not necessarily limited to them.

- *Flow Turning*: This term, first discovered by Culick (24), has been debated extensively. This physical mechanism represents the energy loss when the flow from the solid surface is turned in the direction of the nozzle and oscillatory energy is imparted to it. That this physical mechanism occurs is not debated. What is not accepted is whether it should be included in the linear stability analysis. Flandro, Majdalani, Fischbach and Chibli (25–29) have shown that in the case of tubular and slab grain motors it cancels out with the boundary layer pumping and that it should not be included as a one-dimensional patch as was standard practice to that point. Culick (30) in his analysis of a tubular grain has also confirmed that in the case of tubular grains this term cancels out, but that it may not be true for all SRMs especially in the case of T-Burners. Flandro, Majdalani and French (31) have suggested that flow turning completely disappears when doing a complete energy balance. Van Moorhen (32) has also done a critical study on flow turning, especially on the inclusion of *ad hoc* one dimensional terms in a three dimensional model, as suggested by Culick.

- *Boundary Layer Pumping*: This is a driving term of the same order of magnitude as the pressure coupled response function. It occurs when the oscillations of acoustic waves parallel to the surface are non-uniform and induce a fluctuating velocity normal to the surface. These fluctuations, when in phase with an acoustic wave, can act as an oscillating piston adding energy to the acoustic wave. This is the latest term to be accepted into linear CI theory.

- *Nozzle Dampening*: This term represents the largest dampening mechanism. The flow through a nozzle of an SRM, and indeed other propulsion systems such as liquid and ramjet motors, is choked, which results in the nozzle losses being represented as a function of the specific heat of the gas and the Mach number at the nozzle entrance (30). This loss occurs as some of the acoustic wave is reflected back into the motor while a large portion of the wave travels through the nozzle and exits the motor. This reduces the total acoustic energy. This effect is highest when the mean flow velocity at the nozzle entrance is at a maximum. This results in the nozzle dampening being at a maximum at the initial stages of the burn time as the port area is small and the resulting mean flow velocity is high. The nozzle dampening decreases as the mean flow velocity decreases with the increasing port area.

- *Residual or Distributed Combustion*: This occurs when burning metals couple with the motor acoustics away from the burning surface.

The typical linear energy analysis components are displayed in Table 1.1.

An SRM can be inherently unstable or can require a disturbance, i.e. a pulse, to induce combustion instability as shown in Figures 1.5 and 1.6. An inherently unstable SRM goes unstable without any outside influence. Pulsed instability happens in practice when ejecta either pass through the nozzle and cause a shock wave, or when an external pulse is caused by the collision of the in flight missile or rocket with an outside object. This pulse causes a structural vibration large enough to excite the acoustic modes of the SRM (33).

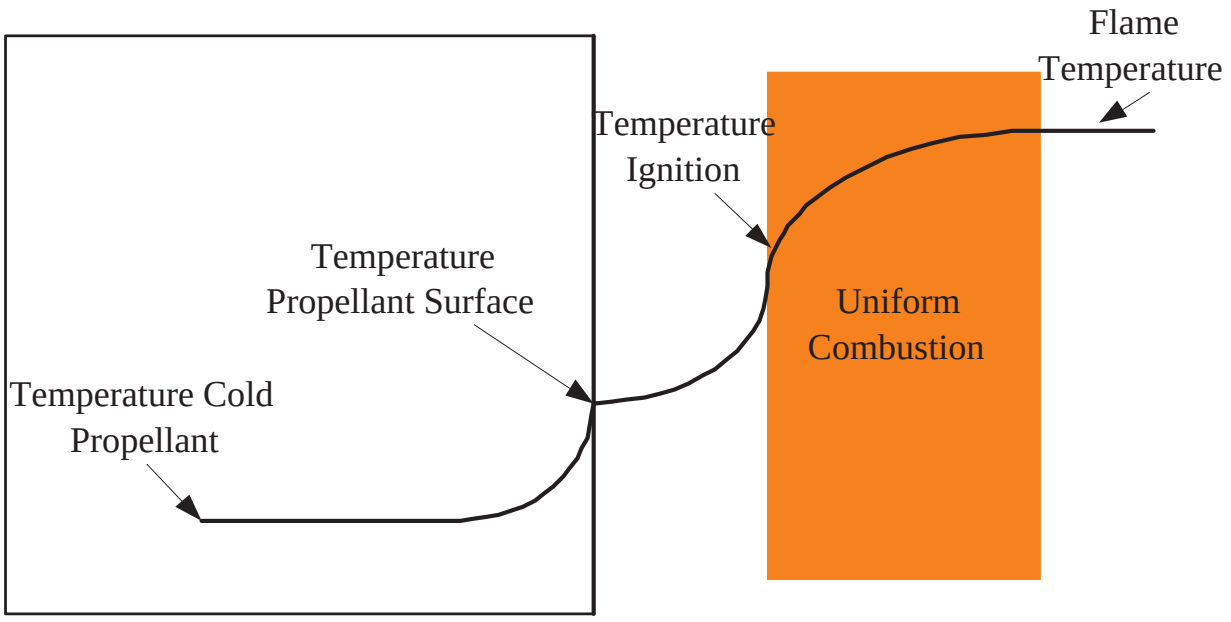

Figure 1.2: QSHOD Model with Uniform Combustion [Redrawn from Culick (30)]

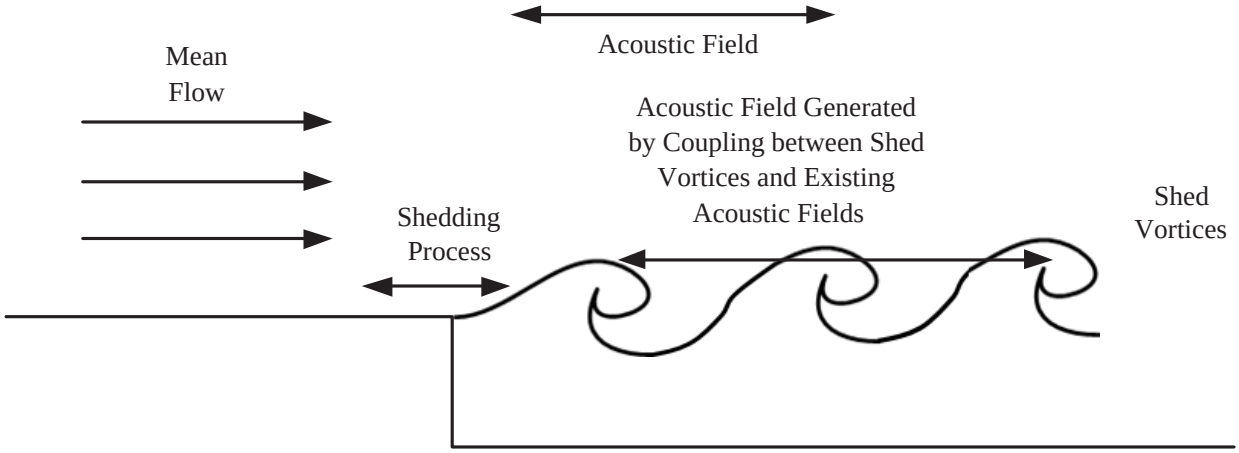

Figure 1.3: Vortex Generation [Redrawn from Culick (30)]

Figure 1.4: Vortices in SRM Window Tests [Sotter and Flandro (181)]

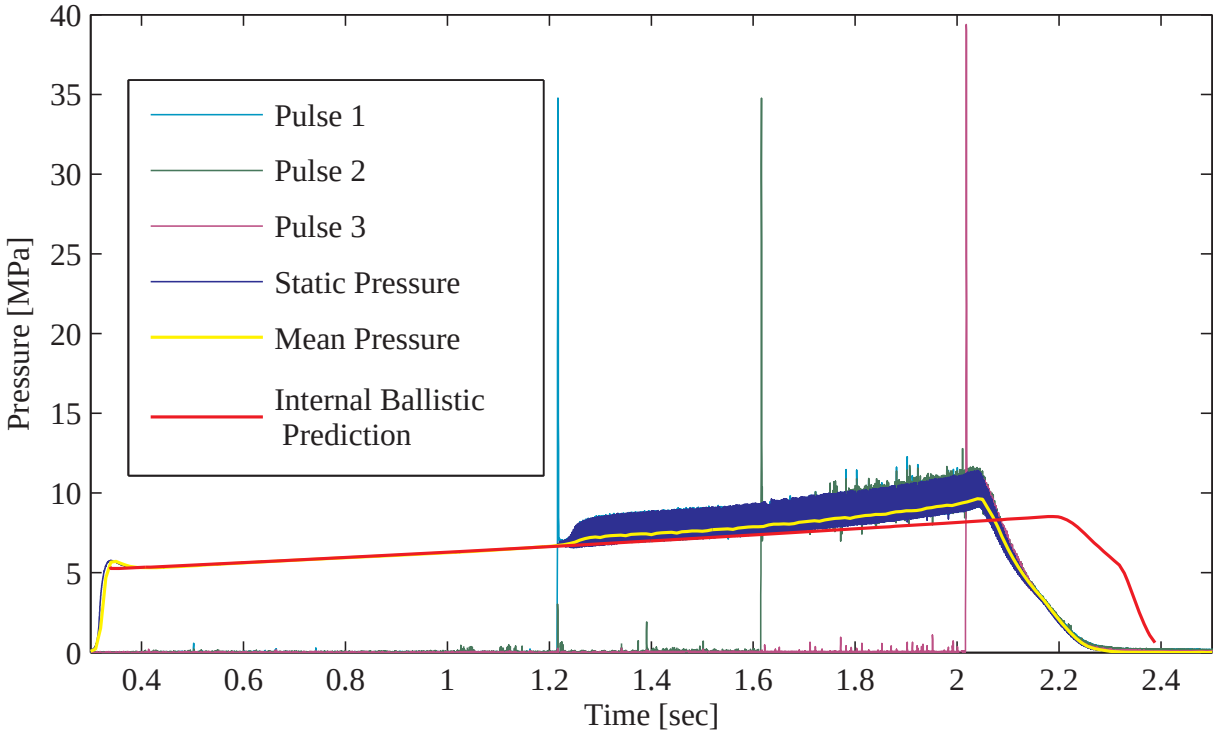

Figure 1.5: Typical Pulse Induced Combustion Instability Pulse Test

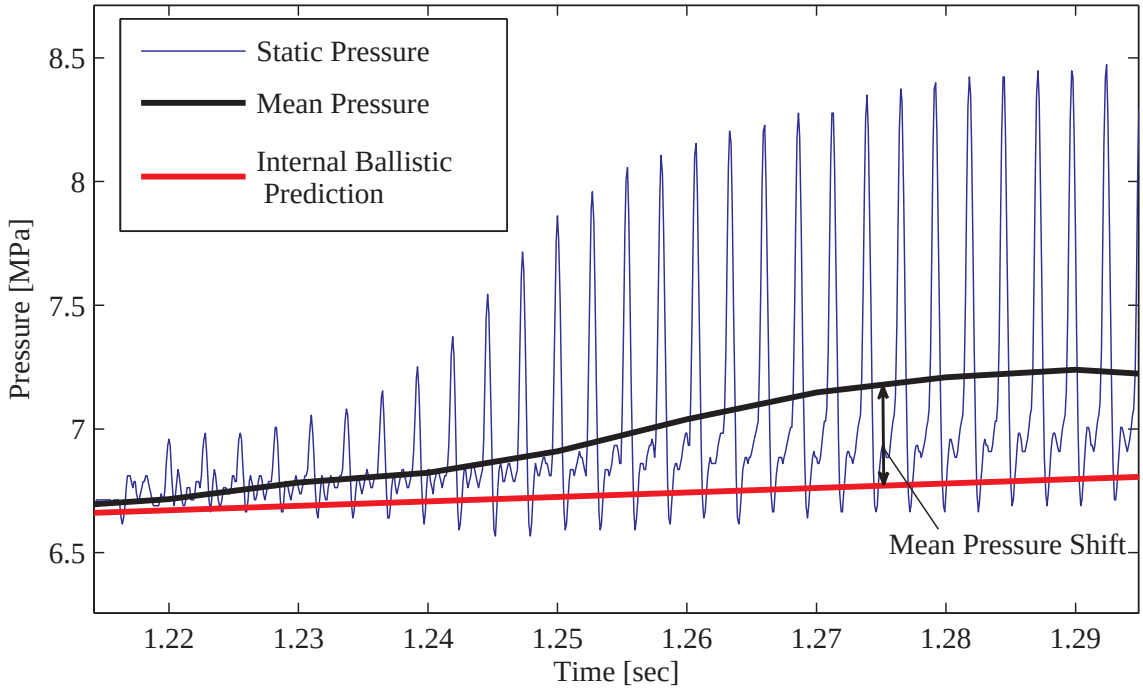

Figure 1.6: Unstable Region

Table 1.1: Summary of Gain And Loss Mechanisms

Gain Effects	**Loss or Dampening Effects**
Combustion Response	Nozzle Dampening
Flow Turning	Particle Dampening
Distributed Combustion	Viscous Dampening
Unsteady Boundary Layer Displacement Effect	Flow Turning
Velocity Coupling	Shock Layer Dampening

Acoustic combustion instability occurs in three different modes as displayed in Figure 1.7:

- Axial, or more commonly Longitudinal Modes;
- Tangential or Transverse Modes; and
- Radial Modes

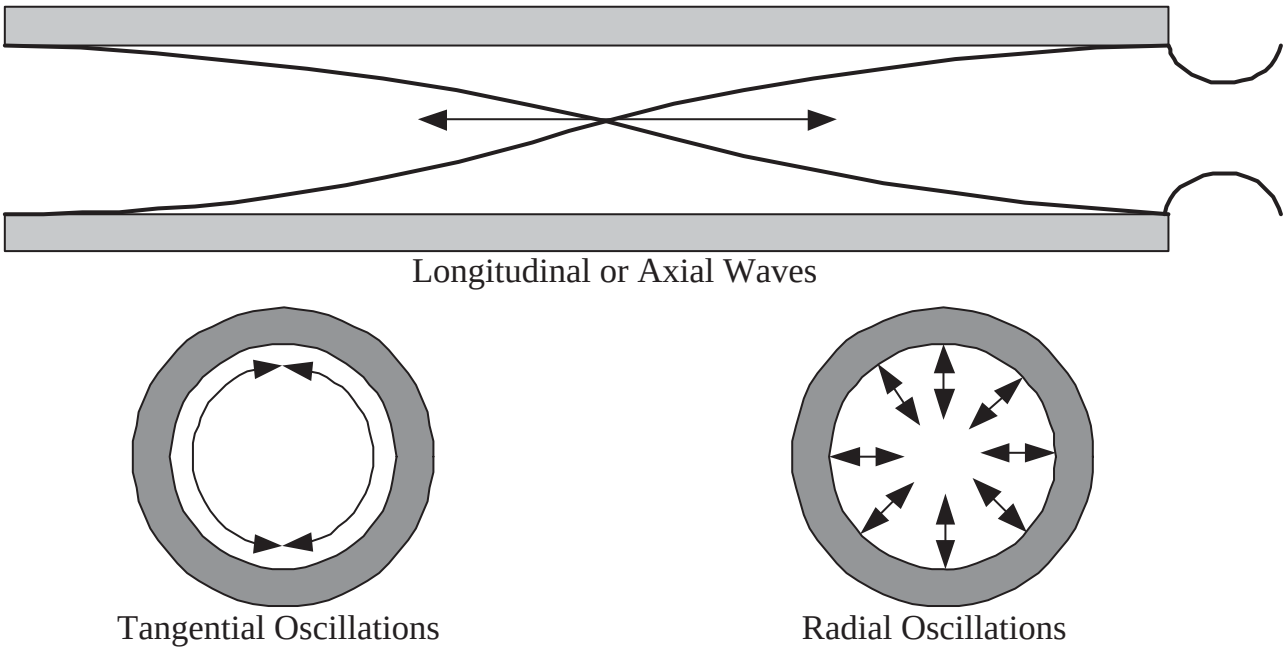

Figure 1.7: Different Types of Oscillations [Redrawn from Blomshield (29)]

Longitudinal and tangential modes are most commonly found in combustion instability. These modes are also the most likely to cause a large DC pressure shift. Radial instability is rare. Both longitudinal and tangential instabilities are found in all propellant families. It has also been found that both can occur in the same motor. However, tangential mode instability is often not associated with aluminized propellants and it is more likely to occur in modern SRMs since the current trend is the development of smokeless propellants (1).

1.3 Outline

The main objective of this study was to establish a program to quantify the combustion response of a propellant and then use this to predict motor stability. To achieve this objective

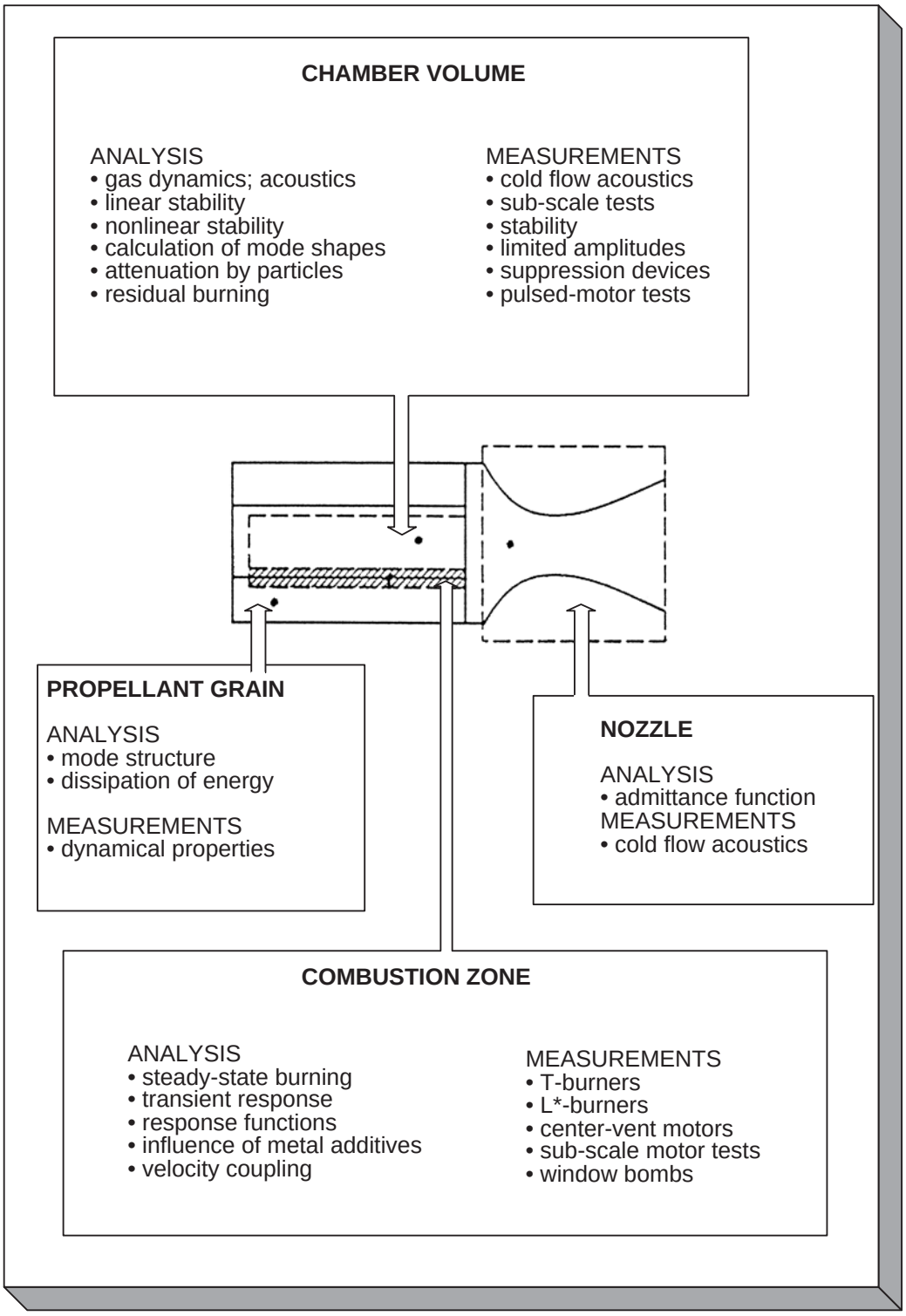

Figure 1.8: Global Summary of the Combustion Instability Problem [Redrawn from Flandro (105)]

it was necessary to establish tools to qualify an SRM. With this focus it was possible to obtain enough data in a cost effective way to make a valid prediction of the stability of a proposed SRM design. This section gives a brief overview of the tasks that were completed and the strategy that was followed to achieve the objective. Figure 1.8 shows how the problem of combustion instability can be divided into four main areas. The focus of this research project was on the chamber volume and the combustion zone.

To achieve these aims, pulse test data was used in new and innovative ways. Currently, a standard procedure does not exist for using pulse test data as a quantitative and qualitative prediction tool for the stability of solid rocket propellants, nor for the data reduction from such tests. Pulse tests are generally used to validate the motor's stability as part of the qualification process. Thus, in this field there was an opportunity to develop testing strategies and data reduction techniques to achieve the goal of quantifying the susceptibility of a solid rocket propellant to instability. This knowledge can be applied to the design process of a solid rocket motor, as a pre-emptive tool against creating an unstable motor. This approach may ultimately produce more qualitative results that will aid in the motor design and will also mark a step forward in the South African SRM industry.

Previous projects (34; 35) have set the foundation for future work to be done. The first three phases have produced the hardware and the data acquisition capacity required for further tests. This dissertation endeavours to establish a reference for future work. The key areas of focus were:

Pulse Testing: One of the key hypotheses of this study was that the pulse test data can be used as a predictive tool. Pulse testing allows for the testing of geometries as well as the determination of the properties of the solid rocket propellant. This can be useful to a SRM designer because correlations can be drawn from the test results of a specific formulation with a specific grain geometry and then applied to the same formulation in a different grain geometry.

Linear Stability Analysis: Linear stability analysis is the first step that needs to be taken in the analysis of the stability of an SRM. The linear terms merely give an indication of the rate of amplitude growth or decay. This analysis is often based on flawed assumptions but can nevertheless give a clear indication of the motor's stability. Linear stability forms part of any non-linear analysis.

Non-Linear Analysis: Most pulsed-instability occurrences are non-linear in nature. In most cases of instability a DC pressure shift occurs; this invalidates one of the primary assumptions of linear stability analysis. The amplitude of the pressure wave increases initially and then steadies out at the limit cycle. The non-linear analysis allows for the trigger point and the limit cycle to be found from a pulsed test. This information can be used in the prediction of the stability of the propellant in a different application or geometry.

1.4 Objectives

As stated before, the objective of this study is to develop a combustion instability methodology to be used by the South African tactical missile industry. Most SRM designers rely on rules of thumb and pre-emptive strategies that reduce the performance of the SRM. The fact that there is only one operational T-Burner (36) (the industry standard for propellant response measurement) in the U.S.A indicates the reliance on such methods above the theoretical assessment of an SRM. This is due to the expense and time associated with operating a T-Burner as well as the lack of confidence in predictive codes. This study focused on obtai-

ning the pressure coupled response of a propellant. Without the pressure coupled response it is not possible to make any priori prediction of a motor stability. Pulsed tubular grain motors were chosen as the device to obtain the pressure coupled response. The assumption was that it is possible to obtain the pressure coupled response at several pressures and frequencies from a single firing. Combustion instability is one of the most published upon niche areas in SRM theory. There are large areas of contention about the validity of frameworks as is shown throughout the dissertation. It is important to develop a method that is independent of any framework. Thus the newly developed analysis methodology must be able to accommodate second order driving terms as well as linearly unstable systems. The velocity coupling response can then be obtained by using the new analysis methodology if the pressure coupled response function is available. The objective of obtaining the pressure coupled response becomes subjective as there is no universal agreement on the linear driving terms or if there are any second order driving terms. However, using the same terms for both the new analysis methodology and the prediction provides the SRM designer with a relative prediction of the motor stability. This provides an opportunity to make an informed decision on which propellant will be most stable in the system. This can reduce the risk of CI being encountered. The pressure coupled response function can be used to predict the linear growth constant of a motor. To make use of this capacity, the ability to predict axial mode instability was developed. This capability allows for the stability of the motor to be predicted, provided the linear terms and the velocity coupling can be obtained. It is hoped that future studies will provide a local capacity to determine the linear terms for complex grain designs.

This study aimed to equip the SRM designer with a tool that can obtain the pressure coupled response function quickly and cheaply. Secondly, this methodology aimed to provide a way to evaluate predictive codes and frameworks by applying the theory to actual data in a way that has not been done before.

1.5 Tasks

To achieve the above objectives the following tasks were completed:

1. Extensive literature survey;
2. Develop hardware: Pulsers and test motor;
3. Calibrate pulsers;
4. Develop data acquisition schemes;
5. Develop data analysis methodology;
6. Develop non-linear axial mode predictive capacity.

1.6 Dissertation Outline

Chapter 2 shows the development of the hardware and is accompanied by Appendix C that presents some sample calculations. The focus is on the development of the pulser hardware, since the pulser is required to produce different pulse amplitudes it was necessary to establish a predictive capability for different pulser configurations. The experimental procedures to

test various pulser configurations are presented. These results were used to develop a unique design optimisation algorithm. The data acquisition scheme is also presented. Chapter 3 presents a rigorous mathematical description of both linear and non-linear CI theory. This chapter is essentially an in-depth literature review that presents all terms required to perform the calculations in Chapter 4 and 5. It presents how the linear growth terms are calculated. It reports the assumptions made to develop these terms and their physical meaning. Three forms are presented, i.e. the volume integrals, surface integrals, and results for tubular grains. The tubular grain results are of most interest for this study as they will be used to calculate the growth and decay constants of the test motor. The volume and surface integrals are presented as these need to be solved for more complex geometries and will hopefully form part of future studies. Several different sets of linear terms are presented and these different sets are compared in Chapter 5. It also presents how the non-linear calculations are performed. A comparative report from literature on the different non-linear methods is also given as the analysis methodology developed Chapter 4 and 5 is dependent on their validity. A brief overview is presented of the most recent developments in the solving of the linear growth terms with the use both of finite element analysis and computational fluid dynamics. Chapter 4 uses the theory presented in Chapter 3 to develop a new analysis methodology. The first section presents a new combustion instability strategy for the tactical missile industry. The focus of this chapter is to use the non-linear methods developed to predict CI as analysis tools. The non-linear equations are used to calculate the mode linear stability. The response can then be calculated assuming all other growth and loss terms can be calculated. This analysis is then extended to accommodate second order driving terms to allow for terms such as velocity coupling to be calculated.

Chapter 5 employs the analysis method developed in Chapter 4. The different sets of linear terms are compared. The implications of the results using these terms are discussed. This process reveals a new interpretation for triggering. The analysis is then extended to determine the velocity coupling response from experimental data. The system dynamics for linearly unstable systems and for second order driving terms are compared and discussed. Finally, Chapter 6 will discuss the main conclusions and contributions of this study. Appendix A provides background on the development of CI theory. It is included as a reference for those interested in further study of CI. Appendix B discusses existing experimental methods and is included as a reference.

Chapter 2

Hardware Qualification and Characterization

2.1 Pulse Testing

Pulse testing has predominantly been used to qualify an SRM. This is to ensure that no instability will be induced by ejecta passing through the nozzle and to a lesser extent due to external shock. The pulser design is based on the pulser used by Blomshield *et al.* (37–40) as part of a NAWC program.

The pulsers were tested in a cold flow motor that was designed and manufactured for this study. A correlation was established to predict the pulser performance.

Pulse testing consists of the following phases:

1. Select motor operating conditions;
2. Select desired pulse amplitude based on the motor conditions;
3. Use shock wave theory to estimate the required burst pressure;
4. Use the current data to select the best possible pulser configuration;
5. Test the configuration and change the orifice and burst plate until the desired burst pressure is acquired;
6. Test the pulser configuration in a cold flow motor setup to confirm program results;
7. Pulse test the live motor;
8. Analyse the data.

2.1.1 Determining the Maximum Pulse Amplitude

Pulses are caused by ejecta particles leaving the motor via the nozzle as shown in Figure 2.1. It is important to know what the maximum possible shockwave that can occur during operation of the motor will be.

A simple model for predicting the pressure pulse was developed by Lovine *et al.* (41). The following assumptions were made:

- Flow in the nozzle is one-dimensional and isentropic;
- Ejecta only affect the instantaneous nozzle and throat area.

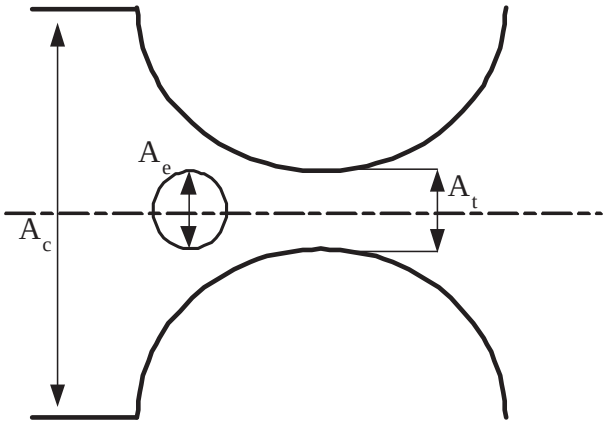

Figure 2.1: Ejecta Passing through the Nozzle

The authors used linear wave propagation theory to express the instantaneous pressure at the nozzle entrance (p) to the initial undisturbed entrance pressure p_1 as follows (41):

$$\frac{p}{p_1} = \left[\left(1 + \frac{\gamma - 1}{2} M_1^2\right) / \left(1 + \frac{\gamma - 1}{2} M^2\right)\right]^{(2\gamma)/(\gamma-1)} \tag{2.1.1}$$

The next step is to determine the Mach number as it passes through the nozzle. Quasi-steady nozzle behaviour is assumed. Thus it is possible to calculate the instantaneous Mach number (41):

$$M_1 = J\left[\left(1 + \frac{\gamma - 1}{2} M_1^2\right)\left(\frac{2}{\gamma + 1}\right)\right]^{(\gamma+1)/2(\gamma-1)} \tag{2.1.2}$$

J is the ratio of the throat areato the nozzle entrance area A_t/A_c. M_1 is replaced by M and J is replaced by $J(1 - f_b)$. f_b is the fraction of the nozzle area that is blocked. It is important to note that the quasi-steady nozzle assumption is most applicable to slow moving particles and tends to over predict pulse amplitude for smaller fast moving particles (41).

Equation (2.1.2) is transcendental for M_1 as a function of J. Assuming that $0.5\,(\gamma - 1)\,M_1^2$ is significantly small compared to 1 allows M_1 and M to be expressed as follows (41):

$$\begin{aligned} M_1 &= J\left(\frac{2}{\gamma + 1}\right)^{(\gamma+1)/2(\gamma-1)} \\ M &= J(1 - f_b)\left(\frac{2}{\gamma + 1}\right)^{(\gamma+1)/2(\gamma-1)} \end{aligned} \tag{2.1.3}$$

Substituting Equation (2.1.3) into Equation (2.1.1) as well as neglecting all terms smaller than 0.1J the following expression is found (41):

$$\frac{p_1 - p}{p_1} = \frac{\delta p}{p_1} = \left[\gamma\left(\frac{2}{\gamma + 1}\right)^{(\gamma+1)/2(\gamma-1)}\right] f_b J \tag{2.1.4}$$

An expression is now obtained that predicts the pulse amplitude δp proportional to the initial constriction ratio J and the fraction of the throat area that is blocked f_b.

The next step is to calculate the required pulser performance to produce a pulse equivalent to the maximum pulse that is possible during operation.

The shock wave amplitude in the connecting tube p_v can be found using the following equation (40):

$$\frac{p_r}{p_c} = \frac{p_v}{p_c}\left\{1 - \frac{(\gamma_{ch}-1)\,(a_c/a_{ch})\,[p_v/p_c - 1]}{\sqrt{2\gamma_c}\sqrt{2\gamma_c + (\gamma_c+1)\,[(p_v/p_c) - 1]}}\right\}^{-[2\gamma_{ch}/(\gamma_{ch}-1)]} \tag{2.1.5}$$

Where p_r is the rupture pressure and the subscripts ch refers to the pulser, c to the motor chamber and v the connecting tube.

Once the wave moves into the chamber the following equation describes the quasispherical shock wave expansion (40).

$$\frac{\delta p}{p_c} = \left(\frac{p_v}{p_c} - 1\right)\sqrt{\frac{1}{1 + 1.75(D_c/D_v)^2}} \tag{2.1.6}$$

D_c is the diameter of the motor chamber and D_v is the diameter of the connecting tube.

Equation (2.1.6) can be used to solve p_v since the chamber pressure p_c is known, the diameters D_v and D_c are known and the desired pulse amplitude δp has been calculated. This is then substituted into Equation (2.1.5) and is solved to obtain the rupture pressure p_r.

The first step is to determine the maximum δp that can occur during operation. Using Equation (2.1.4) and assuming γ =1.2 (typical value for propellant combustion gases) the following result is obtained (41):

$$\frac{\delta p}{p_1} = 0.71 J f_b \tag{2.1.7}$$

Though it has been shown experimentally (41) that $0.6Jf_b$ is a slightly better approximation, the analytical result($0.71Jf_b$) will be used as the first approximation. As the motor burns J changes as the propellant is consumed. This is due to the propellant burning surface regressing and thus A_c increases with time as illustrated in Figure 2.2. Typically the beginning value of J will be 0.5 and the end value of 0.2.

Figure 2.3 plots the pressure amplitude as a percentage of mean motor pressure against J for varying particle sizes. Starting with J=0.5, the expected shockwave is larger and decreases with burn time. It is unlikely that a particle can be large enough to cause a 90% blockage. It has been found in literature that the maximum expected blocked fraction is about 70% (41). Thus, the worst pressure pulse is 25% of the motor pressure at the initial burn time and decreases with time to about 10% towards the end of the motor burn time. Thus, the pulsers are able to deliver a 25% pulse in the early stages of the motor burn time and a 10% pulse towards the end of the burn time.

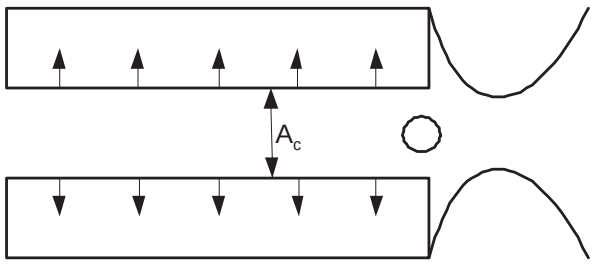

Figure 2.2: Rocket Motor Burning Surface Regression

Using the shockwave theory and the known performances levels of the pulsers, it can now be established whether pulsers are capable of matching the performance required to ascertain if the motor will go unstable under normal operating conditions.

The first parameter is that of chamber pressure. In most motors, the pressure increases as the motor burn time increases. This is usually due to most grains being progressive in nature and thus the surface area increases with time. From Figure 2.4 it can be seen that

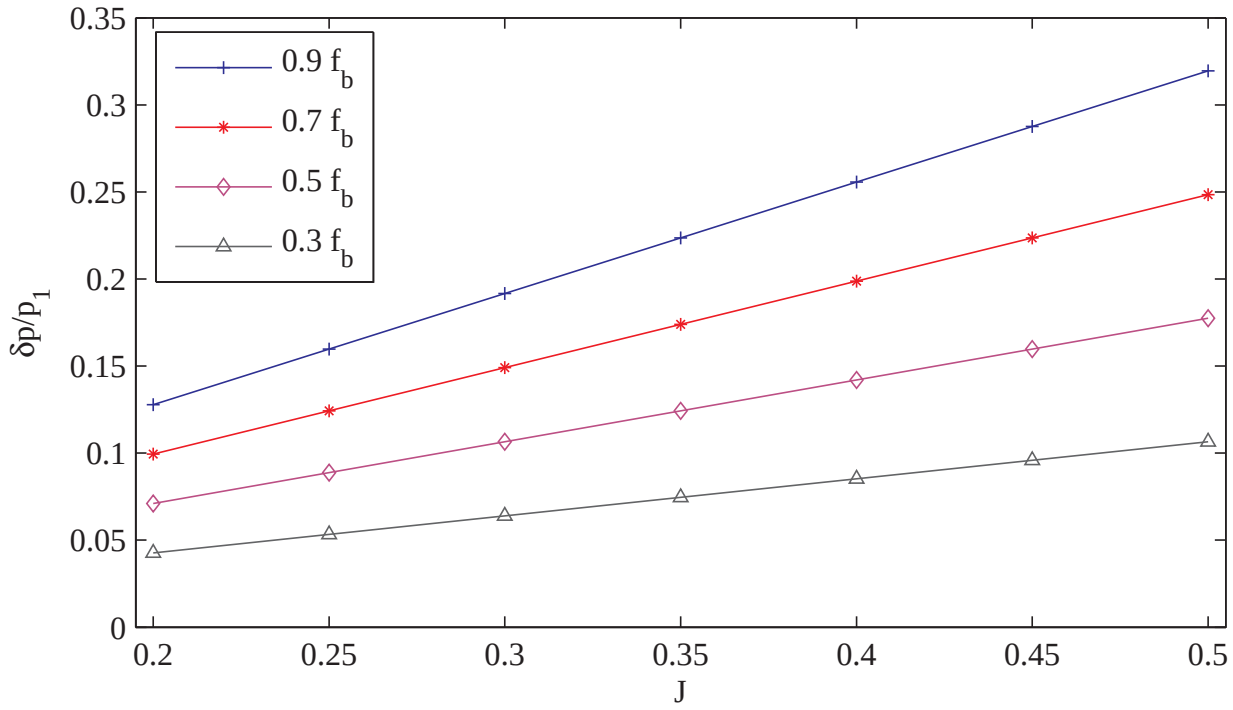

Figure 2.3: Theoretical Pressure Pulse in terms of Burn time and Fraction Blocked

it is easier to obtain a large pulse at lower motor pressure than at higher pressures. As the motor diameter increases, the ability of a particular pulser to give a large shock wave decreases rapidly.

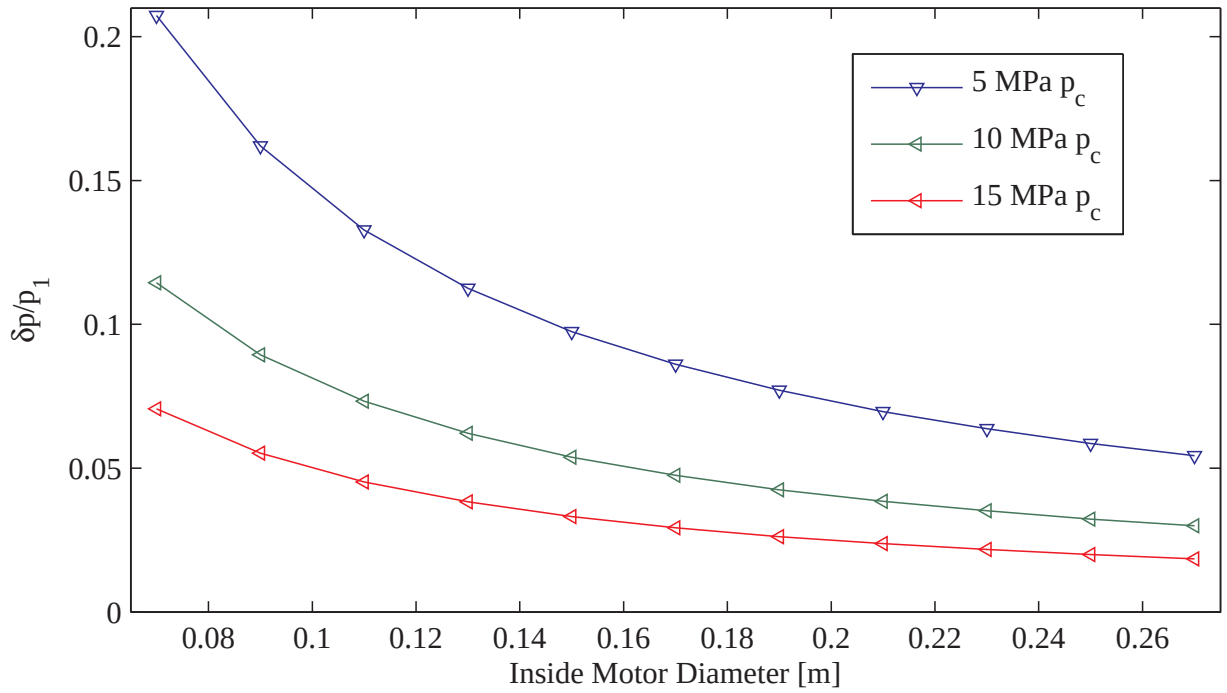

Figure 2.4: Increase in Pressure Shockwave Amplitudes as Motor Pressure Decreases

The next parameter that can be varied is p_r of the pulser. The pulsers used for this study were designed for a maximum combustion chamber of 40 MPa. From Figure 2.5 it can be seen that the increase of 80% in δp equals an increase of 10 MPa in p_r. Again, it must be noted that the shockwave amplitude is a strong function of the increase in motor diameter as shown in Figure 2.5.

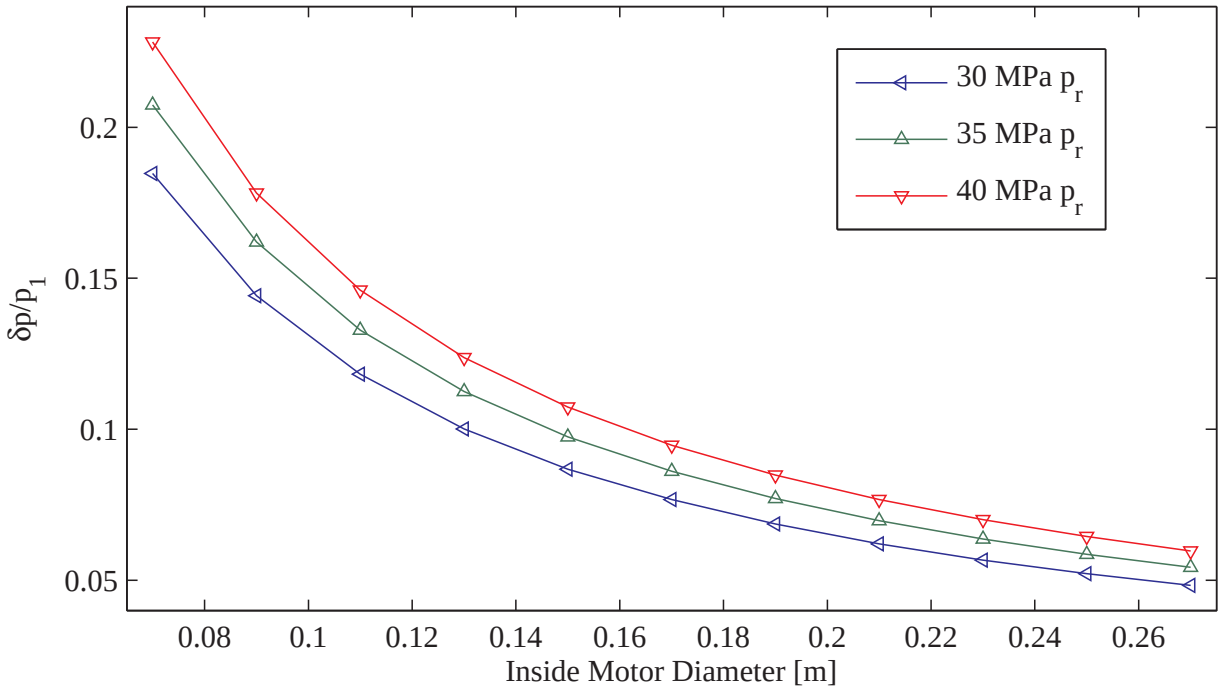

Figure 2.5: Increase in Shockwave Amplitude as a Function of Increased Rupture Pressure

The final variable that can change is D_v. Though a change in diameter can cause a large change in shockwave amplitude, it may not always be feasible to do so, and thus should only be considered as a parameter for change as a last course of action.

The δp that the existing pulsers can produce is large enough to be fully evaluated for a motor with an inner diameter of less than 30cm and operating pressures of less than 15 MPa. By using this method the first two steps are completed. This was all integrated into the pulser prediction program presented in Appendix C.

2.1.2 Pulser Hardware

The pulser consisted of three interchangeable parts as shown in Figure 2.6. This includes the burst diaphragm, orifice diameter and charge amount. This is a relatively simple device and has been used since the first pulse tests in the 1960s (42; 43). The pulser was based on Blomshield *et al.* (37; 40). The available pulser components were:

- Burst diaphragm made from brass shimstock. Two thicknesses were available namely, 0.1 and 0.05mm;
- Three orifice plate diameters of 5.05 mm, 7.49 mm, and 9.02 mm were used. It is preferred that smaller diameters are used since larger diameters often tear rather than

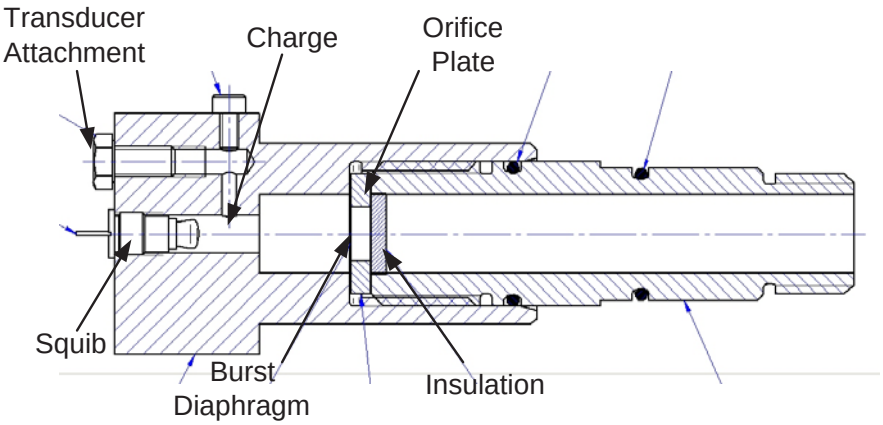

Figure 2.6: Pulser and its Components based on the NAWC Design.

a circular hole being formed. This also reduces the area exposed to the hot combustion gases;

- The maximum charge mass was 200 mg black powder;
- An electric squib containing 90 mg charge was used to initiate the black powder.

Figure 2.7: Cold Flow Test Setup

Different combinations of these parameters were tested by modifying the test motor (cf. Figure 2.7) which was used for live firings. Instead of a nozzle, the aft end had a connection hose to a helium tank and a high speed Kistler pressure transducer (100 KHz) was attached on a modified bulkhead. On the head end, three pulsers were attached as well as a static pressure transducer and another high speed pressure transducer. The pulsers were then fired into the chamber that had been pressurized with helium. Helium at room temperature has similar acoustic properties to combustion gases such as the same speed of sound and ratio of specific heats. On each pulser a transducer was attached so that the burst pressure could be measured The Excel program presented in Appendix C calculates the best pulser configuration to achieve the desired pulse amplitude.

2.1.3 Pulser Prediction and Design

Step 3 is to use the shock wave theory to predict the required burst pressure. Using Equations (2.1.4) and (2.1.6) the required rupture pressure can be estimated. Once the rupture pressure is known, the next step is to select the pulser configuration. Experimental data is used for the dynamics of the burst plate and orifice diameter. The pressure rise is modelled using internal ballistic predictions. The motor chamber pressure can be assumed to be constant.

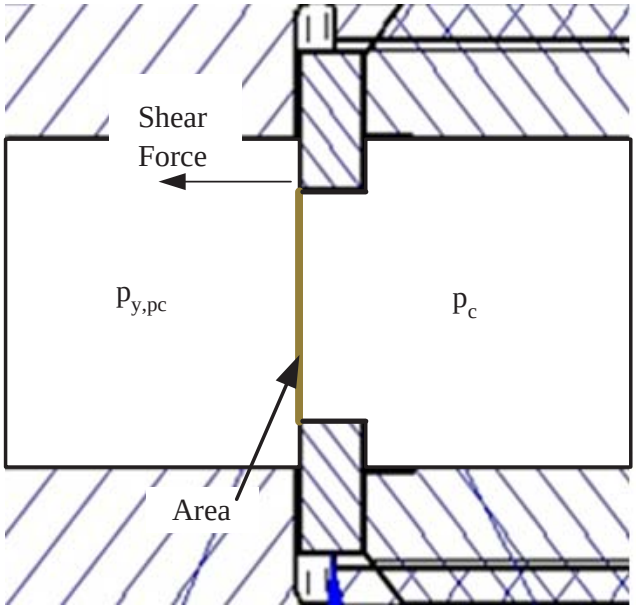

Figure 2.8: Free Body Diagram of Pulser

At the point at which the plate starts to yield, the following equation is valid as derived from Figure 2.8.

$$Area \times p_{y,pc} = Area \times p_c + Shear\ Force \tag{2.1.8}$$

p_{y,p_c} is the yield pressure at a given chamber pressure. At atmospheric pressure, the shear force will be the only resistance:

$$Area \times p_{y,atm} = Shear\ Force \tag{2.1.9}$$

Substituting this result into the original equation yields:

$$Area \times p_{y,p_c} = Area \times p_c + Area \times p_{y,atm}$$

$$Dividing\ by\ \ Area \tag{2.1.10}$$

$$p_{y,p_c} = p_c + p_{y,atm}$$

Between the point where the plate ruptures and the pressure where the plate starts to yield the pressure will rise:

$$p_r = p_{y,pc} + \frac{dp}{dt}\Delta t \tag{2.1.11}$$

It is assumed that Δt, the time it takes for the burst plate to rupture, is constant. $p_{y,atm}$ and Δt are obtained experimentally for a burst plate thickness and orifice diameter combination. This analysis depends on the assumption that these parameters remain constant for all possible chamber pressures. To determine the charge amount, dp/dt is predicted as a function of charge amount. The orifice diameter and burst plate thickness is selected by choosing the configuration which gives the closest value of p_y and p_c to that of p_r.

Rearranging Equation (2.1.11):

$$p_r - (p_{y,atm} + p_c) = \frac{dp}{dt}\Delta t \tag{2.1.12}$$

From the experimental results p_r has been obtained for several configurations. p_c is also known for all tests. By using the experimental results $p_{y,atm}$ and Δt can be obtained.

2.1.4 Pressure-Time Curves

For the first version of the program it was decided to use an empirical model to generate the pressure time curves. The pressure time curves of a 200 mg charge and a 100 mg charge were plotted and a 5^{th} order polynomial was fitted to the curves. These fits can only be used for interoperation and were chosen as they are easy to manipulate numerically. Obtaining the required information to do a full internal ballistic simulation for commercially available black powder is often not possible. It was required to interpolate between 100 mg and 200 mg. To achieve this it was necessary to calculate a scale-up value for each factor in the polynomial that is a function of the amount of powder in the pulser chamber. The 100 mg data curve was selected as the base case. Thus the scale factor was charge divided by 100 to the power of an unknown exponent. The following equation was created:

Table 2.1: Polynomial constants, Exponents and Scale up Factors

Order	200mg	100mg	Exponents
5	2.2E+16	6.9E+13	8.3
4	-5.8E+13	-5.9E+11	6.6
3	6.0E+10	1.9E+9	5.0
2	-2.5E+7	-2.0E+6	3.5
1	7.6E+3	815.9	3.2
0	2.6	0.13	4.3

$$\begin{aligned} p = &\left(\frac{Charge}{100}\right)^{\exp 1} \times 5^{th}\, order\, term\, 100mg \times t^5 + \left(\frac{Charge}{100}\right)^{\exp 2} \times 4^{th}\, order\, term\, 100mg \times t^4 + \\ &\left(\frac{Charge}{100}\right)^{\exp 3} \times 3^{rd}\, order\, term\, 100mg \times t^3 + \left(\frac{Charge}{100}\right)^{\exp 4} \times 2^{nd}\, order\, term\, 100mg \times t^2 + \\ &\left(\frac{Charge}{100}\right)^{\exp 5} \times 1^{st}\, order\, term\, 100mg \times t + \left(\frac{Charge}{100}\right)^{\exp 6} \times 0^{th}\, order\, term\, 100mg \end{aligned} \tag{2.1.13}$$

By solving for each term separately and setting it equal to the corresponding polynomial terms of the 200 mg polynomial, the exponents exp1 to exp6 can be solved for. By using the polynomial with the scale up factors, the predicted data curves in Figure 2.9 were obtained.

From Figure 2.9 it can be seen that the scale up polynomial shows a good correlation with the experimental results. The polynomial constants and the scale up factor exponents are shown in Table 2.1. A sample calculation is presented in Appendix C.

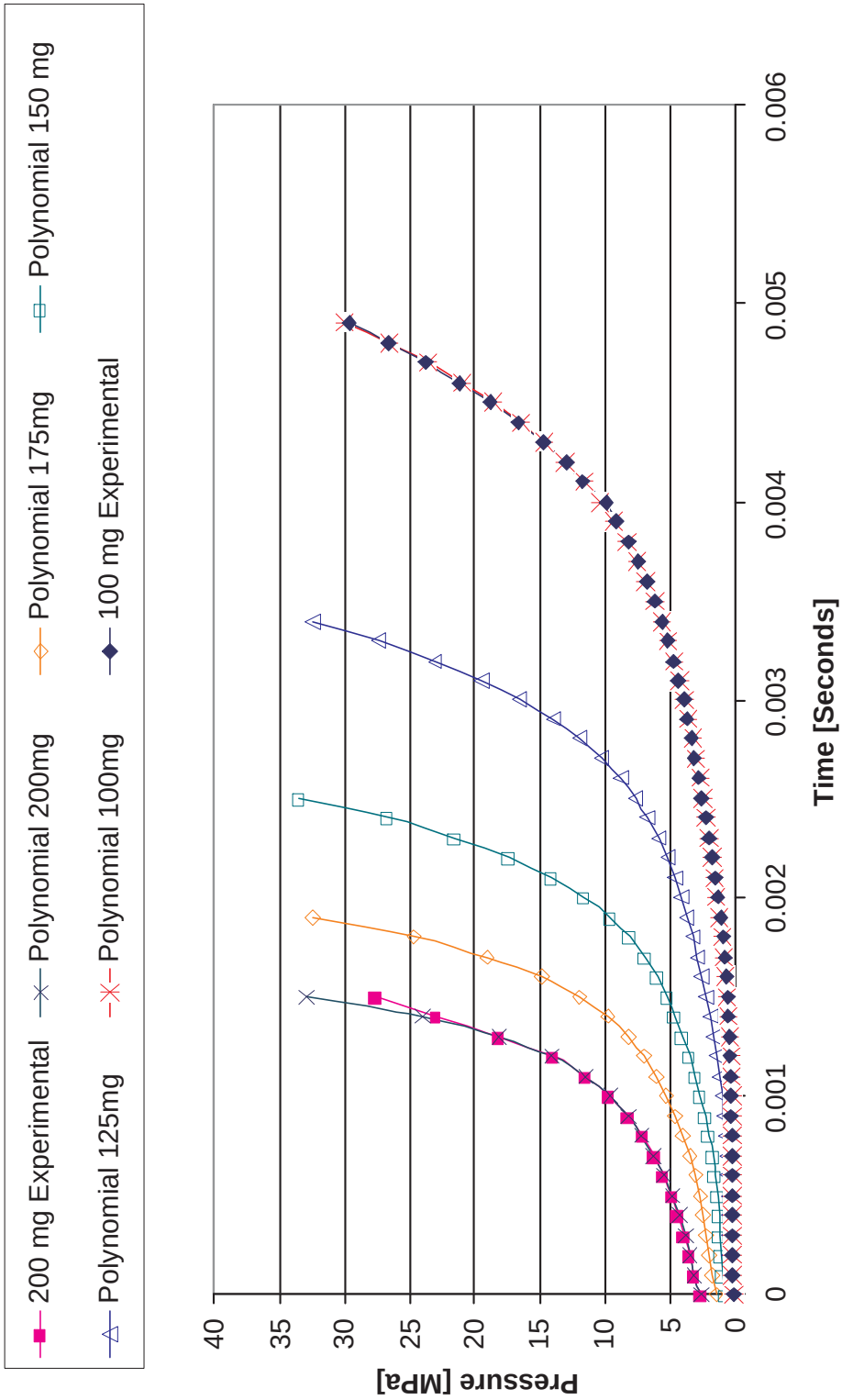

Figure 2.9: Predicted and Experimental Pressure-Time Curves

2.1.5 Determining the Yield Pressure

Three tests were done on each pulser configuration at atmospheric pressure, and two other pressures, usually 7 and 10 MPa. From these tests, pressure curves and rupture pressure at three different motor chamber pressure levels p_y and Δt could be found by applying equation (2.1.11). By fitting 5^{th} order polynomials to the pressure-time curve of each pressure plot it was possible to set up simultaneous equations to solve for yield pressure and Δt. The general forms of the polynomials are:

$$p = 5^{th}order \times (t_f - \Delta t)^5 + 4^{th}order \times (t_f - \Delta t)^4 + 3^{rd}order \times (t_f - \Delta t)^3 + 2^{nd}order \times (t_f - \Delta t)^2 + 1^{st}order \times (t_f - \Delta t) + 0^{th}order \tag{2.1.14}$$

Substituting this equation into equation (2.1.11) and rearranging yields:

$$p_{y,atm} = 5^{th}order \times (t_f - \Delta t)^5 + 4^{th}order \times (t_f - \Delta t)^4 + 3^{rd}order \times (t_f - \Delta t)^3 + 2^{nd}order \times (t_f - \Delta t)^2 + 1^{st}order \times (t_f - \Delta t) + 0^{th}order - p_c \tag{2.1.15}$$

where t_f is the time at which the plate ruptures for each individual pulser time curve. Fitting a 5^{th} order polynomial to each curve and setting them all equal to $p_{y,atm}$ allows for Δt to be solved iteratively. It was found, however, that this does not produce an exact answer. The best possible solution was sought. Excel's Solver was used to find the Δt that gives the closest answer to the actual tests result when used in equation (2.1.14) to determine the rupture pressure. Thus, no exact solution was found for a specific test but the data from all tests for a specific configuration were taken to calculate a Δt that adequately predicts its performance. The deviation of the yield pressure of each individual pulser from the average yield pressure has a direct bearing on the accuracy of the predictions.

In summary, the following procedure was used to determine the yield pressure and Δt:

1. Fit 5^{th} degree Polynomials;
2. Use equation (2.1.15);
3. Set all experimental data sets equal to each other;
4. Use Excel Solver to minimize the standard deviation by changing Δt;
5. The average yield pressure is obtained.

A sample calculation is given in Appendix C.

From the results in Table 2.2 we can clearly see that the standard deviation of the pulsers ranged from 1.2 to 1.5 MPa. Thus the predictions of the computer model were in a confidence range of $\pm$1.5 MPa.

It can also be noted from Table 2.2 that the yield pressures that were obtained are not necessarily the value where the disk starts to burst. It is seen in the case of pulser 2 that if the yield pressure was indeed at 1.26 MPa, it would have burst at the given chamber pressures. However, it can also be seen that the value for Δt is also significantly larger than that of the other configurations. Thus it will still produce the rupture pressures that match the experimental values when used in the computer program.

Finally, the burst pressures of the pulsers ranged from 10 to 30 MPa. An additional configuration was tested, but overlapped with 4 and proved to be less reliable.

Table 2.2: Constants for Computer Program

Pulser	Orifice Diameter [mm]	Bust Plate thickness [mm]	Yield Pressure [MPa]	Yield Time(s)	Standard Deviation	Burst Pressure Range +
1	5.05	0.1	10.9	0.00022	1.218962	20+
2	5.05	0.05	1.3	0.000474	1.27145	14+
3	3.36	0.5	19.2	2.33E-05	1.472278	26+
4	9.02	0.1	6.48	6.56E-05	1.48	10+

The result of atmospheric tests for configurations 2, 3, and 4 were not used due to transducer conversion factors that were incorrect. It is also important to note from the figures in Appendix C.2 that the ignition of the powder is highly non-reproducible. Once the ignition has begun and reaches the top half of the curves, the rate of pressure change is uniform. This will not, however, have a significant effect on testing live rocket motors as the total time is in the order of a millisecond. Therefore, the pulser will, in terms of a motor burn time, not rupture significantly from the desired pulse time.

Finally, it was necessary to evaluate whether a ± 1.5 MPa standard deviation in rupture pressure is acceptable. The goal was to produce a shockwave as close as possible to the desired level. Therefore various rupture pressures were plotted against that of the corresponding shockwave (as predicted by the shockwave theory and quasi-spherical expansion at a constant chamber pressure). Note that the change in shockwave amplitude was not as rapid as that of the rupture pressure. Thus, even if the rupture pressure deviates $\pm$ 1.5 MPa from the desired rupture pressure, the pulsers will still produce a shockwave within an acceptable error range from that which is desired.

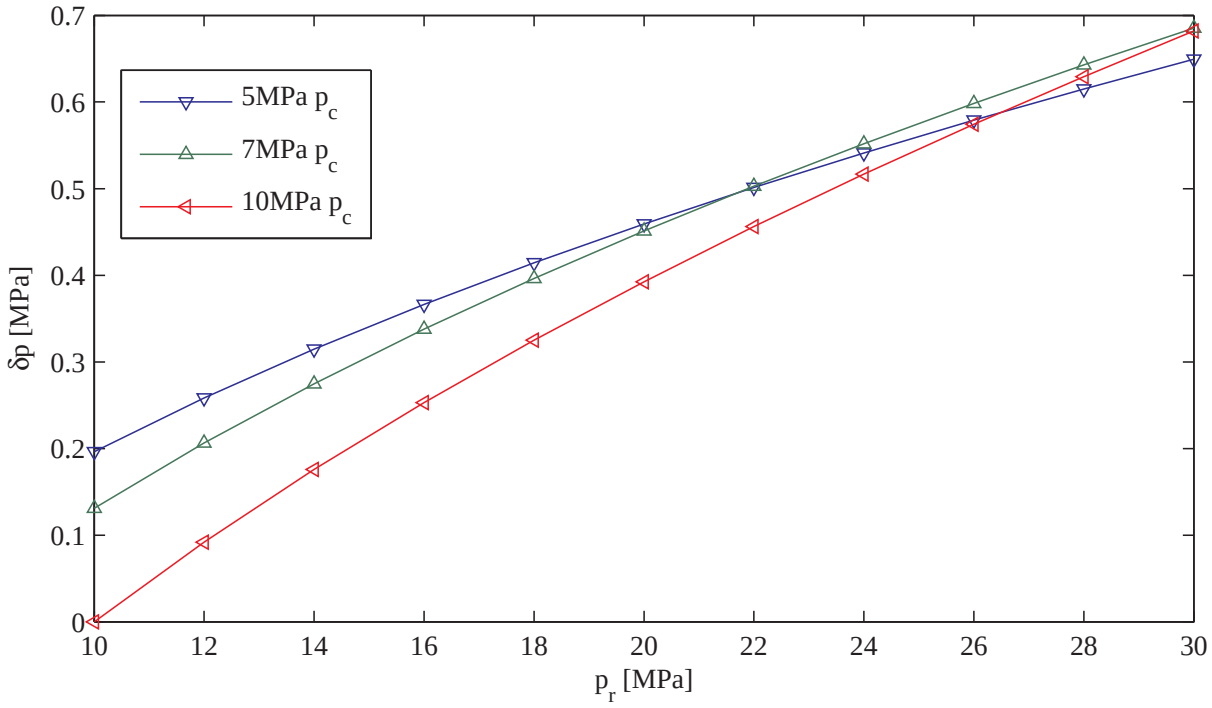

Figure 2.10: Rupture Pressure vs. Shockwave Amplitude

The model at present seems to generate adequate representation of the pulsers. The standard deviation for such a device is to be expected due to the nature of the combustion

process and ignition process. It will, however, allow the user to make a prediction with relative confidence.

5^{th} degree polynomials are a good representation of the pulser data curves. Being able to model the curves as such made numerical manipulation easier. However an analytical model can be developed in the event of powder or squibs being changed. Also, if it is desired at a later stage to create pulsers that can deliver larger burst pressures; such a model will make the design of such pulsers significantly easier. This approach can only be employed when the required data such as burn rate and geometry is available for the black powder. In most cases it is more practical to employ an empirical model based on experimental results as presented here.

It is also shown in Figure 2.10, that a change in the shockwave amplitude is relatively small compared to that of the rupture pressure. Thus, the order of magnitude of the shockwave can be predicted with certainty. The maximum variations of the pulser's rupture pressure will not adversely affect the test results of a live motor firing. Due to space constraints at the head end of SRMs, an adapter will have to be designed on a case to case basis. The users manual for pulser design configurations can be found in Appendix C.3.

2.2 Cold Flow Tests

The hardware, testing procedures, and initial tests were performed in 2005 at Rheinmetall DENEL Munitions as part of a final year project by C.W. Rousseau (35). The pulser prediction capability was developed as part of this dissertation. The following set of equipment was used for the tests:

- 3x Pulsers;
- 200 000 Hz Kistler dynamic pressure transducers;
- 1x Static pressure transducer;
- 1x 30 Bar connection hose;
- 6x Helium canisters;
- 2x Dynamic transducers attached to pulsers;
- 2 x Bulk heads machined for fitting transducers, pulsers and hose;
- 1x Motor chamber;
- 1x Needle Valve;
- 1x Isolation Valve;
- 1x Pressure Regulator;
- 1x Pressure Relief valve;
- Amplifier and analogto digital converter.

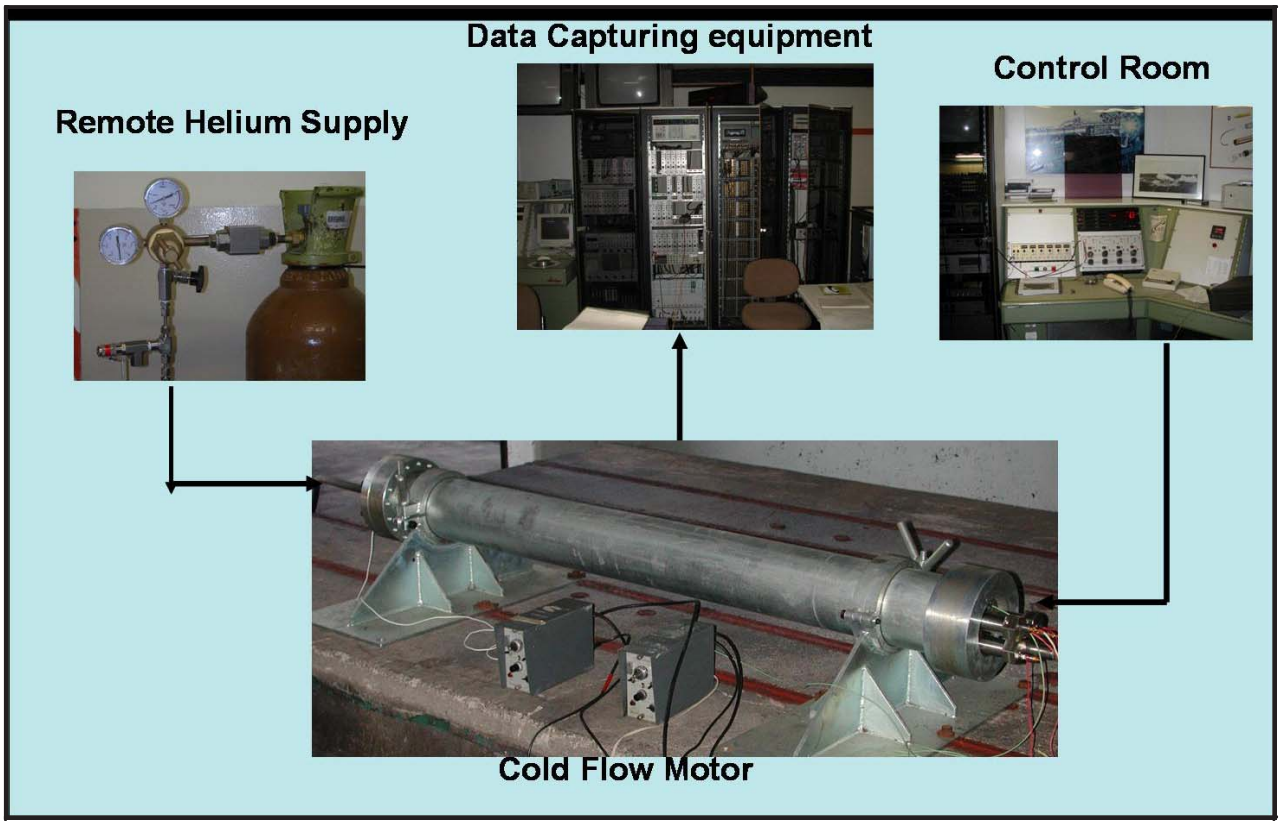

Figure 2.11: Test Setup for a Cold Flow Motor

Figures 2.11 to 2.12 show the test setup for cold flow tests. The three pulsers were attached to the head end of the motor as well as a static transducer and a Kistler dynamic transducer. The static transducer was used to measure the pressure as the cylinder is charged to the correct pressure with helium. Once the motor chamber was charged, the pulsers were fired individually. The shockwave was then measured by the dynamic transducers and analysed to obtain the initial shockwave amplitude. This data was also used to develop the signal analysis techniques that were used for live motor firings.

As discussed in Section 2.1.2 the pulser consisted of three interchangeable components: the charge amount, burst diaphragm thickness, and the orifice plate diameter. A pressure transducer was attached to the pulser as seen in Figure 2.6. The rupture pressure was measured and was used to calculate the yield pressure for a specific orifice and burst diaphragm (as shown in Section2.1.3-2.1.5) . The rupture pressure was also used to verify the shock tube theory by calculating the theoretical shock amplitude and that which was measured (35).

2.3 Live Motor Tests

The purpose of the cold flow tests was to develop dependable hardware. The live rocket motor test is more complex and also more dangerous. Unlike the cold flow test the pulsers are subjected to high temperatures necessitating the addition of insulation as shown in Figure 2.6. The pulsers are fired at specific times based on the time of ignition. The test procedure is as follows:

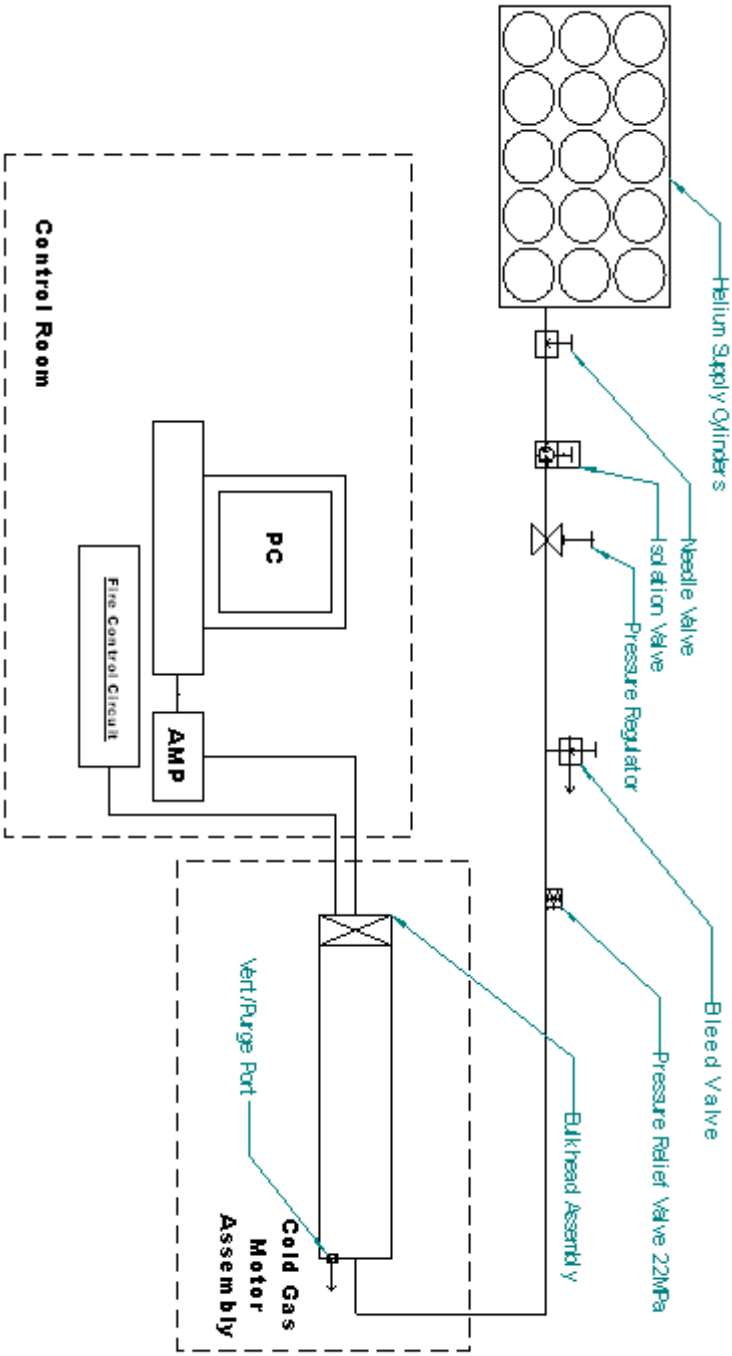

Figure 2.12: Schematic of Cold Flow Motor Test Setup

1. Attach three pulsers to the rocket motor head end;
2. Attach the dynamic Kistler and static pressure transducers to the head end;
3. Attach the igniter;
4. Evacuate area and move all personal to the control room;
5. Initiate ignition sequence.

In a successful firing the motor will ignite without delay. This is important as the pulsers are fired at programmed set times after the igniter is fired. Previous programs have had difficulty in miss-timed pulser firings amongst other problems (37–40).

2.3.1 Data Acquisition Scheme

The data acquisition scheme has constantly been improved throughout this study. The initial tests were done with unfiltered high frequency data and progressed to a filtered scheme as proposed by Blomshield (36) (cf. Figure 2.13). The data quality has been greatly increased using this data acquisition strategy. Key factors are (36):

- Use redundant or second pressure transducer in case of malfunction (it happens regularly that one transducer will fail);
- Minimise the distance between pressure transducer and motor. Extension tubes can decrease frequency response and add frequencies that are not present in the motor;
- Maximize signal to noise ratio;
- Sample 30x expected frequency or at the maximum sampling frequency possible;
- Anti-alias filter data before sampling;
- 12 Bit A-to-D converter minimum, 14 bit or higher preferred;
- Gains in Figure 2.13 set to maximize signal to noise ratio;
- Known noise sources to be minimized (example 60 Hz);

The first three tests (baseline propellant tubular grain, 4 slotted grain and the first SiC grain) performed in this study used a 16 bit analog to digital converter with only raw data channels being recorded. The subsequent tests used the exact data acquisition scheme as presented in Figure 2.13. A 16 bit analog to digital converter was used.

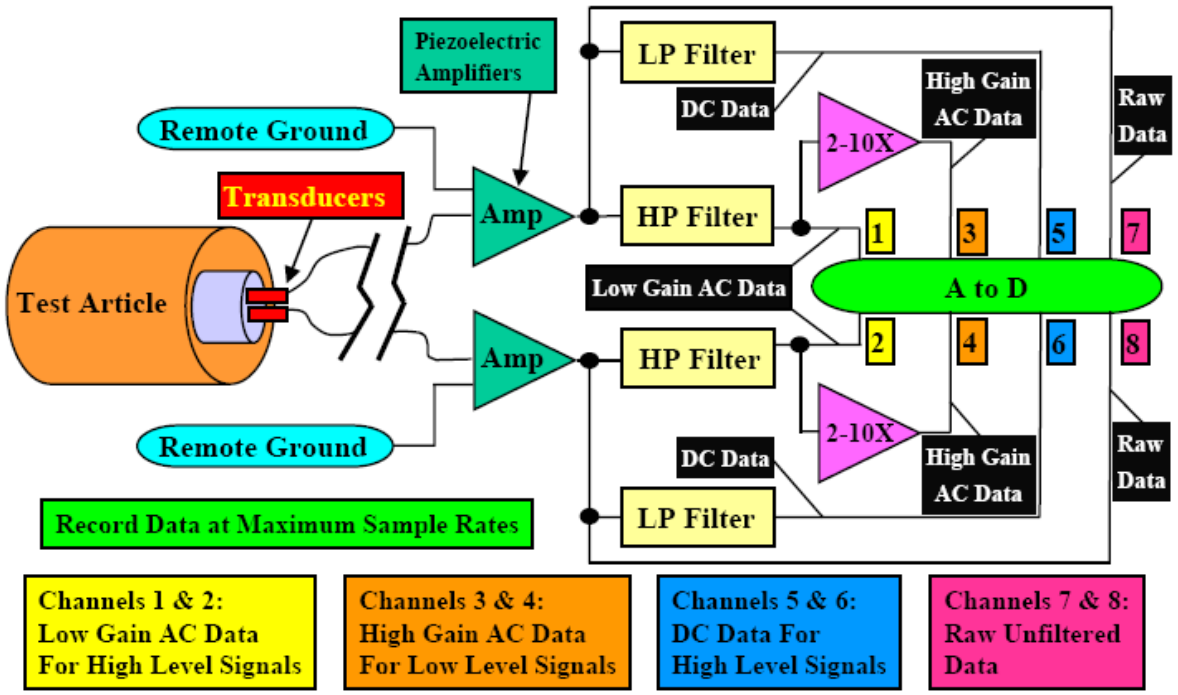

Figure 2.13: Data Acquisition Scheme Proposed by [Blomshield (29). Courtesy F. Blomshield, with permission]

2.4 Conclusions

The capacity to perform pulse tests was established. All aspects were addressed. The ability to predict the maximum pulse amplitude, the required pulser performance and the corresponding pulser configuration were established. The pulser hardware can be configured for a wide range of motors quickly and easily. This new capacity will allow the motor designer to perform a pulse test with minimum effort required.

The testing procedures were established and were carried out with great success. The data acquisition scheme was improved and the quality of results increased correspondingly.

Chapter 3

SRM Stability Prediction Theory

3.1 Introduction

This chapter is essentially an in depth literature survey that presents the notation, sets of linear terms, non-linear prediction methods and second order driving terms used in Chapter 4.. All terms and definitions required for computation are introduced. Furthermore, the terms are also discussed conceptually to establish an understanding of the physical processes. The theory, as indicated previously, can be split into linear and non-linear theory. This work does not represent the author's own work but is included here for convenience.

A large amount of work has been done in the analysis and prediction of combustion instability since 2000 especially by Flandro, Majdalani, Fischbach, French and Chibli on linear stability integrals (5; 5; 25–28; 31; 44–47). All the terms shown here have not been accepted by the entire CI community. The progress in theory is detailed in Appendix A. However, the sets of linear stability integrals are all subsets of the stability integrals presented.

The non-linear theory takes two forms, the shock wave approximation as proposed by Flandro and the non-linear gas dynamics method developed by Culick. Both methods are evaluated. In addition second order velocity coupling is discussed in the non-linear gas dynamics model.

These terms and methods are applied in the analysis of a tubular grain motor to obtain the response function of the propellant. The application of these models is discussed in Chapter 4. The results obtained from these differing analyses are presented in Chapter 5.

Lastly, computational fluid dynamics methods are discussed. This does not form part of this analysis but shows how the response function obtained using this method can be used to predict the motors stability during key periods.

3.2 Notation and Governing Equations

The first step is to establish notation as described by Flandro, Fischbach and Majdalani (47):

$$\begin{cases} \mathrm{p_a}{=}p_a*/p_0 \\ \rho{=}\rho*/\rho_0 \\ \mathrm{T} = T*/T_0 \\ \mathbf{u} = \mathbf{u}*/a_0 \\ r_b = r_b*/L \end{cases} \qquad \begin{cases} \mathbf{F} = \mathbf{F}*/(\rho_0 a_0^2/L) \\ t = t*/(L/a_0) \\ \boldsymbol{\omega}_v = \boldsymbol{\omega}_v*/(a_0/L) \\ e_e = e_e*/a_0^2 \end{cases} \tag{3.2.1}$$

The dimensionless governing equations become:

The mass or continuity equation (47):

$$\frac{\partial \rho}{\partial t} + \nabla \cdot (\rho \mathbf{u}) = 0 \tag{3.2.2}$$

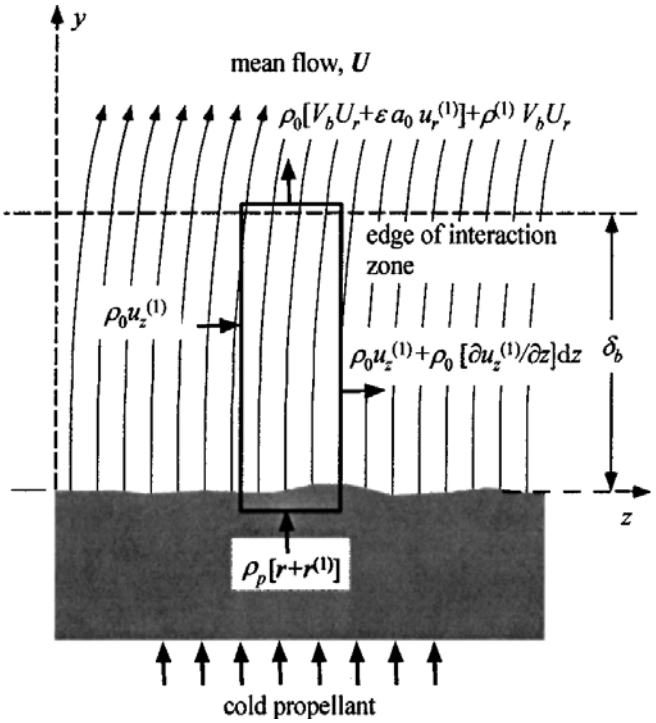

Figure 3.1: Mass balance Across the Combustion Zone [Flandro and Majdalani (25). Courtesy of J. Majdalani, with permission]

The momentum equation (47):

$$\rho \left(\frac{\partial u}{\partial t} + \frac{1}{2} \nabla \cdot \mathbf{u} \cdot \mathbf{u} \times \boldsymbol{\omega}_v \right) = -\frac{1}{\gamma} \nabla p - \delta_{Re}^2 \times \nabla \times \mathbf{u} + \delta_d^2 \nabla (\nabla \cdot \mathbf{u}) + \mathbf{F} \tag{3.2.3}$$

The energy balance (47):

$$\frac{\partial}{\partial t} \left[\rho (e_e + \frac{1}{2} \mathbf{u} \times \mathbf{u}) \right] + \nabla \left[\rho \mathbf{u} (e_e + \frac{1}{2} \mathbf{u} \times \mathbf{u}) \right] =$$

$$\left\{ \begin{array}{l} \dfrac{\delta_{Re}^2}{(\gamma - 1) \, \mathrm{Pr}} \nabla^2 T - \dfrac{1}{\gamma} \nabla \cdot (p_a \mathbf{u}) + \rho u \times (\mathbf{u} \times \boldsymbol{\omega}_v) \\ \\ + \mathbf{u} \times \mathbf{F} + \delta_{Re}^2 \left[\boldsymbol{\omega}_v \times \boldsymbol{\omega}_v - \mathbf{u} \cdot \nabla \times \boldsymbol{\omega}_v \right] \\ \\ + \delta_d^2 \left[(\nabla \cdot \mathbf{u})^2 + \mathbf{u} \cdot \nabla (\nabla \cdot \mathbf{u}) \right] - \sum_{i=1}^{N} h_i^0 w_i \end{array} \right\} \tag{3.2.4}$$

Species mass fractions (47):

$$\rho\left[\frac{\partial Y_i}{\partial t}+u\cdot\nabla Y_i\right]-\frac{\delta^2_{\mathrm{Re}}}{\mathrm{Pr}}\nabla 2Y_i=w_i \tag{3.2.5}$$

Equation of State (47):

$$p=\rho\mathbf{R}T \tag{3.2.6}$$

The Prandtl number and several other viscous reference numbers appear naturally (47):

$$\begin{cases}\mathrm{Pr}\equiv\dfrac{C_p\mu}{\kappa}\\[2ex]\delta^2_{Re}=\dfrac{\upsilon}{\bar{a}L}\\[2ex]\delta^2_d=\delta^2_{Re}\left(\eta/\mu+4/3\right)\\[2ex]\delta_f\equiv\dfrac{\kappa}{\rho_0C_pV}=\dfrac{\kappa}{\rho_0C_p\bar{a}M_b}\end{cases} \tag{3.2.7}$$

Dimensionless variables for modelling chemical reactions (47):

$$\begin{aligned}w&=w*/(\bar{\rho}\bar{a}/L)=Dimensionless\ reaction\ rate\\h^0_i&=(h^0_i)*/\bar{a}^2=Dimensionless\ Heat\ of\ Combustion\end{aligned} \tag{3.2.8}$$

3.2.1 Steady and Unsteady parts

The steady and unsteady parts are separated as follows (47):

$$\begin{cases}\rho=\bar{\rho}+\rho^{(1)}\\p=\bar{p}+p^{(1)}\\T=\bar{T}+T^{(1)}\\u=\bar{M}_b\mathbf{U}+\mathbf{u}^{(1)}\\\omega_v=\bar{M}_b\nabla\times(\mathbf{U}+\nabla\times\mathbf{u}^{(1)}=\bar{M}_b\boldsymbol{\omega}_v+\boldsymbol{\omega}^{(1)}_v\end{cases} \tag{3.2.9}$$

The approach followed by Flandro *et al.* (5; 25–28; 31; 44–46) is adopted here to avoid simplification such as isentropic flow limitations. Furthermore, it also includes heat transfer and viscosity so that the wave system is modelled as superimposed waves of compressibility, vorticity and entropy.

The system energy is defined as (47):

$$\zeta\equiv\rho\left(e_e+\frac{1}{2}\mathbf{u}\cdot\mathbf{u}\right) \tag{3.2.10}$$

For a calorically perfect gas the energy equation becomes (47):

$$\frac{\partial \zeta}{\partial t} = -\nabla \cdot \left\{ \rho \mathbf{u} \left[\frac{T}{\gamma(\gamma-1)} \right] + \frac{1}{2}\mathbf{u}\cdot\mathbf{u} \right\}$$

$$+ \left\{ \begin{array}{l} -\dfrac{1}{\gamma}\nabla\cdot(p_a\mathbf{u}) + \rho u(\mathbf{u}\cdot\omega) \\ \\ +\delta_{Re}^2(\boldsymbol{\omega}\cdot\boldsymbol{\omega} - \mathbf{u}\cdot\nabla\times\boldsymbol{\omega}) + \dfrac{\delta_{Re}^2}{(\gamma-1)\,\mathrm{Pr}}\nabla^2 T \\ \\ \delta_d^2\left[(\nabla\cdot\mathbf{u})^2 + u\cdot\nabla(\nabla\cdot\mathbf{u})\right] + \dot{Q} + \mathbf{u}\cdot\mathbf{F} \end{array} \right\} \tag{3.2.11}$$

The compressive viscous force and conduction are retained and are the source of nonlinear losses associated with steep fronted waves. The time average of equation (3.2.11) is taken to give an equation for the system amplitude (47):

$$-\nabla \cdot \left\{ \rho u \left[\frac{T}{\gamma(\gamma-1)} \right] + \frac{1}{2}u\cdot u \right\}$$

$$2\varepsilon\frac{d\varepsilon}{dt}\langle\zeta\rangle = \left\langle \begin{array}{l} -\dfrac{1}{\gamma}\nabla\cdot(p_a u) + \rho u(u\cdot\boldsymbol{\omega}) + \dot{Q} + u\cdot F \\ \\ +\delta_{Re}^2(\boldsymbol{\omega}\cdot\boldsymbol{\omega} - u\cdot\nabla\times\boldsymbol{\omega}) + \delta_d^2 u\cdot\nabla(\nabla\cdot u) \end{array} \right\rangle \tag{3.2.12}$$

$$+ \left\{ \frac{\delta_{Re}^2}{(\gamma-1)\,\mathrm{Pr}}\nabla^2 T + \delta_d^2(\nabla\cdot u)^2 \right\}$$

The time averaged oscillatory energy is (47):

$$\langle\zeta\rangle = \frac{1}{\gamma\bar{p}}\left\langle \left(\frac{p'}{\gamma}\right)^2 \right\rangle + \frac{1}{2}\bar{\rho}\,\langle\mathbf{u}'\times\mathbf{u}'\rangle \tag{3.2.13}$$

The first term in equation (3.2.13) is the potential energy proportional to the pressure fluctuation and the kinetic energy is proportional to the square of the particle velocity. The particle velocity is the composite of irrotational and rotational parts required to satisfy the boundary conditions.

3.3 Spatial Averaging

The time averaged density is integrated over the chamber control volume. The reference system is defined (47):

$$E^2 \equiv \iiint_V \langle\zeta\rangle\, dV = \iiint_V \frac{1}{\gamma\bar{p}}\left(\frac{p'}{\gamma}\right)^2 + \frac{1}{2}\bar{\rho}\,\langle\mathbf{u}'\times\mathbf{u}'\rangle \tag{3.3.1}$$

The fluctuating variables are defined by factoring out the slowly changing amplitude (47):

$$p^{(1)} = \varepsilon(t)p' \tag{3.3.2}$$

Thus, as shown in (48; 49) the system amplitude can be conveniently written as a composite wave system (47):

$$\frac{d\varepsilon}{dt} = \alpha^{(1)}\varepsilon + \alpha^{(2)}\varepsilon^2 + \alpha^{(3)}\varepsilon^3 + \cdots \quad (3.3.3)$$

At this point it may be necessary to address Culick's critique on this method as presented in (50). His critique is valid in the sense that it may be dangerous to assume all variables and processes are a function of ε, the system amplitude. However, this is the most practically applicable method in open literature. The results that have been obtained to date have shown great promise and are validated by excellent agreement with experimental results (51). Flandro's energy analysis method requires the least amount of experimental data and thus represents the most cost effective method for qualitative predictions of rocket motor stability. The method is limited as an approximation of the wave form must be made to calculate the shock wave losses. The sawtooth approximation for the wave form gives good results for tubular grains, but for more complex grain geometries the wave form does not adequately predict the shock losses (51).

3.4 Flow Field Analysis for a Tubular Grain

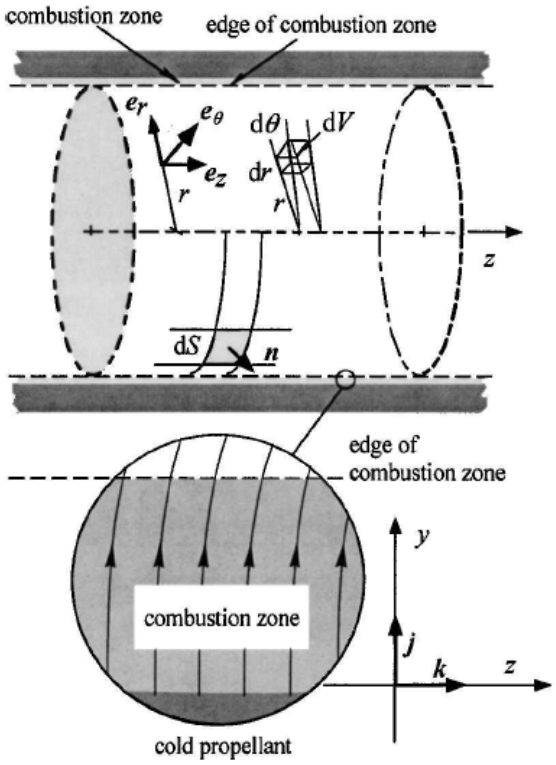

Figure 3.2: Coordinate System Proposed [Flandro and Majdalani (25). Courtesy of J. Majdalani, with permission]

For the validity of any computations it is necessary to correctly represent the unsteady flow fields. Figure 3.2 shows the coordinate system and the geometry for a tubular grain. This is the best defined and researched motor geometry. For this study the motor is of most

interest, thus the complete formulation will be given as presented by Flandro and Majdalani (25).

Starting as Culick in (52) and assuming small-amplitude unsteady perturbations (25):

$$\mathbf{U} = U_r \mathbf{e}_r + U_z \mathbf{e}_z = -r^{-1} \sin x \mathbf{e}_r + \pi z \cos x \mathbf{e}_z \tag{3.4.1}$$

Where the following combination is used repeatedly throughout the analysis:

$$x \equiv \frac{1}{2}\pi r^2 \tag{3.4.2}$$

The continuity and momentum equations are linearised (as is standard combustion instability theory practice) (25):

$$\frac{\partial \rho^{(1)}}{\partial t} + \nabla \mathbf{u}^{(1)} = -M_b \mathbf{U} \nabla \rho^{(1)} \tag{3.4.3}$$

$$\begin{aligned} \frac{\partial \mathbf{u}^{(1)}}{\partial t} + \nabla p^{(1)} = M_b \left\{ -\nabla \left[\mathbf{U} \times \mathbf{u}^{(1)} \right] + u^{(1)} \times \nabla \times \mathbf{U} \times \mathbf{U} \times \nabla \times \mathbf{u}^{(1)} \right\} + \\ \delta_{Re}^2 \left\{ \left(2 + \frac{\lambda}{\mu} \right) \nabla \left[\nabla \cdot \mathbf{u}^{(1)} \right] - \nabla \times \nabla \times \mathbf{u}^{(1)} \right\} \end{aligned} \tag{3.4.4}$$

Where:

- The superscript (1) is first order terms of the perturbation parameter ε;
- The second small perturbation parameter is the surface Mach number, M_b, with only first order terms being retained;
- The viscous forces relative sizes are set by δ_{Re}^2, the inverse square of the Reynolds number based on the radius;
- Viscous terms are retained by assuming δ_{Re}^2=$O(\mathrm{M}_b)$ (same order of magnitude).

The main variables are represented as the sum of the rotational and irrotational components (25):

$$\begin{cases} p^{(1)} = \hat{p} + \tilde{p} \\ \rho^{(1)} = \hat{\rho} = \hat{p} \\ \mathbf{u}^{(1)} = \hat{\mathbf{u}} + \tilde{\mathbf{u}} \end{cases} \tag{3.4.5}$$

The following is assumed:

- The acoustic field is irrotational ($\nabla \times \hat{\mathbf{u}} = 0$);
- The superimposed vortical component is incompressible ($\nabla \cdot \hat{\mathbf{u}} = 0$);
- The assumption of constant entropy allows for the density and the thermodynamic (acoustic) pressure to be treated as interchangeable as shown in equation 3.4.5 ;
- The unsteady pressure in the continuity equation represents a density fluctuation which is of vital importance in the rotational case.

When flow is irrotational, equations (3.4.3) and (3.4.4) yield the acoustic wave solution. For axial modes of a standing plane wave (25):

$$\hat{p} = e^{-ikt}\cos(k_m z) + O(\mathrm{M}_b) \tag{3.4.6}$$

$$\hat{\mathbf{u}} = e^{-ikt}\sin(k_m z)\mathbf{e}_z + O(\mathrm{M}_b) \tag{3.4.7}$$

Where for a closed end boundary:

$$k_m = n\pi R/L \tag{3.4.8}$$

The acoustic solution equations are (3.4.6) and (3.4.7) and are accompanied by corrections for rotational pressure and velocity (25):

$$\tilde{p} = iM_b e^{-ikt}\sin(2x)e^{(\phi+i\psi)}\left(\frac{1}{2}\pi z\right)\sin\left[\sin(x)k_m z\right] + O\left(M_b^2\right) \tag{3.4.9}$$

$$\tilde{\mathbf{u}} = iCe^{-iktr}U_r^{(\phi+i\psi)}\sin\left[\sin(x)k_m z\right]\mathbf{e}_z + O(M_b) \tag{3.4.10}$$

Where C=1.

The exponential factor $\exp(\phi - i\psi)$ shows that the vertical wave can be interpreted as a dampened travelling shear wave. Both are functions of radial position only. The imaginary part is given as (25):

$$\psi(r) = -\left[k_m/(\pi M_b)\right]\ln\tan\left(\frac{1}{2}x\right) \tag{3.4.11}$$

This sets the wavelength and the spatial frequency of the shear wave. The derivative will become important at a later point and is (25):

$$\frac{d\psi}{dr} = \frac{k_m}{M_b U_r} \tag{3.4.12}$$

This is proportional to the reciprocal of the radial mean flow velocity. The real part is given as (25):

$$\begin{aligned}\phi(r) &= \frac{\xi}{\pi^2}\left[1 - \frac{1}{\sin(x)} - x\frac{\cos(x)}{\sin^2(x)} + I(x) - I\left(\frac{1}{2}\pi\right)\right] \\ where: \qquad \xi &\equiv \frac{k_m^2\delta_{Re}^2}{M_b^3} = \frac{S_t^2\delta_{Re}^2}{M_b}, \qquad St \equiv \frac{k_m}{M_b}\end{aligned} \tag{3.4.13}$$

$$I(x) = x + \frac{1}{18}x^2 + \frac{7}{1800}x^3 + \frac{31}{105,480}x^7 + \cdots \tag{3.4.14}$$

The flow field as described has shown good agreement with experimental results. Numerical solutions based on Navier-Stokes equations also return similar results.

All the unsteady energy terms needs to be accounted for. This is achieved by multiplying equation (3.4.3), the continuity equation, by the acoustic pressure and is added to the momentum equation (3.4.4), and multiplied by the composite velocity vector $\mathbf{u}^{(1)}$. The terms are isolated and differentiated with respect to time and terms linear in the Mach number M_b. The following is obtained (25):

$$\frac{\partial}{\partial t}\left[\frac{1}{2}\hat{p}^2+\frac{1}{2}\mathbf{u}^{(1)}\times\mathbf{u}^{(1)})\right]=-\left[\hat{p}\nabla\cdot\hat{\mathbf{u}}+\mathbf{u}^{(1)}\cdot\nabla(\hat{p}+\tilde{p})\right]$$
$$-M_b\left\{\frac{1}{2}\mathbf{U}\cdot\nabla\cdot\hat{p}^2+\mathbf{u}^{(1)}\cdot\nabla\left[\mathbf{U}\cdot\mathbf{u}^{(1)}\right]-\mathbf{u}^{(1)}\cdot\left[\mathbf{u}^{(1)}\times\nabla\times\mathbf{U}+\mathbf{U}\times\nabla\times\tilde{\mathbf{u}}\right]\right\}$$
$$+\delta_{Re}^2\mathbf{u}^{(1)}\cdot\left[\left(2+\frac{\lambda}{\mu}\right)\nabla\left(\nabla\cdot\hat{\mathbf{u}}\right)-\nabla\times\nabla\times\tilde{\mathbf{u}}\right] \tag{3.4.15}$$

The oscillatory energy density is given as (25):

$$e_e=\frac{1}{2}\left[p^2+\mathbf{u}^{(1)}\mathbf{u}^{(1)}\right] \tag{3.4.16}$$

The time averaged oscillatory energy within the chamber is (25):

$$E=\iiint_V\langle e_e\rangle\,dV=\frac{1}{2}\iiint_V\left\langle p^2+\mathbf{u}^{(1)}\mathbf{u}^{(1)}\right\rangle dV \tag{3.4.17}$$

From equation (3.4.15) the system energy is controlled by (25):

$$\frac{\partial E}{\partial t}=\iiint_V\left\langle\begin{array}{l}\overbrace{\begin{array}{l}-\nabla\cdot(\hat{p}\cdot\hat{\mathbf{u}})-\frac{1}{2}M_b(\mathbf{U}\cdot\nabla\hat{p}^2)-M_b\left[\hat{\mathbf{u}}\cdot\nabla(\mathbf{U}\times\hat{\mathbf{u}})\right]\\+\delta_d^2\hat{\mathbf{u}}\cdot\nabla\left(\nabla\cdot\hat{\mathbf{u}}\right)+M_b\left[\hat{\mathbf{u}}\cdot(\hat{\mathbf{u}}\times\boldsymbol{\Omega})\right]+\hat{\mathbf{u}}\cdot(\mathbf{U}\times\boldsymbol{\omega}_v)\end{array}}^{irrotational}\\\overbrace{\begin{array}{l}-\tilde{\mathbf{u}}\nabla\hat{p}-M_b\left[\begin{array}{l}\tilde{\mathbf{u}}\cdot\nabla\left(\mathbf{U}\cdot\hat{\mathbf{u}}\right)+\hat{\mathbf{u}}\cdot\nabla(\mathbf{U}\times\tilde{\mathbf{u}})-\tilde{\mathbf{u}}\cdot\nabla(\mathbf{U}\times\tilde{\mathbf{u}})\\-\tilde{\mathbf{u}}\cdot(\mathbf{U}\times\boldsymbol{\omega}_v)-\tilde{\mathbf{u}}\cdot(\tilde{\mathbf{u}}\times\boldsymbol{\Omega})\end{array}\right]\\+\delta_d^2\tilde{\mathbf{u}}\cdot\nabla\cdot(\nabla\cdot\hat{\mathbf{u}})-\delta_{Re}^2\left[\hat{\mathbf{u}}\cdot(\nabla\times\boldsymbol{\omega}_v)+\tilde{\mathbf{u}}\cdot(\nabla\times\boldsymbol{\omega}_v)\right]\\-\hat{\mathbf{u}}\cdot\nabla\tilde{p}-\tilde{\mathbf{u}}\cdot\nabla\tilde{p}\end{array}}^{Rotational}\end{array}\right\rangle dV \tag{3.4.18}$$

The mean and unsteady vorticity vectors are represented by $\boldsymbol{\Omega}=\nabla\times\mathbf{U}$ and $\boldsymbol{\omega}_v=\nabla\times\tilde{\mathbf{u}}$ respectively. The viscous dilation is defined as (25):

$$\delta_d^2\equiv\delta_{Re}^2\left(2+\lambda/\mu\right) \tag{3.4.19}$$

Where λ is the second coefficient of viscosity. Several terms in (3.4.18) cancel each other out. Further simplifications can also be made by expressing the volume integrals as surface integrals. The right hand side of equation (3.4.18) controls the rate of energy change. This can thus be used to determine the growth and decay (linear part) for a given motor configuration.

The complex wave number is given as (25):

$$k_c=k_m+(\omega_m+i\alpha_m)+O(M_b^2) \tag{3.4.20}$$

- For multidimensional analysis m can consist of three mode integers, but as stated earlier this analysis focuses on the axial case giving the result from equation (3.4.8):
- ω_m + iα_m are in the order of the mean Mach number;

- The frequency correction ω_m is ignored to simplify the calculations;
- The frequency correction is implicitly accounted for by k_m.

There are variables that appear in quadratic combinations. This makes it necessary to take the real parts of velocity and pressure to be used in the equations. Thus (25):

$$\hat{p} = \hat{p}_m \exp(\alpha_m t) \cos(k_m t) \tag{3.4.21}$$

$$\tilde{\mathbf{u}} = \tilde{\mathbf{u}}_m \exp(\alpha_m t) \sin(k_m t) \tag{3.4.22}$$

$$\tilde{\mathbf{u}} = \exp(\alpha_m t) \left[\tilde{\mathbf{u}}_m^{(r)} \cos(k_m t) + \tilde{\mathbf{u}}_m^{(i)} \sin(k_m t) \right] \tag{3.4.23}$$

- Superscripts (r) and (i) refer to cosine and sine multipliers due to complex to real conversions of real and imaginary parts;
- Due to rotational velocity vectors containing the exponential term $\exp(\phi + i\psi)$ this notation becomes necessary.

Substituting these terms into the energy density equation (3.4.16) yields (25):

$$\langle e_e \rangle = \frac{1}{4} \exp(2\alpha_m t) \left[\overbrace{\hat{p}_m^2 + \mathbf{u}_m \cdot \mathbf{u}_m}^{irrotational} + \overbrace{2\hat{\mathbf{u}}_m \cdot \tilde{\mathbf{u}}_m^{(i)} + \tilde{\mathbf{u}}_m^{(r)} \cdot \tilde{\mathbf{u}}_m^{(r)} + \tilde{\mathbf{u}}_m^{(i)} \cdot \tilde{\mathbf{u}}_m^{(i)}}^{Rotational} \right] \tag{3.4.24}$$

By substituting equation (3.4.24) into equation (3.4.17) and differentiating with respect to time the following is obtained (25):

$$\frac{\partial E}{\partial t} = \alpha_m \exp(2\alpha_m t) E_m^2 \tag{3.4.25}$$

Where the energy normalisation is given as (25):

$$E_m^2 = \frac{1}{2} \iiint_V \left[\left(\hat{p}_m^{'} \right)^2 + \mathbf{u}_m \cdot \mathbf{u}_m + 2\hat{\mathbf{u}}_m \cdot \tilde{\mathbf{u}}_m^{(i)} + \tilde{\mathbf{u}}_m^{(r)} \cdot \tilde{\mathbf{u}}_m^{(r)} + \tilde{\mathbf{u}}_m^{(i)} \cdot \tilde{\mathbf{u}}_m^{(i)} \right] dV \tag{3.4.26}$$

- It is written as a squared quantity to indicate that it is positive and definite.

From equations(3.4.6), (3.4.7) and (3.4.10) the necessary information can be obtained to calculate the axial mode oscillation to zeroth order in M_b (25):

$$\hat{p}_m = \cos(k_m z) \tag{3.4.27}$$

$$\hat{\mathbf{u}}_m = \sin(k_m z) e_z \tag{3.4.28}$$

$$\mathbf{u}_m^{(r)} = \sin(x) \exp(\phi) \sin(\psi) \sin\left[\sin(x) k_m z\right] \mathbf{e}_z \tag{3.4.29}$$

$$\mathbf{u}_m^{(i)} = -\sin(x)\exp(\phi)\cos(\psi)\sin\left[\sin(x)k_m z\right]\mathbf{e}_z \tag{3.4.30}$$

The acoustic pressure and velocity mode shapes are related as (25):

$$\hat{\mathbf{u}}_m = -\nabla\hat{p}_m/k_m \tag{3.4.31}$$

By integrating equation (3.4.26) and substituting equations (3.4.27)-(3.4.30), the normalized energy function is found to be (25):

$$E_m^2 = \frac{5}{8}\pi L/r \tag{3.4.32}$$

It is now possible to calculate the growth rate or the linear stability of the system. Before moving on, it is important to note that this method can be extended for more modes than just axial modes. The complexity would increase dramatically. Thus, for this project only axial modes will be evaluated. It has been shown that tangential instability can be more severe but is easily eliminated with the addition of particles (3). Also, axial or longitudinal modes are the most common form of instability and thus, are the main focus.

More complex geometries also complicate mode shapes and the flow dynamics. This is an area that is currently being addressed by various researchers. It will be shown in the next section that it is possible to obtain a formulation in terms of function of surface and acoustic fields. This eliminates the need to evaluate the rotational field directly. The analysis as shown here, is strongly dependent on the assumption of a simple cylindrical motor. The use of finite element analysis and computational flow dynamics is discussed in section 3.6.2.

3.5 Linear Stability

Linear stability has been the foundation upon which combustion instability analyses have been built. Non-linear combustion instability theory is dependent on the quality of linear stability theory. The original framework has been established by Culick (23; 24; 52–54). It has progressed from one-dimensional to three-dimensional analysis. There have been corrections added and removed over time. The following section is included for easy reference. It is important to note that some of the terms have subsequently been neglected or abandoned. They are included for the sake of completeness. For parametric evaluation of these terms the reader is referred to (26; 27). All analysis includes subsets of the physical mechanisms discussed here.

Classical linear stability theory evaluates equation (3.4.18) or the linear part of equation (3.2.12) and can be represented as the linear sum of gains and losses:

$$\alpha_m = \alpha_1 + \alpha_2 + \alpha_3 + \cdots = \sum_{i=1}^{N}\alpha_i \tag{3.5.1}$$

Majdalani *et al.* (26) introduced six new growth rate corrections. This makes the total number of growth or decay rates 10, excluding particle dampening which can be added if necessary. Fischbach *et al.* (28; 29) transformed these volume integrals into surface integrals. This has the great advantage of being independent of rotational flow fields which can be extremely difficult to obtain for a real motor geometry. This makes it possible to predict the stability by obtaining information from the acoustic field by only using a function of

quantities distributed along the control surface. Furthermore, the integrals are manipulated so that they can be used in a computational algorithm.

The final results will be listed here only for the volume integral, surface integral, computational form and analytical result for a tubular grain motor. The volume and surface integral terms are included for future studies wishing to attempt to solve the linear growth constants for more complex geometries. The tubular grain results are of the most interest for this study as they will be used to calculate the growth and loss terms for tubular grain test motor in Chapter 5. The complete formulation and mathematical manipulation of these growth rate integrals have been excellently presented in (25–29) and are not presented here. The physical significance of each contribution is also discussed briefly. This section attempts to shed light on the physical processes at work and how they relate to equation (3.4.18) and (3.2.12). The equations shown here also form the basis of the stability algorithm that was developed.

3.5.1 Irrotational Growth Rate Contributions

The first three irrotational terms in equation (3.4.18) represent the energy gained from the combustion process and the energy lost at the nozzle boundary. These terms are referred to in classical CI theory as pressure coupling and nozzle damping are defined below:

Expressed as a volume integral (25–29):

$$\alpha_1 = \frac{1}{\exp(2\alpha_m t) E_m^2} \iiint_V \left\langle -\nabla \cdot \left[(\hat{p} \cdot \hat{\mathbf{u}}) + \frac{1}{2} M_b (U \cdot \hat{p}^2) \right] - M_b \left[\hat{\mathbf{u}} \cdot \nabla (\mathbf{U} \times \hat{\mathbf{u}}) \right] \right\rangle dV \quad (3.5.2)$$

Surface integral form (28; 29):

$$\alpha_1 = \frac{1}{\exp(2\alpha_m t) E_m^2} \iint_S \left\langle \mathbf{n} \cdot \left[(\hat{p} \cdot \hat{\mathbf{u}}) + \frac{1}{2} M_b (U \cdot \hat{p}^2) \right] - M_b \left[\hat{\mathbf{u}} \cdot \mathbf{n} (\mathbf{U} \times \hat{\mathbf{u}}) \right] \right\rangle dS \quad (3.5.3)$$

Form to be used in computational prediction (28; 29) :

$$\alpha_1 = \frac{M_b}{2E_m^2} \left\{ \iint_{S_b} \left[A_b^{(r)} + 1 \right] \hat{p}_m^2 dS - \iint_{S_N} \left[A_N^{(r)} + U_z \right] \hat{p}_m^2 \right\} \quad (3.5.4)$$

For a tubular grain with quasi-steady short nozzle the following is found (25–29):

$$\alpha_1 = \frac{\pi M_b}{2E_m^2} \frac{L}{R} \left\{ \left[A_b^{(r)} + 1 \right] - [\gamma + 1] \right\} \quad (3.5.5)$$

- The entire surface is not represented; inert surfaces could be incorporated if required.
- Surface losses are usually assumed to be negligibly small, however in some cases rough chamber walls and insulation can have significant dampening affect.

The fourth term from equation (3.4.18) is the volume (dilation) acoustic viscous energy. The volume integral (25–29):

$$\alpha_2 = \frac{1}{\exp(2\alpha_m t) E_m^2} \iiint_V \left\langle \delta_d^2 \hat{\mathbf{u}} \cdot \nabla (\nabla \cdot \hat{\mathbf{u}}) \right\rangle dV \quad (3.5.6)$$

Surface volume integral (28; 29):

$$\alpha_2 = \frac{4k_{_m}\delta_{Re}^2}{3\exp(2\alpha_m t)E_m^2}\iint\limits_S \langle n\cdot(\hat{p}\hat{\mathbf{u}})\rangle\, dS - \frac{2}{3}\delta_{Re}^2 k_m^4 \tag{3.5.7}$$

Form to be used in computational prediction (28; 29):

$$\alpha_2 = -\frac{2k_m\delta_{Re}^2}{3E_m^2}\left[\iint\limits_{S_b} M_b A_b^{(r)}\hat{p}_m^2 dS - \iint\limits_{S_N} M_b A_N^{(r)}\hat{p}_m^2 dS\right] - \frac{2}{3}\delta_{Re}^2 k_m^4 \tag{3.5.8}$$

This reduces for a tubular grain (25–29):

$$\alpha_2 \simeq -\frac{\delta_d^2\pi k_m^2}{4E_m^2}\frac{L}{R} \tag{3.5.9}$$

- α_2 is usually regarded as negligible;
- May not be negligible if turbulence is present due to change in transport properties;
- Particulate dampening and residual burning are not included but can be superimposed.

The rotational mean flow is given as (25–29):

$$\alpha_3 = \frac{1}{\exp(2\alpha_m t)E_m^2}\iiint\limits_V \langle M_b\left[\hat{\mathbf{u}}\cdot(\hat{\mathbf{u}}\times\boldsymbol{\Omega})\right]\rangle\, dV = O\left(M_b^2\right) \tag{3.5.10}$$

It has been shown by Culick (52) that this term is negligibly small, and thus is ignored in further analysis. The next term is the famous or infamous flow turning correction. Following standard combustion instability practice the flow turning is included here. It was however noted by Flandro *et al.* (25) that simply patching this result and excluding other rotational corrections, as with previous work by Culick (24), is not mathematically legitimate. The volume integral is(25–29):

$$\alpha_4 = \alpha_{flow\,turning} = \frac{1}{\exp(2\alpha_m t)E_m^2}\iiint\limits_V \langle M_b\hat{\mathbf{u}}\cdot(\mathbf{U}\times\boldsymbol{\omega}_v)\rangle\, dV \tag{3.5.11}$$

Surface integral(28; 29):

$$\alpha_4 = \frac{M_b}{E_m^2\exp(\alpha_m t)}\iint\limits_{S_b}\left\langle\tilde{\mathbf{u}}^{(i)}\cdot\hat{\mathbf{u}}\right\rangle dS \tag{3.5.12}$$

The form to be used in computational prediction (28; 29):

$$\alpha_4 = -\frac{1M_b}{2E_m^2 k_m}\iint\limits_{S_b}\left\langle\tilde{\mathbf{u}}_m^{(i)}\cdot\nabla\hat{p}_m\right\rangle dS \tag{3.5.13}$$

For a tubular grain(25–29):

$$\alpha_4 \simeq -\frac{\pi M_b}{2E_m^2}\frac{L}{R} \tag{3.5.14}$$

3.5.2 Rotational Flow Corrections

The rotational flow correction from the first rotational term in equation(3.4.18)(25–29):

$$\alpha_5 = \frac{1}{E_m^2 \exp(2\alpha_m t)} \iiint_V \langle -\tilde{\mathbf{u}} \cdot \nabla \hat{p} \rangle \, dV \tag{3.5.15}$$

The surface integral(28; 29):

$$\alpha_5 = \frac{1}{E_m^2 \exp(2\alpha_m t)} \iint_S \langle \mathbf{n} \cdot (\tilde{\mathbf{u}} \hat{p}) \rangle \, dS \tag{3.5.16}$$

Form to be used in computational prediction (28; 29):

$$\alpha_5 = \frac{1 M_b}{2 E_m^2} \iint_{S_b} \hat{p}_m^2 dS \tag{3.5.17}$$

For a tubular grain motor (25–29):

$$\alpha_5 \simeq \frac{1}{2} \left(\frac{\pi M_b}{E_m^2} \right) \frac{L}{R} \tag{3.5.18}$$

- α_5 represents the physical rate of work being done by the boundary layer on the acoustic wave;
- For axial modes it is only necessary to know the axial components of the rotational flow field velocity. This is due to the pressure gradient being in the z direction;
- The radial components of the rotational velocity field are not needed in the calculation of α_5;
- Also referred to as the boundary layer pumping affect.

Equation (3.5.18) has been shown to be equal to the flow turning result but is opposite in sign. It has been shown in (55; 56) that the flow turning is exactly cancelled out by the rotational flow correction. That is (25–29):

$$\alpha_4 + \alpha_5 = 0 \tag{3.5.19}$$

Though it has been shown that these terms cancel out, they are both important in the understanding of the combustion instability processes. Flow turning has been debated since it was first described by Culick, so too has α_5. R.S. Brown in communications with Flandro (25) has claimed that this is merely duplicating the same physical effect. This has resulted in confusion within the combustion instability community. Flandro and Majdalani (25) have shown convincingly that it is indeed two different mechanisms. Culick (30) includes this term in his analysis.

Returning to equation (3.4.18), the second rotational term is ignored as it is in the order of M_b. The third and fourth terms are evaluated together but due to uncertainties at the nozzle entrance these terms are routinely ignored. More recent work (26; 28) has included it in the analysis and hence it is designated as α_{10}. The volume integral (26–29):

$$\alpha_{10} = \frac{1}{E_m^2 \exp(2\alpha_m t)} \iiint_V \langle M_b \left(\hat{\mathbf{u}} + \tilde{\mathbf{u}}\right) \cdot \nabla \left(\mathbf{U} \cdot \tilde{\mathbf{u}}\right) \rangle \, dV \tag{3.5.20}$$

Surface integral (28; 29):

$$\alpha_{10} = -\frac{M_b}{E_m^2 \exp(2\alpha_m t)} \iint_S \langle \hat{\mathbf{n}} \cdot \left[\tilde{\mathbf{u}} \left(\mathbf{U} \cdot \tilde{\mathbf{u}}\right)\right] \rangle \, dS \tag{3.5.21}$$

Form to be used in computational prediction (28; 29):

$$\alpha_{10} = -\frac{1 M_b}{2E_m^2} \iint_{S_N} \left[\left(\tilde{\mathbf{u}}_m^{(i)}\right)^2 + \left(\tilde{\mathbf{u}}_m^{(r)}\right)^2 \right] U_z dS \tag{3.5.22}$$

For a tubular grain(26–29)[1]:

$$\alpha_{10} = -\frac{4}{3}\pi M_b \left\{ \left[\pi^2 + 4\left(\xi + \sqrt{2}\right)^2 \right]^{-1} - \frac{1}{500} \right\} \tag{3.5.23}$$

The next correction is the mean vortical correction which corresponds to the fifth rotational term in equation (3.4.18) (25–29):

$$\alpha_6 = \frac{1}{E_m^2 \exp(2\alpha_m t)} \iiint_V \langle M_b \tilde{\mathbf{u}} \cdot \left(\mathbf{U} \times \boldsymbol{\omega}_v\right) \rangle \, dV \tag{3.5.24}$$

The surface integral (28; 29):

$$\alpha_6 = \frac{M_b}{E_m^2 \exp(2\alpha_m t)} \iint_S \left\langle \mathbf{n} \cdot \mathbf{U} \left(\frac{1}{2} \tilde{\mathbf{u}} \cdot \tilde{\mathbf{u}} \right) \right\rangle dS \tag{3.5.25}$$

Form to be used in computational prediction (28; 29):

$$\alpha_6 = \frac{M_b}{k_m^2 E_m^2} \iint_{S_b} \left(\nabla \hat{p}_m\right)^2 dS \tag{3.5.26}$$

For a tubular grain(28; 29):

$$\alpha_6 \simeq \frac{\pi M_b L}{4E_m^2 R} \tag{3.5.27}$$

- This term is of interest since it is analogous to the flow turning effect. Instead of acoustic velocity, rotational velocity appears ;
- This represents an additional energy source other than the pressure coupling response. Classical theory regarded all contributions as energy sinks or losses; this is a new energy source term;
- Caused by the creation of unsteady vorticity at the boundaries;

[1] Flandro and Majdalani (25) ignored α_{10}

- This term is only at the surface and arises due to the no slip condition for the axial mode. It can be extended to include vortex shedding phenomenon.

The sixth rotational term in equation (3.4.18) is ignored upon transforming this integral to a surface integral, since its parameters are of the order of the mean flow Mach number M_b. The last term of equation (3.4.18) is the viscous dampening (25–29):

$$\alpha_7 = \frac{1}{E_m^2 \exp(2\alpha_m t)} \iiint_V \left\langle -\delta_{Re}^2 \left(\hat{\mathbf{u}} \cdot \tilde{\mathbf{u}}\right) \cdot \left(\nabla \times \boldsymbol{\omega}_v\right) \right\rangle \, dV \tag{3.5.28}$$

Surface integral form (28; 29):

$$\alpha_7 = \frac{-\delta_{Re}^2 k_m^2}{2E_m^2 \exp(2\alpha_m t) M_b^2} \iint_S \left\langle \tilde{\mathbf{u}}^2 \right\rangle \Big|_{r=1} \, dS \tag{3.5.29}$$

Form to be used in computational prediction (28; 29):

$$\alpha_7 = \frac{-\delta_{Re}^2 k_m^2}{4E_m^2 M_b^2} \iint_{S_b} \left\langle \nabla \hat{p}_m \right\rangle \Big|_{r=1} \, dS \tag{3.5.30}$$

For a tubular grain (25–29):

$$\alpha_7 \simeq -\frac{\pi \delta_{Re}^2}{6E_m^2} \frac{L}{R} \left(\frac{k_m}{M_b}\right)^2 = -\frac{\pi M_b \xi}{6E_m^2} \frac{L}{R} \tag{3.5.31}$$

- Viscous dampening increases rapidly with frequency;
- Since the Mach number appears in the denominator this term can be as important as any other term;
- Turbulent mean flows can increase δ_{Re}^2 so that its influence is much larger than the laminar case;
- To evaluate this term correctly an extensive numerical algorithm is required.

3.5.3 Pseudo Pressure Growth Rate Corrections

The last two terms in equation (3.4.18) are the interactions of the velocity flow fields and the pseudo pressure associated with vorticity-driven disturbances. Majdalani and Flandro (26) best explain the pseudo pressure's importance. Since it is not possible to measure the pseudo pressure experimentally and experimental data from combustion instability tests only reflect the pressure component, this term has been easy to ignore. However, cold flow studies by Brown *et al.* (57) and Avalon *et al.* (58) supported the conclusion that the waves observed are compressible rotational waves. Center for Simulation of Advanced Rockets (CSAR) and Office d'Etudes et de Recherches Aerospatiales (ONERA) have also provided data to corroborate this analysis. One of the more important aspects is that both amplitudes must grow and decay at the same rate. Majdalani, Flandro and Fischbach (26) went on to state that for an energy representation of the stability analysis both energies must be accounted for. The historic dismissal of this component was made for problems that did not display

cross-flow and where rotational effects do not penetrate deep into the chamber. As such the purely acoustic representation is only valid where rotational effects are negligible or limited to a very thin layer. However Majdalani and van Moorhem (59) and Majdalani (60) have shown that the rotational region occupies nearly 80% of the motor volume and this was confirmed by a large volume of work performed in the 1990s that also predict large unsteady rotational depths.

The first term is the pseudo acoustical correction (25–29):

$$\alpha_8 = -\frac{1}{E_m^2 \exp(2\alpha_m t)} \iiint_V \langle -\hat{\mathbf{u}} \cdot \nabla \tilde{p} \rangle \, dV \simeq \frac{M_b^3}{E_m^2 k_m^2} \frac{L}{R} \tag{3.5.32}$$

From equation (3.5.32) its can be seen that it is in the order of M_b^3 and thus can be ignored. The final term to be evaluated is the pseudo rotational correction (25–29):

$$\alpha_9 = -\frac{1}{E_m^2 \exp(2\alpha_m t)} \iiint_V \langle -\tilde{\mathbf{u}} \cdot \nabla \tilde{p} \rangle \, dV \tag{3.5.33}$$

Surface integral form(28; 29):

$$\alpha_9 = -\frac{1}{E_m^2 \exp(2\alpha_m t)} \iint_S \langle \mathbf{n} \cdot \tilde{\mathbf{u}} \tilde{p} \rangle \, dS \tag{3.5.34}$$

Form to be used in computational prediction (28; 29):

$$\alpha_9 = -\frac{1}{2E_m^2} \iint_{S_N} \left[u_m^{(r)} p_m^{(r)} + u_m^{(i)} p_m^{(i)} \right] \, dS \tag{3.5.35}$$

For a tubular grain (25–29):

$$\alpha_9 \simeq \frac{9\pi^2 M_b}{200 E_m^2} \frac{L}{R} \tag{3.5.36}$$

This term is of the same order as α_6 and must thus be retained. It also represents a destabilising agent. Particle dampening can be calculated as presented in Section 5.3.2.1.

3.5.4 Flandro and Fischbach Analysis Circa 2007

A set of linear growth rate constants has been suggested by Flandro, Majdalani, Fischbach and French (31; 47) and has been incorporated in to the SSP code. Only four terms were included, namely pressure coupling, nozzle dampening, displacement effect α_5 ("*rotational flow correction*" or "*boundary layer pumping*") and viscous dampening α_7. Flandro and Fischbach (20; 21) further stated that the boundary layer term is in fact a physical description of velocity coupling. A response function $B_b^{(r)}$ was introduced for the rotational flow correction also referred to as boundary layer pumping. The rotational flow correction is expressed as (20):

$$\alpha_{Rotational\ Flow\ Correction} = \iint_{S_{b||}} \bar{M}_b B_b^{(r)} \hat{p}_m^2 dS \tag{3.5.37}$$

For axial modes $B_b^{(r)} = 1$ (61). This is identical to the result for α_5. Flandro *et al.* (31) has shown that by incorporating all the rotational terms and performing a complete energy balance, flow turning, driving and dampening are counterbalanced and does not cancel the rotational flow correction any more. This is the key difference between the results previously discussed. It does not seem at present that consensus has been reached as is shown in the next section.

This system of growth functions results in motors that are linearly unstable. Flandro and Fischbach (20; 21) have reasserted the belief that CI is always present but that the amplitude grows so slowly that the amplitude rarely exceeds transducer noise levels.

3.5.5 Culick's Standard Analysis for Tubular Grains

The growth and loss terms that should be included in the analysis have been a subject of debate in recent times, little of which has been published. This debate has focused on the inclusion or exclusion of flow turning and boundary layer pumping. Culick (30) ignored surface pumping and flow turning terms for the special case tubular grain where these terms have been shown to cancel out. However, he noted that equity between the flow turning and surface pumping terms may not hold in certain cases. Culick illustrated this view by performing an analysis on the flow fields of a T-Burner.

The view that flow turning disappears when a full energy balance is applied does not seem to be shared by Culick. Part of this investigation is to evaluate the agreement of these two results with experimental data.

Thus Culick's analysis for a tubular grain is reduced to simply two terms if there is no particulate dampening. These terms are nozzle dampening and the combustion response. These terms are expressed as (30):

$$\alpha_{Nozzle} = \alpha_N = -\frac{\gamma - 1}{2}\frac{\bar{a}}{L}\bar{M}_N \tag{3.5.38}$$

$$\alpha_{pressure\ coupling} = \alpha_c = \frac{\bar{v}_b}{R}R_b^{(r)} \tag{3.5.39}$$

This set of terms, with the addition of particulate dampening, almost always results in a linearly stable system. Thus, additional mechanisms must then be responsible for triggering. This is discussed in subsequent sections, in particular the inclusion of velocity coupling.

3.6 Non-linear Stability

3.6.1 Flandro's Energy Balance Method

Having resolved the linear contribution or the first term on the right hand side for equation (3.3.3), it is possible to proceed to the second term or non-linear effects. The section that follows is an extension of (47–49) and is detailed more recently in (5; 31; 62). The last set of terms in equation (3.2.12), after temporal and spatial averaging is:

$$\iiint_V \left\langle \frac{\delta_{Re}^2}{(\gamma - 1)\,\mathrm{Pr}}\nabla^2 T + \delta_d^2(\nabla \cdot \mathbf{u})^2 \right\rangle dV \tag{3.6.1}$$

This is the entropy gain and energy loss associated with steep fronted waves. This term has traditionally been ignored because it is only of significance when there are very steep

gradients in particle velocity and temperature. If a very small section of the chamber volume encompassing the shock layer (that is formed by the steepening wave system as shown in Figure 3.3) is considered the following derivation can be made.

By treating the shock wave as an area of non-uniformity (as shown in Figure 3.3), equation (3.6.1) can be manipulated to yield the energy loss for a steep fronted wave:

$$\begin{aligned}\left(\frac{dE}{dt}\right)_{shock} &= -\frac{S_{port}}{\gamma\left(\gamma-1\right)}\frac{\left(s_2-s_1\right)*}{C_v} \\ &= \left(\frac{\varepsilon_{shock}}{\bar{p}}\right)^3 S_{port}\left(\frac{\gamma+1}{12\gamma^3}\right)\end{aligned} \tag{3.6.2}$$

This leads to the following approximation:

$$\alpha^{(2)} = -\frac{(\gamma+1)}{3E^2}\left(\frac{\sigma}{2\gamma}\right)^3 S_{port} \tag{3.6.3}$$

Where σ is dependent on the waveform that is assumed and S_{port} is the area of the shock front. For axial or longitudinal waves this is the cross-sectional area of the duct at a convenient location. This non-linear dampening mechanism is the primary loss mechanism and is vital in understanding the limit cycle. When the limit amplitude is reached the wave amplitude is steady. Therefore, from equation (3.2.12) the limit amplitude can easily be determined:

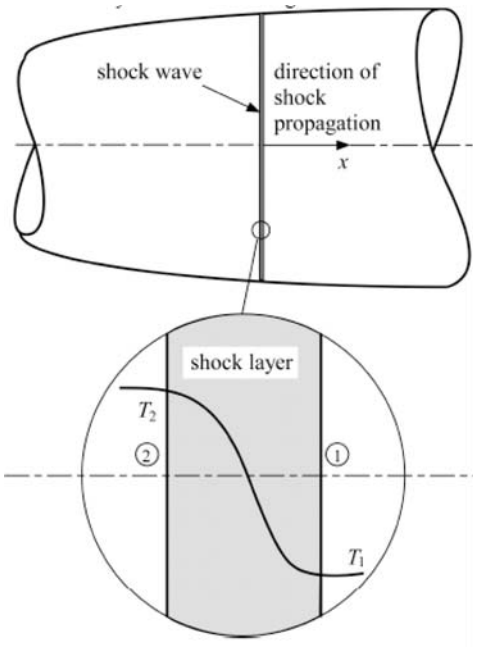

Figure 3.3: Shock Layer Structure [Flandro *el al* (31). Courtesy of J. Majdalani, with permission]

$$\varepsilon_{limit} = -\frac{\alpha^{(1)}}{\alpha^{(2)}} \tag{3.6.4}$$

This is only of use if the second order term is negative. Flandro (31) has noted that no driving mechanisms have been found that are second order and that all second order

interactions are negative. Good estimates of limit amplitude have been found as long as the linear stability estimate is valid.

The triggering amplitude is a controversial subject. True triggering is when the oscillations are at its lowest limit cycle and is then pulsed to a higher limit amplitude by adding sufficient energy above a critical point. However, this has not been observed. Motors that have shown "triggering" are actually linearly unstable motors. These motors are not linearly stable and are pulsed into higher limit amplitudes. The oscillations are always present, but grow extremely slowly and are observed as transducer noise and are barely noticeable at the end of the burn time. When the motor is disturbed with sufficient energy in a form of a pulse, the steep fronted wave can be formed. Flandro *et al.* (31) has stated that true triggering has not been observed.

3.6.1.1 DC Pressure Shift

As mentioned previously, the DC pressure shift or mean pressure shift is often observed. It is closely linked to the growth of the limit amplitude of the acoustic wave. It has been demonstrated (31) that the mechanism that drives oscillations is the same as that for the DC pressure shift.

In validating this approach, it is believed by Flandro, Fischbach and Majdalani (31), that the *ad hoc* terms such as velocity coupling, burning surface velocity rectification and "acoustic erosivity" can finally be discarded. From the continuity equation (3.2.2) the source of the DC pressure shift is readily obtained. By expanding and time averaging the equation, non-linear terms are also retained. The following is obtained(31):

$$\frac{d\bar{p}}{dt} = -\nabla \cdot (M_b \bar{\rho}) - \frac{\varepsilon^2}{\gamma} \nabla \langle p' \mathbf{u}' \rangle \tag{3.6.5}$$

Equation (3.6.5) represents the quasi-steady mass flux from the surface and the mass leaving through the nozzle. By integrating over the volume of the chamber the following is obtained:

$$\frac{d\bar{p}}{dt} = \left\{ \begin{array}{l} -\dfrac{1}{\bar{V}} \iint\limits_S \mathbf{n} \cdot \left(\rho \bar{M}_b \mathbf{U} \right) dS \\ \\ -\varepsilon^2 \left(\dfrac{1}{\gamma \bar{V}} \right) \iint\limits_S \mathbf{n} \cdot \langle p' \cdot \mathbf{u}' \rangle \, dS \end{array} \right\} \tag{3.6.6}$$

The first integral can be evaluated using classical internal ballistics. The second term is that which causes the DC pressure shift and is of the second order in wave amplitude. So the rate in mean pressure shift can now be expressed as:

$$\frac{d\bar{p}}{dt} = \frac{1}{\bar{V}} \left[\beta_{DC} r_b S_b - \bar{p} \left(\frac{2}{\gamma + 1} \right)^{\frac{(\gamma+1)}{2(\gamma-1)}} S_{throat} \right] - \frac{\varepsilon^2}{\gamma \bar{V}} \iint\limits_S \mathbf{n} \cdot \langle p' \cdot u' \rangle \, dS \tag{3.6.7}$$

Where:

$$\mathbf{n}\cdot\langle p'\mathbf{u}'\rangle = \begin{cases} -\dfrac{1}{\gamma}M_b A_b^{(r)}\left\langle (p')^2\right\rangle & (a)\,Waves\,Normal\,to\,Surface \\ \\ -\dfrac{M_b}{\gamma}\left(A_b^{(r)}+1\right)\left\langle (p')^2\right\rangle & (b)\,Waves\,Parallel\,to\,Surface \end{cases} \tag{3.6.8}$$

It is now possible to evaluate the response function. When the new mean pressure is reached, equation (3.6.7) is equal to 0. This means the pressure is no longer changing:

$$0 = \left[\beta_{DC}\frac{(p_0\bar{p})^{n-b}}{a_0}S_b - \bar{p}\left(\frac{2}{\gamma+1}\right)^{\frac{(\gamma+1)}{2(\gamma-1)}}S_{throat}\right] - \frac{\varepsilon^2}{\gamma}\iint\limits_S \mathbf{n}\cdot\langle p'\cdot\mathbf{u}'\rangle\, dS \tag{3.6.9}$$

By using the results from equation (3.6.8) and manipulating algebraically, the admittance can be calculated as follows:

$$\frac{p_{\lim}}{p_{std}} = \left[1+\frac{\varepsilon^2 C_2}{4\gamma^2}\left(A_b^{(r)}+C_1\right)\right]^{\left(\frac{1}{1-n_b}\right)} \tag{3.6.10}$$

where:

- n_b is the burning rate exponent;
- The pressure ratio is that of the measured mean pressure to the expected mean pressure if there is no instability;
- C_1 is 0 when waves are normal and 1 when they are parallel.

$$C_2 = \frac{1}{S_b}\iint\limits_S \psi^2(\mathbf{r})dS \tag{3.6.11}$$

C_2 accounts for the effective mode shape of a wave. For longitudinal waves it can be assumed to be approximately 0.5. It is now possible to solve for the admittance function.

It is important that the value for the admittance function (obtained from the mean pressure shift) is compared to the admittance function found from the linear stability analysis. This gives two possible paths to the same answer and allows for comparison from pulse testing a tubular SRM. Thus, three different methods can be employed to calculate the admittance function. That is from T-Burner data, from performing a mean pressure analysis, and from the non-linear analysis of the limiting amplitude on a tubular SRM.

3.6.1.2 Simulating and Predicting Motor Behavior

The next step is to simulate this behaviour. This is done by solving two coupled non-linear differential equations:

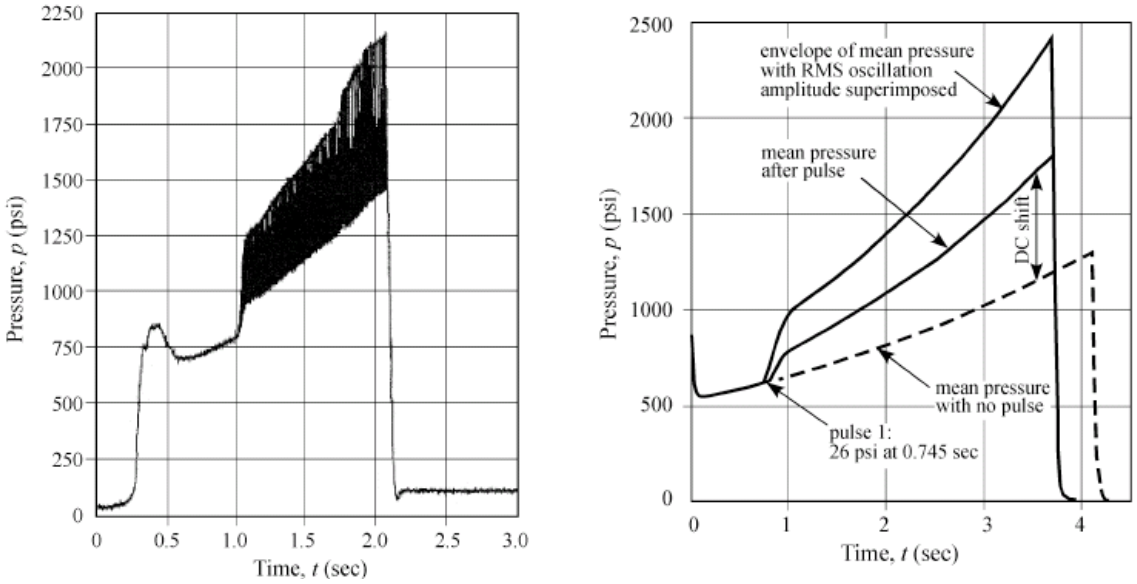

Figure 3.4: Using complete analysis result for a real motor [Flandro *el al* (31). Courtesy of J. Majdalani, with permission]

$$\begin{cases} \dfrac{d\varepsilon}{dt} = \alpha^{(1)}\varepsilon + \alpha^{(2)}\varepsilon^2 + \cdots \\ \\ \dfrac{d\bar{p}}{dt} = \beta_{DC}^{(1)} + \beta_{DC}^{(2)}\varepsilon^2 \end{cases} \tag{3.6.12}$$

These sets of equations are comparatively easy to solve numerically. However, as illustrated in the previous section the input data are not easily obtainable and the mode shapes (amongst others) need to be evaluated carefully. For any practically applicable algorithm all these parameters need to be solved. Many of these terms have not fully been evaluated for more complex geometries of SRMs. Figure 3.4 shows the preliminary results that compare well with experimental data.

There is large scope in this area to contribute to the evaluation of certain terms for complex geometries and the expected waveforms.

3.6.1.3 Modifications to the Energy Balance Method Circa 2007

Flandro and Fischbach (20) have modified the method described above. The shock wave assumption has been replaced with the non-linear gas-dynamics method. This may possibly be motivated by the fact that though this method returns good results, there are some problems, in particular with the superposition of a wave form, for more complex geometries that adequately represents reality. Thus, a seeming under prediction has been observed using the sawtooth approximation (51). The shock wave approximation may also have been abandoned due to the fact that the non-linear gas dynamics method (to be discussed next) gives superior results and that computational effort is no longer a deterring factor. This is discussed more thoroughly in a subsequent section where these methods are compared.

Essentially the shock wave method is replaced by the non-linear gas dynamics method. This results in three differential equations that need to be solved simultaneously; the mode amplitudes up to a specified number, typically 20, the phase shift for each mode, and the

mean pressure shift. The equations as shown in (20) do not provide enough information to reproduce the results. Thus Culick's (63; 64) non-linear gas dynamics method is used to calculate the mode amplitudes with phase shift ignored. Thus, only the equation for mean pressure shift is used in the analysis (20):

$$\frac{d\bar{P}}{dt} = \left\{ \begin{array}{l} \left(\dfrac{\bar{a}^2}{\gamma V}\right) \left(\bar{\rho} S_b \left(b \bar{P}^{n_b}\right) - \bar{P} \dfrac{\gamma}{\bar{a}} \left(\dfrac{2}{\gamma+1}\right)^{\frac{(\gamma+1)}{2(\gamma-1)}} S_N \right) \\ \\ -\dfrac{\bar{a}(\pi R L)}{2\gamma^2 V} \bar{P} \sum\limits_{m=1}^{\infty} r_m^2 \left\{ \bar{M}_b \left(A_b^{(r)} + B_b^{(r)} \right) C_2 \right\} \end{array} \right\} \tag{3.6.13}$$

3.6.2 Culick's Non-Linear Gas Dynamics Method

Culick (63; 64) proposed a solution scheme that consists of the following steps (65; 66):

1. Derive approximate conservation equations for two phase flow;
2. Decompose the flow field into a steady and unsteady field;
3. Derive non-linear wave equations for pressure fluctuations;
4. Represent the unsteady velocity and pressure spectral components as linear acoustic modes;
5. Apply method of least residuals (Galerkin's method[2]) to obtain non-linear governing equations for the amplitudes of the acoustic modes;
6. Apply time averaging to simplify equation;
7. Obtain approximate solution for non-linear amplitude equations.

The general form for the non-linear wave equation and boundary conditions (step 2 and 3) (63–66)(Papirizos and Culick's (65) nomenclature will be used):

$$\frac{\partial^2 p'}{\partial t^2} - a^2 \nabla^2 p' = h \tag{3.6.14}$$

$$\mathbf{n} \cdot \nabla p' = -f_c \tag{3.6.15}$$

The terms h and f_c are general non-linear functionals dependent on the acoustic and steady flow fields. These functionals contain all contributing mechanisms such as combustion, gas/particle, non-linear gas dynamics, and boundary conditions.

The spatial and frequency domains' characteristics have been shown, by both experimental and numerical results, to be approximated by linear acoustic analysis. This means that non-linear equations (3.6.14) and (3.6.15) represent a perturbation of linear oscillations within a rigid boundary. Also functions h and f_c are small compared to the corresponding linear terms. Equation (3.6.14) and its boundary condition equation (3.6.15) can be solved by using standard perturbation theory and expressed as an unperturbed acoustic field (63–66):

[2]Methods for converting continuous operator problems to a discrete problem.

$$p' = \bar{p}\sum_{n=1}^{\infty}\eta_n(t)\psi_n(\mathbf{r}) \tag{3.6.16}$$

$$u' = a\sum_{n=1}^{\infty}\frac{\dot{\eta}_n(t)}{\gamma k_n^2}\nabla\psi_n(\mathbf{r}) \tag{3.6.17}$$

$\psi_n(\mathbf{r})$ and k_n are solutions of the eigenvalue problem (63–66):

$$\nabla^2\psi_n + k_n\psi_n = 0 \tag{3.6.18}$$

Where:

$$\mathbf{n}\cdot\nabla\psi_n \tag{3.6.19}$$

The Galerkin method is now applied to equations (3.6.14) and (3.6.15) and p' and u' are solved for. The following second order non-linear equations of the acoustic modes, η_n are obtained (65; 66):

$$\ddot{\eta_n} + \omega_n^2\eta_n = F_n \quad for \quad n \geq 1 \tag{3.6.20}$$

Where:

$$F_n = \frac{1}{\bar{p}E_n^2}\left[\psi_n h dV - a^2\oiint \psi_n f_c dS\right] \tag{3.6.21}$$

$$E_n^2 = \int \psi_n^2 dV \tag{3.6.22}$$

$2\alpha_n\dot{\eta}$ and $2\theta_n\omega_n\eta_n$ represent the linear interactions and the non-linear gas dynamics is represented by the summation equation. For small fluctuations, $|\eta_n| \ll 1$, η_n can be represented as follows (63–66):

$$\eta_n(t) \approx r_n cos(\omega_n t - \phi(t)) = A_n(t)sin(\omega_n t) + B_n(t)cos(\omega_n t) \tag{3.6.23}$$

A_n, B_n, r_n and ϕ_n are functions varying slowly in time. Time averaging can thus be used to derive approximate equations for A_n(t) and B_n(t)(63–66):

$$\frac{dA_n}{dt} = \frac{1}{2\pi}\int_t^{t+(2\pi/\omega_n)} F_n cos(\omega t')dt' \tag{3.6.24}$$

$$\frac{dB_n}{dt} = -\frac{1}{2\pi}\int_t^{t+(2\pi/\omega_n)} F_n sin(\omega t')dt' \tag{3.6.25}$$

The scheme described here by equations (3.6.14)-(3.6.25) is applicable to any system experiencing combustion instability, as long as the non-linear functionals h and f_c are small compared to the linear wave equation. The limit cycle is a primary consequence of these perturbation terms. Thus for accurate prediction of the limit cycle, the functionals have to be modelled accurately.

3.6.2.1 Longitudinal Modes in a Tubular Grain Motor

The mode shape for the longitudinal mode:

$$\psi_n = cos(k_n x) \tag{3.6.26}$$

The natural frequency in radians:

$$\omega_n = \frac{a\pi n}{L} \tag{3.6.27}$$

Culick (63–66) has obtained second order non-linear equations for the mode amplitudes η_n by retaining h and f:

$$\ddot{\eta_n} + \omega_n^2 \eta_n = 2\alpha_n \dot{\eta} + 2\theta_n \omega_n \eta_n - \overbrace{\sum_{i=1}^{n-1}(C_{ni}^{(1)} \dot{\eta}_i \dot{\eta}_{n-i} + D_{ni}^{(1)} \eta_n \eta_{n-i}) - 2\sum_{i=1}^{\infty}(C_{ni}^{(2)} \dot{\eta}_i \dot{\eta}_{n+i} + D_{ni}^{(2)} \eta_n \eta_{n+i})}^{Non-Linear\ Gas\ Dynamics} \tag{3.6.28}$$

Where

$$\begin{aligned} C_{ni}^{(1)} &= -\frac{1}{2\gamma i(n-1)}\left[n^2 + i(n-i)(\gamma-1)\right] \\ C_{ni}^{(2)} &= \frac{1}{2\gamma i(n+i)}\left[n^2 - i(n+i)(\gamma-1)\right] \\ D_{ni}^{(1)} &= \frac{(\gamma-1)\omega_1^2}{4\gamma}\left[n^2 - 2i(n-i)\right] \\ D_{ni}^{(2)} &= \frac{(\gamma-1)\omega_1^2}{4\gamma}\left[n^2 + 2i(n+i)\right] \end{aligned} \tag{3.6.29}$$

In equation (3.6.28), the linear contributions are represented by the growth, α_i, and the frequency shifting, θ_i, and the non-linear gas dynamics by the two summation equations. Time averaging is now applied to equations (3.6.24), (3.6.25) and (3.6.28) which give (63–66):

$$\frac{dA_n}{dt} = \alpha_n A_n + \theta_n B_n + \frac{n\beta_c}{2}\sum_{i=1}^{n-1}(A_i A_{n-i} - B_i B_{n-i}) - n\beta_c \sum_{i=1}^{\infty}(A_{n+i}A_i - B_{n+i}B_i) \tag{3.6.30}$$

$$\frac{dB_n}{dt} = \alpha_n B_n - \theta_n A_n + \frac{n\beta_c}{2}\sum_{i=1}^{n-1}(A_i B_{n-i} + B_i A_{n-i}) + n\beta_c \sum_{i=1}^{\infty}(A_{n+i}B_i - B_{n+i}A_i) \tag{3.6.31}$$

β_c represents the only term arising from the non-linear gas dynamics:

$$\beta_c = \frac{(1+\gamma)\omega_1}{8\gamma} \tag{3.6.32}$$

Excellent agreement has been found for small to moderate fluctuations ($p'/\bar{p} < 0.10$) when comparing the averaged equations (3.6.30),(3.6.31) and the second order differential equation (3.6.28). This method can be expanded to larger fluctuations by adding a term for the D.C. pressure shift, D_n(65):

$$\eta_n = D_n + A_n sin(\omega_n t) + B_n cos(\omega_n t) \tag{3.6.33}$$

Paparizos and Culick (65) have presented truncated equations for dA_n/dt and dB_n/dt for longitudinal modes in a cylindrical motor:

$$\frac{dA_n}{dt} = \alpha_n A_n + \theta_n B_n + \overbrace{\frac{n\beta_c}{2}\sum_{i=1}^{n-1}(A_i A_{n-i} - B_i B_{n-i})}^{term1} - \overbrace{n\beta_c \sum_{i=1}^{m-n}(A_{n+i}A_i - B_{n+i}B_i)}^{term2} \quad (3.6.34)$$

$$\frac{dB_n}{dt} = \alpha_n B_n - \theta_n A_n + \overbrace{\frac{n\beta_c}{2}\sum_{i=1}^{n-1}(A_i B_{n-i} + B_i A_{n-i})}^{term3} + \overbrace{n\beta_c \sum_{i=1}^{m-n}(A_{n+i}B_i - B_{n+i}A_i)}^{term4} \quad (3.6.35)$$

This is based on the observations that for higher modes of the acoustic spectrum large dissipation of energy occurs. The limit amplitudes for higher modes can be considered negligible. Ananthkrishnan, Deoy and Culick *et al.* (19) stated that for first mode instability four modes must be retained in the analysis and eight for second mode instability.

3.6.3 Comparison of Non-linear Methods

These methods have rarely been compared. French, who is responsible for the combustion instability modules in the SPP and SSP codes, has presented two such papers (45; 51). French (51) has shown (Figure 3.5) that similar results are obtained for Flandro's Energy Balance method and Culick's Gas Dynamics method. Key findings include (51):

- The contrast between Flandro's method and Culick's is that the energy balance method assumes a sawtooth waveform;
- The energy balance method needs to be reformulated so that the mode shape amplitudes can vary with time. This will allow for more complex acoustic shapes to be evaluated;
- The gas dynamics allows for the overall motion to grow to its final form with respect to time;
- The energy balance method requires less computational time;
- The energy balance method provides a physical interpretation of non-linearity and the ability to evaluate the effects of instability on slowly varying physical properties;
- The gas dynamics method is more flexible as it handles unusual cases such as the second mode being unstable.

French (51) evaluated three different scenarios: a stable cylindrical motor with the stability parameters varied; an unstable cylindrical motor with the stability parameters varied; and motor with star aft section with the number of modes varied. The gas dynamics method uses the stable and unstable modes stability parameters and the energy balance method uses only the unstable mode stability parameter. It is necessary to evaluate this key difference. Findings for the first case were (51):

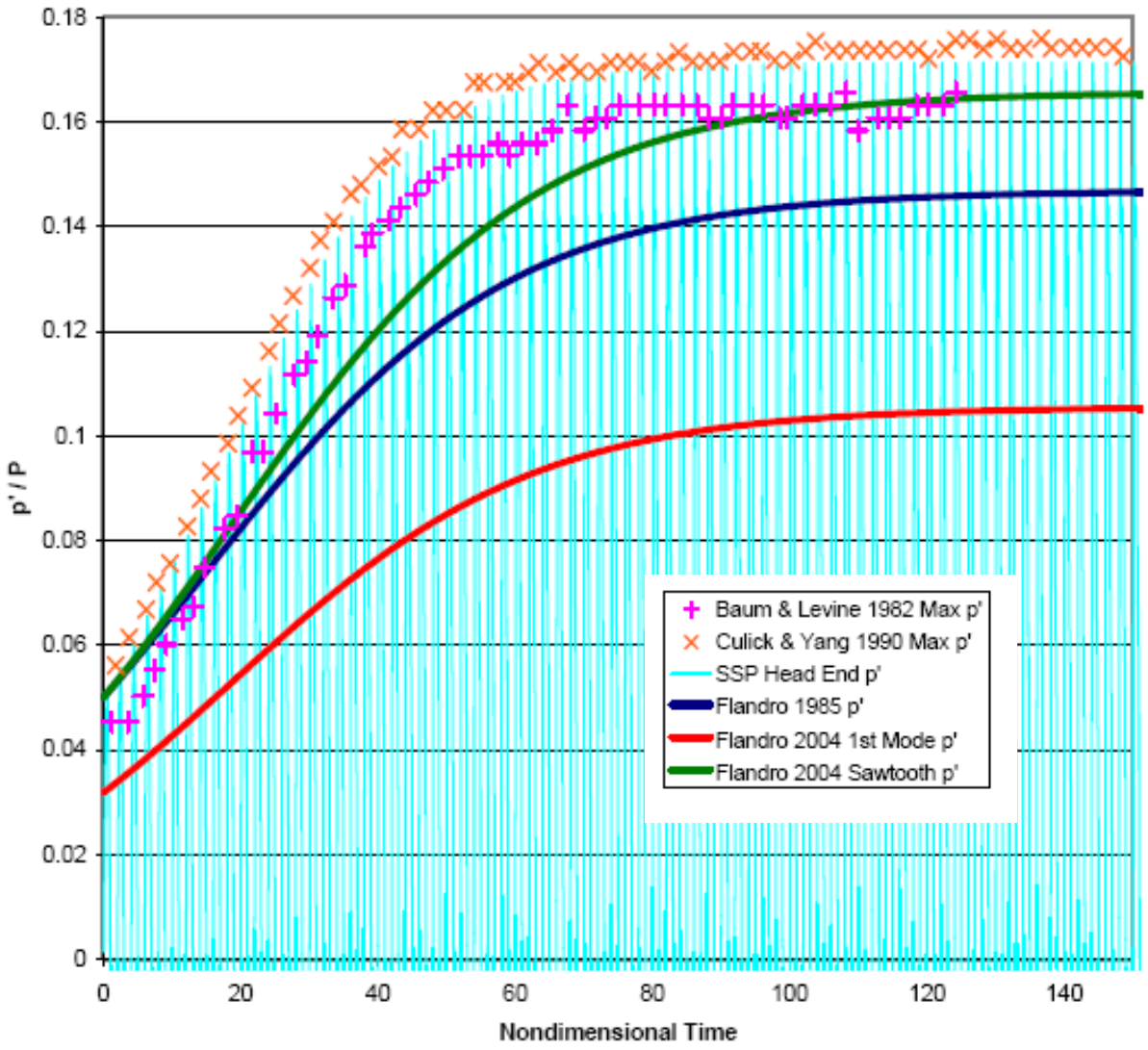

Figure 3.5: Comparison of Non-linear Methods [French (51). Used with permission from Software and Engineering Associates, Inc., Carson City, NV]

- There is a limit to using time averaging for the gas dynamics method. If the stable mode parameters are set too close to zero relative to the unstable mode, the system of equations become unstable;
- The more negative the stability parameters of the stable modes the sooner modes level out to a constant value;
- The limit cycle versus the stability parameter is linear until time averaging breaks down. This was predicted by the energy balance method.

For the second case:

- The amplitude of the unstable mode increases linearly with increasing unstable mode stability parameters;
- Trends confirm the energy balance method assumptions.

Third Case:

- Internal reflection can occur in axial varying SRMs;
- A travelling square wave was observed;
- It would be expected that the travelling shock wave would invalidate the energy balance method but a jump in pressure was observed indicating a gain in entropy;
- Increasing the number of modes in the gas dynamics method decreases the amplitude of spurious waves but increases their number.

This clearly shows that both methods are capable of giving good results. The level of complexity of Culick's method makes it difficult to apply. However, it is much more flexible in its application. It also requires more input information. Each stability parameter is in essence another frequency at which the propellant pressure coupled response must be found. This in itself represents a significant stumbling block for its practical application. However, as is shown above, more accurate results can be found and can be used to great effect as an analysis tool, since multiple modes can be evaluated. Flandro's method only requires one stability parameter simplifying the calculation. The DC pressure shift can also be incorporated. This makes it much more useful as a design tool, but limited as an analysis tool. The designer has much clearer indication of the physical interpretation of non-linear effects and how they vary with the slowly changing parameters using Flandro's energy balance method. However, the wave form assumptions must be re-evaluated to vary with time to increase accuracy.

3.7 Incorporating Non-Linear Combustion Terms

By using the gas dynamics method it is possible to include second order non-linear effects for combustion. This is of particular importance if triggering is to be investigated. Culick (30) argues that through trial and error "*numerical experimenting*" it has been shown that non-linear acoustics can not be responsible for the triggering of the stable limit cycle. This cannot be strictly proven as this implies another non-linear affect needs to be accounted for and this results in another degree of freedom. Combustion is the most likely candidate to produce such phenomena. Burnley, Culick and Swenson (17) and Burnley (67) have shown that non-linear combustion and gas dynamics together reveal triggering. Their methods are detailed here.

The higher order non-linear combustion contributions can be included in equation (3.6.28) for longitudinal modes (65):

$$\ddot{\eta}_n + \omega_n^2\eta_n = 2\alpha_n\dot{\eta} + 2\theta_n\omega_n\eta_n - \overbrace{\sum_{i=1}^{n-1}(C_{ni}^{(1)}\dot{\eta}_i\dot{\eta}_{n-i} + D_{ni}^{(1)}\eta_n\eta_{n-i}) - 2\sum_{i=1}^{\infty}(C_{ni}^{(2)}\dot{\eta}_i\dot{\eta}_{n+i} + D_{ni}^{(2)}\eta_n\eta_{n+i})}^{Non-Linear\ Gas\ Dynamics} + (F_n)_{other}^{NL} \tag{3.7.1}$$

Two alternatives can be considered. Firstly, that second order-pressure coupling (a non-linear response function) can be introduced as a function of the linear response function.

Burnley (67) has presented such a model but has shown that triggering is not shown for reasonable values of the two parameter solution. Thus, this model is ignored. The second possibility is the ever controversial velocity coupling.

3.7.1 Velocity Coupling

Velocity coupling has its origins in the observation that flow parallel to the burning surface increases the burning rate. Increased convective heat transfer is the most intuitive cause for the increased burn rate. This phenomenon has been observed in many practical applications and has led to many *ad hoc* and first principle models to model its effect. Hart, Bird and McClure (68) were the first to introduce this concept into the realm of acoustic instability (67). This effect introduces a kinematic non-linearity.

Most, if not all, early velocity coupling models have been abandoned. These initial models were intentionally simplistic (to be used in computer codes) and lacked any real theoretical basis. Baum and Levine in 1983 (69) introduced an *ad hoc* model that showed good agreement with experimental results.

This *ad hoc* model expresses the total mass flow of the grain as a function of linear pressure coupling and non-linear velocity coupling (17; 67; 69):

$$\dot{m} = \dot{m}_{pc}\left[1 + R_{vc}F(\mathbf{u})\right] \tag{3.7.2}$$

Here $\dot{m}^{pc}$ represents the mass flux due to pressure only. R_{vc} is the constant that reveals the sensitivity of the propellant burning to velocity parallel to the surface. F($\mathbf{u}$) is set equal to $|\mathbf{u}'|$ since the burn rate augmentation should depend on the magnitude and not the direction of the flow (17; 67; 69).

$$\dot{m} = \dot{m}_{pc}\left[1 + R_{vc}\left|\mathbf{u}'\right|\right] \tag{3.7.3}$$

It was further assumed by Burnley (67) and Burnley, Culick and Swenson (67) that the mean flow has no influence on the propellant surface and thus is only a function of the perturbed velocity. This was done to simplify the numerical calculations by avoiding complications due to variable mean flow. Steady erosive burning was also ignored. After much manipulation, Burnley (67) arrived at a forcing function for combustion in the form (17; 67):

$$(F_n)^{BL}_{comb} = \frac{\bar{v}_b}{E_n^2}\left\{C_1\int\frac{\partial}{\partial t}\left(\frac{p'}{\bar{p}}\left|\mathbf{u}'\right|\right)\psi_n dS + C_2\int\frac{\partial\left|\mathbf{u}'\right|}{\partial t}\psi_n dS - C_3\int\frac{p'}{\bar{p}}\frac{\partial}{\partial t}\left(\frac{p'}{\bar{p}}\right)\psi_n dS\right\} \tag{3.7.4}$$

Where:

$$\begin{aligned} C_1 &= R_b R_{vc} \\ C_2 &= \frac{R_{vc}}{\bar{\gamma}} \\ C_3 &= \frac{2}{\bar{\gamma}}(R_b - 1) \end{aligned} \tag{3.7.5}$$

Due to discontinuities this method cannot be handled in the traditional time averaging fashion. A sgn[3] function is introduced. Handling of this discontinuity is fully explained in (67) and will not be covered here. For longitudinal modes Burnley (17; 67) presents:

[3]The sgn function is an odd mathematical function that extracts the sign of a real number.

$$(F_n)^{BL}_{comb} = \frac{2(L/D)}{\bar{\gamma}\pi^2}\frac{\bar{v}_b}{a}\left\{ \begin{array}{l} -2R_b\bar{R}_{vc}\sum_{i=1}^{\infty}\sum_{j=1}^{\infty}\left[\frac{\dot{\eta}_i\dot{\eta}_j}{i} - i\omega_1^2\eta_i\eta_j\right]I^{(A)}_{nij} \\ +\frac{4\omega_1^2\bar{R}_{vc}}{\bar{\gamma}}\sum_{i=1}^{\infty} i\eta_i I^{(B)}_{ni} - 4\omega_1(R_b-1)\sum_{i=1}^{\infty}\sum_{j=1}^{\infty}\eta_i\dot{\eta}_j I^{(C)}_{nij} \end{array} \right\} \quad (3.7.6)$$

$$\begin{array}{l} I^{(A)}_{nij} = \int_0^{\pi} cosn\tilde{x}[sin(i-j)\tilde{x} + sin(i+j)\tilde{x}]sgn(u')d\tilde{x} \\ I^{(B)}_{ni} = \int_0^{\pi} cosn\tilde{x}sini\tilde{x}sgn(u')d\tilde{x} \\ I^{(C)}_{nij} = \int_0^{\pi} cosn\tilde{x}[cos(i-j)\tilde{x} + cos(i+j)\tilde{x}]d\tilde{x} \end{array} \quad (3.7.7)$$

Burnley went on to include a threshold velocity. This was based on the observations of Ma, van Moorhem and Shorthill (70). Their investigation on dry ice showed that there is a threshold acoustic velocity above which the mass flux increases linearly with the Reynolds number. They found that the mass flux below this point is essentially constant. It was found that this increase was due to the increased heat transfer as the system became turbulent. This implies that the SRM will only become unstable if a pulse is of a large enough magnitude so that turbulent flow is induced at the burning surface. No such assertions were made by Burnley or Culick but in part it explains the distaste certain researchers have for the velocity coupling models and its *ad hoc* nature. The true physical implications of the assumptions were not fully investigated but rather the theoretical results of the assumptions. For a more complete discussion on threshold velocity and the functions derived, the reader is referred to Burnley *et al.* (17), Burnley (67) and Ananthkrishnan *(*et al.) (19; 71). This does not form part of this investigation and is not be discussed further.

Dynamic systems theory[4] through the use of the continuation method[5] is applied. This was first presented by Jahnke and Culick (16) as a method to investigate non-linear instability. The results are not discussed in detail here. The system of second order differential equations is reduced to first order and the first modes growth constant is typically used. Though second mode stability can also be evaluated in this way. This results in bifurcation[6] diagrams, which can indicate a zone of triggering, in particular Hopf Bifurcation plots are encountered[7]. For a more complete discussion on these results the reader is referred to Jahnke and Culick (16) Burnley *et al.* (17), Burnley (67) and Ananthkrishnan, Deoy and Culick (19; 71).

3.8 Computational Fluid Dynamics Methods

The focus up to this point has been to obtain analytical solutions. This approach is applicable for relatively simple geometries such as cylindrical grains. This becomes very difficult for more complicated geometries, which requires a different approach. Computational flow dynamics (CFD) allows for the solution of flow fields in complex geometries and is applicable

[4]Dynamical systems theory is an area of applied mathematics used to describe the behaviour of complex dynamical systems, usually by employing differential equations or difference equations

[5]Numerical Continuation is a method of computing approximate solutions of a system of parameterized non-linear equations

[6]Bifurcation occurs when a small smooth change made to the parameter values (the bifurcation parameters) of a system causes a sudden 'qualitative' or topological change in its behaviour

[7]Bifurcation in which a fixed point of a dynamical system loses stability as a pair of complex conjugate eigenvalues of the linearization around the fixed point cross the imaginary axis of the complex plane

to a wider range of conditions since fewer assumptions are made in the formulation. The finite element analysis (FEA) is used to calculate the acoustic mode shapes by calculating the Eigen functions. With the ever increasing computational capacity this method has become more feasible.

CFD has been applied with success to the problem of combustion instability. Notably Baum and Levine (69; 72–75) have applied these methods with success. The Ariane 5 experienced vortex driven combustion instability, which led to a large amount of work being done on the prediction of CI and the development of an in house CFD code MOPTI (76–81). One of the major findings of the Ariane 5 work was that a vortex in a stream do not require sharp edges or obstructions to form. This has been called "*Parietal vortex shedding*" due to it forming close to the walls (30). This phenomenon is associated with large boosters and will not be investigated further here.

French has worked on such modules for SSP/SPP codes (45; 82–86) and his method is be outlined here.

This method comprises of five steps(84):

1. Create a grid of the geometry at a given time step;
2. Determine acoustic modes (FEA) from the grid;
3. Determine steady flow fields (CFD);
4. Determine unsteady flow fields from steady flow fields;
5. Evaluate the stability integrals using the acoustic mode shapes, as well as steady and unsteady flow fields.

Steps 1 and 2 do not fall within the scope of this dissertation and are not be discussed. French and co-authors have written several articles (83; 84; 86–89) on these two steps and the reader is referred to them for further reading. Step 3-5 is the next phase of development and represents the ability to do stability assessments for more complex rocket motors. This is also one of the main focus areas in current combustion instability research in particular the inclusion of gas dynamic effects such as vortex shedding. Though this analysis is not be part of this thesis it is included as part of general combustion instability theory. The basic framework for a CFD study is outlined by French and Dang (84) and is given here.

By assuming that the Euler equations describe the fluid motion in a motor chamber and by performing a perturbation analysis for a harmonic motion, the system of equations reduces to the acoustic Helmholtz equation. This is expressed in terms of pressure and is driven by the dynamic properties of the combustion process (similar to Culick's gas-dynamic approach)(84):

$$\nabla^2 p' + k_c^2 p' = h \tag{3.8.1}$$

$$\frac{\partial p'}{\partial \mathbf{n}} = -f_c \tag{3.8.2}$$

The form of h and f_c varies according to the non-dimensional parameters and the choice of combustion processes. The terms included also vary from analysis to analysis; i.e. in a segmented rocket motor vortex shedding may be important but it may not have a significant role in tactical motors and can thus be ignored. The partial differential equation can be solved using an eigenfunction expansion of the pure acoustic waves. The pure modes or eigenfunction satisfy the Helmholtz partial differential equation(84):

$$\nabla^2\Phi_m + k_m^2\Phi_m = 0 \tag{3.8.3}$$

$$\frac{\partial\Phi}{\partial\mathbf{n}} = 0 \tag{3.8.4}$$

p' can be expanded in terms of m pure modes. Tensor notation for index i is be used. Note that it is not summed for m. These modes can be for any axial, tangential or radial mode(84):

$$p' = c_i\Phi_i \tag{3.8.5}$$

Equation (3.8.1) is multiplied by Φ_m and equation (3.8.3) by p' and subtracted from each other. After much manipulation and taking advantage of the fact that mode shapes are orthogonal and a non-trivial volume integral only occurs when $i = m$, the following is obtained:

$$(k_c^2 - k_m^2)c_m \iiint \Phi_m^2 dV = \iiint h\Phi_m dV + \oiint f_c\Phi_m dS \tag{3.8.6}$$

The perturbed frequencies are assumed near the pure mode's frequency, but shifted in phase and amplitude. M_b is chosen as the perturbed parameter (55; 84):

$$k_c = k_m + M_b(\omega_m - \alpha_m) + O(M_b^2) \tag{3.8.7}$$

Squaring equation (3.8.7) ,substituting into equation (3.8.6) and taking cognisance of $E_m^2 = \iiint \Phi_m^2 dV$, the following is obtained (84):

$$\omega_m - i\alpha_m = \frac{\iiint h\Phi_m dV + \oiint f_c\Phi_m dS}{2k_m M_b E_m^2} \tag{3.8.8}$$

For linear stability analysis:

$$\alpha_m = -\Im\left[\frac{\iiint h\Phi_m dV + \oiint f_c\Phi_m dS}{2k_m M_b E_m^2}\right] \tag{3.8.9}$$

The third step is to calculate the steady flow fields using a CFD code. This approach varies from package to package. The output from the CFD software package must include: gas pressure, temperature, density, and velocity vectors. This output can be used to calculate h and f_c in equations (3.8.1) and (3.8.2). It is important to remember that even with advances in computational power, it is still not feasible to produce a continuous simulation. Instead, "snap shots" of critical periods can be done to evaluate the motors stability.

The fourth step is to calculate the unsteady rotational velocity computations. There are two approaches. Firstly, compute the unsteady flow and subtract the desired mode shape. The second is to compute the rotational flow field directly by using the acoustic mode shape as a boundary condition. The second approach is outlined here. Flandro (55) has shown that for a non-slip boundary condition to be maintained the unsteady rotational velocity must cancel the irrotational field at the boundary. The unsteady flow rotational velocity are equated as (55):

$$\nabla\cdot\tilde{u} = 0 \tag{3.8.10}$$

$$ik\tilde{u} = M_b\left[\nabla(\tilde{u}\cdot U - \tilde{u}\times\Omega - U\times\omega'\right] + \delta_{Re}\nabla\times\omega' \tag{3.8.11}$$

Equation (3.8.11) after some manipulation can be expressed as two differential equations (84):

$$\frac{\partial \tilde{u}}{\partial t} + [\tilde{u} \cdot \nabla \bar{u} + \bar{u} \cdot \nabla \tilde{u}] = \delta_{Re}^2 \nabla^2 \tilde{u} \tag{3.8.12}$$

$$\frac{\partial \tilde{u}_0}{\partial t} + \tilde{u} \cdot \nabla \bar{u} = \delta^2 \nabla^2 \tilde{u} \tag{3.8.13}$$

These equations can be discretised using the finite volume method. To ensure that the no-slip condition is met, the rotational velocity vector and the acoustic velocity vector are assumed equal and opposite ($\tilde{u} = -\hat{u}$). This method requires that each mode be evaluated separately.

The steady flow analysis, unsteady rotational velocity, and mode shape calculations form part of the terms h and f_c. This allows for the stability integrals to be solved using equation (3.8.8).

3.9 Conclusions

Combustion instability theory is an ever evolving field. There are several schools of thought that have resulted in several different interpretations of the experimental results. It is also significant to note that Russian CI theory is becoming available for the first time. In the future this work may reveal perspectives which can facilitate a more complete understanding.

This study uses both the linear and non-linear theory presented here. The linear theory is the area with the most contention as there is still a significant difference in opinion as to which linear terms should be included. This study uses all three sets of linear stability growth constants and evaluates the difference in the results.

The non-linear methods seem to be less contentious as the gas dynamics method seems to be the method of choice. The shock wave method, however, should not be discounted as it captures all significant trends and can be an invaluable tool for a motor designer when there is limited response function data available.

This study uses these methods as analysis tools to quickly and cheaply obtain response functions for propellants.

The CFD methods are becoming more attractive with increased computational power but is not pursued here.

Chapter 4

Response Function from Pulse Testing

4.1 Stratagy

The T-Burner, as mentioned in Appendix B, has several disadvantages such as large test matrices, high maintenance and subjective data analysis. However, overall it is by far the most useful and successful laboratory scale device for obtaining the admittance/response function of a propellant. The main disadvantage is the amount of test runs and the corresponding man hours required to operate it. This can, however, be kept to a minimum by carefully choosing the test matrix based on the SRM harmonics and operating pressures. This study develops a methodology to derive a response function from pulse testing circular grain motors. Ideally, it would have been advantageous if the data obtained from such an analysis could have been corroborated by T-Burner results for the same results. The response function obtained varies depending on the set of linear growth terms used. The addition of T-burner data would have allowed for the validity of the linear set of equations to be evaluated.

The goal of this research should be kept in mind. The goal is to establish an economically feasible strategy that will aid in avoiding instability problems. This research should also help increase the understanding of combustion instability and SRM dynamics as a whole and thus improve the quality of the product. Figure 4.1 illustrates how this can be achieved in a cost effective manner. Putting this infrastructure into place will greatly increase the local capacity to effectively deal with combustion instability. Firstly, by having the tools to predict stability for a specific SRM with a particular propellant; and secondly, if a motor is found not to be stable during the development stages, to quickly and cost effectively address the problem.

In addition to the T-Burner, use of pulse testing can greatly reduce the total number of tests required for a normal T-Burner analysis. It is shown that combustion instability theory can adequately predict the loss mechanisms of radially burning SRMs. Thus, the admittance/response function can be obtained as well as an indication of the relative amplitudes of the different modes. This will give an indication of what can be expected in operational SRMs with the same propellant.

The following section will illustrate that due to progress in linear theory (Chapter 3) combined with an increase in computational power, it is now possible to calculate the admittance/response function from pulsed tubular grain motor tests.

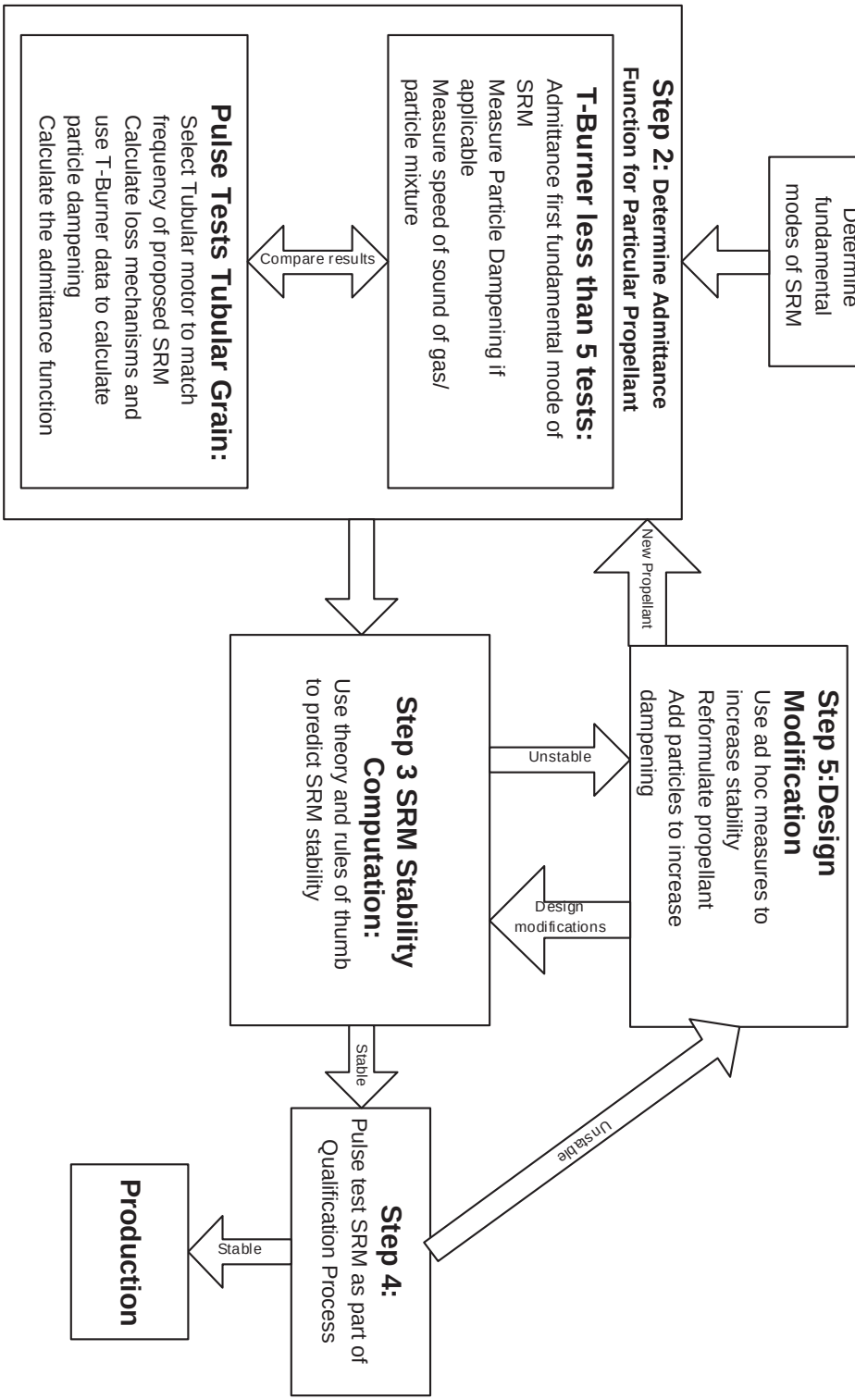

Figure 4.1: Proposed Combustion Instability Strategy

4.2 Admittance and Response Function from Pulse Tests

In the open literature, no one has attempted to obtain admittance/response function from a pulse test of a subscale tubular motor. The main purpose of this research is to establish an economically feasible test strategy. This data is used to predict the stability of a motor. The pulse test hardware and test procedures are used with the qualification process of full scale SRMs to show that a motor is stable to all possible pulses that can be reasonably expected during SRM operation. The hypothesis is that it is possible to pulse test a tubular grain SRM containing a specific propellant with a similar modal content. Also, that all predominant loss mechanisms can be calculated for a tubular grain which is the best understood. Thus, the energy gained due to interaction with the propellant surface can be found. This is essentially the same concept used for T-Burner analysis. However, the flow fields have become considerably more complicated. There is also flow parallel to the burning surface. The following assumptions are made:

- Flow fields in a tubular grain are well understood and characterised;
- The growth and loss mechanisms in a tubular grain can be calculated;
- The modal content of the motor are multiples of the fundamental mode, i.e. the acoustic wave can be decomposed into individual modes;

The second assumption that the tubular grain flow fields can be determined analytically allow for analytical results to be obtained for the linear stability integrals, as shown in Chapter 4. The second assumption is based on the large volume published on the subject since 2000, as shown in Chapter 4. By systematically evaluating the different sets of linear terms and comparing the results to that for similar propellants, an indication is obtained of the validity of these sets. The third assumption implies that the acoustic signal obtained from tests can be decomposed and the mode α value can be solved for using the non-linear theory presented in Chapter 4.

Possible advantages of this method:

- One test obtains a pressure coupled response value for many frequencies;
- The relative amplitudes of the different modes can be found in respect to the fundamental mode, i.e. mode coupling is included;
- The admittance/response function is averaged over a larger area;
- Combustor dynamics are more closely simulated;
- The tests are performed in the best characterized geometry;
- A reduction in the amount of tests as well as man hours required to perform tests;

Possible disadvantages:

- Difficulty in obtaining all loss mechanisms;

- Requires more information on combustor dynamics, such as nozzle losses, flow fields, etc;
- Vortex shedding occurs only in certain cases and may not be accounted for. It can add energy which may be wrongly attributed to the pressure coupled response;
- May lead to empirical data fitting to parameters such as acoustic velocity and pressure;
- No data to measure it against, i.e. T-Burner data;
- All errors will be contained in the admittance/response function.

It is this author's belief that the current status and understanding of combustion instability has progressed enough to avoid the disadvantages. It, however, requires great care and considerable work. These obstacles are not be insurmountable. Through systematic analysis of different linear growth terms this study also serves to establish confidence in the calculation of the linear and non-linear stability of an SRM. This is discussed in Chapter 5.

Thus, for a new rocket motor the method consists of the following:

- Determine the proposed motors first fundamental frequency and mean operating pressure;
- Alter the length of the tubular motor to match the first fundamental mode of the motor and choose a nozzle that will generate the same mean pressure;
- Determine the energy losses from theory;
- Pulse test the motor;
- Analyse the data;
- Calculate an admittance/response function;
- Use the obtained admittance/response function to predict the stability of the proposed motor.

By using this technique the number of tests required to determine a usable admittance/response function is reduced. This gives a more accurate reflection of what is to be expected in the SRM. By using this method the stability of an SRM for a particular propellant can be calculated quickly, cheaply and thus the quality of the SRM can be improved.

Pulse testing can be divided into two tests: cold flow tests and live motor tests. Cold flow tests are used to characterize the pulsers themselves and to ensure that the pulsers function properly before proceeding to live motor tests. Live motor tests are used to obtain the response of a propellant to an acoustic disturbance.

4.3 Calculating the Admittance and Response Function

The response and admittance function are both used in linear analysis as shown in Chapter 3. The following equation is used to relate the response and admittance functions for a tubular grain motor:

$$\frac{v_b}{R} R_b^{(r)} = \frac{a_0}{R} \frac{\pi}{2} \frac{M_b}{E_m^2} \frac{L}{R} (A_b^{(r)} + 1) \tag{4.3.1}$$

4.3.1 Composite Wave Assumption and Superposition

Culick(2; 50; 90) and Flandro (5; 31; 47–49) have shown that analysis is greatly simplified by realizing that the waves are composites of the chamber normal modes. The composite steep fronted wave can be described as: (5; 31; 47–49):

$$p'(\mathbf{r},t) = \epsilon(t)\sum_{n=1}^{\infty} Ar_n(t)\psi_n(\mathbf{r}) \tag{4.3.2}$$

For a port with constant cross section:

$$\begin{cases} Ar_n(t) = \left(\dfrac{8n}{4n^2+1}\right) sin\left(\dfrac{n\pi a_0}{L}\right) \\ \psi_n(r) = cos\left(\dfrac{n\pi z}{L}\right) \end{cases} \tag{4.3.3}$$

This approach has been shown to conform to all experimental features of non-linear combustion instability and greatly reduces computational effort (5; 31; 47–49). Thus, it is also possible to us a FFT(Fast Fourier Transform) algorithm to decompose the wave in to the individual modes.

4.3.2 Flandro's Energy Balance Method

From Equation 3.6.12 it is possible to obtain an admittance/response function from the acoustic wave amplitude and the mean pressure shift. Assuming that shock wave losses are the only non-linear mechanism, the change in acoustic wave amplitude for longitudinal modes becomes for a tubular grains (45; 48; 49):

$$\frac{d\epsilon}{dt} = \epsilon\alpha_m - \epsilon^2\left(\frac{\gamma+1}{6\gamma}\right)\frac{\bar{a}}{L} \tag{4.3.4}$$

When the limit amplitude is reached $d\epsilon/dt = 0$. Thus equation 4.3.4 can be rearranged to give:

$$\alpha_m = \epsilon_{limit}\left(\frac{\gamma+1}{6\gamma}\right)\frac{\bar{a}}{L} \tag{4.3.5}$$

The admittance/response function is contained within α_1. Rearranging equation 3.5.1:

$$\alpha_1 = \alpha_m - \sum_{i=2}^{N}\alpha_i \tag{4.3.6}$$

Internal ballistic data is used to calculate the α values. The admittance/response function is then calculated for each mode individually. An admittance/response function can also be obtained from the mean pressure shift. When the new mean pressure is reached $dp/dt = 0$. This means that the pressure is no longer changing (31):

$$0 = \left[\beta_{DC}\frac{(p_0\bar{p})^{n-b}}{a_0}S_b - \bar{p}\left(\frac{2}{\gamma+1}\right)^{\frac{(\gamma+1)}{2(\gamma-1)}}S_{throat}\right] - \frac{\varepsilon^2}{\gamma}\iint_S \mathbf{n}\cdot\langle p'\cdot\mathbf{u}'\rangle\, dS \tag{4.3.7}$$

Using the results from equation (3.6.8) and after some algebraic manipulation, the admittance/response can be calculated as follows (31):

$$\frac{p_{\lim}}{p_{std}} = \left[1 + \frac{\varepsilon^2 C_2}{4\gamma^2}\left(A_b^{(r)} + C_1\right)\right]\left(\frac{1}{1-n_b}\right) \tag{4.3.8}$$

- n_b is the burning rate exponent;
- The pressure ratio is that of the measured mean pressure to the expected mean pressure if there are no instability;
- C_1 is 0 when waves are normal and 1 when they are parallel.

$$C_2 = \frac{1}{S_b}\iint_S \psi^2(\mathbf{r})dS \tag{4.3.9}$$

C_2 accounts for the effective mode shape of a wave. For longitudinal waves it can be assumed to be approximately 0.5 (31). It is now possible to solve for the admittance/response function. This method is limited to the first mode only. Flandro accounts for the losses due to non-linear gas dynamics as a single shock front. This greatly simplifies the prediction of stability; however, it has limitations as an analysis tool.

4.3.3 Culick's method

Culick's method allows for more than one mode to be evaluated. One of the major obstacles for this method has been computational expense. The number of calculations required increases exponentially as the number of modes are increased. In the mid 80s to early 90s a large amount of work was done following on from Culick's analytical work (63; 64) and Levine's numerical work (91; 92). Many analyses only considered the first two modes to reduce computational effort. This is no longer an obstacle.

The result shown in Figure 4.2 is calculated from the values for α and θ as presented by Culick (50). Identical results are obtained by French (45) for the same data set. Figures 4.2:(a-c) show the results when the published θ values are used, Figures 4.2:(d-f) show the results if θ for all modes are set equal to zero. Identical results are obtained by French (45; 51). French (93) stated: "*we are fixing the linear phase shifts to zero, until we find a compelling reason not to do so*".By inspecting equations 3.6.35 and 3.6.32 it is noted that the frequency shift essentially transfers energy from A_n to B_n and vice versa. Figure 4.2: (a-c) shows that A_n and B_n are 180° out of phase. Using random θ values do not alter the limit amplitude, it only alters the period of oscillation of A_n and B_n and thus the time it takes to reach the limit amplitude.

By recognizing that when A_n is at its maximum, B_n is equal to zero and also that when dA_n/dt is equal to zero, dB_n/dt is at a maximum, the converse is also true. When θ_n is set to zero, either A_n or B_n is at a maximum, and correspondingly the matching amplitude is set to zero. Essentially it is assumed that all modes are in phase with either A_n and B_n at a maximum or a minimum. It can be shown that for odd modes, n= 1,3,5,...:

$$\begin{aligned} B_n &= r_n sin(\frac{\pi}{2}n) \\ A_n &= 0 \end{aligned} \tag{4.3.10}$$

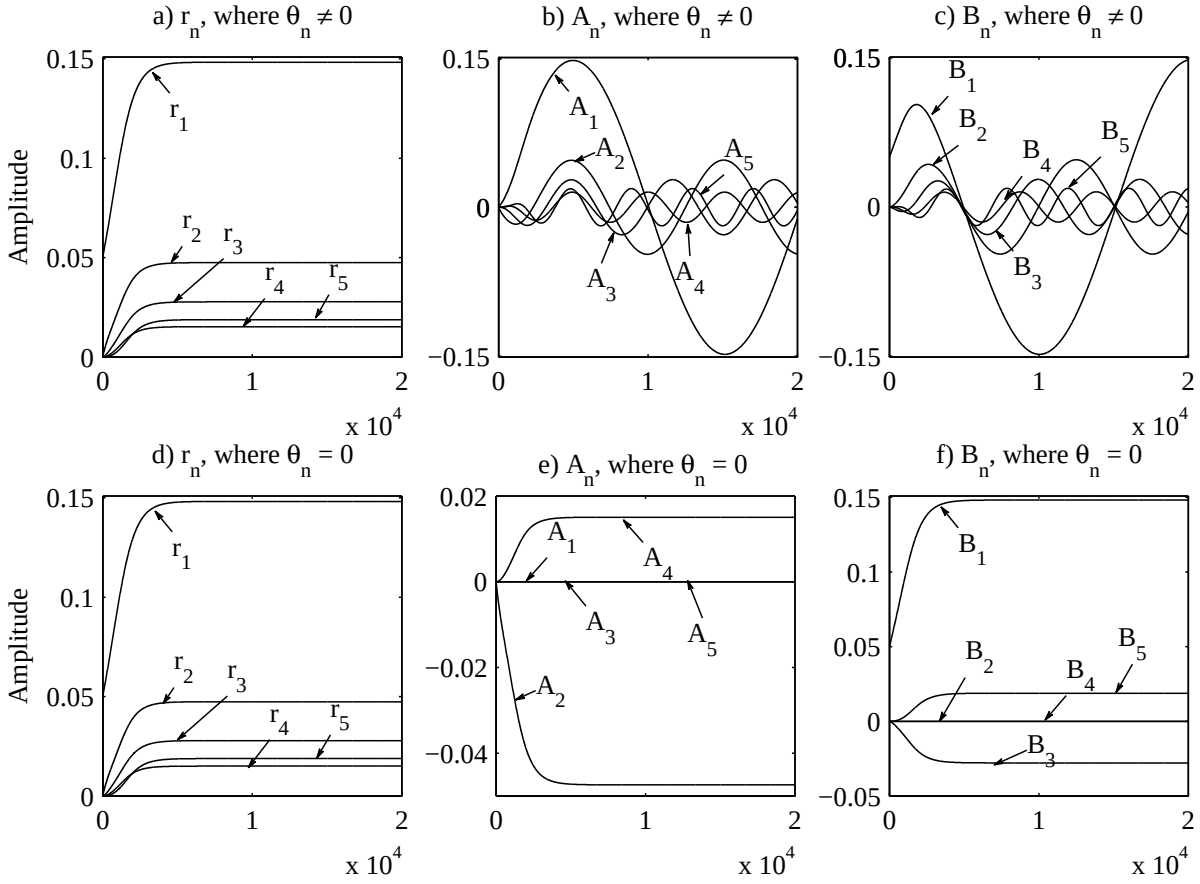

Figure 4.2: Amplitude [p'/P] vs. Time Steps[0.00001s], produced from Culick's Tubular Grain Data

For even modes, n= 2,4,6,. . . :

$$\begin{aligned} A_n &= r_n cos(\frac{\pi}{2}n) \\ B_n &= 0 \end{aligned} \tag{4.3.11}$$

Furthermore, it is now possible to obtain α_n for each mode using equations 3.6.34 and 3.6.35. For odd modes, n= 1,3,5,...:

$$\alpha_n = -\left[-\theta_n A_n + \overbrace{\frac{n\beta_c}{2}\sum_{i=1}^{n-1}(A_i B_{n-i} + B_i A_{n-i})}^{term3} + \overbrace{n\beta_c \sum_{i=1}^{m-n}(A_{n+i}B_i - B_{n+i}A_i)}^{term4} \right] / B_n \tag{4.3.12}$$

For even modes, n= 2,4,6,. . . :

$$\alpha_n = -\left[\theta_n B_n + \overbrace{\frac{n\beta_c}{2}\sum_{i=1}^{n-1}(A_i A_{n-i} - B_i B_{n-i})}^{term1} - \overbrace{n\beta_c \sum_{i=1}^{m-n}(A_{n+i}A_i - B_{n+i}B_i)}^{term2} \right] / A_n \tag{4.3.13}$$

The mode amplitudes, r_n, published by French (45) are used. Exactly the same α values are obtained (cf. Table 4.1).

Table 4.1: Mode Stability α $[s^{-1}]$

Mode	1	2	3	4	5
Published(45; 50)	81.4	-316	-561	-874	-1256
Calculated	81.4	-316	-561	-874	-1255

When using this method it is important to remember that equations 3.6.34 and 3.6.35 are truncated. The last several modes' α values will be erroneous since their value is more strongly linked to the subsequent modes. When only 5 modes are used only α_1 and α_2 are correct. As more modes are added the values of α_3 and α_4 change until their values are no longer affected by higher modes. By inspecting term2 and term4 of equations 3.6.34 and 3.6.35 it can be seen that these terms are only interconnected to higher modes. An iterative process is used to evaluate for a specific mode if enough modes are taken into account to return a valid α.

4.4 Velocity Coupling

The velocity coupling model presented by Burnley *et al.* (17) and Burnley (67) needs to be modified to fit into the frame work described in the previous section. Applying time averaging to each mode individually in equation (3.7.6) and truncating in a similar fashion as Paparizos and Culick (65) produces the following result for dA_n/dt:

$$(F_n)^{BL}_{comb} = \frac{2(L/D)}{\bar{\gamma}\pi^2}\frac{\bar{v}_b}{a}\left\{\begin{array}{l} -2R_b\bar{R}_{vc}\sum_{i=1}^{m-n}\sum_{j=1}^{m-n}\left[\frac{A_iA_j}{4i}-\frac{iB_iB_j}{4ij}\right]I^{(A)}_{nij} \\ +\frac{4\omega_1\bar{R}_{vc}}{\bar{\gamma}}\sum_{i=1}^{m-n}\frac{B_i}{2}I^{(B)}_{ni}-4(R_b-1)\sum_{i=1}^{m-n}\sum_{j=1}^{m-n}\frac{A_iB_j}{4j}I^{(C)}_{nij}\end{array}\right\} \quad (4.4.1)$$

For dB_n/dt:

$$(F_n)^{BL}_{comb} = \frac{2(L/D)}{\bar{\gamma}\pi^2}\frac{\bar{v}_b}{a}\left\{\begin{array}{l} -2R_b\bar{R}_{vc}\sum_{i=1}^{m-n}\sum_{j=1}^{m-n}\left[\frac{B_iB_j}{4i}-\frac{iB_iB_j}{4ij}\right]I^{(A)}_{nij} \\ -\frac{4\omega_1\bar{R}_{vc}}{\bar{\gamma}}\sum_{i=1}^{m-n}\frac{A_i}{2}I^{(B)}_{ni}-4(R_b-1)\sum_{i=1}^{m-n}\sum_{j=1}^{m-n}\frac{B_iA_j}{4j}I^{(C)}_{nij}\end{array}\right\} \quad (4.4.2)$$

To solve equation (3.7.7) it is assumed that the crossover as indicated by $sgn(\mathbf{u}')$ from negative to positive is $\pi/2$ as was shown for the first mode by Burnley (67). It is assumed that this is also valid for the second mode. This analysis is restricted to only the first two modes. It is assumed that for higher modes that the velocity coupling is negligible and thus is set to zero. The higher modes are handled as in the previous section.

The above analysis may not yield the same results as those published for the same velocity coupling values. However, this shows the flexibility of the new methodology being investigated here. This method allows for the analyst to obtain an experimental velocity coupling response function. This means that these values are no longer just an estimate based on the experience of the analyst.

4.5 Conclusions

This section shows how CI theory can be manipulated to be used as an analysis tool. The most significant modification is to Culick's non-linear gas dynamics method. By realising that the phase shift has little or no impact on the final wave amplitude reduces the number of unknowns to one, allowing it to be used as an analysis tool.

Though Flandro's shock wave model can be used, it is limited as it can only evaluate one mode. The aim here is to evaluate as many modes as possible. The gas dynamics method has some significant advantages in prediction when there is limited response information and computational effort is a concern. However, computational effort is increasingly less of an issue. The saw tooth function does not seem to yield as good results when complex geometries are considered. However, it is used for initial calculations for the sake of completeness.

Within this new methodology it is possible to evaluate any linear theory. This will allow the application of these theories upon experimental data and direct comparison to each other. Velocity coupling can also be integrated if there is pressure coupled response data. This achieves one of the goals of this study which is to develop a framework for the analysis of pulse tests independent of the set of linear gain and loss terms.

Chapter 5

Results and Discussion

5.1 Introduction

The following section discusses the results obtained from the tests performed using the methodology presented in Chapter 4. The analysis was split into linear and non-linear analyses. Both interpretations of CI were investigated. Firstly, the classical interpretation that the system is linearly stable and requires second order driving terms to exhibit non-linear instability was investigated. Secondly, the assertion that all SRMs that exhibit non-linear instability are linearly unstable and that no second order driving terms are required was investigated.

The non-linear method predominantly applied here is Culick's gas dynamics method as it allows for multiple modes to be evaluated. Flandro's shock wave approximation only allows one mode to be calculated and thus it is limited as an analysis tool. It is shown in this section that both methods yield similar results for a tubular grain. The linear analysis comprises the interpretation and terms described in Chapter 3. For the sake of brevity, the method presented by Flandro, Madjdalani, Fischbach and Chibli is referred to as Flandro 2002 (25–28; 31; 44; 45; 47), Culick's standard analysis as Culick 2006 (30) and Flandro and Fischbach's set of terms is referred to as Flandro 2007 (20; 21). When this analysis is applied to a system it is assumed that the system is linearly unstable and Flandro's assertion that all motors are indeed linearly unstable is true. By evaluating the velocity coupling model it is assumed that the system is linearly stable and true triggering occurs. This requires the pressure coupled response function to calculate the velocity coupling. Only the Al motor tests were used to evaluate this as it is the only set of tests to yield enough data to allow for such a calculation. This set of data was also the only set of data to be completely captured using the improved data capturing scheme.

The different interpretations are used to predict the motor behaviour. The effects of these different methods on the prediction are evaluated and compared. Again only the Al tests yield enough data to allow for this to be evaluated.

5.2 Motor Tests

Three propellants have been tested to date. All of these have been HTPB/APC propellants with 86.5% solids loading. The first motor contained no stability additives, the following three motors contained 1% SiC and the last two motors contained 4% Al. For the initial tests the pulsers were set to rupture at a maximum pressure of 35 MPa except for the third

SiC motor which was pulsed at 50% of the maximum rupture pressure. The maximum pulse amplitude was desired as this would give the best chance of inducing non-linear acoustic instability. The first motor shown in Figure 5.1 was pulsed three times at 1.2, 1.6 and 2.0 seconds respectively. The pulsers were set to give the maximum pulse possible. The motor went unstable after the first pulse displaying all the classical phenomena that are associated with non-linear combustion instability, that is, a steep fronted wave was formed with a limiting amplitude and consisting of modes that are multiples of the first fundamental frequency. A 1 MPa pressure shift was also observed.

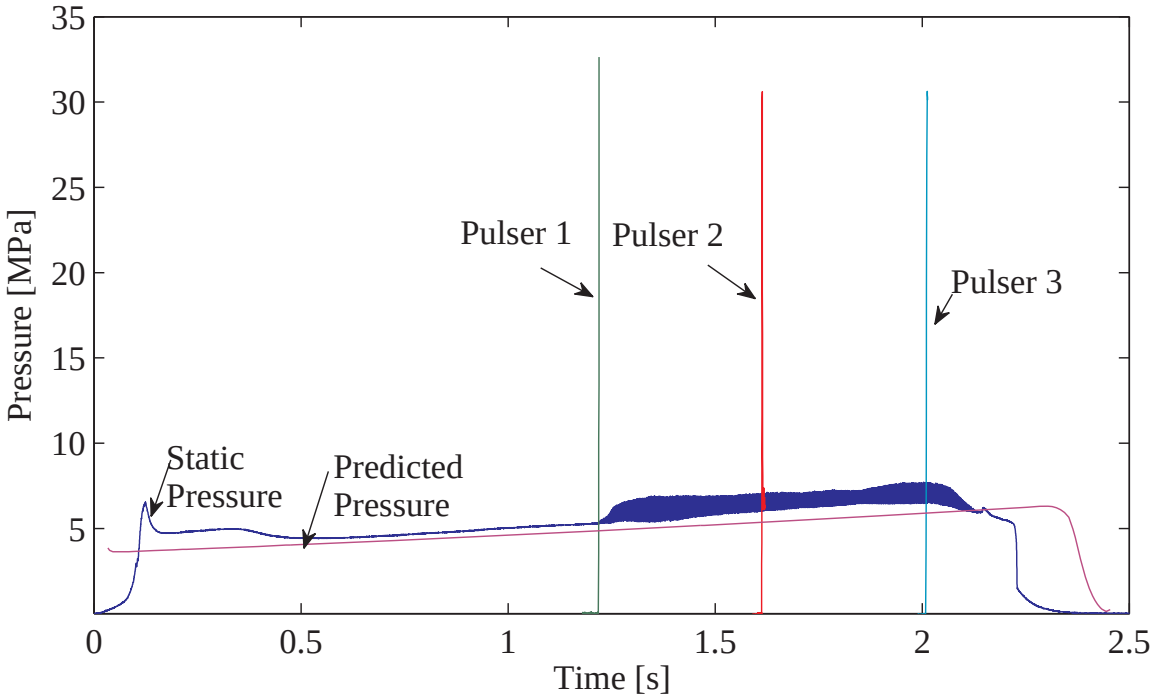

Figure 5.1: First Motor Firing Pressure Profile Prediction and Experimental Results

The second set of motors contained propellant with 1% SiC. Three tests were performed as shown in Figure 5.2. The first test operated at the same pressures as the first motor without stability additives and only went unstable after the third pulse. This showed that the particle dampening does indeed increase the motor stability. The second test was performed at a higher pressure with the motor going unstable after the first pulse. The same test was repeated with the pulsers set to rupture at 50% of the maximum rupture pressure. This decrease in rupture pressure reduces the shock wave amplitude by 50%. This motor remained stable after the first pulse but went unstable after the second. These tests showed two very important aspects. Firstly, motor stability decreases towards the end of the burn time due to the decrease in nozzle dampening. As discussed in Chapter 1, acoustic energy is lost as a portion of the acoustic wave passes through the nozzle and exits the motor. As the mean velocity decreases at the nozzle inlet, less of the acoustic energy is carried through the nozzle. This is confirmed by inspecting Equation (3.5.38). The typical decrease in nozzle dampening for the tubular grain motor is displayed in Figure 5.3. Secondly, these two tests at the same operating pressures with different pulse amplitudes show that there is indeed a threshold value for the pulse to induce combustion instability with a limiting amplitude. Figure

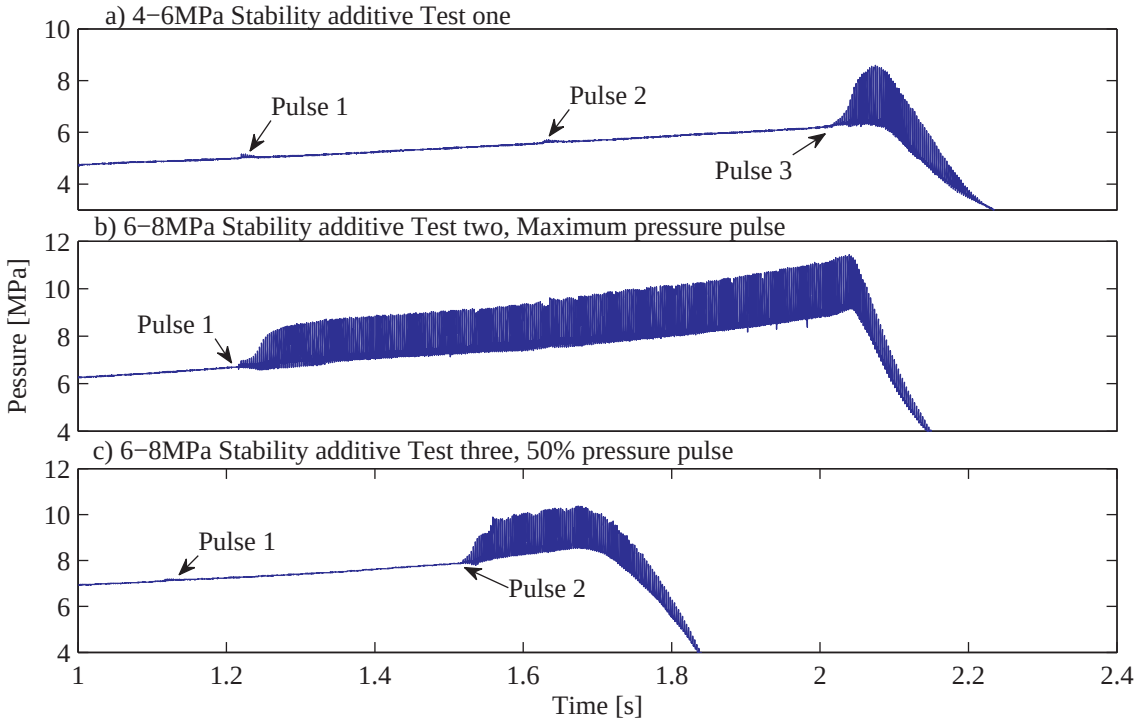

Figure 5.2: Motors with Stability Additives Pressure Time History

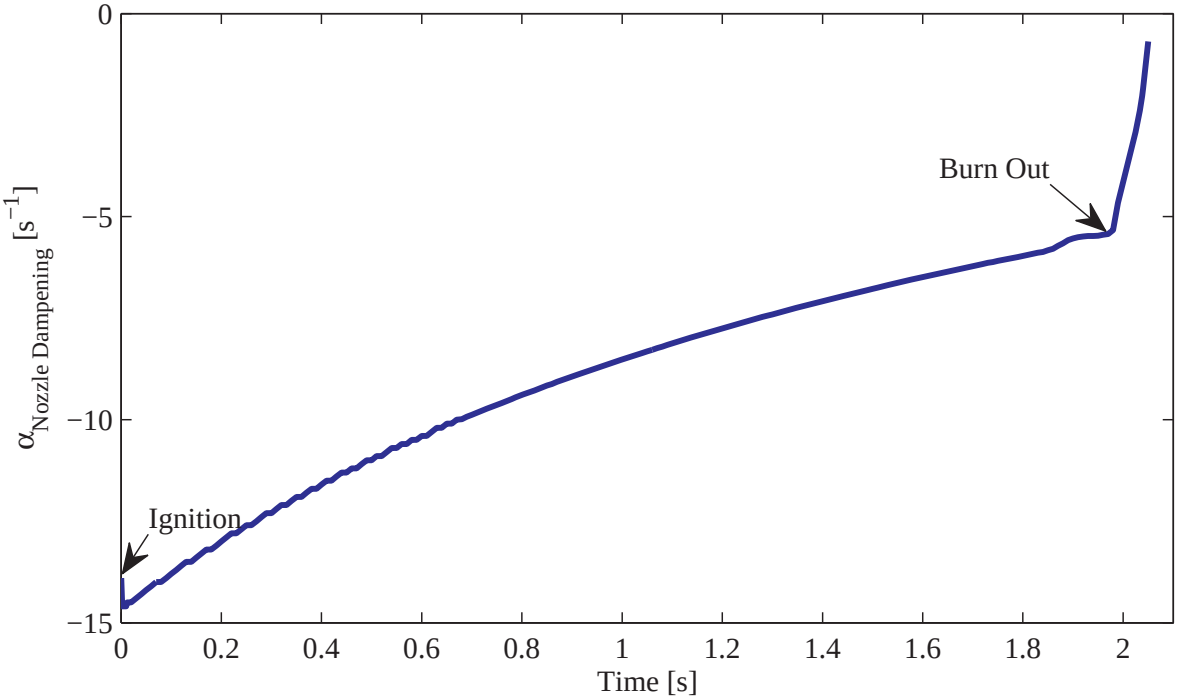

Figure 5.3: Typical Decrease in Nozzle Dampening for a Tubular Grain Motor

5.4 shows the tests done with 4% Al. The first test also operated between $4-6$ MPa and remained stable to all pulses. The second motor operating pressure was increased and was also pulsed unstable towards the end of the burn time. This was a rather surprising result as it would be expected that 4% Al particle loading would provide sufficient dampening to prevent this from occurring. This test, however, again confirmed that if a motor is pulsed with a sufficiently high pulse it can indeed induce non-linear CI. This was also the only test set that was performed using only the improved data capturing scheme.

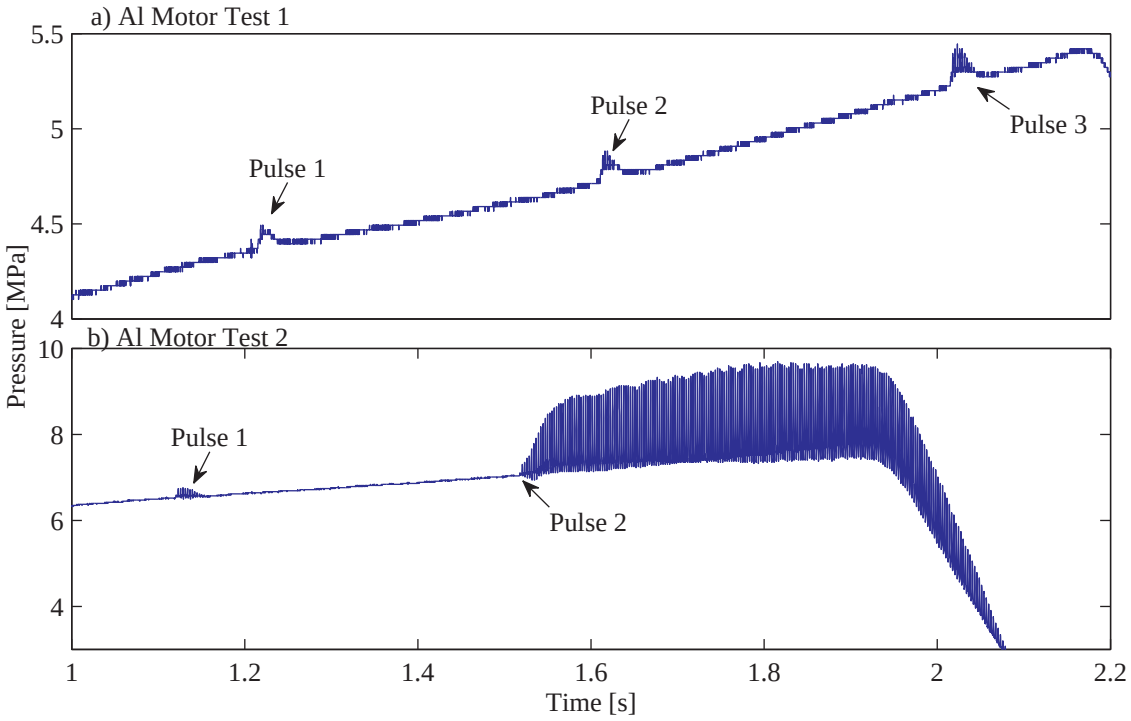

Figure 5.4: Pressure Curves Al Stability Additive Tests

All tests were performed successfully. The pulsers performed as expected and were fired at the time steps required. These tests show that the capacity to perform these tests has indeed been established. Full scale tests have been performed successfully using this test setup. However, this data will not be discussed in this text.

5.3 Analysis with No Second Order driving Terms

5.3.1 Cylindrical Motor Data Analysis

The first test was a tubular grain motor that was pulsed tested with a HTPB/APC composite propellant with no stability additives to serve as a baseline. After firing a pulse, oscillations occurred and a mean pressure shift was observed. The signal was then divided into windows equal to the period of the first longitudinal mode. These windows were then evaluated using an FFT (Fast Fourier Transform) algorithm. This is a relatively simple method for calculating the amplitude growth of the individual modes. Figure 5.5 show the results from this analysis. The longitudinal or axial frequency for a tubular grain can be calculated as

follows:

$$f = n\frac{a_0}{2L} \qquad n = 1, 2, 3..... \tag{5.3.1}$$

Table 5.1 shows the agreement between the predicted mode frequencies and the FFT algorithm.

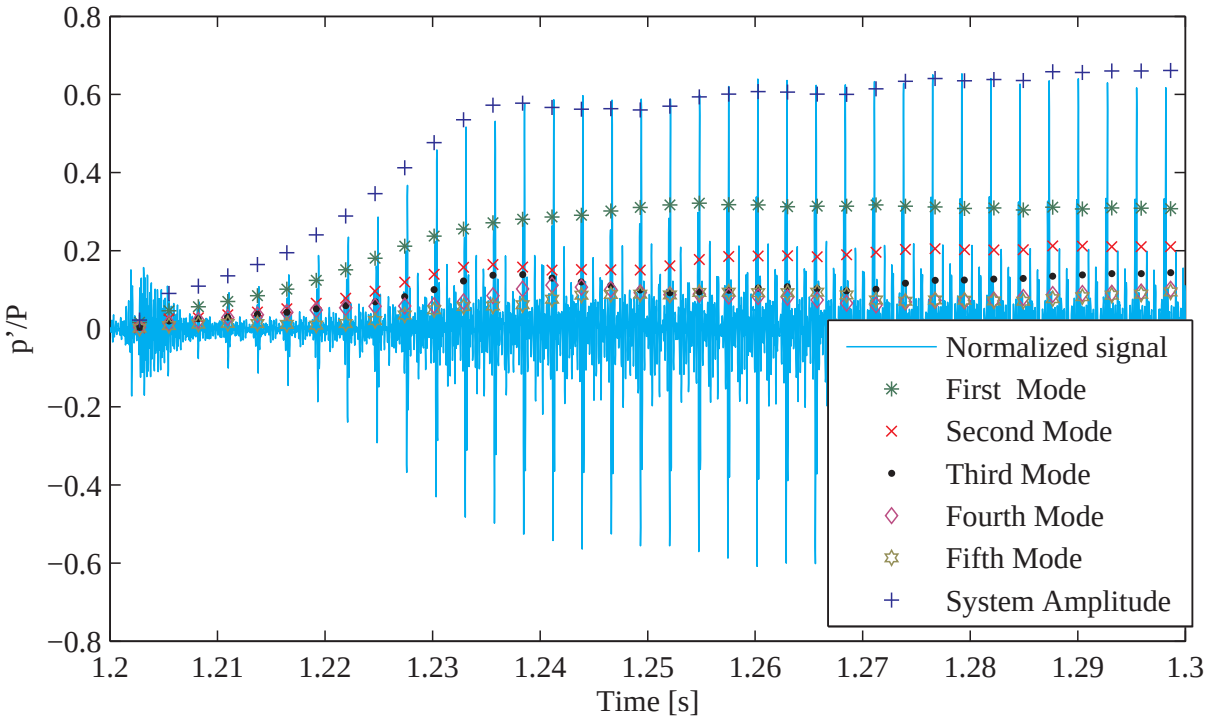

Figure 5.5: Pulsed Motor Firing and Individual Modes

Table 5.1: Frequencies Calculated using Equation (5.3.1) and FFT Analysis Results

Mode	1	2	3	4	5
Equation (5.3.1) [Hz]	386	772	1157	1543	1929
FFT [Hz]	391	782	1173	1564	1955

In Figure 5.5 it can be seen that after the initial plateau region is reached the amplitude remains constant for several cycles, and then the limiting amplitude readjusts to changing motor conditions. This is due to the dynamic behaviour of the motor. Once instability occurs, the limiting amplitude constantly readjusts to increasing burning area, increased volume, change in mean pressure, and changing mean flow velocity. The limit amplitude reached first will be used since this is the point closest to stable operating conditions. At this point the normalized system amplitude is 0.15. To solve for the α values using Culick's non-linear gas dynamics method all terms in equations (4.3.12) and (4.3.13) need to be calculated. An MATLAB algorithm was developed to calculate the summation terms from the mode amplitudes obtained experimentally. The mode *alpha* values can then be solved for. To perform this analysis 25 modes were used to obtain the α_{1-10} on Table 5.2 using Culick's method.

Table 5.2 gives α_1 obtained from both methods and α_{2-10} from Culick's method. Flandro's method obtains $\alpha_1 = 35.6s^{-1}$, for a system amplitude of $\epsilon \approx 0.15$. The linear analysis gives $A_b^{(r)} = 1.61$ (Flandro 2002). α_1 obtained using Culick's method is $38.3s^{-1}$ with $A_b^{(r)} = 1.67$ (Flandro 2002). This shows relatively good agreement between the two methods. This result shows that using cylindrical motors to obtain an admittance function is indeed possible.

Table 5.2: α_{1-10} $[s^{-1}]$ at 5.3 MPa

Mode	1	2	3	4	5	6	7	8	9	10
Flandro	35.6	-	-	-	-	-	-	-	-	-
Culick	38.3	59.9	64.5	31.7	-32.4	-80.1	-103	-232	-240	-242

Initial investigation by Rousseau and Knoetze (94) showed that with the Flandro 2002 set of linear equations the analysis was limited by the small ξ approximation. This approximation limited the analysis to modes with values of ξ that is less than 1. By returning to the derivation of α_7 by Majdalani, Flandro and Fischbach (26), an approximation of the following equation for α_7 is found without the small ξ, (26):

$$\alpha_7 = -\frac{1}{5}\xi^{-2}(1 - 2\xi + 2\xi^2 - e^{-2\xi}) \tag{5.3.2}$$

Figure 5.6 shows that as ξ becomes larger than 1, the small ξ approximation deviates dramatically and starts to tend towards infinity. The function without the small ξ assumption trends towards an asymptote as ξ becomes larger. Interestingly, α_6 and α_7 become equal and opposite when $\xi > 100$. The analysis performed here uses the function for the small ξ for values less than 1 and the function without the small ξ approximation for values greater than 1. Figure 5.6 shows the difference in results with and without the small ξ approximation.

Figure 5.7 shows the admittance/response function calculated from the α values obtained using Culick's gas dynamics method. This curve shows good qualitative agreement with those of Blomshield *et al.* (95; 96) (cf. Figures 5.7 and 5.8). Blomshield *et al.* used a similar propellant with an HTPB binder and an array of stability additives for their T-Burner investigation. The trends observed are similar with the peak response being observed between 800-1200 Hz. Blomshield (96) presented the response function for several families of propellants. Figure 5.8 shows the response functions for propellants most closely matching the burn rate and composition of the propellant evaluated here. Though direct comparison should be avoided due to different binder formulations and particle sizes, it does provide a guideline to the response function values that should be obtained.

From Figure 5.8 it can be seen that the maximum response obtained is 2, while most sets of data have a maximum response function below 2. Comparing this to the results from the analysis performed here (cf. Figure 5.7) it is clear that the Culick 2007 linear analysis gives values greatly exceeding the expected range. The peak response function using this method is 6.5. This is expected, since this interpretation of non-linear instability requires second order driving mechanisms such as velocity coupling to explain non-linear CI. Flandro 2002 gives values that are substantially less and fall within the pressure coupled response values. This is due to the inviscid vortical correction α_6 which adds an additional driving mechanism. It is interesting to note as the modes increase and ξ increases correspondingly, that the values of Culick 2006 and Flandro 2002 converge. This is due to α_6 and α_7 effectively cancelling each other out reducing Flandro 2002 essentially to Culick 2006. Flandro 2007

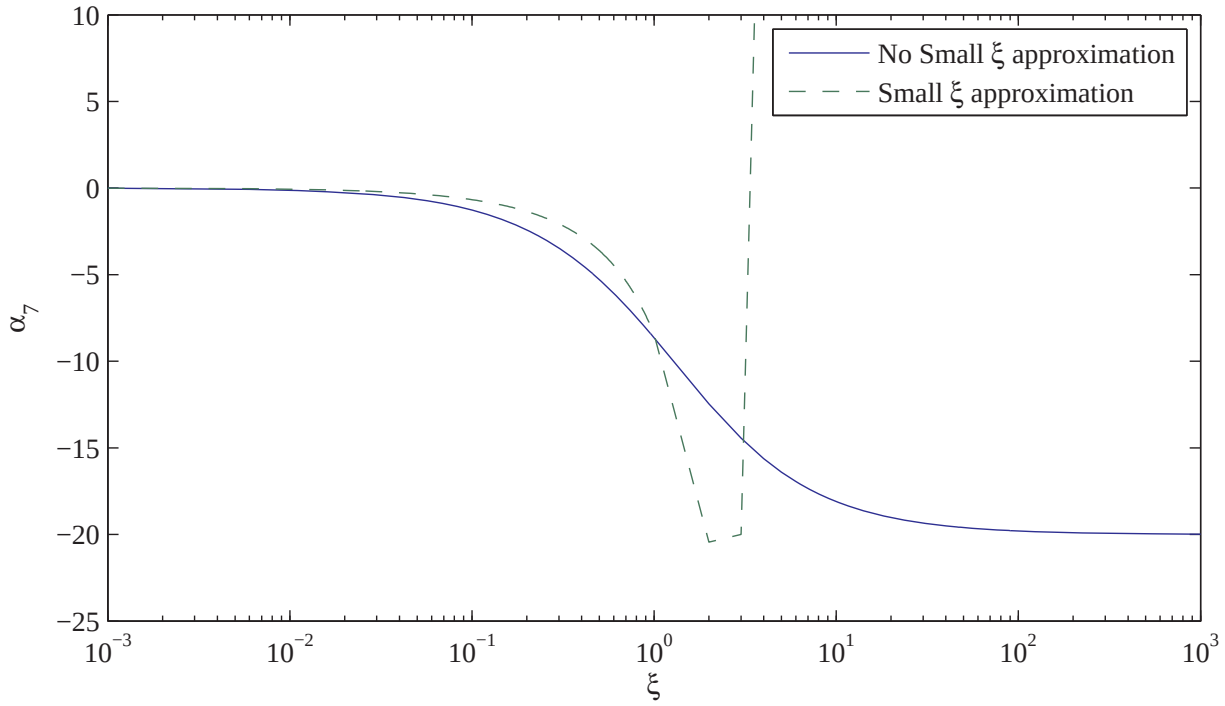

Figure 5.6: α_7 with and without ξ approximation, $M_b = 0.01$ and $\bar{a}/R = 5000$

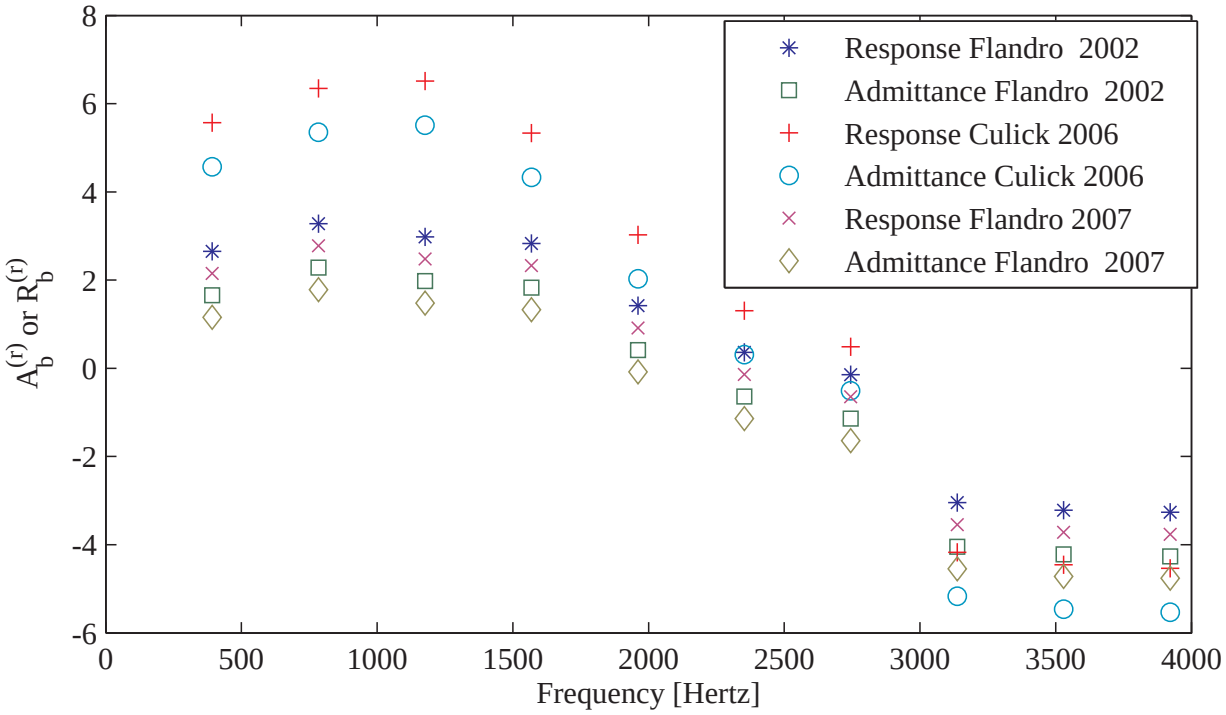

Figure 5.7: Admittance/Response Curve Obtained for Propellant with No Stability Additives

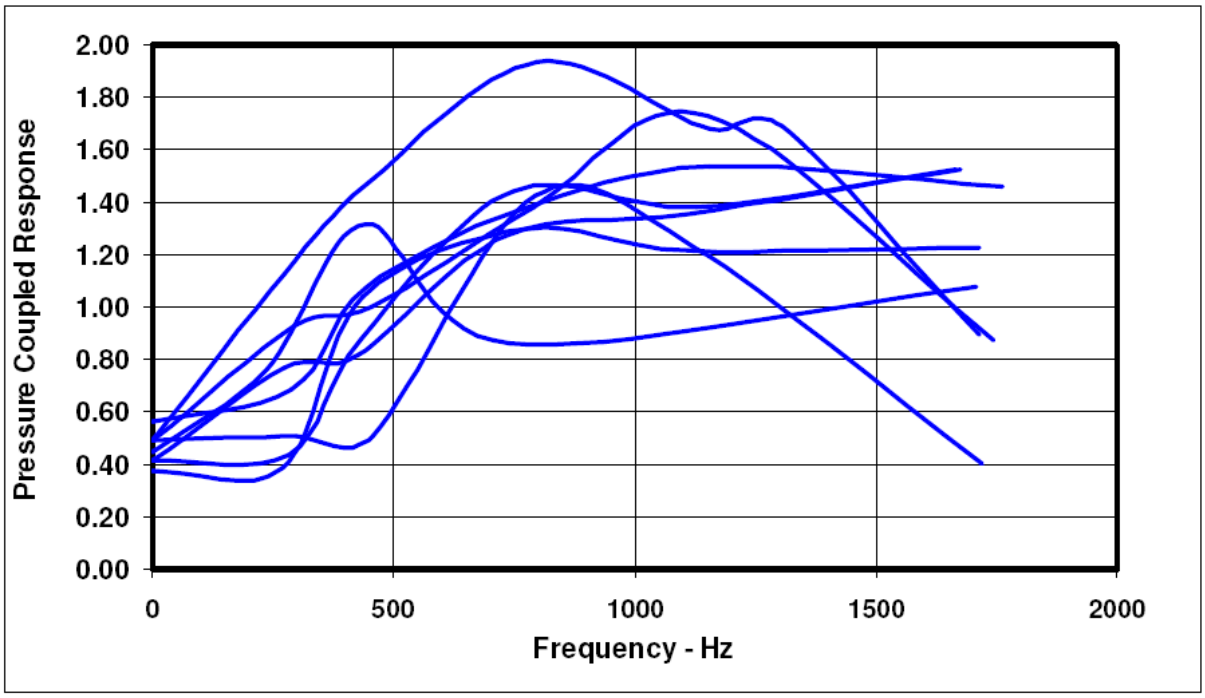

Figure 5.8: Typical Pressure Coupled Response for Set of Reduced Smoke Inert Binder APC Propellants operating at 6.9 MPA, with a Burn Rate $\approx$ 6.6 mm/s [Blomshield (96), Courtesy of F. Blomshield, with permission]

reduces the response function even more. The inviscid vortical correction is ignored here which would have resulted in an even smaller peak response function. No reason is given for its exclusion but it is assumed that subsequent investigation may have revealed some flaws in its formulation. It would appear that the linear model of Flandro and co-workers gives much better results. However, it is important to remember that their linear theory is not universally accepted. Their study was in part to address the shortcomings of the standard analysis that almost always predicts a stable system. This result would appear to show that their study has improved the linear analysis. In the absence of T-Burner data it is not possible to draw any verifiable conclusions.

Culick's standard analysis is unlikely to yield reasonable results as non-linear driving is accounted for by higher order mechanisms. The Flandro 2002 model has seemingly been abandoned by the original authors. Thus, the Flandro 2007 set of linear equations is used for the remaining analysis of non-linear instability as it returns the most reasonable results.

Another significant difference in these two analyses is the use of different results for energy normalization. Flandro and co workers use $E_m^2 = \frac{5}{8}\pi R/L$ and claimed a 25% relative improvement in results (97; 98). Culick used the standard energy estimate of $E_m^2 = \frac{1}{2}\pi R/L$. Since the improved normalization constant has not been universally accepted, the standard normalization function is used for the analysis presented here. To make these integrals conform to the standard energy normalization function the stability integrals are multiplied by a factor of 5/4. This results in a slight reduction in the response function obtained.

The admittance value obtained from the mean pressure shift is found to be $A_b^{(r)} = 4.6$. This corresponds more closely with the admittance found for the 3^{rd} and 4^{th} modes. There is clearly some refinement required to be able to use this method with confidence as mentioned by Flandro (31).

5.3.2 Motor with Stability Additives

5.3.2.1 Stability Integrals

Particle dampening is an extremely useful tool as a suppressing agent of CI. Modern tactical motors are required to be reduced smoke and in such systems ZrC particles have become the particles of choice. However, adding particles reduce the SRM performance (more inert particles mean less APC). Table 5.3 shows the reduction in the theoretical specific impulse with increasing stability additive weight fraction. A 2% reduction in specific impulse is predicted for a 1% inert stability additive propellant.

Table 5.3: Specific Impulse [s] for Varying Inert Particle Loading Calculated using the *Calculation of Complex Equilibrium Compositions Program* (100).Nozzle with an Nozzle Expansion Ratio of five at Sea Level.

Mass Fraction Inert [%]	0	0.5	1
Specific Impulse at 5 MPa	250.8	248.1	245.2

The linear stability integrals do not need to be altered for this motor. The particle dampening can be added to equation 4.3.5. The most commonly used expression for particulate dampening is used (95):

$$\alpha_p = \frac{C_m}{(1+C_m)} \frac{\omega}{2} \frac{\omega\tau_D}{1+(\omega\tau_D)^2} \tag{5.3.3}$$

The relaxation time τ_D is given as:

$$\tau_D = \frac{\rho_p D^2}{18\mu} \tag{5.3.4}$$

5.3.2.2 Pulsed Test Results for SiC Additive

For these motors 1% SiC replaced an equivalent mass of APC. SiC is not commonly used in composite propellants. Its use in the South African industry comes from its use in double base propellants. The use of SiC comes from the British use in the double base systems, most notably some of their cast double base rockets. SiC appears to be the additive of choice. The British had been using and testing suppressants as early as the early 1960's (99). The only publication on this work that the author could obtain is: *The Suppression of Combustion Instability by Particulate Dampening in Solid Rocket Motors* by G.I. Evans[1] and P.K. Smith (99). This details a large range of particle additives that were evaluated within the British development of various rocket motors. SiC is also less expensive than ZrC and easier to obtain, making it more attractive to the South African SRM industry. ZrC however is superior in composite propellants as its melting temperature is 3813 K compared to the decomposition temperature of SiC of 2973 K (99). Double base propellants have lower flame temperatures than composite propellants (see Table 5.4). The decomposition temperature of SiC is not exceeded in a double base system. However, composite propellants can exceed the decomposition temperature and thus the particle dampening effect is lost. The *Calculation of Complex Equilibrium Compositions Program* (100) also calculates that

[1]A significant figure in the British rocket community and holder of several patents on cast double base propellants. One such patent uses the inhibitor system to provide silica particles for particle dampening.

SiO and SiO_2 will form. It has as yet not been possible to collect samples of the suppressant particles post fire to confirm this result. This can have an effect on various aspects of the calculations performed and is discussed briefly in this section. An additional advantage of ZrC is that with its higher density, fewer particles at a given diameter per unit volume gas are required to obtain the same dampening. This improves the light scattering coefficient and thus reduces plume visibility (99).

Table 5.4: Typical Flame Temperature for Composite and Double Base Propellants Calculated using the *Calculation of Complex Equilibrium Compositions Program*(100)

Pressure [MPa]	5	10	15
Typical Double Base Propellant Flame Temperature [K]	2430	2432	2433
Typical Low Smoke Composite Propellant Flame Temperature [K]	2933	2963	2978

This motor was also pulsed three times only going unstable after the third pulse (cf. Figure 5.2). Two approaches were followed to evaluate the data from the two pulses that were damped out. The classical linear analysis is employed:

$$\epsilon(t) = e^{\alpha t} \tag{5.3.5}$$

The natural logarithm is taken of the normalised amplitude, a straight line is fitted to the data and the slope of this line is α. As with the unstable case the decaying wave's data is windowed and evaluated with the FFT algorithm. Fitting a straight line to this data gives an α for each mode. Figure 5.9 shows the non-linear prediction using α_1 obtained from the linear analysis. The experimental results deviate from the predicted values due to the transducer noise being of the same order as the decaying wave. Using the linear analysis, on both the system amplitude and the amplitude of the first mode, the same value for α was obtained. This indicates that using the FFT algorithm does give a correct result and that the α values obtained are representative of the modes stability.

The second method used was fitting Flandro's energy balance equation (4.3.4) to the system amplitude. This method is once again limited as it can only be used to obtain the α value for the first mode. The α values obtained using both methods showed excellent agreement (cf. Table 5.5).

Table 5.5: α $[s^{-1}]$ for Modes one to five

Mode	1	2	3	4	5
Pulse 1 at 5.0MPa					
Flandro	-46.4	-	-	-	-
Linear	-44.7	-50.7	-78.7	-84.2	-104
Pulse 2 at 5.6MPa					
Flandro	-39.1	-	-	-	-
Linear	-46.0	-41.0	-73.1	-84.7	-111
Pulse 3 at 6.3MPa					
Flandro	72.3	-	-	-	-
Culick	72.3	67.7	-8.14	-159	-382

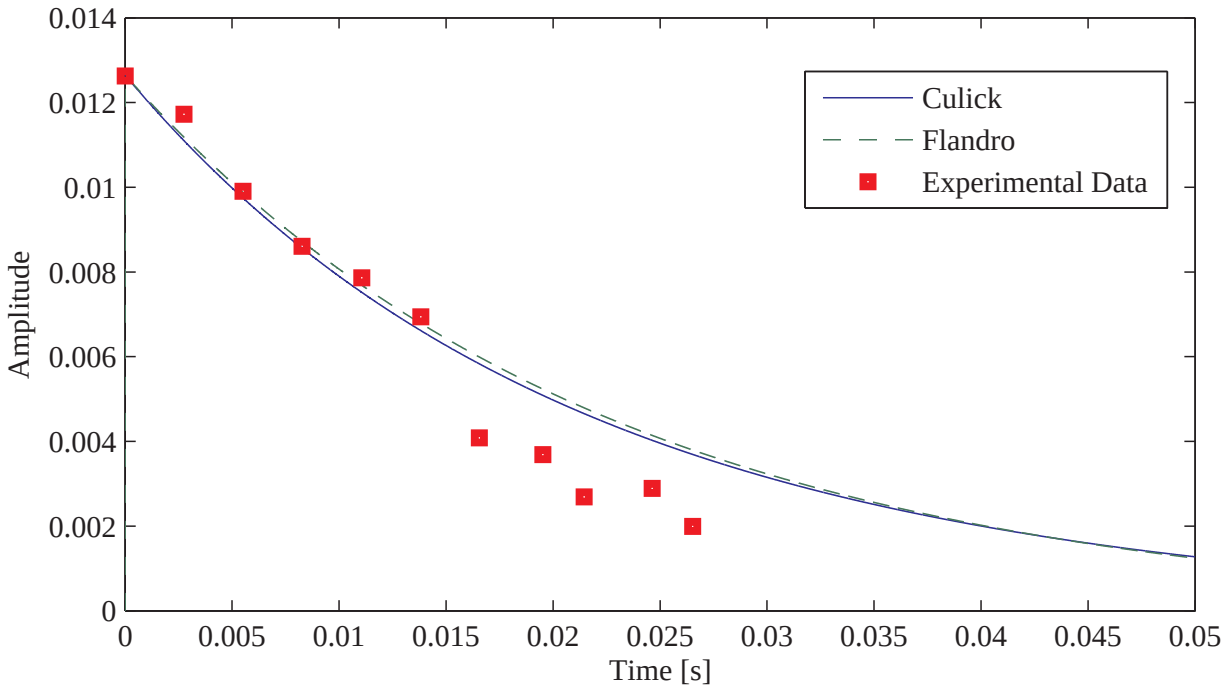

Figure 5.9: Stability Prediction from Linear Analysis

The data analysis used for the third pulse is the same as for the motor with no stability additives. The limit amplitude is found using the FFT algorithm. Both Culick's and Flandro's methods were used. From the results in Table 5.5 it can be seen that the additives have increased the motor stability greatly. It can also be seen that the stability decreases with burn time. It should be noted that investigations by Baum and Levine (75; 101) and Blomshield *et al.* (39; 40) have found that stability decreases towards the end of the burn time. This can be attributed to increased pressure in progressive burning grains (increased response), decrease in mean flow velocity and decreased nozzle dampening.

Figures 5.10 and 5.11 show the response functions obtained for the propellant. Flandro 2002 and Flandro 2007 give results that are well below that which would be expected when compared to Figure 5.8. Culick 2006 gives a response function that would seem to be more representative of the propellant family. This would seem to contradict the findings of the previous section. There are two possible conclusions: a) Flandro and co-worker's analysis is still incomplete and cannot account for motors that remain stable after a pulse b) That boundary pumping is not instantaneous and does not need to be accounted for when the pulse is damped out. Culick (2) has warned that though the inclusion of the mean flow interactions is no longer a subject of debate, the precise form is still a controversial topic. Though some of these terms have been accepted, by Culick (30), his assertion remains that second order terms are responsible for triggering and the occurrence of non-linear instability. However the second conclusion may be the key to understanding and predicting "*triggering*" within the interpretation that the motor is linearly unstable and that there are no second order driving terms or at the very least these terms are much smaller than first expected.

Culick (30) defines boundary pumping as: *a fluctuating velocity induced normal to the surface if the acoustic velocity tangential to the surface is not uniform, a direct consequence of continuity. This motion makes the surface appear as an effective oscillating piston tending, if the phase motion is suitable, to drive the wave in the chamber.* The important phrase in

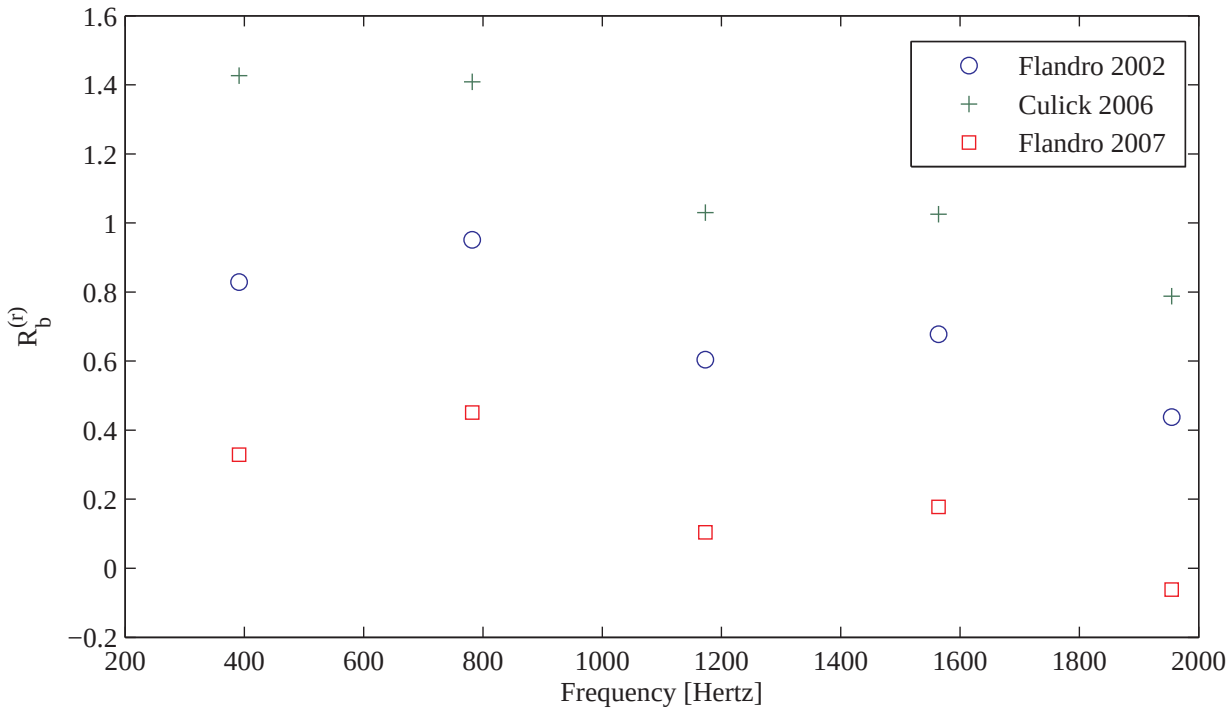

Figure 5.10: Response Function Obtained from Test One, Pulse 1 for Propellant with Stability Additives

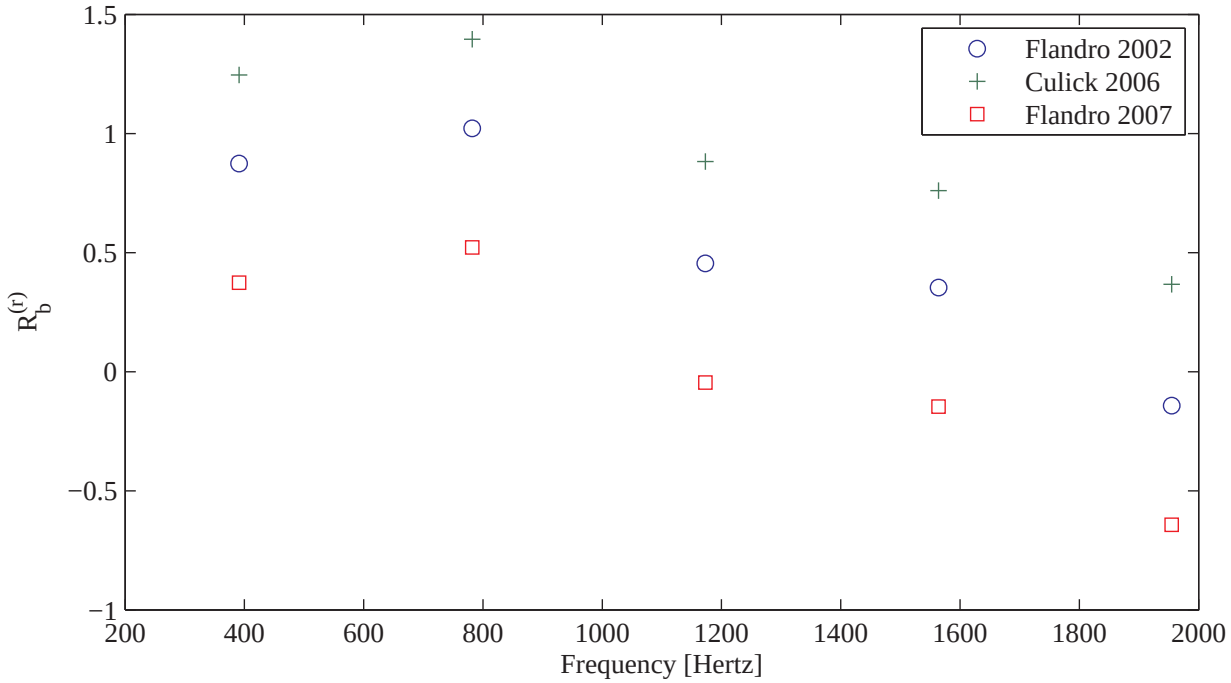

Figure 5.11: Response function Obtained from Test One, Pulse 2 for Propellant with Stability Additives

this context is *if the phase motion is suitable*. It is likely that there is a lag between the time that the pulse occurs and when the boundary pumping is in phase with the oscillations. If the boundary pumping is not in phase the system is stable and thus decays. If the pulse does not decay completely allowing for the boundary pumping to start oscillating in phase, the motor α becomes positive and thus instability is induced. In all tests that went unstable the amplitude decayed for 1-2 cycles before starting to grow. A second possible criterion is that the pulse must be of a certain magnitude to initiate boundary pumping. This would be analogous to the velocity coupling threshold. This possibility is investigated in Section 5.4.

SiC is not commonly used and little could be found that has been published on its use. To this authors knowledge the only use of SiC as a stability additive outside of South Africa has been double base systems developed in the United Kingdom in the 1960s and 1970s use SiC. The results of this work have not been published on extensively as mentioned earlier. It was chosen due to its good thermal properties, high melting temperature (2730°C), and availability. SiC in this reactive environment may form SiO_2 as discussed earlier. If it takes place, this reaction at the propellant surface may have a significant effect on the response of the propellant. At the motor operating temperature SiO_2 is a liquid; this can result in particle agglomeration altering the particle size distribution causing the particle dampening predictions to be incorrect. Direct comparison with the reduced smoke results shown by Blomshield (96) should be avoided as the stability additive in this case is ZrC. Attempts to calculate the particle post fire from samples collected from a collector behind the motor failed, because the glue on the adhesive metallic tape prevented the SEM analysis being performed. SiC has been shown to provide adequate particle dampening at the operating pressures and corresponding flame temperatures in this study.

Figure 5.11 shows that Flandro 2002 and Culick 2006 are relatively close together. This is due to the increase in viscosity with pressure. The values for ξ ($\xi > 10$) are high compared to the first pulse thus the difference between α_6 and α_7 is significantly less resulting in the two analysis being closer together.

It should also be expected that the response function should increase with pressure. This is not the case. This is due to the subjectivity of the linear analysis. Due to the transducer noise being the same order of magnitude as the pulse, this can result in the FFT algorithm returning distorted results. As with the T-Burner, it is up to the analyst to determine which points should and should not be included. As the modes increase this effect is even greater. Thus the analysis is limited to only five modes. The improved data capturing methodology proposed by Blomshield and discussed in Chapter 2 had not yet been incorporated in the test data acquisition routine. Using the high gain signal the noise to signal ratio is significantly less, allowing for less subjective analysis.

All three motors ultimately went unstable. Figures 5.12 and 5.13 show the response function obtained from the analyses. The first motor does not seem to follow the trends of the other two tests. This data may be erroneous because at the time of the pulse the motor was nearly burned out. The increased local burning rate may have caused the grain to burn through to the inert surface at certain points. Since the grain was also relatively thin at this point it may have caused cracking and resulted in additional surface area. This was also the last test that was performed not to use Blomshield's data acquisition scheme. This may account for the higher modes being negative compared to the positive values for the other two tests.

The second and third tests yielded results that seem to fit what is expected. The response function increases slightly with pressure as shown in Figure 5.13. Unlike the first test and the motor without additives, the higher modes response does not become negative. Though

it is possible for the response to be negative it is generally not at such low frequencies. This is due to the improved data acquisition scheme employed eliminating much of the distortion caused by noise.

The response from the linear analysis is generally lower than that from the non-linear analysis (cf. Figures 5.10, 5.11 and 5.12). This indicates that some other driving mechanism may be present. The linear analysis results were at lower pressures than that of the non-linear analysis results, however, this difference cannot account for the discrepancy in results. This would indicate that even with boundary layer pumping there are still some driving mechanisms not accounted for. Yet again, without T-Burner data, it is not possible to pursue or verify any of these conjectures.

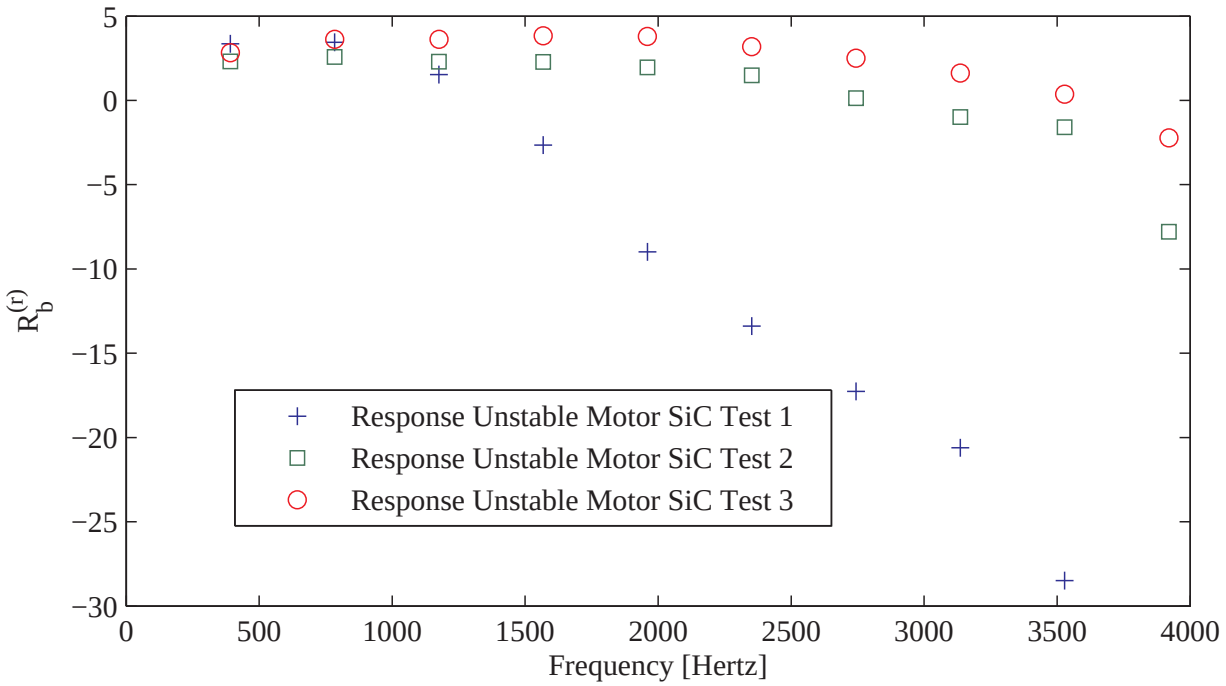

Figure 5.12: Response Obtained for Unstable Motors with SiC Stability Additives

5.3.2.3 Pulsed Test Results for Aluminium Additive

Two motors with 4% Al, a 300% increase in particle loading by mass over the SiC motors, have also been tested, as shown in Figure 5.4. These motors proved significantly more stable than their SiC counterparts, due to the increase in particle loading and different particle size ranges. The first motor, with an expected operating range from 3.5-5.5 MPa, was pulsed three times at maximum pulse strength and remained stable. The second Al motor had an operating range between 5-8 MPa and went unstable after the second pulse. The increased particle loading makes this motor significantly more stable than the SiC motors. Figures 5.14 and 5.15 display the absolute value of particle dampening for the first three modes at 5 MPa, calculated using equation (5.3.3). The size distribution of these particles obtained from the suppliers is also displayed. By comparing these figures it is shown that the Al particle size distribution overlaps to a larger extent with the particle size required for optimal dampening. The SiC particle distribution is much larger than the Al particle

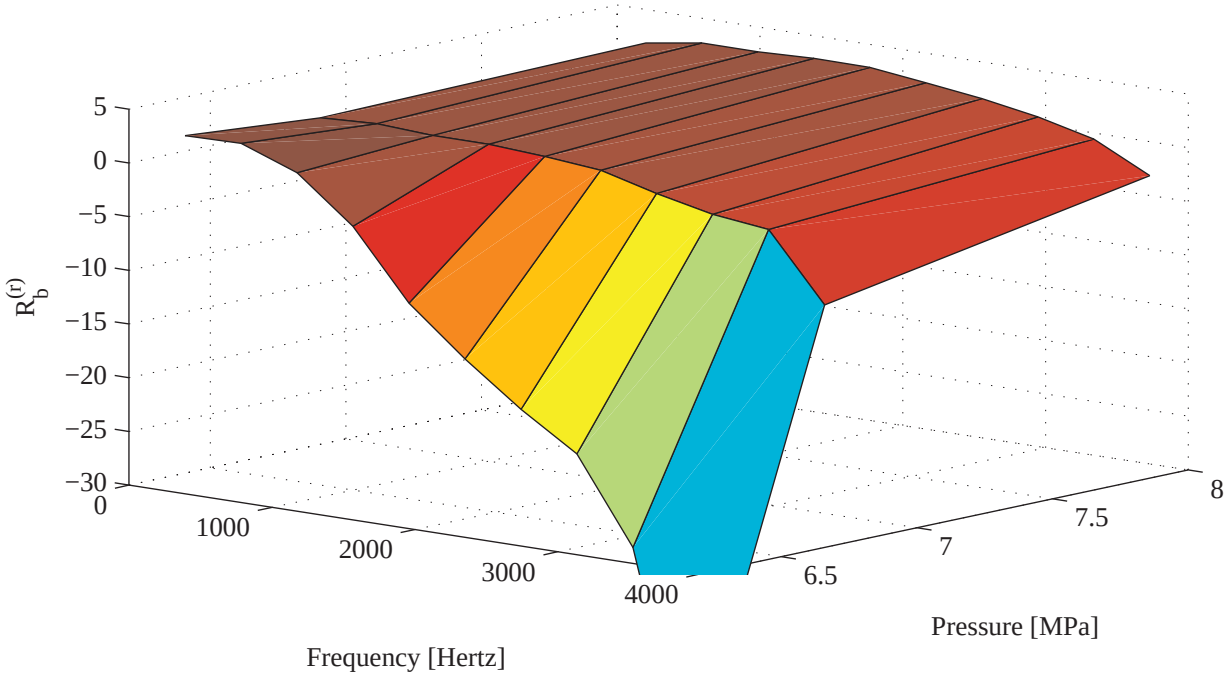

Figure 5.13: Surface Plot Response Obtained for Unstable Motors with Additives

distribution making it less effective in dampening the first mode which is expected at ≈ 390 Hz (Table 5.1). It is also likely that as the Al_2O_3 forms and agglomeration occurs, the finer particles will form larger particles moving more of the particle distribution into the size range for optimal suppression. To fully model CI with Al combustion residual combustion needs to be included with an agglomeration model of the particles. This should be done in future studies.

There were four sets of linear data. Unlike the SiC tests, the data acquisition scheme proposed by Blomshield (36) was implemented as presented in Section 2.3.1 for all these tests. This allowed for more modes to be evaluated. Figure 5.16 shows the true advantage of this testing regime. From two tests 36 response function points had been obtained (or 46 including the pulse that went unstable). This is a dramatic reduction in the man-hours required for a skilled operator to run T-Burner tests. From the surface plot it can, however, be seen that this method is still subjective. There are some data points that do not fit the general trends. It is up to the analyst to decide up to which mode to perform the analysis. However, this is no more subjective than that of the T-Burner analysis.

The surface plot can be used to interpolate between points. This data can be used to predict the stability of a motor at the required pressure and burn time. The analyst may have to remove some outliers within the data analysis adding to the subjectivity, but in general the first 4-6 modes give results with few outliers. As the mode numbers increase the analysis becomes more difficult. For instance, the first pulse was damped out significantly quicker. This means that higher modes may not have been activated. However, since only the first four modes are required to calculate the limit amplitude (19), it should be possible to calculate the motor stability or the level of instability with high a degree of certainty.

Finally a non-linear analysis was performed (cf. Figure 5.17). This analysis employed the Flandro 2007 set of linear equations. The mode α values were calculated using the non-linear gas dynamics method. As with the previous analysis, this analysis returned higher than expected response function values than that which were obtained from the linear analysis.

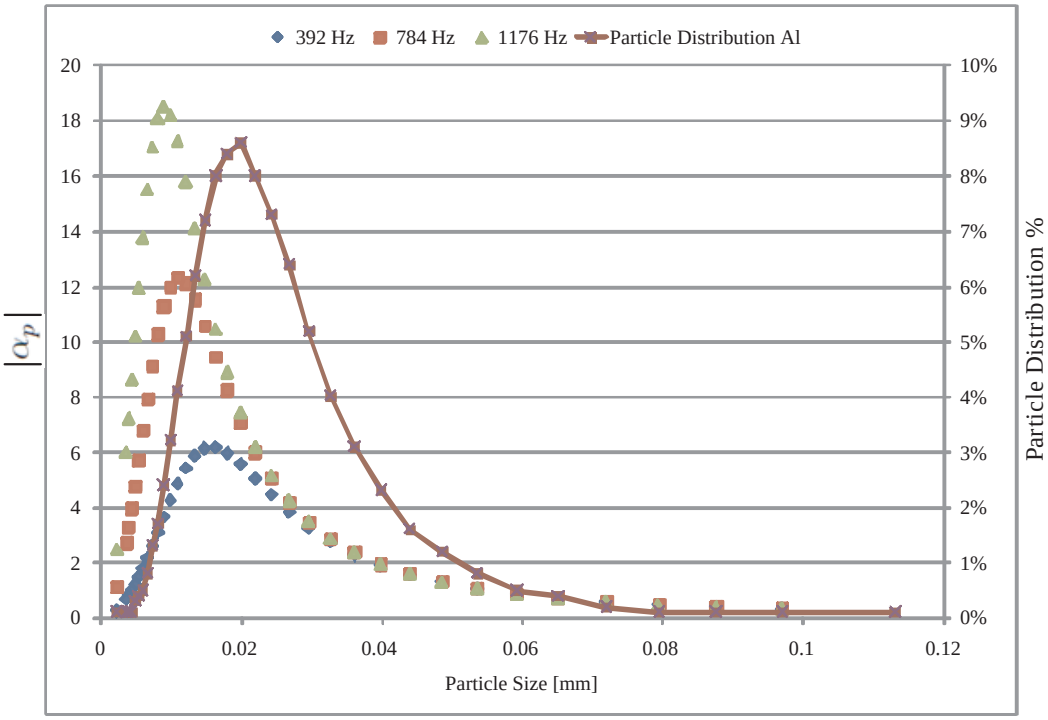

Figure 5.14: Al Particle Distribution from Supplier and the Absolute value Particle Dampening at 5 MPa

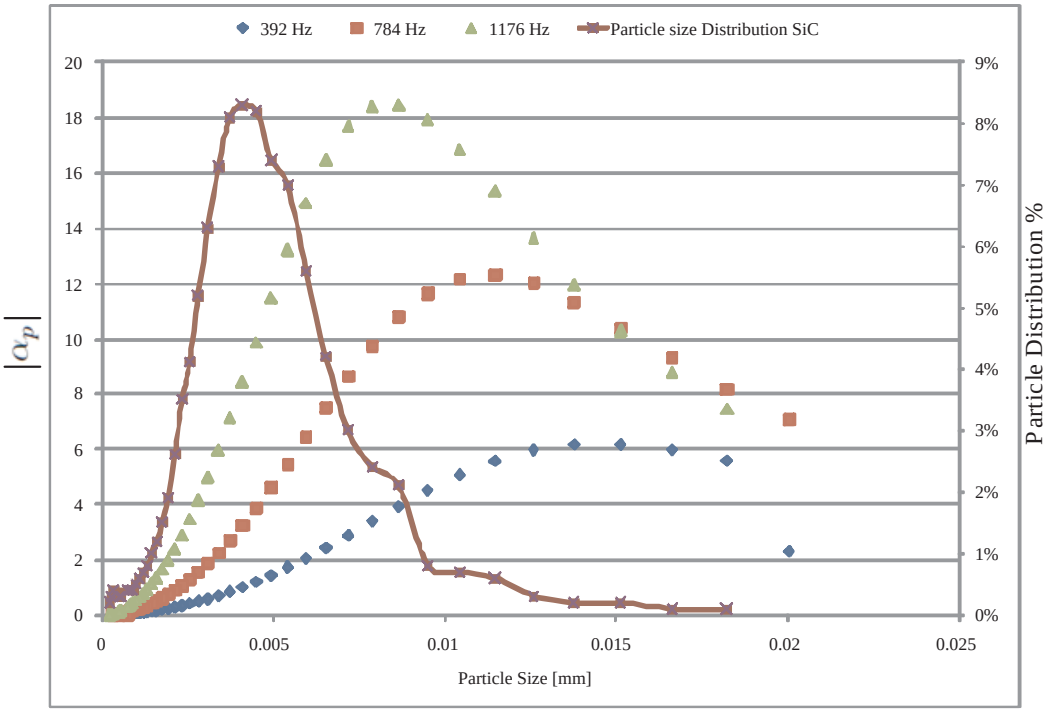

Figure 5.15: SiC Particle Distribution from Supplier and Relative Dampening of Various Modes

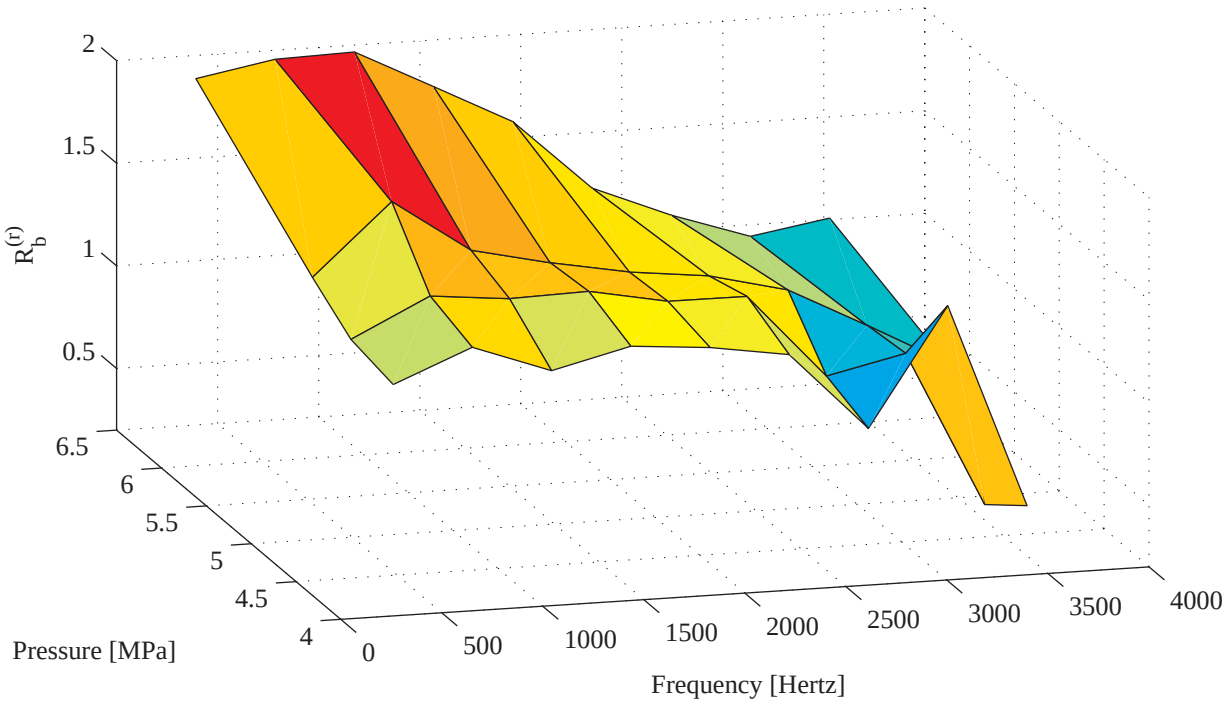

Figure 5.16: Surface Plot of the Response Function from Linear Analyses

It would appear that even with addition of the boundary layer pumping that there is still some unaccounted driving force.

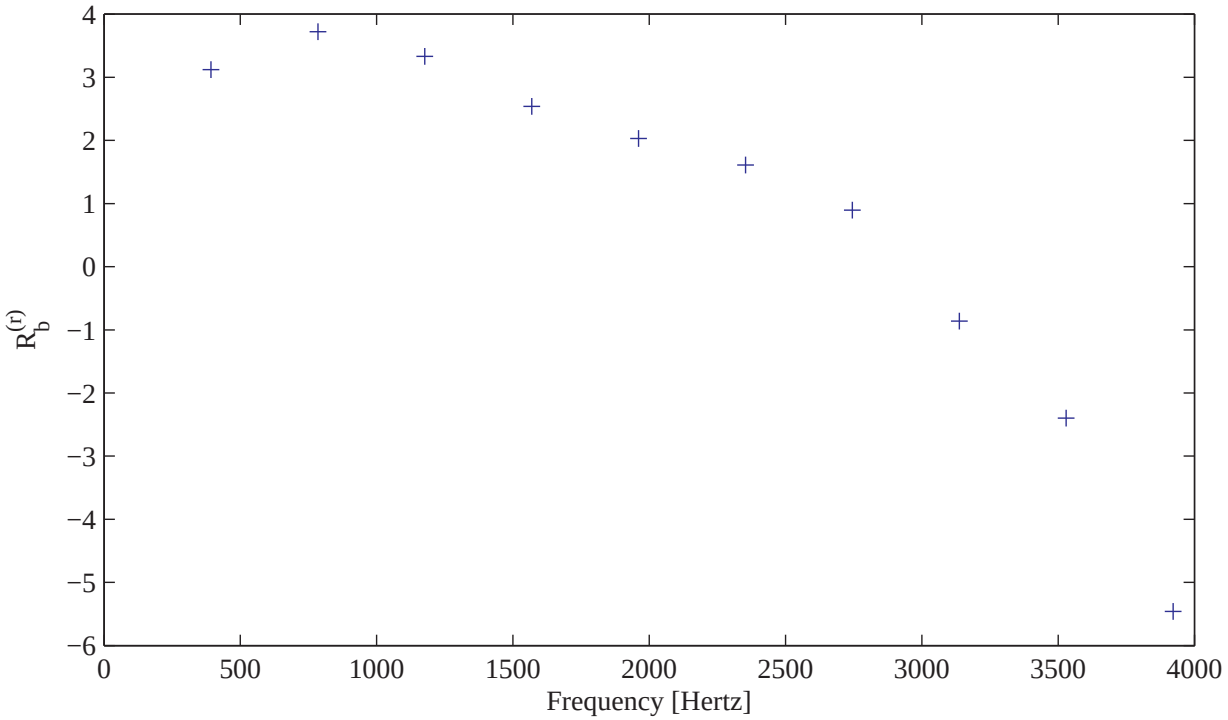

Figure 5.17: Response Function from Non-Linear Analysis

5.3.3 Conclusions for Analysis with No Second Order driving Terms

The linear analysis on pulses that decayed showed that the Culick 2006 model returned the most reasonable results. For unstable operation the Flandro 2007 set of equations returns the most reasonable results. However it still appears that there are some driving mechanisms that are not accounted for. Even when including the inviscid vortical correction into the Flandro 2007, this analysis does not reconcile the two sets of linear equations nor does changing the value for the energy normalization function.

Assuming that there are no second order driving mechanisms, a new methodology for quantifying triggering would seem to appear using the Flandro 2007 model. Assuming that boundary layer pumping is not instantaneous and/or is only activated by a significantly large pulse, allows the motor designer to make an assessment of the pulse magnitude required to initiate the formation of a limit amplitude and the associated DC pressure shift. This represents a new opportunity for motor designers to evaluate whether the motor is indeed stable to any pulse that can occur during normal operation.

The Al test most dramatically demonstrated the reduction in tests required to obtain enough information to perform a motor stability analysis. Two motor firings replaced 46 T-Burner tests. In a tactical missile environment the increased propellant required is negated by the reduction in man-hours. In this environment where new experimental propellant with limited quantities are not used it is possible to cast several motors from a batch of propellant without significantly reducing the amount of burn rate motors or full scale motors. Typically, 3-6 CI motors can be cast with the amount of propellant used in a single full scale motor. If the results from this analysis method can be compared with T-Burner data, it will allow for researchers to evaluate the stability integrals and methodologies directly with experimental results. Since T-Burner data was not available it was not possible to draw any verifiable conclusions about which linear set of equations returns the best results. It must be stated, however, that when a relative analysis between two propellants for the same application is performed, this method still holds great promise in providing reliable data as long as the same linear analysis terms are used throughout. Such an analysis will yield a response function for both propellants revealing the potential of the propellants to drive CI and thus allows the SRM designer to choose the propellant least likely to cause instability.

5.4 Analysis with Second Order Driving Terms: Velocity Coupling

5.4.1 Introduction

As discussed in Chapters 3 and 4, second order driving terms have been the subject of much research. There has been little work done on second order pressure coupled driving terms as it has been shown not to reveal triggering. The main focus of the research into second order driving mechanisms has been velocity coupling. Thus, the focus of this section will be to obtain the velocity coupling response function.

Velocity coupling is in some ways analogous to the erosive burning analysis. Erosive burning is commonly observed in SRMs, especially at ignition, as the port area at this point is relatively small i.e. high velocity flow in the motor. This higher flow velocity results in increased mixing in the flame zone, increasing the heat released due to combustion and, finally, increasing the heat transfer to the propellant surface resulting in increased burn rate. The flow can also augment the local transport properties in the boundary layer increasing the heat transfer to the surface. The flame zone can also be slanted due the incoming flow increasing the radiant heat feedback to the propellant surface. All these mechanisms can contribute to the augmentation of the burn rate. This usually manifests as a "*hump*" at the start of the motor operation. Alain Davenas (102) gives a good account of the rules of thumb developed over the years to avoid and make a priori prediction of erosive burning. Armed with this knowledge it is possible to make a quantitative estimate for the erosive burning that will be experienced by a motor of a particular design. An experienced internal ballistician can even use the erosive burning to create a neutral thrust profile. There exists many models to predict erosive burning such as the Modified Lenoir-Rollibard, Standard Lenoir-Rollibard and the Green and Saderholm Model (103). These models have different advantages and disadvantages, however all these models augment the burn rate by assuming that the burn rate is some function of the flow rate through the port. In most cases they also incorporate a threshold value above which erosive burning occurs. This can take the guise of a hydraulic perimeter, the port perimeter, or some threshold gas flow value. Most of these models are "*tuned*" post fire to be able to predict the erosive burning adequately. There exists fundamental models but they require input data that are simply too expensive or time consuming to obtain. In this author's personal experience, as an internal ballistician it is relatively easy to calibrate these models post fire to predict the erosive burning for other grains from different batches of propellant.

Velocity coupling and erosive burning share two important physical characteristics. Firstly, both augment the burn rate due to gas velocity parallel to the burning surface. Secondly, both seem to have a velocity threshold above which these phenomena occur. In application of these semi-empirical models and prediction using these models both these phenomena also share some similarities. In most cases internal ballisticians use the above semi-empirical models that allow them to make accurate predictions once experimental results are available. More fundamental models are ignored due to their complexity. In the same way, the SRM designer can use an *ad hoc* velocity coupling model that is also semi-empirical to assess the stability of the motor. In most cases the velocity coupled response function is a best guess without any experimental data to base it on. This is, of course, not done because fundamental models are complex but because no such model as yet exists (boundary layer pumping has been proposed as such model and is discussed later in this context). Finally,

semi-empirical models can be of great help to the SRM designer as long as they are able to accurately simulate SRM behaviour with minimal experimental values required.

Velocity coupling in the CI context has always been referred to as an *ad hoc* model. This is because the driving is attributed to the acoustic velocity even though the mechanism of this interaction is unknown. Thus, as with erosive burning, an equation can be derived that will mimic the system behaviour adequately and allows the fitting of this phenomenon to experimentally obtained data or best guess of the analyst. There have been attempts in the past to obtain the velocity coupling values from lab scale experimental devices but these devices do not seem to be commonly used. Here then lies an opportunity to develop such a method to obtain the velocity coupled response function experimentally. Though this model is not a fundamental model it may be possible, as with most erosive burning models, to obtain constants for the velocity coupled response that will allow adequate prediction of the system dynamics. This is attempted here.

As mentioned in Section 3.7 the acoustic velocity augments the mass flux when the flow is turbulent, as shown by Ma *et al.* (70). Majdalani and van Moorhem (59) has shown that the flow is indeed turbulent in a rocket motor with mass transpiring from the walls. Thus it can be safely assumed that velocity coupling will take place in an SRM. Thus it will not be assumed that there is a velocity threshold as proposed by Burnley *et al.* (17). Instead, the triggering should be expected to occur naturally without the application of an artificial threshold constant as found by Ananthkrishnan *et al.* (19). This is investigated in the analysis presented here.

There is one aspect of the velocity coupled/erosive burning phenomena that cannot be addressed in this analysis. That is the change in geometry. Devices to obtain erosive burning constants for propellants have all been abandoned. This is due to the effect of the geometry on the flow profile. In a typical star profile the flow velocity parallel to the surface will not be the same throughout the cross section. Thus, in the same cross section there can be variable augmentation of the burn rate. As mentioned earlier, it is often cheaper and easier to only evaluate this in the full scale motor relying on experience and rules of thumb. In the same manner the velocity coupled response obtained for a tubular grain may or may not be directly applied to the analysis of a more complex geometry.

5.4.2 Velocity Coupling Analysis

The analysis is similar to that of the analysis without any second order terms. However, additional input data are required such as the response function of the propellant. The analysis can be broken down into seven steps:

1. Perform FFT analysis of the data.

2. Choose an appropriate time step or an average mode amplitude from the FFT analysis.

3. Calculate the motor linear stability α values for at least ten modes using a response function from either stable pulse test results or T-Burner results.

4. Calculate the weighting functions (equation (3.7.7)) using the trapezoid rule for the first two modes.

5. Calculate the non-linear gas dynamics from the input wave amplitudes using equations (4.3.12) and (4.3.13).

6. Equations (4.4.1) and (4.4.2) are added to equations (4.3.12) and (4.3.13).

7. Solve for $\bar{R}_{vc,2}$ instead of the mode α.

For this analysis the response data are provided from the pulses that remained stable. The response is then extrapolated to the pressure at which instability occurred (see Figure 5.4). The mode α values are calculated using the Culick 2006 set of stability integrals at the motor conditions at onset, as shown in Table 5.6[2]. Adding equations (4.4.1) and (4.4.2) to the non-linear analysis, it is possible to solve for the velocity coupling response for the first two modes. The weighting function equation 3.7.7 are numerically calculated using the trapezoid rule for the first two modes. Burnley's (67) numerical technique to calculate the functions for higher modes could not be reproduced with the limited information presented.

Table 5.6: α values for modes one to ten calculated using response function values from Figure 5.16.

Mode	1	2	3	4	5	6	7	8	9	10
α $[s^{-1}]$	-20.5	-14.6	-28.5	-41.0	-68.3	-96.6	-118.2	-124.0	-114	-1000

Performing this analysis (as with the response function) is subjective as can be seen from experimental results in Figure 5.18. The experimental results for higher mode values seem to oscillate even with the improved data capturing scheme. This is most likely due to the acoustic wave constantly having to readjust to the changing geometry of the motor. Thus, it is necessary to decide which time step is the truest reflection of the experimental data. The results vary significantly with the value of higher modes. When the higher mode value is in a trough, the weighting function tends to predict a high velocity coupling value as the lower modes do not contribute energy to the system. If the modes are at a peak value, a lower velocity coupling response is calculated as the higher modes contribute energy to the system. When the system is then simulated with these values, the first mode is either over- or under-predicted. The numerical analysis presented here is sensitive even for small changes in velocity coupling response. To avoid this, an average value for each mode should be calculated for several time steps once the limit amplitude is reached. It may be necessary to check the values obtained by simulating the system of waves by using the values obtained. The last mode that is evaluated in this case, Mode 10, seems to have an unreasonably high amplitude. This is due to the truncation error. Thus, to minimize its affect on the rest of the system, the mode α is set to -1000.

In this analysis $\bar{R}_{vc,1}$ and $\bar{R}_{vc,2}$ are found to be 0.46 and 0.8 respectively. The mode amplitudes are predicted by integrating equations (3.6.34) and (3.6.35) forward in time. Velocity coupling is included by adding equations (4.4.1) and (4.4.2) to the right hand side of equations (3.6.34) and (3.6.35). This was performed in MATLAB. Figures 5.18 and 5.19 show the result obtained for these values. The first mode's amplitude is predicted correctly, but the second and third modes are less than their experimental counterparts. This may be due to the truncation and errors as well the assumptions related to the weighting functions (equations (4.4.1) and (4.4.2)). However this is an adequate representation of the mode instability when the primary concern is the system limiting amplitude.

Velocity coupling has been pursued as it allows for the triggering amplitude to be predicted as well as representing unaccounted driving from the linear terms. For the R_{vc} values,

[2]Mode 10 is assigned a value of -1000 to limit its effect on the analysis.

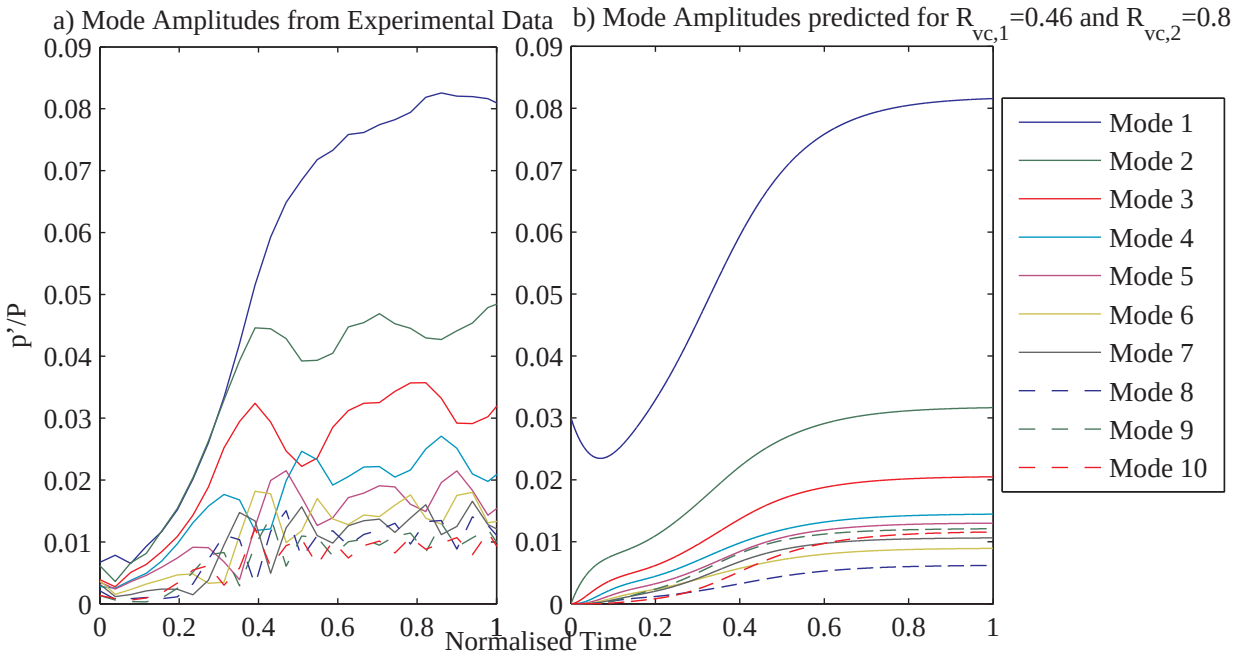

Figure 5.18: Experimental and Predicted Mode Amplitudes. Prediction made using Velocity Coupled Response.

the triggering amplitude is found to be p'/P=0.16. The onset of combustion instability was caused by a pulse of p'/P= 0.09. This is a relatively large disagreement. This is most likely caused by the α values. If other driving mechanisms were to be added the triggering amplitude will decrease with the increasing α values. It is important to note that triggering can only occur if the mode α values are negative. A linearly unstable system will result in a limiting amplitude regardless of the initial amplitude.

It is interesting to note that as with the experimental data the amplitude initially falls and then starts to grow. This is due to the higher modes starting at zero amplitude. Initially, energy is transferred to the higher modes causing the first mode amplitude to decrease. However, as the higher modes' amplitude increase, so does the driving from the velocity coupling function. Thus, the first mode starts to increase in amplitude. Figure 5.19 shows that if the higher modes are given an initial amplitude greater than zero, the second mode's initial amplitude of p'/P= 0.002 is assigned and all higher mode amplitudes of p'/P =0.0001 is assigned. The triggering amplitude is decreased to 0.06p'/P, which is less than that for the initial pulse amplitude that resulted in CI in this motor. This would indicate that it predicts reasonable triggering amplitude. It should also be noted that the triggering amplitude obtained is sensitive to the initial mode amplitudes and great care should be taken in assigning values for the initial amplitudes. In particular, if the first mode amplitude exceeds 50% of the initial mode amplitude of the system amplitude, then the system does not converge to a limiting amplitude but instead tends to an infinite amplitude. Thus, this analysis does give a velocity coupling threshold naturally. It is also very instructive to note that the limiting amplitude is also determined by the modal composition of the pulse. The initial pulse consists of several frequencies that as yet are not an ordered wave. As the wave synchronises and becomes coherent, energy transfer can start taking place between modes. If the velocity coupling is of a great enough magnitude this wave will then start to grow to a limiting amplitude. It is not clear from Burnley *et al.* (17) if the ratio of the initial mode

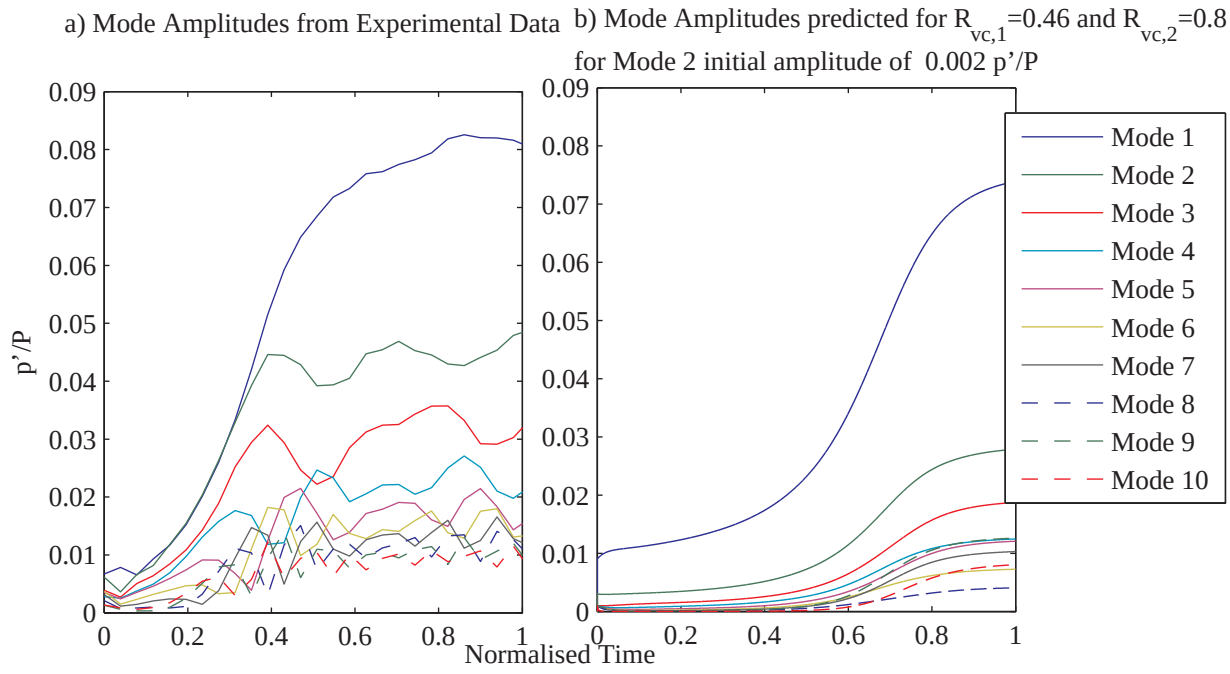

Figure 5.19: Experimental and Predicted Mode Amplitudes. Prediction made using Velocity Coupled Response with Higher Modes Initial Amplitude greater than Zero.

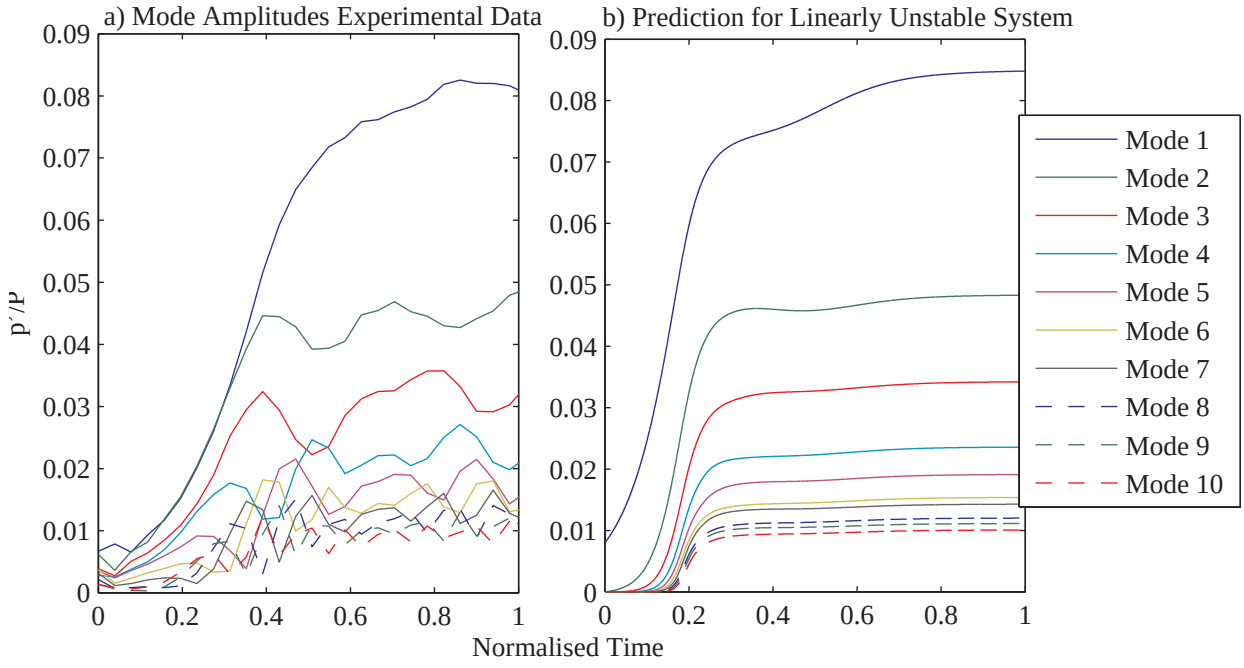

Figure 5.20: Experimental and Predicted Modes Amplitudes. Prediction made using Positive α Values.

amplitudes was evaluated. It is clear from the analysis presented here that this ratio of the various modes can have a significant impact on the triggering amplitude. This appears to be a significant factor that may have been overlooked or not adequately been reported on.

The largest discrepancy is the time taken to reach the limiting amplitude. The velocity coupling model takes longer to reach the limiting amplitude. The second and third mode amplitudes do not match the experimental amplitudes.

Figure 5.20 shows that by using positive mode α values (obtained experimentally), the time taken to reach a limiting amplitude is comparable. This difference may be due to the assumptions made to include the velocity coupling model or may in fact be a deficiency of this model. As Burnley's (17; 67) time averaged equations are not available and much of the numerical manipulations are not discussed, it is not possible to comment on his velocity coupling. This analysis, however, shows that it is possible to get an experimentally obtained velocity coupling response function. The analysis presented here can be improved upon by investigating Burnley's velocity coupling models more vigorously in order to evaluate more modes. However this mathematical endeavour does not fall within the scope of this project.

5.4.3 Discussion: Velocity Coupling vs. Boundary Layer Pumping

As mentioned on numerous occasions the most common criticism levelled against velocity coupling is that it is an *ad hoc* model since there is no satisfactory theoretical description of the interaction with the acoustic wave. It is based purely on the observation that the acoustic velocity parallel to the burning surface has an impact on the burn rate through convective heat transfer. It is also apparent that such a mechanism inherently contains two key aspects of non-linear triggered instability, i.e. a threshold characteristic and inherent non-linearity.

The interaction between the acoustic velocity and the burning surface is of particular importance when the flow is turbulent, as shown by Ma *et al.* (70). In a rocket motor with mass injection from the walls, it has been shown convincingly by Majdalani and van Moorhem (59) that the boundary layer is indeed turbulent. Thus, this cannot be the source of triggering as the acoustic velocity is not responsible for causing a transition from laminar to turbulent flow. Since it is not possible to ascribe the triggering amplitude to a particular change in transport properties, researchers have included artificial threshold velocity functions to extract the triggering amplitude. Ananthkristan *et al.* (19) claimed to have produced a velocity coupling model that naturally reveals the threshold nature desired but make no assertion of the physical mechanism it represents. These models have been shown to accurately reproduce the system dynamics if calibrated correctly.

Evaluating the boundary layer pumping in this context, i.e. a mechanism used to explain that apparent threshold nature of non-linear triggered instability and its non-linear nature, it becomes apparent that this mechanism represents a possible physical interpretation of velocity coupling or at least a subset of this interaction. Flandro (20) has stated: "*A mythology has grown over the years attributing unexpected (usually nonlinear) unsteady behaviour to mechanisms involving parallel incidence. These are often referred to as "velocity-coupling" since an acoustic velocity component parallel to the interface is expected. However, a verifiable theory based on fundamental physical interactions has yet to be devised. Consequently* ad hoc *models are often invoked that require unrealistic values of parameters (e.g. the velocity coupled response function) that cannot be supported experimentally. On the other hand there are mechanisms based on careful analysis that can be attributed to parallel wave incidence at a burning surface or an injector interface.*" This mechanism based on "*careful*" analysis is

boundary layer pumping. Boundary layer pumping is due to the oscillation of the boundary layer induced by parallel acoustic velocity.

By imagining the boundary layer as a hard surface that cannot be penetrated by the acoustic wave and that this surface is supported by some form of piston or spring, as presented in Figure 5.21, some of the properties of boundary layer pumping is revealed. By assuming that the spring must be displaced by a certain distance to induce harmonic motion of the surface, it becomes apparent that there is an inherent threshold, i.e. the acoustic wave needs to be of sufficient magnitude to cause the surface to oscillate. When the wave moves along the surface, the local force decreases on the surface and the spring can decompress. This decompression returns some of the energy back to the acoustic wave.

The process of the solid propellant being converted to gas is represented by the springs. As with the springs, energy will be stored by compressing the gases flowing from the surface. However, this compression will also increase the convective heat transfer to the surface increasing the mass flux from the propellant surface. Thus, not only will energy be stored but energy will be added to the acoustic wave, causing it to grow in amplitude. This driving from the increased mass flux from the surface would typically be non-linear. As in the case of composite propellants the increased burn rate is related by Veille's law $r = aP^n$, i.e. the mass flux will increase non-linearly with the increase in pressure.

This is an over simplified representation of the effect of boundary layer pumping, but it does illustrate that this mechanism inherently contains the phenomena that velocity coupling attempts to address. That is, a threshold velocity and the non-linearity of pulse induced CI. It should then be possible through further careful investigation to reformulate the boundary layer pumping integral not only to predict the final driving from this mechanism but also to give a means of predicting the triggering amplitude.

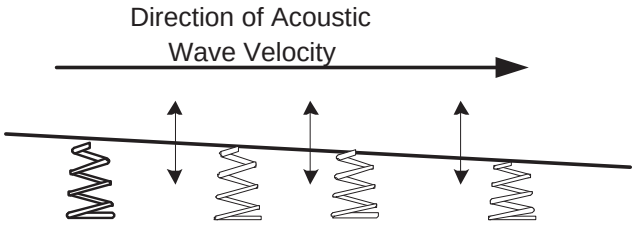

Figure 5.21: Hypothetical Representation of the Boundary Layer Pumping Mechanism

As stated earlier, the velocity coupling function is analogous to the erosive burning problem. Erosive burning is predicted using semi-empirical models due to their ease of use and because they are easy interpret in terms of flow velocity within the motor. In the same way, velocity coupling provides the internal ballistician with an interpretation that is easy to understand in terms of acoustic velocity. Boundary layer pumping in contrast is more difficult to obtain especially if a complex geometry is being investigated.

Velocity coupling models, due to their numerical nature, have the additional advantage that they can be used in the active control of CI as presented by Isella and Culick (18) and Isella (104). Although this would not be a practical solution on tactical size missiles with short burn times, the advantages for long burn times motors such as liquid, hybrid and ramjet rockets is clear. In liquid rockets the complex and heavy baffle systems often used to suppress instability can be discarded and replaced by a dump combustor as proposed by Isella (104) (the reader is referred to this reference for a detailed description of this control system). For a

liquid rocket, reusable hardware can be manufactured to perform pulse tests to obtain enough velocity coupling data at various operating pressures and operating conditions to create an effective control system. The ability to instrument at various locations and to include such instrumentations on the operational motor makes such a control system possible. The fact that the interior volume is relatively simple compared to a complex geometry of an SRM with a boost-sustain motor makes calculating the stability integrals a relatively simple task. The method described here can be used in such a case to obtain the required velocity coupling inputs.

As discussed here it is possible that velocity coupling and boundary layer pumping are indeed two representations of the same phenomenon. Assuming this to be true, in the tactical missile environment calculating the stability α value would be a more practical solution. Since the only experimentally obtained values required is the pressure coupled response function (as long as the capacity exists to calculate the stability integrals for complex motor geometries). The addition of a threshold characteristic into the boundary layer function based on momentum will allow the prediction of the triggering amplitude without having to resort to velocity coupling. It is important to remember that in the tactical missile environment the desired outcome is to answer the question: *will the motor remains stable for all conceivable scenarios.*

The velocity coupling models presented recently by Burnley and Culick (17) and Anathikishan *et al.* (19) can be used in active control systems, which on large, expensive systems would be a viable option. The major disadvantage of the velocity coupling model is that it generally yields results for a particular case only and that these results may not be directly applicable to different geometries. It is unfortunate that the velocity coupling constants presented here could not be used for the prediction of the stability of more complex motors and evaluated experimentally. The analysis method presented here allows for both the velocity coupling and boundary layer pumping to be evaluated as the source of non-linear instability.

5.4.4 Conclusions Analysis with Second Order Driving Terms

Velocity coupling can be calculated using pulse test results from tubular grains. This is of particular interest as there is no experimental method currently that allows for this to be done. Though there is no universal agreement on the validity of velocity coupling this method will allow for it to be evaluated.

The velocity coupling model used here adequately predicts the system amplitude and first mode amplitude. It is, however, important to note that velocity coupling was only included for the first two modes. The response is also significantly slower than that of the actual system. This is either due to the assumptions made to allow for the velocity coupling model to be evaluated or it points out some limitations of the model. To allow for the velocity coupling to be evaluated, a large amount of mathematical manipulation is required. As the numerical models presented in the literature were not available, and in some aspects difficult to reproduce, it is not clear if these errors occur due to errors in this transformation process or are simply limitations of the model. If these are limitations of the model they have not been reported on. Regardless of the limitations of the velocity coupling model employed here, it has been shown that velocity coupling response function can be obtained experimentally if pressure coupled response values are available. The application of the analysis methodology presented here can be applied to other systems such as liquid, hybrid or ramjet motors to obtain velocity coupled response. This can be of great value if active control of CI is feasible for the system.

The triggering amplitude can be evaluated. This is of course of great importance to any motor designer. Great care should be taken when assigning initial amplitude values. Assigning zero values to higher modes increases the triggering amplitude. Assigning initial values to higher modes greatly decreases the triggering amplitude. Great care should be taken in assigning these values as it will greatly influence the results obtained. However, as more tests are evaluated using this methodology, it should be possible to formulate general guidelines to assist the SRM designer in selecting the relative amplitudes of the modes to be able to predict the triggering point accurately.

The effect of the geometry on the velocity coupling constant could not be evaluated in this study. It is hoped that future studies will provide opportunities to do so.

5.5 Conclusions

The objectives of this dissertation have been achieved. It is possible to obtain a pressure-coupled response function for a propellant using pulse tested tubular grain motors. Furthermore, it has been shown that it is possible to obtain up to 46 response function data points from a single test. The assumption that linear stability theory had progressed to a point where the gain and loss mechanisms are accounted for, has partly been invalidated. Though there has been significant work done in the last decade to better quantify the physical mechanisms that drive CI, there is no consensus on what should and should not be included.

This is not a practical hindrance to the application of the analysis presented here. It allows the analyst to select the set of equations of preference. As long as the analysis is done consistently, the analyst will be able to make an assessment of the stability of an SRM for a specific propellant. It will most certainly allow the analyst to make a selection of the most stable propellant for the particular application.

The analysis presented here has inadvertently become a tool to evaluate the different linear theories. Since it can accommodate any linear interpretation it is not biased to any particular viewpoint. The inclusion of second order driving terms into the analysis also for the first time provides a viable means of obtaining the velocity coupled response function. It is hoped that the analysis presented here will be used to analyse other sets of data by fellow researchers.

The analysis has shown that when the set of linear terms is used that predicts a linearly unstable motor the response function obtained when the pulse is damped out is not reasonable. This has led to the conclusion for this interpretation to be valid; that some of the driving terms must be non-instantaneous and/or require a pulse of sufficient magnitude to initiate the driving. This set of equations returned a reasonable response function when the motor exhibited non-linear pulsed instability.

When the classical linear analyses that predict linearly stable systems are employed, reasonable results for the response function are obtained when the pulses are damped out. As can be expected, unreasonable results are obtained when non-linear instability is encountered. However, this analysis can be combined with second order driving mechanisms such as velocity coupling.

The application of this analysis methodology is not limited to SRMs only. The velocity coupling analysis can be applied to long burn time systems to calibrate an active CI control system.

A new flexible analysis tool that can be applied to any system with axial mode instability has been developed. This analysis methodology will allow researchers to systematically evaluate growth and decay constants. This may in time bring a better understanding of the CI process and bring consensus on what terms should and should not be included.

Chapter 6

Conclusions and Contributions

6.1 Conclusions

The objective of this study was to develop a new combustion instability strategy for the South African tactical missile industry. The focus was to obtain the pressure coupled response function from tubular grain pulse tests. A new method for obtaining the pressure coupled response function form pulse tests has proven successful. Realising that the phase shift has little impact on the final amplitude it was possible to create an algorithm to solve for the mode α values when a motor displays instability. The mode amplitude values could be obtained using an FFT algorithm. The linear analysis is less complicated but still allows for multiple modes to be evaluated. Several tasks had to be completed to make this analysis possible. The literature survey identified the most relevant sources that were presented in Chapter 3. It was possible to formulate a new strategy for obtaining quantitative propellant pressure coupled response functions. The literature presented in Chapter 3 was used to construct a new analysis methodology. Thus, the first task of this study was accomplished.

The hardware required to perform CI tests was developed. The pulser's performance was shown to be reproducible. The pulser hardware has been used for full scale tests and the software to predict their performance has been shown to be accurate. The reusable motor hardware has proven to be easy to use and to instrument. The data acquisition was improved over the course of this study and thus results obtained were improved as the study progressed. Tasks 2-4 was completed as defined by Section 1.5.

This method shows great promise in providing useable data. It is possible to replace significant amounts of T-Burner tests with a single pulse motor test. In the case of the motors with Al, two tests replaced 46 T-Burner tests. Such a large set of tests can take days if not weeks to perform. Even though more propellant is required than for a T-Burner, the time in man hours saved can be significant. In a tactical missile environment the amount of propellant required can be routinely obtained. Thus the 5^{th} task of this study, to develop a data analysis methodology, was completed.

All linear theory and interpretations of CI can be investigated using the analysis method presented here. There is much conjecture about linear theory and about what should and should not be included. Linear theory is based upon a myriad of assumptions about the physical mechanisms present within the motor. With a few exceptions most of them cannot be measured directly. This method described here gives insight into how these different interpretations affect the results.

It is clear from the analysis here that the Flandro 2002 and Flandro 2007 models do

not calculate reasonable values for the pressure coupled response when the motor remains stable. However, much better results are obtained from the non-linear analysis. This then provides insight into the possible triggering mechanisms. The results points to boundary layer pumping being non-instantaneous and that there is a lag between initial pulse and the boundary layer moving in phase with the oscillations. Systematic tests can reveal the location of such pulse tests and it may ultimately be possible to formulate a fundamental criterion for the required amplitude and lag. This brings the SRM designer closer to answering the most pertinent question, i.e. *will the motor remain stable under all conceivable operating conditions and eventualities.*

Culick's linear model does not seem to return reasonable values when non-linear CI is encountered but does calculate reasonable values when linear analysis is applied. This forces one to consider other second order models such as velocity coupling. This too can be incorporated in the method presented here. As an *ad hoc* model it must however be approached with caution. It can also be combined with the Flandro 2002 and 2007 models.

It must be noted that predicting motor behaviour with positive α compares more closely with the experimental results. This has been shown to be true for several cases by Flandro, Perry and French when re-evaluating Brownlee's early investigations (5). The velocity coupling can be modified to better simulate the system dynamics but there is an ever present danger of data fitting. The validity of the velocity coupling model can only be verified by obtaining a velocity response from one motor and predicting the stability limit of a second motor with different internal geometry and/or free volume and then to evaluate the stability limit experimentally. This does not fall in the scope of this project. However, this method provides experimentally obtained values for the velocity coupled response for the first time. This analysis verifies that the 6^{th} outcome of this study was achieved by establishing a predictive capacity for longitudinal mode instability.

There were several aspects that were ignored such as vortex shedding, particle agglomeration, and residual combustion. Simulation of these phenomena represent challenging projects within themselves. However the largest limitation to the verification of this method is the lack of T-Burner data. With such data it would be possible to compare the response functions obtained directly and as a result draw substantiated conclusions. This unfortunately could not be done within this study. It is hoped that future collaboration with other researchers will give such opportunities.

6.2 Recommendations

The following recommendations are made for future studies using the newly developed pulsed tubular grain analysis:

1. The results from this study should be compared with T-Burner results for the same propellants.

2. Alternatively, this analysis should be performed on pulse test motors from the NAWC combustion instability program and compared with the T-Burner results for the corresponding propellant. This may lead to a collaborative program with NAWC researchers.

3. The analysis of Al propellant motors can be improved by including residual combustion and particle agglomeration and should be included in future studies.

4. Future studies should attempt to replicate the CFD analysis presented in Section 3.8. This will allow for the stability of more complex motors to be evaluated.

5. The velocity coupled response function obtained using this analysis should be used to predict the stability of a full scale SRMs.

6.3 Contributions

The objectives of this study were reached. As was outlined in Chapter 1 all the building blocks to be able to successfully perform pulse tests were established. The pulsers and motor hardware were tested and evaluated and have performed as desired. The ability to calibrate the pulser to give the desired performance was demonstrated. The data acquisition was improved over time and in doing so the quality of the data obtained.

These data can also be analysed successfully and software using the Matlab environment was developed to quickly and easily analyse the data obtained. These tools were successfully used in other investigations.

The ability to model the non-linear mode amplitudes was also established using the Matlab environment. This prediction capacity however is limited to axial modes and not tangential modes but could possibly be modified to be able to handle tangential modes. The limitation of this model, however, is the input of the linear terms. For even slight deviations from cylindrical rocket motors, the various linear terms become extremely difficult to predict and FEA and CFD analyses are required. It is hoped that future projects will establish this capacity locally.

A completely new methodology was developed for obtaining the response function of a propellant. Realising that the phase shift can be neglected leaves only one unknown per equation that must be solved for. This method has the potential to replace up to 30 T-Burner tests in a single firing. However, this method is dependent on the ability to predict the other gain and loss mechanisms. Thus, it can also be used as a powerful research tool. In combination with T-Burner data it will be possible to directly evaluate different sets of linear inputs. Non-linear terms such as velocity coupling can also be incorporated. This method promises to be a flexible tool for evaluating CI theory.

Though not all aspects could be verified, all assumptions and methods are based on experimental results and in large part on accepted CI framework, i.e. splitting the analysis into linear and non-linear. Regardless of the researcher's standpoint on specifics on both linear and non-linear models a method now exists to investigate these standpoints and draw conclusions based on experimental data. This study has contributed a new testing methodology to the field of CI research. It is hoped that future studies and international collaboration will further validate the method presented.

Appendices

Appendix A

Combustion Instability History

A.1 Reported Cases of Combustion Instability

The following section contains some cases where combustion instability was found in motor systems as detailed by Blomshield[1] (1). This section will illustrate the prevalence of combustion instability in SRM's as well as what was done to fix these problem. The following are some of the more interesting cases encountered in the industry.

- **Sergeant Theater Ballistic Missile**: This motor was developed by the Jet Propulsion Laboratory for the U.S. Army between 1953-1962. This motor had a star perforated grain with a polysulphide-AP propellant which contained no aluminium. This motor encountered tangential combustion instability. The roll torque encountered was so strong that the casing was scored on the outside as the motor rotated in its restrains on the test stand. These roll torques were also found later on in the flight tests. The problem was never completely fixed and by the time the motor went into service the motor was obsolete. This motor served as impetus to further study combustion instability leading to the pulse testing study by W.G. Brownlee.

- **SUBROC**: The initial tests of this motor were performed using quarter and half length motors. This was done in order to minimize cost. However, when the full length motor was tested with the same aluminium particle size, it was found that severe axial mode instability was present. This is a classic case of non-linear instability with multiple harmonic modes present producing a DC pressure shift of 3.4MPa and oscillation amplitudes of 2.8MPa. The first attempt to fix the problem was several mechanical changes. This however proved futile. A host of possible changes were proposed. It is noteworthy that all emphasized that the aluminium particle size had to be reduced and all sources of debris be removed to avoid ejecta pulsing. 50% of the aluminium was replaced by a finer aluminium. This seemed to solve the problem. In a later test instability occurred and it was finally decided to use 100% finer particles. No further occurrence of instability occurred. The combustion instability delayed the project by four months and a corresponding increase in costs.

- **MK-27 TARTAR**: This is an anti-aircraft, ship launched missile. It had a dual boost-sustain motor with polyurethane aluminized Ammonium Perchlorate(AP) boost

[1]Fred S. Blomshield is a research Scientist and Senior Member of the AIAA. His research includes a large volume of work on pulse testing.

propellant and polyurethane nitroguandine AP sustain propellant. Slight longitudinal oscillations were observed in the boost phase. Toward the end of the sustain phase, more severe oscillations were observed that caused a DC pressure shift. The nozzle was altered by moving it from the upstream end to the downstream end of the blast tube. To improve the long term storage, the geometry was changed to decrease the mechanical stresses on the grain. The propellant formulation remained the same. The tests on the new geometry showed that there was a significant increase in the mean pressure during the sustain period. It was assumed that ejecta pulsing were responsible and all possible sources of ejecta was reduced. Also the web at the head end of the motor was increased. This increases the volume of the aft plenum and finally the igniter exterior surface was also insulated. This seemingly solved the problem.

- **TOW Flight Motor**: This motor was for an anti-tank missile. It was only 6 inches long and 5 inches in diameter. The grain was bonded to the head end of the motor. Burning occurred on the inside and outside diameter as well as the end face of the motor. Though the measuring devices of the time had a very limited frequency response, it was clearly observable that the motor was unstable in the first and second tangential modes. A DC pressure shift also occurred. This motor had to be flashless and smokeless and therefore the propellant was a double-base. This also meant metal additives could not be used. Baffles were used, placing these baffles around the outside of the grain and between the grain and the case. Several configurations were used before the instability was removed.

- **MINUTEMAN Wing I Stage III Missile:** During routine evaluation tests five flight failures of this missile occurred. This motor (already being in service) was placed under scrutiny due to the unacceptably high failure rate during random test. It was required to discover what proportions of the fleet were defective and which ones were not. Upon reviewing production documentation, it was found all five motors were from the last half of the production run. The aluminium powder used was from the same company and same designation but from different plants. Therefore it was deducted that the aluminium used in the beginning and the end of production were not the same. At the same time combustion instability of this motor was then investigated further. This motor had displayed instability throughout its development, but no significant difference was found between the magnitude of the oscillations of the two sets of motor. However upon reviewing the flight data it was noted that the frequency response had altered. The spectrum had changed. The most severe oscillations were now at a different frequency. This in turn means that the coupling between the wave and the mechanical structure had altered affecting the flight control system. Two efforts were then launched. First to determine why the new frequency caused malfunction within the control systems and secondly, how did the new aluminium change the combustion instability frequency spectrum. The first option was pursued since this allowed for a quick fix. It was found that a hydraulic line had the same resonant frequencies. This was attached to a spring loaded piston. When the vibrations became sufficiently large, the piston became dislodged and the control system could not return to a neutral position. The piston was replaced by a piston which could not be dislodged. All the motors from the second half of production had to be removed from silos and refitted with the new piston. At the same time the new dynamics of the aluminium were being studied. It was found the burn characteristics were significantly different. This was

probably caused by the amount or condition of oxide coating. In response the U.S. Air Force established an in-house program on combustion instability of SRMs. This program also funded the development of a computer program.

- **SLUFAE**: This motor displayed first mode longitudinal oscillations. Thus one percent 12μm AL_2O_3 was added. This removed the instability only for new instability to occur at 1500 Hz (one of the resonant modes). They found a unique solution by using a Helmholtz resonator that had the same frequency at the head end of the motor. This dampened the oscillations.

- **MK-36 Reduced Smoke SIDEWINDER**: The motor was adapted from a aluminized motor to a smokeless motor due to the changing needs in SRM performance. In performing this conversion, non-linear longitudinal mode instabilities were encountered. These instabilities caused DC pressure shifts that caused concern. Since it was not possible to use metal oxides to damp oscillations due to the motor's reduced smoke requirement. A further requirement is that it needed to be stable against pulsing. Thus the grain geometries were varied. The key slot geometry appeared to be stable, but due to some slight changes in propellant to achieve the desired burn rate it proved unstable as well. The star grain geometry also proved to be unstable. The final solution was to design a unique forward finocyl grain geometry. This grain geometry balanced the fin and cylinder burning areas according to velocity coupling theory. The principle is that the ratio of the burning area upstream oscillatory pressure node(zero pressure oscillation) and the area downstream of the node towards the aft end, should be constant and close to unity. The geometry consisted of three unique sections: a cylinder, 10 slots and an oval. The fix however that was finally adopted was to replace some AP with RDX. This removed the low-frequency pressure-coupled and the velocity coupled response. This was confirmed by T-Burner tests. 1% ZrC was also added to improve stability. These measures proved adequate and the motor was found to be stable in over 70 tests.

- **EX-70**: This motor was a research and development motor. It experienced excessive longitudinal mode oscillations which produced unacceptable thrust oscillations. A reduced smoke AP/HTBP propellant was used. Finer AP particles were also used to increase the burning rate. The nozzle throat size was increased to maintain the thrust time trace. The adjustment to the AP reduced the Pressure-coupled and Velocity Coupled response at the longitudinal mode frequency. Changing the nozzle increased the flow speed and thus the velocity coupled response was reduced and the increased throat size also increased the dampening of the nozzle.

- **SENTRY**: This missile defence motor was developed by Thiokol, which had an extremely high burning rate 12.7cm/sec at 6.9MPa.This motor went violently unstable and exhibited longitudinal mode acoustic instability. It was assumed, from predictions based on the high aluminium content, that this motor would be stable. T-Burner tests were performed to ascertain the effect of particle size of the aluminium particles. From these tests it was seen that finer particles drove the distribution more than larger particles. Theory supported this conclusion as the increased burning surface of the smaller particles was more pertinent in the driving of combustion instability than that of larger particles with a longer burning time. The Sentry program was cancelled. However valuable information was obtained from this program.

The cases above show that combustion instability is a common problem in SRMs. These instabilities can be found at any stage of development. It is important to be able to predict and eliminate combustion instability. This requires three tasks to be accomplished. Firstly, a prediction needs to be made on the stability of the motor. Secondly, the motor must be tested to ensure that the motor will be stable. Thirdly, one needs to identify what changes have to be incorporated in the case of possible instability.

It can also be seen that the combustion instability can be and has been solved in several ways. Some were as simple as changing the propellant formulation. Others required a redesign of the motor internal geometry such as adding baffles or in one exceptional case by adding the Helmholtz resonator. All these solutions require an understanding of the problem, in order to obtain the best possible solution without adversely affecting the motors performance.

A.2 Development of Combustion Instability Theory

This section was written as part of the initial literature survey of this study. The literature presented in the body of the dissertation was identified through this study. It is included here in the hope that it will serve as a valuable reference for those who wish to further study combustion instability in solid rocket motors. The following section is based on the author's research and the material that was available in the open literature.

This section is not meant to be authoritative but to outline the vast amount of work that has been done in the field since 1960. It will also demonstrate the limited technological aid available to early researchers. Combustion instability is the single most complex engineering challenge faced in the SRM industry and is often misunderstood. The approach to this problem in large part has been passive. Due to very limited predictive tools most SRM developers would normally develop a motor using rules of thumb. Only after combustion instability occurs a quick fix is sought. The development of computational power will also be referenced to show how the tools required to analyse the data and model combustion instability have developed. It will also establish a firm conceptual understanding of combustion instability. The papers referenced are determined by the relevance to the field as well as the number of citations in other publications.

The foundation for combustion research has been laid by few researchers, Grad 1949, Green 1956, Hart and McClure 1959, and Culick[2] 1968. Their work created the theoretical framework for combustion instability in both liquid and solid rocket motors (105). The following sections have been divided into decades.

A.2.1 1958-1970

1958: Edward W. Price manufactures first T-Burner. First integrated chip is developed.

1959: Harvard Mark I is turned off for the last time

[2]F.E.C. Culick is currently the Richard L. and Dorothy M. Hayman Professor of Mechanical Engineering and Professor of Jet Propulsion at CALTEC, Member or the Technical advisory Committee (TAC), Active member of the International Academy of Astronautics, and a Fellow of the AIAA. Has also participated in the reconstruction of the Wright Flyer.

Hart and McClure 1959 published a paper entitled "Combustion Instability: Acoustic interaction with a Burning Surface" (106) that has been widely referenced (2; 22; 25; 31; 107–124). This paper attempted to explain and predict the interaction between sound waves and the combustion surface. It was limited to simply understanding the finite transfer rates of heat and mass through the induction zone. The Model consists of and assumes the following:

- Heat and Mass Transfer equations;
- Gases were assumed ideal and assumed that there is no variation in molecular weight;
- Specific heat and thermal conductivity are assumed constant;
- The rate of conversion was assumed to be a function of the temperature and a thin reaction zone (Arrhenius);
- Combustion zone is treated as adiabatic;
- All reactions outside the induction zone are regarded as boundary conditions;
- It takes advantage of a relatively short transit time to solve the time-dependence of the heat flow;
- The burn rate's dependence on pressure is assumed known;
- The mass transfer is rewritten in terms of flame velocity;
- Pressure is assumed as spatially homogeneous and a time-dependent forcing function;

Upon completion of a "laborious" and "abstract" development of the model, the authors were quick to note the model was highly simplified and that there are several inadequacies viz:

- All time dependent reaction rate chemistry is suppressed by the adiabatic solutions;
- The solid phase chemical reactions are rudimentary;
- Specific heat and heat thermal conductivity are assumed constant and that there is no reaction in induction zone;
- Theory is entirely thermal. Diffusion of reactant products and active species are ignored. Neglecting these effects were neglected which in the authors words was "sinful";
- This theory cannot predict the growth of the perturbations and is only valid for relatively small ones. It is a linear model;
- The effort was to determine the periodic solution for acoustic interaction.

From this analysis it is clear to see that these researchers were severely hampered by what was practically possible. The assumptions made merely in the chemical reactions were simplistic. It is however understandable since a thermodynamics program capable to solve such reactions did not exist at the time. Hart and McClure along with Bird and Cantrell authored and co-authored many papers on combustion instability. See references (4; 106; 107; 107–109; 115; 125–134).

1960: "Transport Phenomena"' by Bird R.B., W.E. Steward and E.N. Lightfoot is published. IBM releases the 1400 series for business. COMBOL is is invented.

1961: First industrial robot put into operation by General Motors.

M.R. Denison and E. Baum published the paper "A Simplified Model of unstable burning in Solid Propellants" (22) which is referenced by (2; 4; 6; 13; 45; 69; 75; 118; 119; 121; 124; 130–135). The model is based on describing the physical process as a step increase in pressure. The response to this step change is assumed to consist of two phases. The disturbance, being rapid in nature would cause the combustion zone to move closer to the surface rapidly. It would then (Second Phase) readjust slowly as the surface temperature adjusts to the new conditions.

This affects the mass transfer at the surface opposed to a new pressure that would generally increase the mass flux more substantially. This is because the surface temperature could not adjust rapidly enough to a steady state value. The relative motion between the combustion zone and the surface becomes small as the mass flux from the surface must equal that leaving the combustion zone. Thus the flame temperature drops as the surface temperature stabilises to the new steady state value. The reduction in flame temperature requires that heat be lost from the gas phase. This means there is a sudden increase in heat flux.

The solid now responds gradually to the increased heat flux thus initiating the second phase where the combustion zone now readjusts. This adjustment of the combustion zone as a result of the solid phase is relatively slow when compared to the effect due to the gas velocity. This leads to the quasi steady state assumption. It assumes that at each instant such a state can be derived. If the "proper" heat flux to the solid surface and the "proper" temperature distribution in the solid is attained simultaneously, steady state is achieved. If, however they do not correspond, the constant readjustments of the solid may lead to unsteady burning.

Applying this reasoning to periodic oscillations, the gas phase is assumed to adjust faster than the solid phase. It is also assumed that the gas phase will adjust faster than the periodic oscillations since the gas phase adjustment constant is small when compared to the period of the oscillations. Thus in the gas phase there are assumed to be no time lags. If the frequency is sufficiently low it may even be possible for the solid phase to keep up with the constant change. At higher frequencies the time lag of the solid becomes important. At even higher frequencies the heat flux will not affect the heat distribution in the solid. As a result this analysis is not valid for extremely high frequencies.

This model consists of:

- Gas phase conservation equations;
- Gas phase perturbation relationships: Assumes the quasi steady state pressure, temperature and mass flux is the sum of the steady and perturbed value;
- Transient heat conduction of the solid;
- It incorporates pressure as a step function;
- It also assumes that the pressure varies sinusoidally;
- Establishes stability criteria based on steady state parameters.

From the result is possible to establish if a disturbance will return to steady state, if the amplitude will increase with no limit or steady oscillatory solution will be obtained.

The Following assumptions were made:

- Mass and energy transport is assumed to closely approximate steady state;
- Homogeneous propellant is assumed;
- The gas phase reaction is assumed to be adequately described by an nth order reaction. Gas phase reactions are typically more complex than this implies;
- Vaporization of the propellant is idealized. Solution of the linearized equation is valid only for small amplitudes.

This work established many conditions under which the propellant will remain stable, go to small amplitude or grow without limit. The inability of the model to predict a large amplitude and the limit cycles is due to its linear nature. This model laid the early foundation for linear analysis.

1962: Mariner II has Motorola transmitter on its trip to Venus.

"Command Initiation of Finite wave Axial Combustion Instability in Solid Propellant Rocket Engines" by L.A. Dickenson (43) was one of the first papers published on pulse testing (41; 114; 130; 131; 136–138). Though this is merely a brief outline of this methodology, it serves as a historic indicator to the establishment of pulse testing. This testing strategy has become a standard within the industry as part of the qualification process of SRMs. Concurrently Brownlee was establishing the same testing within the Canadian programs. He Published a paper on the experimental findings and testing methodology in 1964(42). It will become clear that early investigations were severely hampered by the quality of data capturing as well as the capacity to analyze this data.

1963: Doug Engelbert Patents the first Mouse. ASCII is developed to standardize data exchange between computers.

1964: The programming language BASIC is released.

"Interaction between Sound and Flow in Acoustic Cavities: Mass, Momentum and Energy Considerations" by Cantrell and Hart (108) and referenced by (4; 23–25; 46; 54; 57; 90; 112; 124; 139–144). This model attempts to apply combustion instability theory more directly on the actual case of a SRM or T-Burner as opposed to the more combustion orientated papers discussed previously.

The authors firstly look at the case of the energy balance of a cavity. In a cavity with non-reacting walls and constant volume, the energy balance is relatively easy by finding what mechanical work is done at the boundaries. Since a SRM is in essence a cavity with reacting and receding walls, the analysis is vastly more complex. It was noted that three possible techniques could be used:

- Transform the problem into an analogous problem without flow as done in (127);
- Determine the flow fields to the first order perturbation; or

- Explicitly considering the mass, momentum and energy balance.

The authors used the third option. Firstly, they established the neutral stability criterion:

- Consider the isentropic and irrotational relations for mass, momentum and energy conservation;
- Neutral stability is found by integrating and time averaging of the mass, momentum and energy equations;
- Integrating over volume removes all spatial dependence;
- Time-averaging of any linear, harmonic, acoustic field eliminates this quantity (integral of harmonic motion over time is equal to zero). Thus a second order treatment is developed.

The generic application of this analysis is limited because no volume loss is accounted for. The assumptions of isentropic and irrotational behavior also limit its applicability.

The second step is to determine the growth or decay rate at the burning surface:

- The burning surfaces' admittance needs to be calculated;
- The growth rate is determined from the excess of acoustic gains over acoustic losses;
- The losses are determined by measuring the rate of decay after the burnout. However flow fields differ and should be taken into account;
- A direct approach is used to calculate the growth rate as employed for a cavity with no flow. The starting point being the energy-growth-rate equation in a container with no flow;
- For a chamber with flow it is found that neither the energy nor the change in energy can be expressed in terms of first-order acoustic fields;
- The approach is modified by using mass and momentum equations so that the terms other than first order terms cancel each other out;
- Thus, by developing the model, it is found that it is indeed possible to evaluate the growth constant in terms of first order acoustics;
- Insisting that the final equation be in terms of only first order acoustics, however means the theory forfeited the ability to interpret the result in terms of energy flux and energy density;
- However, it was now possible to directly obtain the growth and decay.

$$2\alpha = -\left\{ \frac{\left\langle \int_s dS \bullet \left[p_1 v_1 + \frac{p_1^2 v_0}{\rho_0 v_1} + \rho_0 (v_0 \cdot v_1) v_1 + \frac{p_1}{c_0^2}(v_0 \cdot v_1) v_0 \right] \right\rangle}{\left\langle \int_V dV \left[\frac{1}{2}\rho_0 v_1^2 + \frac{p_1^2}{2\rho_0 c_0^2} + \frac{(v_0 \cdot v_1) p_1}{c_0^2} \right] \right\rangle} \right\} \tag{A.2.1}$$

The authors have now established an equation (A.2.1) that gives the growth rate in terms of the first order flow fields. The growth-rate describes the combined effects of mean flow, wall losses and the response of the propellant. The authors applied this analysis to a T-Burner and a radial burning cylindrical SRM.

To do this it is necessary to perform several integrations over the first order acoustics fields as can be seen from equation (A.2.1). At the time, however, determining the flow fields was an extremely long process. It was complicated by the mean flow and acoustic losses and gains at the boundaries. So, by inspecting the order of magnitudes it was found by assuming no-flow no-loss fields still leads to a satisfactory result. It is again evident that the route of oversimplification was taken due to a lack of computational power at the time of this project.

The application to T-burner and radial SRM will not be discussed here. The main result is equation (A.2.1). Though previous analysis had been done on interpreting the results of T-burners in particular, this paper did much to resolve the discrepancies between previous works. The approach that followed gave a more general result and is applicable to both high and low frequencies. The analysis was however limited by the fact that the non-isentropic boundary condition and dissipation in the acoustic medium were not considered.

"Non-linear Axial Combustion Instability in Solid Propellant Motors" by W.G. Brownlee (42) established pulse testing in SRMs (1; 5; 28; 31; 33; 46; 53; 62; 69; 75; 121; 126; 136; 138; 145–147; 147; 147; 148). Over 400 tests were performed at the Caltech Propulsion Laboratory and the observations have become known as the Brownlee-Marble observations. F.E. Marble was the professor under whose direction Brownlee performed these experiments.

The results from these tests showed reproducible results. It has also long been regarded as the true test of any model on combustion instability. The same propellant formulation was used for all tests with various grain cross sections being used. The findings from the research were as follows:

- Dependence of the axial instability on the restriction ratio K_n;
- Steady burning characteristic: At constant pressure the burning rate increases until 50% of the web is burnt out. It then decreases until burnout. The burning rate r_b is greater at 100% web burnt than when 0% is burnt. This phenomenon is independent of flow effects, radiative heat transfer etc. To be able to compare the data for a propellant with its fixed properties, several firings at different web fractions are required;
- Developed a correlation between pressure and the restriction ratio K_n;
- Geometric Scaling: Two motors separated by a scaling factor of 4 were investigated. It was found that the two motors results were indeed parallel to each other, with the larger motor being more stable than the smaller motor. This was due to the decrease in peak-to-minimum ratio of the wave amplitude. At the time not enough tests were performed on a larger motor. It appeared, however that the increase in stability was not necessarily proportional;
- Motor Length: Low values of length and diameter ratio tend to inhibit axial instability while for higher values it is correlated by K_n;
- Grain Cross Section: The instability is mainly affected by the surface area and that the effect of the geometry can be correlated by K_n. The instability of a slab rocket seems less severe and is probably due to the wall losses;

- Propellant additives: By adding 5% aluminium alloy it was found the stability was increased substantially. It was further increased when pure aluminium was used;
- In performing the stability tests on the subscale motor using additives it was found that the stability was not increased. Though no explanation is given the author claims that subscale motors are not suitable for relative stability tests.
- The increase in stability does not increase proportionally with increase in additives. Too much additives may be as detrimental as too little or no additives.
- Longitudinal and Tangential instability: Tangential instability seems to conform to the K_n correlation. It also seems to not be present in aluminized propellants. The most interesting aspect is that tangential instability dampens longitudinal modes. The mechanism proposed is that longitudinal modes is a strong function of velocity coupling, and that a rising tangential mode prevents the longitudinal mode from coupling with the surface of the burning propellant. Therefore, the longitudinal mode is robbed of a primary source of energy. Tangential mode instability seemed to be more severe with an increase of 50-70% DC pressure shift when compared to that caused by longitudinal modes.

The Brownlee-Marble observations will be revisited when discussing modern data reduction tools and predictive methods as proposed in (5).

1965: Gordon Moore's observes that the amount of transistors per unit area doubles every 24 months and is termed "Moore's law".

"Theory of Combustion Instability in Solid-Propellant Rocket Combustion" R.W. Hart and F.T. McClure (4) is widely referred by other authors (5; 12; 23; 25; 31; 46; 53; 77; 78; 124; 136; 139; 140; 142; 149–153) and "Experimental Solid Rocket Combustion Instability" by E.W. Price[3] (121) is also widely referred to (23; 53; 123; 131; 136; 142; 154; 155). Both these papers are in depth reviews on combustion instability circa 1965 and provide road maps for future work. Though these works are widely referenced they will not be discussed in detail as they add nothing new to combustion instability theory. These articles serve as historical markers and set out a clear framework to the problem as well. They positively identified many terms that have become common combustion instability terminology.

The paper by Hart and McClure focuses on the progression of combustion instability theory. The acoustic gains and losses are discussed as well as the prevailing mathematical description of the gains and losses. It must be noted that these results are generalised forms of work that were previously published. The combustion process is also discussed with particular attention being given to the pressure and velocity coupling.

1966: The Amateur Computer Society the first Personal computer club is established by Stephen Gray.

1967: IBM create first floppy disk

1968: Intel is founded

In the time period from 1966-1968 some of the the most influential papers were published on the subject by F.E.C. Culick (23; 52; 124; 156) and referenced by (2; 5; 12; 13; 25; 27; 28;

[3]E.W. Price is a Regents' Professor Emeritus in the School of Aerospace Engineering. Is a fellow of the AIAA. Is a member National Academy of Engineering. He is also credited with the invention of the T-Burner

31; 46; 52; 55; 55; 59; 64; 78; 119; 124; 132; 133; 135; 142; 153; 157–162). Culick was credited by another authority in the field of combustion instability, G.A. Flandro, by acknowledging that he(Culick) provided instability a "World Class framework" (105). Culick's "A Review of Calculations for Unsteady Burning of a Solid Propellant" published in 1968 will be the focus as it is an end product of the previous publications.

Three traits of the analysis have become known as the QSHOD Approximation:

- The model is linear thus only the stability boundary is investigated;
- Quasi-steady gas phase;
- The propellant is assumed one-dimensional and homogeneous;

The analysis starts with defining the admittance function, A_b, as it is the simplest problem that requires knowledge. A full development of admittance function and its calculation will be discussed in a later section. The admittance function can be described as a complex quantity and is dependent on the material properties and the frequency. The real part of A_b is the fraction of the fluctuating velocity that is in phase with the pressure. The rate of work done at the surface is proportional to the real part of A_b viz. $A_b^{(r)}$. If the real part is positive the waves will grow or be driven. For a larger$A_b^{(r)}$, the greater the likelihood that combustion will drive combustion instability.

Viewing the admittance function in terms of reflecting traveling waves it becomes clear that velocity response is not addressed adequately. It also becomes clear that determination of the admittance function from laboratory devices was in its infancy and much development was still required. These analysis become important in establishing a boundary condition for analytical treatment of waves in the combustion chamber.

The different analysis are broken into three categories: Time-lag theories, pure heat transfer theories, and what was termed as "complete" Calculations. The first two analysis are regarded as obsolete and are discussed briefly by Culick. He pointed the short comings of especially the Time-Lag theories out.

From Culick's research it can be found that the problem is divided into three areas:

- Solid phase: Treated as a homogeneous layer up to the surface, unanimity seems to exist regarding the solution of the gas phase;
- Gas phase: Analysis differs mainly in regard to the gas phase;
- Interface region: Collapsed to a plane and provides the matching condition between solid and gas phase.

As stated earlier the analysis is one-dimensional, and the materials properties are averaged over chemical composition. No means existed at the time to deal with the three-dimensional properties of composite propellants. Approximations had been attempted but inhomogeneities and the influence of metal particles had not been studied adequately.

Culick's work opposed to the majority previous work does not attach the coordinate system to the burning surface. When unsteady burning occurs, the interface moves relative to the mean position and the surface oscillates harmonically with the pressure oscillations. Culick uses an inertial system: that is the origin is fixed to the average position of the burning surface, with the burning rate measured from laboratory tests indicating the movement of the surface. This approach being analogous to airfoil theory.

The problem as stated before is separated into three areas: solid; interface; and gas phase.
Solid Phase:

- Mass and momentum are trivially solved;
- Energy equation in terms of temperature is used;
- Introduces a dimensionless frequency parameter;
- Takes account of the motion of vaporization of the surface;

Solid-Gas Interfacial Region:

- Three important relations: conservation of mass and energy and the conversion of solid to gas;
- Mass and energy are determined by considering small control values;
- Collapses the region so that accumulation of energy and mass within the region can be neglected;
- "Jump" (a sudden increase or decrease in parameters) conditions are found when unsteady mass and energy transfer occur both up and downstream;
- Since the mean gas density($\bar{\rho}$), is much smaller than the propellant density(ρ_p), the term $\bar{\rho}/\rho_{prop}$ is assumed negligible;
- Arrhenius law is assumed to hold true for conversion from solid to gas. Unlike previous work, the dependence on pressure is included;
- Time-lag is introduced arbitrarily to represent the lag or lead between surface temperature and pressure. It is ultimately ignored as no means existed to calculate them from chemical kinetics;
- Arrhenius law assumption has little significance as the crux of the matter is that mass flux responds to surface temperature and pressure. Thus the linear relationship derived must hold;
- A relationship which accounts for the mass conservation at the surface and the conservation of energy at the interface now exists.

Gas Phase:

- Most involved part of problem;
- Uncertainty exists on which approximations can be used for which propellant;
- Limited success achieved with simplest analysis;
- Simplification seems possible due to the dominance of the response of the solid phase;
- Uncertainties over what level of simplification will be representative;

- Analysis starts with the diffusion of the separate species using mass, concentration and energy balances;
- Lewis Number is assumed to be unity;
- Conservation of momentum is reduced to the pressure being uniform throughout but varying with time. This is due to long wave lengths and low speeds;
- The energy, mass and concentration are coupled to the change in density. At the time this was a large obstacle;
- To avoid the change in density the frequency is assumed sufficiently small that the time derivatives are negligible known as the quasi-static assumption;
- As stated in (22) the thermal response is much faster than that of the solid;
- Many, but not necessarily all chemical reaction are faster than the solid thermal response;
- Thus the quasi-static assumption appears to be a valid approximation under some circumstances;
- The gas phase equations are independent from the frequency;
- The mass transfer and the admittance functions variation will only be a function of the slow response of the solid.

The analysis up to this point is similar to much of the previous work and has been called "thermal theories" by Culick. This is because to the focus is on the heat transfer; diffusion of mass seemed to be a minor concern.

After discussing the theories that fall in between the thermal and more complete theory, the discussion proceeds to that of more complete calculations. The analysis now moves to the flame structure and chemical reaction in the interface zone. Culick discusses the work of several authors and their assumptions regarding flame structure. He shows that regardless of the assumptions made concerning the flame structure a two-parameter form of the response function exists. The details of each analysis will not be discussed, the common elements are:

- Solid phase reactions occurs in the thin burning surface. This is possibly not appropriate as the surface is not smooth as well as the occurrence of reaction in the solid phase. Including the assumption that the decomposition of the propellant does not occur at lower temperatures than that at the surface;
- Gas phase is treated as quasi-steady;
- Isentropic assumption makes it possible to avoid detailed consideration of the flame structure;
- Whether the isentropic assumption is made or not the response function is in the same form.

Isentropic assumption is shown to be invalid. As elements pass through the flame, their entropy values vary. This variations can possibly carry on to the edge of the flame zone and then is carried away by the flow. Thus an entropy or temperature wave is created with a much shorter wave length than that of the acoustic waves (entropy cannot be measured directly but the temperature variations can be measured). There are dissipative affects present and if they are sufficiently large the entropy fluctuations could be ignored at a particular plain. If the region is thin, then the admittance function could be calculated using the isentropic assumption. It has also been shown that the attenuation of these waves is not significant and that the dampening length large if only thermal conductivity is considered. At the time the first attempts were being made to measure the temperature fluctuations in order to determine the entropy fluctuations. It is important to note that the temperature fluctuations become important when attempting to calculate the admittance function.

Analysis is born out of the need to be able to interpret observed results. The response function is important due to its central role in combustion instability. The purpose of this analysis is to be able to interpret experimental results and ultimately to categorise propellants in terms of a small number of parameters. It is painfully obvious at this point in time that quantitative analysis of all aspects is not possible, the calculations that have been reviewed are inadequate to accommodate the necessary number of measurements. The specifics of the short comings when compared to experimental data from L* and T-Burners will not be discussed as the shortcomings have already been highlighted.

Culick's paper clearly lays out a framework for the problem, and gives an in-depth look at the status of combustion instability theory circa 1968.

R.L. Coates and M.D. Horton presented "'Design Considerations for Combustion Stability"' (145) is a departure from the abstract theory that has been discussed thus far. They provide practical and usable design guidelines. They subdivide the problem into three areas: L* instability, pulsed instability and acoustic instability. As mentioned earlier L* instability is a strong function of geometry and thus a simple correlation is presented.

Pulse induced instability was briefly discussed. At this point not much work had been performed and little data was available from pulse tests. However the following guidelines are presented:

- Found in SRMs with a length to diameter ratio higher than ten;
- There exists a critical pressure;
- Is sensitive to temperature and the restriction ratio;

Concluding that there is no way to predict if a motor will indeed be unstable. They stress being pre-emptive by insuring there will be no pressure pulses that can induce instability. This entails decreasing the possible sources of ejecta particles.

Acoustic instability here refers to spontaneous occurrence of oscillations. Referring to Culick's work (124) they point out that the current theoretical models are of little use as most parameters required are unknown. Furthermore, it is unlikely that they would be known in the near future. There analysis is based on T-burner results and the direct application to a SRM. The stability criteria simply being if the total acoustic energy gain is negative the motor is stable and if positive the system is unstable. The analysis for the first longitudinal mode is as follows:

- Determine the growth constant α_g from the T-burner test as shown in Chapter B. Unlike later work an admittance function is not calculated. Instead, the acoustic energy generation is calculated. The acoustic generation can then be manipulated to be applicable for a SRM of any geometry;

- The wall losses are calculated empirically;

- The particle losses are calculated assuming that wall and particle losses are predominant and all other loss mechanisms can be neglected. Subtracting the wall losses from the decay constant α_d found from the T-burner test.

- The final loss mechanism considered is termed chamber losses this include wall dampening and nozzle losses. This is calculated from a resonant curve. The resonant curve is generated by constructing a model of the motor using a real or simulated grain. The nozzle is covered with an anechoic(no echoes) coating. The motor is then filled with a cold gas (helium typically). The criteria being ratio of the product of absolute temperatures, molecular weights, and ratio of specific heats of the cold gas and the combustion gases are equal to one. A microphone and speaker is then used to create a resonant curve. It is important to remember this resonant curve is only valid for a singal moment during the burn time thus it would be necessary to generate several such curves at different points during the motors burn time.

This analysis is relatively simple and easy to apply. This is an entirely linear model but, as a preliminary calculation in the design stages can give a strong indication to the stability of the motor.

1969: Laser Printer is invented by Gary Starkwaether

A.2.2 1971-1980

1970: Intel announces the 1103 memory chip with the capacity to store 1000 bits of information classified as Random Access Memory (RAM) Intel also releases the Intel 4004 the first microprocessor. A computer programming language ADA is developed by U.S. Department of Defence capable of designing missile guidance systems.

The 1970's was in many ways again dominated by the work published by Culick (24; 53; 54; 63; 64; 90; 142). These works attempt to progress the theoretical understanding. Other research can be classified into two parts interpretation of experimental results; and the advent of numerical techniques for computer analysis towards the end of the decade. The 1960's attempted to establish the fundamental theory and experimental procedures. The results from these analyses at best could be described as general trends to aid a SRM designer to avoid combustion instability.

"Stability of Longitudinal Oscillations with Pressure and Velocity Coupling in a Solid Propellant Rocket" by Culick (53) and is (2; 5; 25; 27; 28; 31; 46; 55; 69; 70; 82; 139; 147; 150; 157; 161). In contrast to (124) this work is more concerned with a SRM system as a whole and is parallel to (23) with the fundamental difference being that the oscillations are parallel to the burning surface and the mass flux is normal to it.

The mass flux normal to the traveling wave as a dampening mechanism is credited by R.L. Coates[4] (150) as enhancing the understanding of acoustic instability although not experimentally proven at the time. It has become known as "flow turning". This term became a topic of debate for several decades. The main emphasis of the article is that of studying longitudinal or axial waves.

The standing waves are regarded as one-dimensional with flow fields being three-dimensional. It is however not necessary to construct a three-dimensional representation as it is shown in (23) that the main effects of mean flow can be reduced to convection of wave energy and is represented by a volume integral of the convective operator acting on the volume density of acoustic energy. Since the energy of the wave (when one-dimensional) depends only on the axial position it is only then that the axial component of flow velocity becomes important, implying that the one-dimensional representation is sufficient. The analysis follows:

- To couple surface behavior with motions parallel to its surface. New source terms must be introduced;
- The SRM is assumed to be radial burning. Thus the longitudinal direction remains straight with a variable cross sectional area;
- A mass balance of the gases is performed as a one-dimensional approximation. The gases are treated as one component "average" with constant specific heats obeying the ideal gas law. Viscous forces and heat transfer within the gas is ignored;
- Influence of small particles are taken into account based on the evidence presented in (163–166) and are treated in an average way as a fluid;
- A mass balance of the particles are performed;
- Momentum equation combines momentum of the gases and particles;
- Combining the mass balance with the combined momentum equation and rearranging the result the momentum equation for gas flow is derived;
- A term F, which represents the drag force per unit volume between particles and the gas, is part of the momentum equation;
- This force is regarded as the principle dampening factor of acoustic waves;
- An energy balance is performed for gas and particles;
- Thermal energy of particles is ignored;
- It is assumed that the particle and gas energies entering from the burning surface is equal to that of the local average;
- Mass equations are again used to eliminate the cross sectional area from the left hand side of the equation;
- Kinetic energies are eliminated;

[4]R.L. Coates authored and co-authored many papers in the 1960's and 1970's with M.D. Horton. The focus of their work was T-Burners

- The equations are manipulated to finally attain an equation in which $\eta = (1/\gamma \ln p)$ is given as the normalized variable.

In this analysis the points of interest are that of the mean and fluctuating motions that are parallel to the surface. The mass flux as stated earlier is normal to it. Thus the mass flux should dampen such motion. It was not clear at the time what the exact mechanism is that sustains such motions. It was also important to note since this is a one-dimensional analysis of a three-dimentional problem many details are lost or "'smeared out"'. For instance, how spherical waves from a burning surface interfere to form a standing wave cannot be explained. The authore notes this was done to avoid over complicating the problem by attempting to answer such questions. The details are locally averaged for such interaction over the chamber cross section, and then included in the source terms.

The next step is to linearize the problem followed by finding the approximate complex frequencies and mode shapes. The following sections are essentially mathematical manipulation. Thus they will not be discussed here and much of it will be discussed in detail in other sections. The major contribution of this paper was to introduce the dampening of the mass flux normal to the velocity parallel to the burning surface as well as the inclusion of particulate dampening. It is also clear that velocity coupling is a major obstacle in using the proposed analysis. Culick makes it clear at this point that still much analytical work needs to be done.

1971: Pascal programming language is invented by Niklaus Wirth

The Paper "Non-Linear Growth and limiting amplitude of acoustic Oscillations in Combustion Chambers" by Culick (90) was an attempt to solve the non-linear problem. It is clearly evident, that at that time, there was insufficient knowledge to construct a simple, realistic, non-linear model. The interaction between pressure fluctuations and burning remain linear up to substantial amplitudes in the case of SRM. The losses of energy consist of: the nozzle, attenuation of particles in the gas, and the viscous losses at the surface. The nozzle loss is assumed linear whereas the particle attenuation and surface losses are regarded as non-linear. Thus only two processes are considered non-linear. The approach however, cannot be applied shock waves as they are non-linear in nature and extremely so. This analysis could also be applied to afterburners and other combustion chambers, the main focus is solid rocket motors.

The general formulation of the governing equations are the same as that in (23; 53) but the terms that include particle attenuation and surface losses are not linearized. To calculate the amplitude of the oscillations, it is assumed that the spatial features vary only slightly with linear classical forms. Thus the analysis is only concerned with the non-linearity with time and not the wave forms. The admittance function is introduced. Since the admittance function is a complex number, it is preferable to represent the imaginary part as a real number. From this point on the paper is again largely mathematical manipulations. Culick proceeds to apply the analysis to T-burners and SRMs.

In the case of SRMs, it is noted that the assumption that the surface response is linear may not be appropriate. This is because energy requirement at higher amplitudes may become a significant part of the total energy release due to the combustion process. Again velocity coupling may also play an important part. An interesting result is that for an extremely large α, the energy required to drive the oscillations would only be about 1% of the total energy released from the combustion process. Though the interaction may be

non-linear at the time nothing was known of such behaviour. This could only be included in a heuristic way by adding additional function (emperical in nature) to the response function. Researchers in particular Flandro argue that this is merely adding an extra degree of freedom and such a function should arise naturaly from a fundemental analysis (55). Again the lack of knowledge of velocity coupling is raised.

This analysis (though not applicable to shockwave phenomena such as is typical of Pulsed Instability) does lend itself to analysis of other practical problems of combustion instability. This analysis also provides a frame work into which other non-linear phenomenon can be incorporated.

1972: C programming language is invented at Bell labs by Dennis Ritchie.The compact disc is invented.

"Oscillatory burning of Solid Propellants including Gas Phase Time Lag" by J.S. T'ien (118) represents a departure from the Quasi-Static gas phase assumption. The limitations of the quasi-steady state is that the period of oscillation needs to be much larger than that of the gas residence within the flame. This makes it inapplicable to higher frequencies. Dynamic effects can only be evaluated when the period of oscillation is smaller or comparable to the solid thermal lag-time.

Analysis of non-quasi-steady gas phase:

- The flame is assumed one-dimensional, premixed and laminar;
- One step forward chemical reaction;
- Specific heats, molecular weights and the coefficient of heat conduction is assumed constant;
- Lewis Number assumed to be unity;
- The energy, mass in terms of chemical species, and continuity balances are performed;
- The equations for the reaction rate of the fuel and oxidizer is substituted into the energy, species and continuity equations and are introduced as non-dimensional variables;
- The reaction rate is rewritten in terms of mass fractions of fuel, oxidizer and product;
- A perturbed analysis is performed;
- Since the wave length is always much longer than the flame thickness, pressure is assumed as a function of time only. The analysis to this point represents a quasi-static analysis;
- T'ien eliminates the density by using the ideal gas law. He states that the mean temperature is equal to the mean velocity in the mass, energy and continuity equations into which the rate equations were substituted;
- Three equations are obtained that create a fifth order system. Solved using numerical techniques.
- The boundary conditions at the flame edge $x \rightarrow \infty$ (x is the distance from the solid surface), firstly assumes that the mass fraction of the fuel and oxidizer equals zero. The

second is more complex for steady state viz. the change in temperature equal to zero. However this analysis is not concerned with the steady state and such analysis would not be valid for high frequencies. Thus it is assumed that the flow close (but outside the flame) is isentropic. In essence the entropy of each particle remains constant as it is leaving the flame. An expression for this is derived in terms of temperature and pressure and changing the coordinate system so that the edge of the flame is zero. The equation is then differentiated, non-dimensionalized and yields the boundary condition. In reality the distance of entropy decay of the wave is too great to make applicable as a boundary condition for chamber acoustic instability. Thus the derived equation is used at an appropriate location;

- The following boundary and the remaining two are at the surface of the propellant. The first comes from the fact that the oxidizer and fuel mass fractions are determined by propellant composition. Thus the mass flux at the surface composition can be determined and is perturbed.

Solid Phase analysis:

- The usual assumption of homogeneous propellant is made as well as a no condensed-phase chemical reaction;
- The fourth boundary condition is obtained from the heat transfer from the solid to the gas that yields a relationship between surface temperature and temperature gradient;
- The fifth boundary condition comes from combining the Arrhenius law and the continuity equation. As with the other equations it was perturbed and non-dimensionalized.

With the advent of numerical techniques and increased access to computers, it was possible do perform this analysis. Many of the simplifying assumptions were to make the calculations possible. T'ien uses the Runge-Kutta method to solve the three differential equations and the five boundary conditions. Apart from moving away from the quasi steady-state assumption, it shows that technology had advanced to a point where such analysis could be possible.

1973: First Cell Phone call made at Motorola.

"The Stability of One-Dimensional Motions in a Rocket Motor" by Culick (24) is essentially the same analysis as (53) and serves to highlight modifications and attempts to clarify some points. It also serves to provide necessary results for companion paper(54). Therefore, the modifications and clarifications will be discussed here and serve as bridge to when the three dimensional case is discussed in the companion paper. The modifications and clarifications are as follows:

- The variable cross section is approximated as zeroth order or an order of magnitude approximation. This produces more accurate results and allows the results to be compared to the three dimensional case;
- As previously the conservation equations are linearized and a wave equation for pressure is established;

- The mean flow and particulate effects matter are represented. Residual burning term is also introduced;
- The boundary condition is inhomogeneous due to the direct affects of: surface combustion, particulate matter, the exhaust nozzle and mean flow;
- For analyzing stability of disturbances, it is necessary only to consider the harmonic motions. The problem reduces to solving the complex wave number;
- The difference in gas temperature leaving the surface and the gas temperature is accounted for;
- The difference of particulate temperature and average gas temperature is accounted for.
- Applying the solution of the complex wave number as in (53) an equation is found in which the acoustic energy fluctuation is given as a function of the combustion, exhaust nozzle, mean flow/acoustic surface interaction, particulate matter, residual combustion, and moment addition at the boundary contributions.

In the discussion of coupling between combustion and wave motions a distinction is made between the case where the velocity is parallel and perpendicular to the burning surface. It is necessary to distinguish between the two cases. In both cases fluctuations are normal to the surface. The parallel and perpendicular denotes the local acoustic fields and can in both cases be expressed in terms of the admittance function. For more detailed understanding of the coupling it would be required to proceed further. However for the study of stability of motors and interpreting laboratory data, this is sufficient. As long as it is recognized that two functions are required when considering the coupling between combustion and wave motions.

1974: The Intel 8080 becomes the standard of the micro computing industry.

It seems appropriate at this time to introduce G.A. Flandro[5] though he had published papers as early as 1964. "Solid Propellant Acoustic Admittance Correction" in 1974 (167) is one of his first widely recognized publications. His research has become prominent in the mid-nineties to the present. He authored and co-authored many papers on the subject of combustion instability. Flandro's paper (167) as with Culick's (24) emphasises that when calculating the admittance function from T-Burner data, one must also consider the orientation of the wave to the burning surface. Laboratory tests and their data reduction will be discussed in detail at a later stage.

1975: One of the first PC's Altair 8800 shipped by MIT; first flight simulator demo is shown; first PC programming language is developed by Paul Allen and Bill Gates; and Apple is founded by Steve Wozniak and Steve Jobs.

The companion paper to (24) "Stability of Three-dimensional Motions in a Combustion Chamber" by Culick (54) is also widely referred to (2; 5; 16; 25; 31; 46; 55–57; 63; 77; 78; 144; 152; 157; 168; 169). The main purpose of this paper is to incorporate the viscous processes

[5]Dr. Flandro is the first professor to fill the million-dollar Edward J. and Carolyn P. Boling Chair of Excellence in Space Propulsion at UTSI. He has published extensively on non-linear combustion instability in particular.

as one-dimensional estimates into the three-dimensional analysis. This paper adds nothing new to the subject as noted by the author, but attempts to clarify some assumptions. Three-dimensional analysis is essentially the same as the one-dimensional case in that analysis starts with mass, momentum and energy balances. However, when one considers the harmonic motion this leads to an Eigen value problem for a three-dimensional space. The solution for a wave number of the n^{th} order can be found in (23).

Incorporating one-dimensional results into the three-dimensional analysis in large part revolves around the orientation of the wave to that of the burning surface. To account for the limiting cases of parallel and perpendicular acoustic velocity, a mathematically intensive procedure is used. It will not be discussed here. It is, however, apparent when the author applies this analysis to the pulsed motor firing performed by Brownlee and Marble (by using the admittance function based on E.H. Perry's T-Burner analysis) that, if the analysis is correct, a different admittance function is required for parallel and perpendicular velocity. The author notes that the T-burner analysis may also have been erroneous. The dependence on the laboratory results in any analysis again becomes evident. The results of any analysis is dependent on the quality of the experimental data and this project will attempt to address the issue.

Culick revisits Cantrell's paper (108) that was discussed earlier. This analysis was also three-dimensional and many of the results are identical to that obtained by Culick (24). There are however some limitations and differences. They include:

- Cantrell and Hart's analysis does not include viscous effects;
- Proposed that the stability be studied by analysing the rate of change in energy within the chamber;
- Residual combustion is not accounted for;
- Influence of particles are ignored;
- Particle dampening is not accounted for;
- Total energy of the system is considered when only the change in acoustic energy should be considered;
- Analysis is linear.

Culick finally points out that his analysis (though linear) could be extended to the non-linear case. This is an illustration of how theory consumes and eliminates each other.

1976: The 5.25 inch floppy is invented and Intel 8086 is released.

"Non-linear Behavior of Acoustic waves in Combustion Chambers I and II" are companion papers by Culick (63; 64) and are widely referenced (2; 5; 16; 31; 46; 64; 170–172). The main drawback at the time was the fact that elaborate numerical computations based on the governing differential equations were unsuitable because of the unknowns regarding the input information. The governing equations (as partial differential equations) are converted to to a set of ordinary non-linear differential equations in time for the normal modes of the chamber. Culick mentions several times throughout the text the desire to simplify the results

to a point where the numerical computations can be performed cheaply. The work is based on the linear analysis of (24; 54) and extends the work of (90).

The first part of this paper deals with the formal aspects. Much of these analyses have been discussed previously. Some model refinements and simplifications were:

- The wave is regarded as having a fixed shape with an amplitude that varies with time;
- The existence of all standing waves are accounted for. Thus the unsteady field can be synthesised from its Fourier Components;
- Interaction between entropy waves and acoustic waves are ignored;
- Second order differential equations are reduced to first order differential equations;
- Method of averaging is used: Essentially observed instabilities are periodic with amplitudes changing slowly over time. Thus equations for amplitude and phase can be found by averaging the second order differential equations over an interval τ;
- It is assumed that the fractional changes of the amplitude and phase are small during the interval of averaging;
- The general result has both linear and non-linear parts. This is especially useful since the linear components are clearly shown and easily incorporated;
- An analytical solution is only possible when considering two modes. For more than two modes it has to be solved numerically.

The second part of the paper deals with specific cases. It is important to remember that the approximate analysis is based on a iteration/perturbed method. The first case is the linear and non-linear attenuations of waves by gas/particle interactions:

- The Reynolds number for the particles diameter generally falls outside Stokes' Law region. This introduces a new non-linear influence to the problem;
- The numerical technique employed uses the linear solutions as an initial guess. Using it in an iterative procedure produces the next approximation and thus avoids solving the non-linear laws for drag force and heat transfer;
- The larger the particles the higher the harmonic content due to reduced drag (for the same amount of loading there is a significant increase in surface area as the particle size decreases). Conversely smaller particles dampen out higher frequencies;
- Particles change the speed of sound with a corresponding shift in frequencies;
- Demonstrates that non-linear generation of harmonics has a marked influence on the character of the attenuation of waves;
- The value for the decay constant changes dramatically as the wave dies out.

Non-linear viscous losses on an inert surface:

- Viscous losses influence can be significant in stabilizing the system;

- The presence of oscillations can increase heat transfer and can cause structural problems;
- Incorporates experimental results into the analysis of the first section;

Influence of transient surface combustion is of particular interest since all energy comes from the response of the burning surface:

- The simplest representation is used;
- "'True"' transient behaviour is ignored to obtain formula that are "inexpensive" to use;
- Only surface combustion is considered. The same approach, however, can be applied to residual burning;
- Response function same as proposed in (90).

Finally, Culick applies the analysis to stability of Longitudinal Modes:

- Analysis simplifies significantly when considering only longitudinal modes;
- Four linear contributions are considered: nozzle losses, condensed material in the gas phase(particles), surface combustion, and flow turning("one dimensional approximation to inelastic acceleration of flow issuing from lateral surface" (64));
- Using the numerical analysis of two motors and comparing the results to that of the approximate analysis;
- Comparing the approximate and numerical results, it was found that there was a difference in results. Since good results had been obtained for particle dampening and the same response function was used in both cases, the nozzle influence was found to be embedded in the data. The nozzle attenuation of the approximate analysis is altered to match the numerical analysis;
- Only 20 cycles were completed (0.02222sec) for the second motor. The numerical and approximate analysis do not match. Two reasons are given: firstly, since only the first twenty cycles were considered the numerical results may lead to incomplete results. If, however, a limiting amplitude was reached after 20 cycles, the approximate analysis gives incorrect results;
- It is clear from this linear analysis that non-linear interactions are active even at such low amplitudes.

From this analysis it becomes apparent yet again that the researchers work is seriously constrained by computational power. Terms such as "inexpensive" are often used. This illustrates the lack of tools and also the lack of the availability of these tools to be able to fully test their models.

Culick's perturbed wave model has been consumed and modified over time. Researchers have added further corrections such as rotational corrections and turbulent mean flow. The work done by Culick established the framework for the work to follow.

1977: Apple, Commodore and Radio Shack release mass market PCs. Apple becomes incorporated.

1978: Dan Bricklin develops VisiCalc the first spreadsheet.

1979: Half a million Computers in use in the U.S.A

"Velocity Coupling in Oscillatory Combustion in Solid Propellants" by E.W. Price (173) clearly illustrates the difficulty to quantify and incorporate velocity coupling into stability predictions. The work discussed previously focuses on the pressure coupled response as a function of the propellant and not a as function of position in the flowfield. It has been well established that the flowfield can affect burning rate (erosive burning). This interaction is (analytically speaking) a formidable undertaking as it will have to account for increased heat transfer, mixing in combustion zone, and shear stress at the propellant surface.

Spatial variance is inescapable when considering erosive burning. Previous work has simplified the problem by taking an average over the cross section of the flow channel. This means that the flow parallel to the surface is one-dimensionalized. By its very nature such a step is contradictory as certain burning processes are explicitly eliminated by such an assumption. Researchers, however, have achieved to some degree (by use of experimental results and subsidiary modeling) to minimize this "impropriety". Researchers since has confirmed, however, that the response can not be ascribed to pressure fluctuation alone.

The term "'velocity coupling"' is born out of the one-dimensional analysis because it could be ascribed to a single variable such as mean velocity. This effect is assumed locally additive to an independent pressure coupled response. Experiments have been set up to determine such a response as a counterpart to the pressure coupled response.

Another problem apart from one-dimensionalising 2 or 3 dimensional problems, is that is not plausible to assume the same response will occur at each location along the wall flow. Due to the dramatic change in conditions with location. This makes it impossible to produce a velocity coupled response as a property of the propellant.

Price goes on to note that at the time it was not possible to determine: a) how rigorous a combustion model will have to be used to obtain useful results for parallel flow; or b) if the response could be modelled, firstly, as separate to the pressure oscillations and the local parallel flow into independent variables; and secondly, whether the two independent variables can be expressed as properties of the propellant.

Finally, Price advocates for the abandonment of the one-dimensional representation even if this would mean a drastic increase in complexity as well as labour required in order to compute the stability with more rigorous models.

During the last part of the decade the first attempts at using finite element analysis was introduced by Hackett (123; 134). In spite of some work that was done on the numerical techniques during this period, not one seems to enhance the understanding of combustion instability.

A.2.3 1980-1989

The 1980s were dominated by the progress made by Baum, Levine, and Lovine in numerical techniques to solve the combustion instability problem. They used Culick's model and extended it. Favourable results were obtained, but many issues were still not completely resolved, most notably that of velocity coupling. The ability of their analysis to predict the waveforms in even complex geometries, however, was a great step forward.

Concurrently Flandro developed an energy balance method that was less computationally intensive. His objective was to create an intermediate model that could aid the SRM designed in a semi-quantitative way. He also developed the first comprehensive model to incorporate vortex generation.

During this period the focus seems to have shifted from trying to develop holistic models to producing more correct models for certain phenomena and incorporating it into the framework provided by Culick. The topics such as admittance functions, vortex generation and velocity received much attention during this period.

1980: Paul Allen and Bill Gates are hired to create operating system for IBM. They obtained the rights to use an existing program from Seattle Computer Products to create DOS.

1981: IBM releases the IBM-PC with MS-DOS operating system. Osborne I, the first successful portable computer is released. Xerox introduces the graphical work station which influences both Apple and Microsoft Windows operating systems.

1982: Commodore 64 is released with 64 kilobytes of RAM and becomes the best selling computer of all time. HX-20 from Epsom is the first portable notebook computer. Intel releases the 80286 processor.

"Approximate Analysis of Non-linear Instability with Shock Waves" by G.A. Flandro (48) was initially ignored by the combustion instability community. A later study presented in (45) showed excellent agreement with both Baum and Levine's work as well as that of the Culick and Yang. This sees a move away from perturbed models to an energy balance model with a steep fronted wave. Shockwaves have been considered before by other authors (130; 174). Seemingly, it had been ignored up to this point since much of the previous work concentrated on linear analysis. This work attempts to reassess the importance of shockwave behaviour. Due to its relative simplicity and also that the results obtained using this analysis has been verified, made this model and its subsequent improvements useful as an initial means to evaluate the experimental results.

The models main purpose is to predict the limiting amplitude. Key factors, assumptions and methods are:

- Non-linear heat transfer and viscous effects are considered negligible when compared to the shockwave losses;
- Linear losses and gains are well represented;
- Steepening occurs at low amplitudes and in a short time period. Therefore, shockwaves are assumed to be present at all times as it approaches the limit cycle. It is found that initially the waves are weak acoustic waves that can be modelled as standing normal acoustic waves of the chamber. It also shows that the steepening of the wave is a consequence of the non-linear gas dynamics;
- Single shockwave with stationary waveform is considered for this analysis (although it is often found that multiple shockwave fronts may be present that greatly complicate both experiments and analyses);

- The traveling shockwave is connected to the motor acoustics. This implies then that it is possible to superimpose standing acoustic eigenfunctions to represent the standing wave.

- By using this analysis pressure and velocity fluctuations are found to be functions of the mean pressure, the relative amplitude, speed of sound in the chamber and the motor length. The relative amplitude is regarded as a slow function of time and the singular perturbation theory is used to solve both time scales present in these equations. It is necessary, however, to distinguish between events occurring on the fluctuating pressure scale which is significantly more rapid than the change in wave amplitude, mean geometry and thermodynamic conditions.

- Multiple shock fronts can be incorporated using a superposition of a single shock Fourier series;

- The energy of the wave structures is given as a volume integral that ignores the mean flow Mach number;

- The shockwave losses due to viscous and thermal effects are found to be non-linear. The losses are given in terms of shockwave area assuming a single one-dimensional shockwave;

- In considering combustion instability a stationary waveform is assumed as the limit cycle is approached. The energy coupling between modes can then be ignored;

- The amplitude is due to the balance between linear losses and gains;

- The non-isentropic shock losses are considered the principle non-linear loss.

It is of course important to make any model applicable to the geometry and grain configuration. The next step was to make this model specifically applicable to a cylindrical motor with a nozzle where the tubular grain with arbitrary length and position is also considered. This specific application will be discussed later and will be accompanied with a full mathematical description. The results and conclusions are:

- The results using the above analysis correspond favourably with actual test data;

- It is noted that low smoke propellants are used;

- Other losses such as particulate losses, wall losses, and velocity coupling mechanisms need to be clarified;

- It is found in pulse testing that protruding edges of the propellant can cause complicated waveforms;

- Low smoke and smokeless propellants in simple geometries are dominated by shock wave affects. It is important to note that metalised propellants have been phased out in modern SRM systems. As a result shock wave phenomena are more prevalent;

- Small chamber irregularities can cause non trivial losses;

- The author notes that this analysis at this point is only applicable to simple geometries.

J.D. Baum, J.N. Levine and R.L. Lovine published many influential papers between 1982 and 1988. These include (41; 69; 72–75; 101; 138; 138; 175) and have been influential in subsequent works (2; 5; 25; 27; 33; 37; 40; 50; 62; 75; 101; 146–148; 152; 153; 161; 170; 176). The range of topics covered by these works include numerical techniques, modeling, pulse testing, pulser modeling, acoustic refraction and cold flow tests. It is best to view this body of work as one entity that culminates in the final work: "Pulsed Instability in Rocket Motors: A comparison Between Predictions and Experiments" (74). Thus, the review of this work will start with the initial modeling and proceed to the results when compared to experimental data. Pulser Modeling and pulse testing will be discussed in detail in a subsequent section. The numerical techniques will not be discussed in detail. It is, however, noted that the technology at this point had developed to a point where it was possible to compare various such schemes. Therefore, much of the value of this work resides in the progress made in utilising numerical tools and the use of the ever-growing computational power. The published papers (73; 101; 175) merely describe the different results when using different schemes.

Their model, approach and objectives is best described in "Modeling of non-linear Longitudinal Instability in solid rocket motors" (75). The objectives were to further the understanding of the physical mechanisms as well as to, develop a comprehensive analytical model that can be used as a predictive tool in the SRM design process.

The approach consists of: Using the model of Levine and Culick (92) which is based upon Culick's non-linear theory (24; 54; 63; 64; 90) and modifying it to include: shock capturing finite difference schemes, velocity coupling, and also included the ability to model pulsers. The two main components of the non-linear analysis are a finite difference solution of two phase flow and a coupled solution of the non-linear transient propellant burning rate.

The model development key factors, assumptions and methods are:

- The gas is ideal, non-reacting and inviscid (except when interacting with particles) with constant specific heats Prandtl number, etc;
- Flow is Quasi-One dimensional;
- Cross sectional area is neglected;
- Metal particles are completely oxidised (no residual burning) and result in: inert particle spheres; uniform size distribution; uniform internal temperatures, negligible volume within motor cavity, different size particles that do not interact, and particles at a given location and size have the same velocity and temperature at the same location (thus acceleration and heat exchange is instantaneous);
- Particles and gas enter normal to the burning surface at the instantaneous flame temperature of the propellant;
- The effects of propellant surface inclination and non-isentropic flame temperature variations are accounted for;
- The equations of motion in terms of conservation of mass, momentum and energy are constructed as subject to the above assumptions;
- The equations of motion are supplemented with the ideal gas law, a steady state burn rate equation and a correlation for particle drag force in terms of the Reynolds number;

- The boundary conditions are: if the head end is inert, the particle and gas velocities are zero. Particles and gas are at thermal and dynamic equilibrium and particle density or distribution is obtained from the particle to gas weight ratio of propellant. The nozzle is treated as a Mach number boundary condition. The solution is terminated at the nozzle entrance;

- A non-linear transient burn rate model is utilised. It attempts to develop a complete non-linear pressure coupled response and a simplified velocity coupled model. The model of Denison and Baum(22) is extended to non-linear form.

- The assumptions of the current model include: Homogeneous gas and solid phase, the solid is converted to gas in an infinitesimally thin surface, only variation in the normal direction to the burning surface is considered, reactions within the propellant are ignored, quasi-steady gas assumption again employed, flame is attached to the surface, heat release from the surface to flame edge is uniform, gas reaction rate is function of pressure only, metal within propellant is not directly accounted for, specific heats and thermal diffusivity are constant.

- The Arrhenius equation is modified to account for pressure coupled surface reaction;

- The transient burning rate reduces to a non-linear heat conduction equation;

- Shock capturing finite difference scheme is employed. Several methods are discussed. These methods are discussed in more detail in (73; 175);

- Velocity coupling proves once again to be troublesome, due to the lack of understanding of the fundamental physical mechanism. This is because it was not the objective to develop a new model for velocity coupling, but to demonstrate that the non-linear model is capable of predicting several ad hoc functions. It was found that a heat transfer augmentation only produced significant non-linear affects at unrealistic velocity coupled responses. Thus a burn rate augmentations model was employed. This alters the burn rate to account for the acoustic velocity;

- Pulsers are also included into the model and will be discussed later in more detail.

One of the major advances is that this model was the first capable of treating complex geometries. It is indeed possible to analyze grain geometries with discontinuous cross sectional areas. It is even able to predict a secondary shockwave due to a reflection from a discontinuity within the solid rocket motor. The shock wave finite difference capturing scheme has proved itself to be capable of predicting complex wave forms. As a result this analysis is rather complex and requires an integrated numerical method as opposed to Flandro's approach (48; 49) that uses an energy balance method to predict the limiting amplitude and then superimposes the wave form. This simplifies the problem significantly. It is also shown that the DC pressure shift seems to be governed by the frequency and the propellant.

Triggering has been a source of much speculation. No prior analysis is capable to predict triggering of such complex wave structures commonly found in actual motors. Much insight is gained into the actual wave dynamics as stated in (48). After the initial disturbance, a weak acoustic wave is formed that quickly steepens into a traveling shock wave. Due to the non-linear gas dynamics energy is removed from the fundamental mode and fed to the higher harmonics which dampen the fundamental mode. If the amplitudes are sufficiently

large they will interact with the burning surface that feeds the higher harmonics with energy which in turn transfers energy to the fundamental mode as shown in Figure A.1. The authors describe the ability of the analysis to reproduce such behaviour as gratifying. It also seems that the triggering is caused by velocity coupling.

Mean pressure results are also of interest. It was found that for the three propellants tested, the normalized wave amplitudes differed in each case. In one case the wave amplitude increased with mean pressure in the other it increased with an increase in mean pressure, and one propellants response seemed to be independent of the mean pressure.

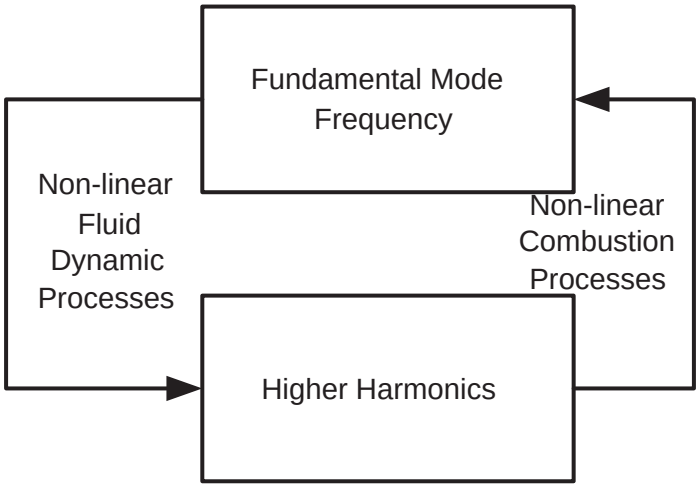

Figure A.1: Triggering Process [Redrawn from Baum and Levine (75)]

The effect of grain length has a direct effect on the fundamental modes. The longer the motor the lower the frequency. This is important to note because the response function of the propellant is often a function of frequency as well as pressure. The analysis can predict many of the observed data trends. It however could not reproduce the normalised wave amplitudes variations in normalized wave amplitudes as a function of frequency. The response function is thus deemed adequate to predict trends so that propellants can be compared, but not to accurately yield individual propellant variations. It is also shown that if accurate calculations are to be made, it is necessary to establish the propellants response function frequency behaviour. The frequency versus response function has a significant affect on the observed wave form and instability.

The fact that the motors are often more unstable toward the end of the burn time, seems to be a result of the internal volume increase and a corresponding decrease in mean flow velocity. This in turn seems to increase the non-linear driving mechanisms.

This analysis represents a large step forward in non-linear combustion instability analysis. This analysis has the ability to predict complex wave forms. However, it is stressed by many researchers as a ground rule that is true for all models, predictions are only as good as its input data. Again it is emphasised that better combustion response models are needed to improve the ability to predict and treat the combustion instability problem.

1983: THX is established, 10 million computers in the U.S.A. and Microsoft Widows is announced. Time Magazine nominates the PC as the machine of the year, the first non human nominee.

1984: 3.5 floppy disk becomes an industry standard. Apple Macintosh is introduced does not require typed commands uses graphical interface. Yellow book of CD-Rom standards is written.

1985: GNU manifesto is published. Intel release the 808386 a 16 MHz processor incorporates 275,000 transistors and can access up to 4 gigabytes of memory sells for $299.

"Energy Balance Analysis of non-linear Combustion Instability" by Flandro (49) builds

on the analysis presented in (48). The acoustic energy balance is extended into the non-linear regime (i.e. third order energy analysis). The assumption that the relative amplitudes remain of the Fourier components of the shock waves remain fixed, greatly simplifies the analysis.

The main aim of Flandro's work is to bridge the gap between extensive numerical investigations and simplified conceptual models. It merely attempts to understand the parametric affects of the volume, burning surface area, placement of propellant surface areas, operating pressures, and the nozzle configuration in a semi-quantitative way. Such a model of relative simplicity could greatly aid the SRM designer. It was found that this analysis corresponds very well with the result of numerically intensive techniques as discussed earlier. The model development is much more rigorous than that proposed in (48). The full mathematical development will be discussed later as it will form a basis to evaluate the results from this research program.

It is interesting to note that velocity coupling is not included in an *ad hoc* manner. Flandro argues that such terms should occur naturally within the model development. That in the past the velocity coupling has simply been used to add a degree of freedom in the experimental data analysis. It is further shown that many of the characteristics of velocity coupling occur in the second and third order combustion corrections. It is also noted that the non-linear combustion response (which is not considered) will not play an important part, but at this point in time no non-linear corrections have been brought to the linear pressure coupling response. No theory or non-linear pressure coupled response existed at this time and was the subject of future work. It is also apparent that access to quality linear data is also problematic.

1986: Apple introduces the Mac Plus with one megabyte of RAM. Microsoft is listed on the stock exchange. There are now 30 million computers in the U.SA..

The work discussed up to this point has detailed mostly the United States approach to the combustion instability. The French at the same time have developed a successful program. One of the distinguishing characteristics is the use of multiple devices to determine propellant admittance functions. F. Vuillot and P. Kuentzmann's paper "Flow Turning and Admittance Correction: an Experimental Comparison" (177) compares the admittance function obtained: a) using the Admittance correction technique proposed by Flandro (167); and b) using Culick's flow turning effect correction (23; 24; 54). Culick's flow turning term had come under scrutiny after the publication by M.K. van Moorhen (32). Both techniques were employed to obtain an admittance function. The experimental apparatus employed was a toothed-wheel apparatus. It was found that the Admittance correction gave better results. The test apparatus and the results will be discussed in detail in the section on experimental devices and analysis in Chapter B.

Velocity coupling remains to be a contentious issue among researchers. Brown R.S., A.M. Blackner et al's "Coupling Between Acoustic Velocity Oscillations and Solid-Propellant Combustion" (161) attempts to address this problem. The analysis consists of a cold flow experimental apparatus. The effects of the velocity on heat transfer are investigated. It was found that the results from both the linear and non-linear velocity coupling models did not correspond to the data obtained.

The linear model assumes that the heat transfer coefficients will oscillate sinusoidally with the axial position. The heat transfer coefficient maximum should correspond to the point where the acoustic velocity is at a maximum. This however was not observed.

The non-linear model expected that the heat transfer coefficient should not correspond to the acoustic waves until a threshold velocity is exceeded. This also did not correspond to the data. This in some part explained why previous models predicted unrealistically large velocity coupling contributions.

From the results the authors concluded that the model for velocity coupling should be reformulated. This further implies a complete reinterpretation of stability predictions. They conclude that all laboratory burners used to evaluate velocity coupling should be re-evaluated.

"Vortex Driving Mechanisms in Oscillatory Rocket Flow" by G.A. Flandro (178) gives a practical theory on vortex shedding that is compatible with practical systems analysis. It had been long established that vortices form within motors and had been shown by using windowed tests by Swithebank (179; 180) as early as 1963 (see Sotter and Flandro (181) for window test results). This study also provides the designer with the tools to avoid vortex driven oscillations by giving attention to the grain and internal ballistics. A more rigorous description of vortex generation will be given in a later section. This work eliminates some deficiencies in existing theory. For SRMs these difficiencies are:

- Aimed at far field radiation effects;
- Geometrical features unique to SRMs are not represented;
- Oversimplification of vortexes is assumed.

The following as assumed in the analysis:

- Irrotational acoustic oscillations;
- Incompressible vortical oscillations;
- Inviscid ideal gas;
- Isentropic flow in acoustic domain.

Figure A.2 shows the interaction between the vortices and hydrodynamic affects. From this figure it is clearly seen that the vortices and the acoustic field form a feedback loop.

1987: Chipsets begin to be found on Motherboards. IBM Introduce VGA. Windows 2.0 is released.

1988: 45 Million PCs in the U.S.A. Liquid Crystal is discovered by Friedrich Reintzer.

1989: Intel release the 486Dx with 1 000 000 transistors and has the ability to multi task.

A.2.4 1990-2000

The research in the 1990's sees even more dependence on computational power and the ever increasing numerical library that can be applied to solving various mathematical problems. There is seemingly a complete departure from the one-dimensional analysis. Researchers are no longer constrained by the expense of computational power.

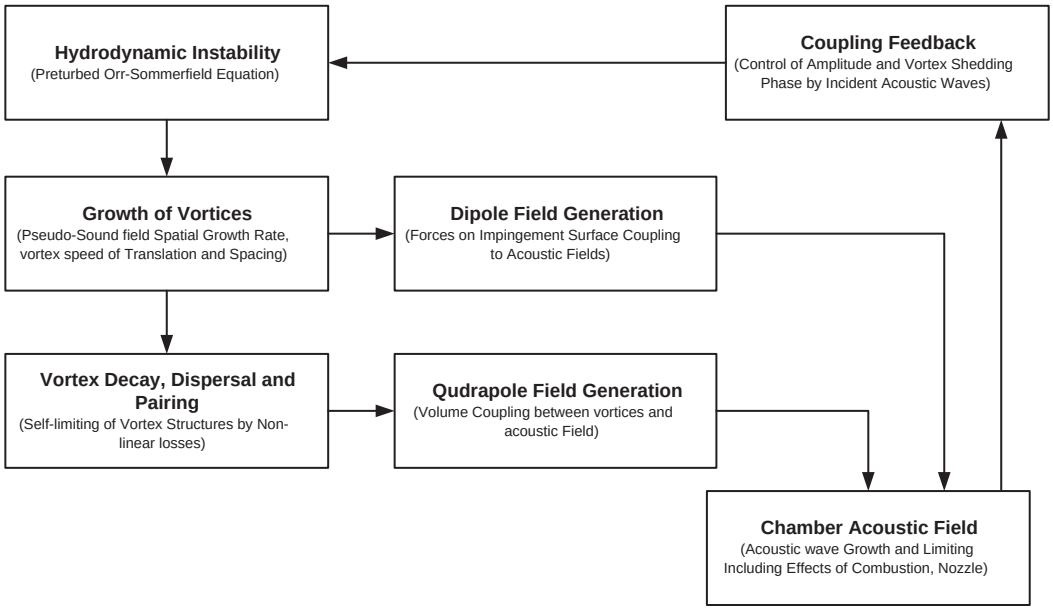

Figure A.2: Analysis of Hydrodynamic/Acoustic Interaction [Redrawn from Flandro (178)]

Considering the problem in three-dimensions also brings about a greater understanding of the physical mechanisms at work. Many answers concerning the flow-turning phenomena is found. Assumptions such as irrotational flow and no-slip condition is discarded. The research also became more specific. Researchers attempted to resolve some of the issues within the traditional combustion instability framework. Again velocity coupling and flow turning receives much attention.

1990: Hypertext system is developed by Tim Burners-Lee and Robert Cailliau. Microsoft Windows 3.0 is released. "'The World"' becomes the first commercial internet dial-up provider. Archi the first search engine is introduced. NiMH batteries are used commercially.

F.S. Blomshield et al published a series of papers (37; 38; 40; 147) on pulse testing of SRMs that has been influential in subsequent publications. A Large test set of motors were evaluated at the Naval Weapons Center at China Lake, California. Much of the work performed at DENEL Munitions is based on the hardware and procedures detailed in these papers. This will be discussed at length in a later section.

The analysis of this data employed by Blomshield et al has been under some debate. Subsequent researchers proposed differing methods of analysis and improving existing methods. The main contribution of this work is a large set of quality data on pulsed motors that researchers can use to evaluate their work with. It also serves as a caution to all SRM designers that Pulsed Instability can not be ignored or viewed as academic. Standard ballistic testing will not reveal the possibility of non-linear instability. It is recommended in the strongest terms that pulse testing should be part of all SRM qualification processes.

Some of the results and conclusion from this experimental study are:

- The severity of Oscillations increase with motor pressure. It has been established that pressure coupling decreases with pressure, but so do other components in the standard linear analysis. Nozzle dampening, for example, also decreases. This lowers the overall stability limit. This is largely due to the decrease in nozzle throat area

which corresponds to a lower mean flow velocity. The lower mean flow velocity as a parameter for stability was previously mentioned by Baum and Levine(101);

- Velocity response was found to depend on the mean pressure and frequency and to be of similar form as proposed by Baum and Levine (72) and Culick et al (92). Therefore, velocity response is negligible under a certain velocity or pressure amplitude threshold followed by a linear dependence on mean acoustic velocity;

- As pressure increases, the pressure threshold decreases appreciably. Thus a motor may not exhibit velocity response at lower pressure but significant velocity coupling at higher pressures;

- As pressure increased, the relative pulse amplitude required, decreased significantly.

1991: Intel introduces the 486SX processor in an attempt to lower computer costs. LINUX is introduced by Linus Torvald. The World Wide Web is launched.

Acoustic boundary layers have become more prominent in the analysis of combustion instability as illustrated in "Acoustic Boundary layers in Solid Propellant Rocket Motors Using Navier-Stokes Equation" by F. Vuillot and G. Avalon (77). Due to the increased computational ability to model multidimensional flow processes within SRMs, it had become apparent that the acoustic boundary layers that form above the burning surface may be critical in determining SRM stability. These boundary conditions control the energy exchange. The propellant responds to the local instantaneous oscillatory and steady flow. Thus to be able to derive a velocity coupling model the boundary layer needs to be fully understood. The author notes that this particular study is the preliminary steps in being able to model unsteady flow fields within SRMs due to the progress in computational speed and memory that can now be envisioned.

The Use of full numerical solution of two-dimensional, laminar, compressible, unsteady Navier-Stokes equation allows that the full features of a SRM two dimensional flow field can be incorporated. The results and conclusions from this analysis are as below:

- Flow turning losses that are usually considered a surface term, is erroneous due to boundary-layer extension;

- The assumption that the admittance function is constant with chamber length is erroneous;

- The admittance function found using this analysis greatly differed from those found from previous analysis;

- The boundary layer can extent throughout the chamber volume towards the end of the motor;

- This analysis correctly predicts trends but is inappropriate when thick boundary layers are observed;

- The flow is found to be rotational and thus invalidates much of the existing linear stability analysis being employed at the time.

1992: Intel 486DX with clock doubling function is released

"Response of Propellant Combustion to a Turbulent Acoustic Boundary Layer" by R.A. Beddini and T.A. Roberts (162). They investigate the effect of the boundary transition from laminar to turbulent flow. Even a small level of turbulence can cause an appreciable burn rate increase by predominantly increasing heat transfer from the flame zone to the propellant surface. From previous laminar studies it can be concluded that due to the boundary layer thickness it may be that the burning surface does not experience much acoustic velocity oscillations and hence no velocity coupling. Thus other mechanisms must be considered.

Whether or not this transition will occur in an actual SRM is a function of several complex factors such as large mass injection rates, surface roughness and the actual combustion process. This study's objective was to ascertain the general trends of reactive acoustic boundary-layer transition to turbulence on the propellants surface, under supposed homogeneous propellant conditions and assesses the resulting response. The Results and Conclusions from this analysis are:

- Despite simplifying assumptions it is apparent that the interaction is non-linear and spatially dependent;
- The occurrence of threshold acoustic amplitude for significant response (triggering), "full wave" rectification occurs relative to the harmonic acoustic velocity outside the boundary layer. A DC pressure shift and the resulting increase in the propellant regression rate are all confirmed analytically;
- The magnitude of response is sensitive to surface roughness and gas-phase heat of reaction (flame-zone thickness).
- Response to acoustic velocity oscillations can be independent of erosive burning. This is contrary to many earlier analyses;
- The acoustic transition susceptibility of the propellant increase with pressure;
- The phase shift of the regression rate response relative to harmonic or external axial velocity can yield a significant "apparent" pressure response when analysed with linear theory;
- Velocity response at even moderate acoustic pressure amplitudes is highly non-linear and has significant harmonic content.
- It is believed further study in this area can significantly contribute to the understanding of these coupling mechanisms.

1993: 50 World Wide Web servers are known to exist. Intel Pentium processor is released which runs at 60MHz and has 3.5 million transistors.

1994: Red Hat Linux is founded.

Culick publishes "Some Recent Results for Non-linear Acoustics in Combustion Chambers" (50). This paper is an excellent review of the work done on combustion instability. It defines all areas of the problem and give both a quantitative and qualitative description. Much of this review is based on his work done in the 1970's, especially (63; 64; 90) and maps

the progress of the work of other researches such as Baum and Levine, and Flandro. It shows where improvements have been made by subsequent research. The analysis is extended to third order non-linear equations. Since much of this work has been discussed previously, it will not be repeated.

It is however appropriate to mention Culick's critique of Flandro's energy balance method. Flandro's analysis suggests that the third order acoustics indeed play a role in triggering to a stable limit amplitudes. This is contrary to that found by numerical and approximate analyses by other researchers. The main assumption that all time dependent variables can be found in a single quantity, was criticized. This implies all modes must share the same time dependence which is not supported by theory nor be experimental evidence. Furthermore transient motions are modelled incorrectly and since these motions are dependent on their history in many respects, it becomes apparent that describing a system with so many degrees of freedom by using a single quantity, may be dangerous. Culick, however, states that the analysis should not totally be disregarded and that many important factors are highlighted, and that the predictions are realistic. It is suggested that a more "rigorous foundation" could reconcile the analysis with other work.

The approximate analysis (using truncation of modes and time-averaging) has been one of the main numerical tools in solving non-linear equations. C.C. Jahnke and F.E.C. Culick introduce the use of dynamic systems theory to the study of combustion instability in "Application of Dynamical Systems Theory to Non-linear combustion instability" (16). This analysis builds on Culick's previous work (63; 64; 90) using Galerkin's Method . Since these methods use time averaging and truncation of modes it is important to understand the affects of these assumptions. This can only be achieved by solving the original system of non-linear equations.

To simply vary the parameters arbitrarily and then compute the numerical simulations is rather tedious. Thus, it is suggested that the elementary dynamic systems theory could be used. From this a bifurcation diagram is constructed which in turn can be used to isolate parameters of interest. A dynamic systems' theory will not be discussed here but, can form an important part of any analysis that is developed from this study. Again the growth of numerical techniques and computational power makes such analyses possible.

1995: Java is introduced. Windows 1995 is released.

"Effects of Vorticity on Rocket Combustion Instability" by Flandro (55) is one of his most influential papers. This is a separate issue from that of vortex shedding discussed earlier. Vorticity is generated in compliance to Crocco's theorem that vorticity is due to unsteady axial pressure gradient across mean flow stream lines. Thus there is an energy transfer mechanism between acoustic pressure oscillations to rotational waves as shown in Figure A.3. This analysis adds rotational corrections, however, not all possible corrections to Culick's model are incoperated. The Standard Stability Prediction Program (SSPP) (based on Culick's linear model) has been known to predict that a motor is stable but upon qualification is found to exhibit longitudinal mode oscillations.

Flandro attributes these failures to the following assumptions: flow is irrotational in classical models and vorticity affects are not explicitly accounted for; and Oscillatory slip flow is allowed based on the belief that viscous stresses and vorticity transport are negligible due to strong surface blowing. The addition of velocity coupling and flow turning corrections are introduced, but have not been validated experimentally or theoretically.

Culick's flow turning correction assumes that gas motion is normal to the propellant

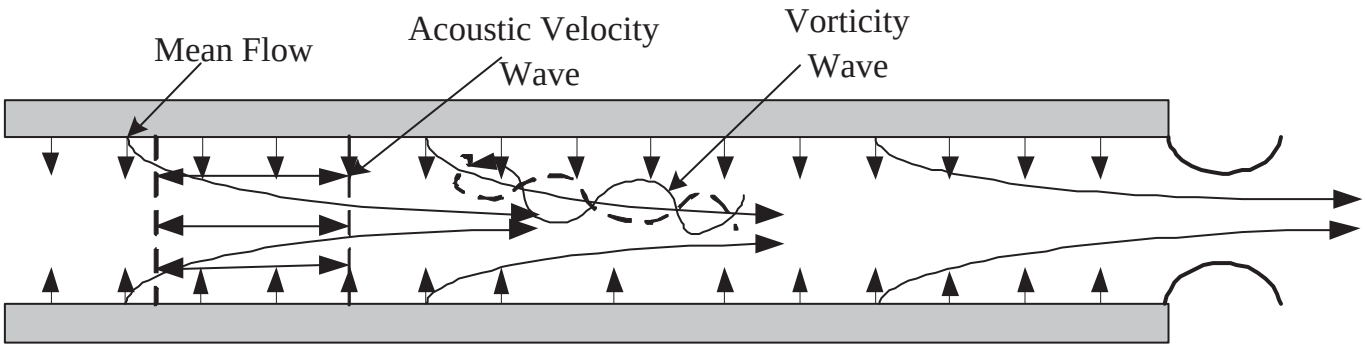

Figure A.3: Vortices Generation [Redrawn from Flandro (55)]

boundary. This departs from multidimensional theory that places no restriction on the velocity components parallel to the burning surface. This damping term is not included in three-dimensional combustion instability and is simply corrected by patching the one-dimensional result.

In a previous study by Flandro in 1974 (167), acoustic boundary layer theory was employed to determine corrections to the stability algorithm. This was based on the idea that flow-turning losses was due to no-slip boundary conditions in the one-dimensional calculations. This analysis demonstrated that vorticity has an effect on the stability of a system. However, the thin acoustic boundary layer resulted in a misinterpretation of the results. The entire flow field is in fact affected not just the thin surface layer. Thus the terminology of acoustic boundary layer is inappropriate.

Rotational flow must be accounted for as it is responsible for acoustic mode shape distortion and modification of the radial velocity fluctuations. The admittance or response function used previously cannot account for this and thus cannot be a complete boundary condition. Key results and conclusions are:

- The inviscid flow is a useful limiting case of the viscous analytical solution. It proves to be appropriate through-out the combustion chamber for many SRM instability problems that involve lower order axial modes;

- The appearance of completely equivalent flow-turning affect in three-dimensions. This is a result of convective forces that involve the generation of unsteady vorticity at the burning surface. The volume integral of convective acceleration can be reduced to a surface integral with inward mass flux. This validates Culick's patching of the one-dimensional results;

- Flow turning is found to be spatially dependent on the square of the unperturbed plane wave velocity mode shape;

- The gradient of oscillatory pressure parallel to the surface causes a loss due to a velocity fluctuation normal to the lateral boundary by mass conservation. This causes a momentum exchange between incoming and bulk flows as defined by (2);

- A strong rotational/acoustic coupling is found to exist and represents a new driving mechanism;

- Incorporating these corrections vastly improve the stability predictions to a point where variance can be attributed to uncertainties concerning admittance function measurements.

The affects of flow turning is further discussed by Flandro (56) in his paper"On Flow Turning"

1996: Intel Pentium releases a 200MHz processor. Deep Blue an IBM computer beats Garry Kasparov in one of two chess matches chess.

1997: Intel releases the MMX (MultiMedia eXtension) chip and the Pentium II 233 MHz processor.

"On the Origin of the DC Shift" by S. Malhorta and G. Flandro (182) discusses the physical mechanisms of the DC shift. The author sets out by giving experimental evidence of the DC shift. The DC shift is one of the most important phenomena. It is therefore essential to include this in any analysis. There have been several mechanisms that have been proposed:

- Burn rate increase;
- Increased burning area;
- Mechanical distortion of the surface;
- Temperature rise in the bulk of the propellant;
- Macroscopic fracture of the grain; and
- Interference of the vortex flows;

Burn rate increase is seemingly the only mechanism that can fully explain all experimental data. Thus the analysis focuses on the gas dynamics that can cause such interactions. Since all observed phenomena must be explained, vorticity must be considered. Using this approach it is possible to connect the DC pressure shift to the vorticity correction. It demonstrates a mechanism that can carry hot combustion gases from the interior to the cooler combustion zone. This effect is two fold: increased heat transfer, and the mechanical momentum forces the flame closer to the surface. Both result in an increased burning rate.

1998: Intel releases Celeron processor.

1999: Intel Pentium III is released a 500MHz processing chip.

A.2.5 2000-Present

2000: Approximately 1 billion PCs have been shipped worldwide.

It seems appropriate that the new millennium be started off by another paper by F.E.C. Culick: "Combustion Instabilities: Mating Dance of Chemical, Combustion, and Combustor Dynamics"(2). This gives the status of combustion instability research. It is important to give a full review of this status report in order to tie together the time line that has been

developed. It gives details of the objectives and current research being performed by the Multidisciplinary University Research Initiative (MURI). The main areas that have slowed down the development of methods to solve the problem include:

- Lack of Funding or availability of funds over short time spans;
- Little collaboration between corresponding communities of research;
- The intrinsic limitations of the experiments currently used. The non-uniform high temperature and chemically active environment makes measurement both in-situ and non-intrusive very difficult. The fact that the measurements are taken over a short time scale also complicates the analysis.

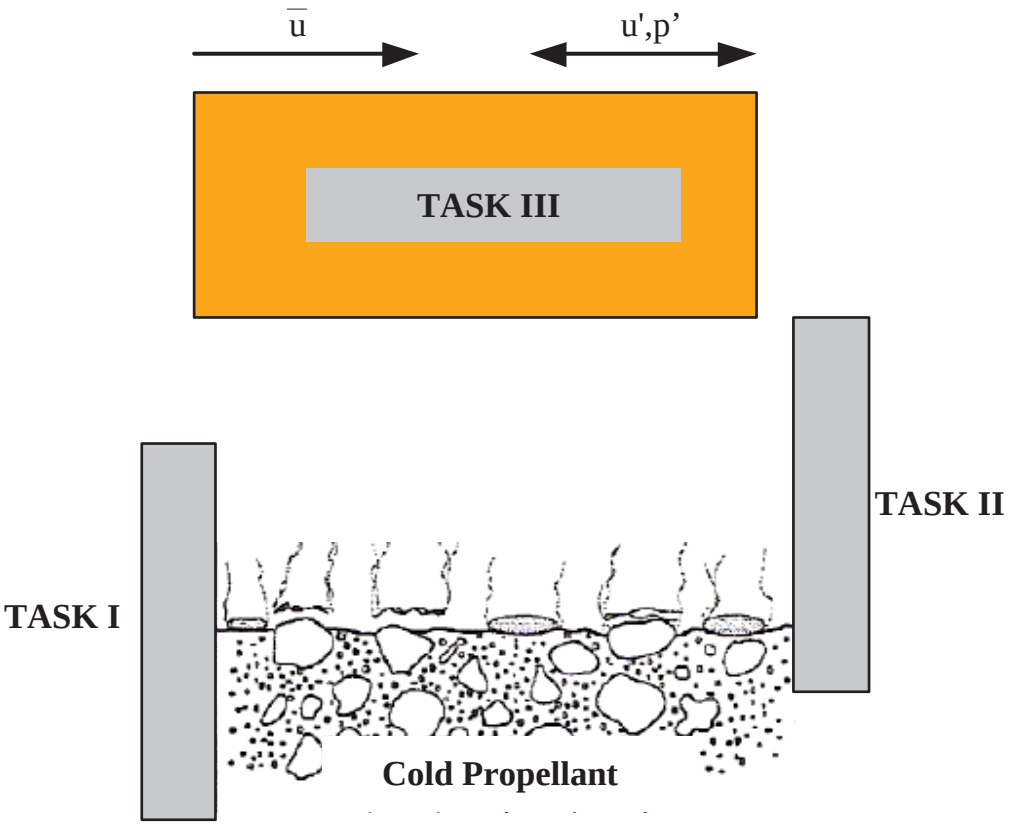

Figure A.4: Integration of Tasks [Redrawn from Culcik (2)]

Figure A.5 illustrates the fields of study that need to be combined to be able to fully understand combustion instability. Combustor dynamics (Task III in Figure A.5) refers to the entire SRM system. It ties together the motor mechanical dynamics with the combustion dynamics. It is important to remember that combustion instability does not refer specifically to the combustion process, but the complex interaction of the combustion with the motor acoustics and the complex energy transfers between losses and gain mechanisms. The relationship between combustor and combustion dynamics is shown in Figure A.6.

Combustion dynamics (Task II in Figure A.5) refers to the response of a combustion process to local values such as local velocity, temperature and pressure. The scale difference between combustor and combustion dynamics is in the order of $10^3 - 10^6$. Thus it is reasonable

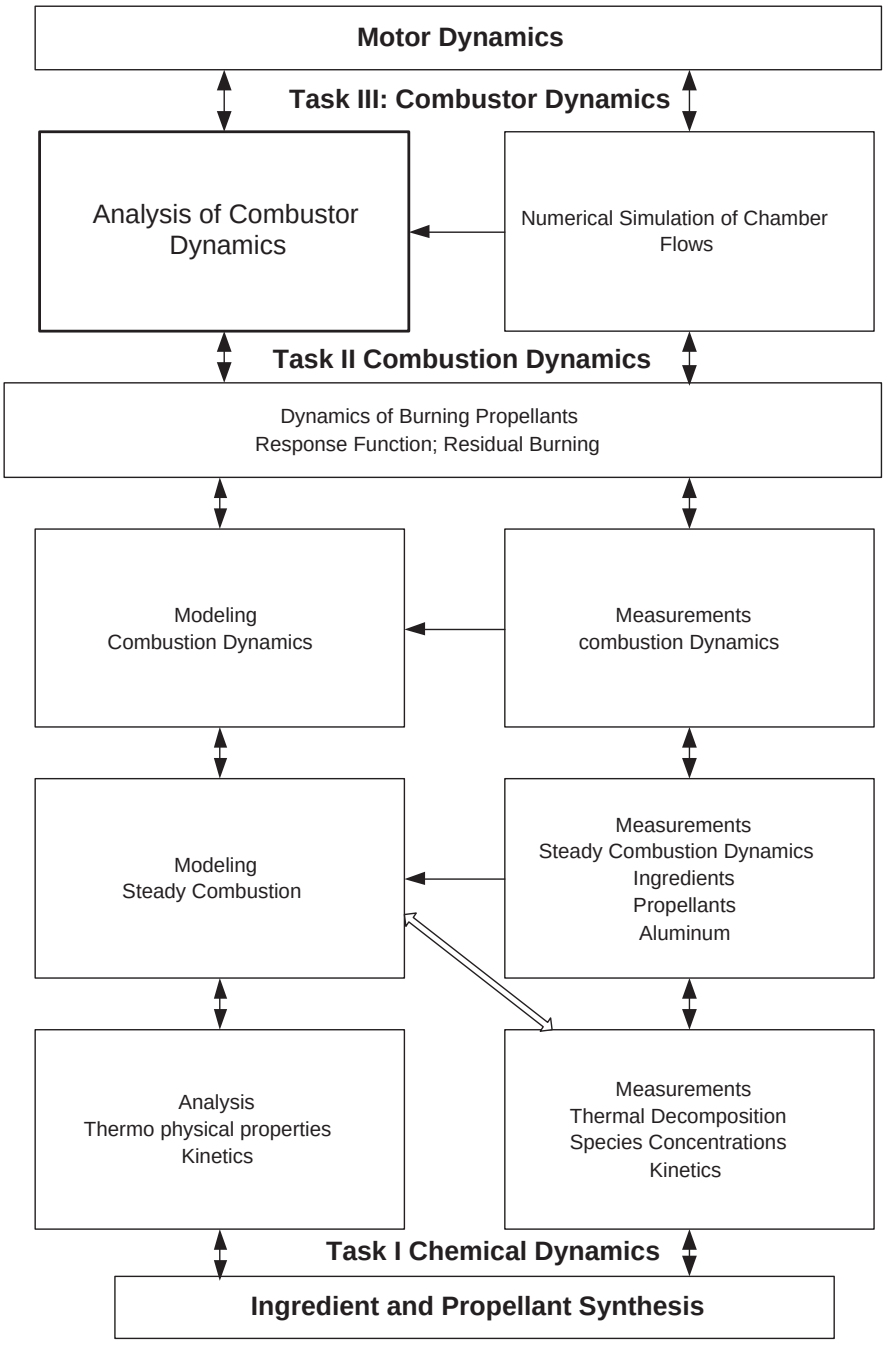

Figure A.5: Overview of Research [Redrawn from Culick (2)]

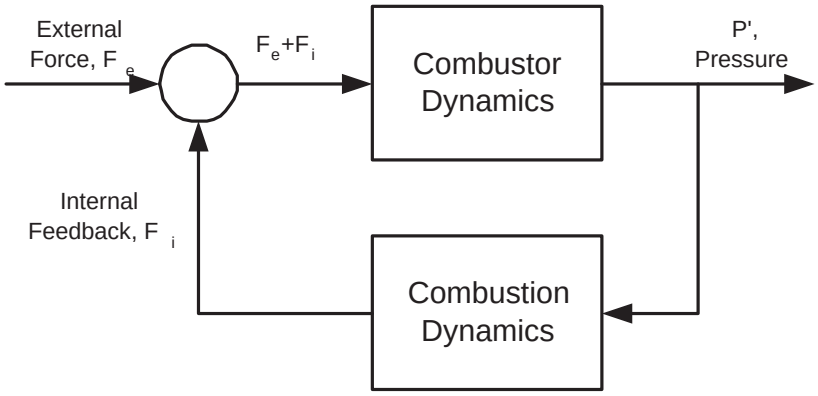

Figure A.6: Combustion Instability Represented as a Feedback Loop [Redrawn from Culick (2)]

to assume that the response of a propellant can be averaged. This of course leads to the response function and serves as the connection between combustor and combustion dynamics. The spatial averaging however does not eliminate the model of heterogeneities on a small scale. Any model must thus typically be a function of oxidizer size, residual combustion, and higher order moments.

Combustion dynamics(Task I in Figure A.5) is of course a macroscopic consequence of a massive amount of microscopic processes. These include energy transfer via conduction; convection; radiation; and the physical and chemical kinetics. The modes of energy transfer are a part of the combustion analysis and the required information on kinetic processes must be supplied independently by Task I.

Combustor Dynamics incoperates the entire system and is essentially the sum of all interactions. The following must be investigated when considering the combustor dynamics:

- First task is to determine the frequencies and the mode shapes of the SRM. This assumption is supported by experimental evidence that the unsteady motion in the combustion chamber can be interpreted as the time evolution of a collection of coupled non-linear oscillators. These oscillators are correspondent with the acoustic modes of the chamber;
- Combustion processes and the flow within a combustion chamber are astonishingly complicated, yet, the pressure record is a simple accurate observation. (Through approximation it should be possible to represent this record. It should of itself not contain direct solution of partial differential equations describing chemical and physical behaviours but rather this data is embedded within the pressure history.)
- A systematic approach is employed to construct equations proven through experience (cf. Culick's framework). This is based on two parameters: the Mach number and mean flow that define both linear and non-linear behaviour.
- Spatial averaging is used to bridge the gap between the applications to macroscopic scale of partial differential equations local in space. Methods include Raleigh and Galerkin's methods. Both are methods of least residuals.
- Three kinds of waves can exist: acoustic, entropy, and vorticity waves;
- Acoustic waves propagate at the speed of sound within the motor, the vorticity and entropy waves are convected by the mean flow;

- Entropy waves can be regarded as spots of temperature difference from the mean.
- Acoustic waves dominate due to: other waves carry no pressure fluctuations within the limits of small amplitudes; acoustic waves are weakly affected by the other waves; and even small pressure fluctuations can cause a significant local response of the propellant if a small fraction of the increased energy release is converted to mechanical energy;
- Determine the linear stability: The typical loss and gain terms are summed. These include nozzle, particle, and surface combustion;
- No disagreement exists in terms of the inclusion of losses or gains associated with the generation of acoustic waves in the linear computations. There is still some controversy on the precise form of the contribution.
- Flow turning must be included in the analysis, the new loss mechanisms identified by Flandro (55) such as vorticity interactions with acoustic waves should be ignored since they are quickly destroyed by viscous losses.

The dynamics of surface combustion are:

- "Unquestionably the most important remaining problem relating to Combustion Instabilities"(2);
- Reconciling three greatly varying in the length scales complicates the problem. This is where all three dynamics come together;
- The response and admittance function are still fundamental to the analysis. Determining the pressure coupled response is vital;
- No theory exists for velocity coupling;
- Response function is still determined by using the two-parameter solution as outlined in (124);
- Experimental methods are inadequate to give the required data, that is the frequency range and mean pressure of real SRMs;
- Several methods of data measurement are being evaluated with little success;
- T-burner is still the most reliable device in the hands of an experienced operator;
- Large variance in response functions obtained for the same propellant at same frequency and pressure ranges using different techniques;
- Over the fifty years of research several "rules of thumb" have accrued.
- Many of these "rules of thumb" are not available to the general combustion instability community.

Calculation of non-linear Combustor Dynamics:

- Linear models can be extended to incorporate non-linearities;

- Linear analysis essentially gives the linear stability. If a motor is stable the problem is solved. However, no calculation can guarantee stability due to low confidence in input data, especially with regards to the response function;
- An explanation is needed for the sensitivity of the combustor dynamics to small changes in propellant composition;
- The sensitivity cannot be solely attributed to a change in response function. If the parameters of the two-parameter solution were to vary as such to induce such changes, it would (during natural course of events in a test device or motor) exhibit large pressure excursions. Secondly it occurs in the dynamic environment of a motor. Thus it is important to carry a time evolution of motions and determine the affect on the response function;
- Velocity coupling is suggested as a possible mechanism to explain the variance in stability for even small changes in propellant composition. It also seems to be a dominant affect on certain instabilities.

2001-Present: Dual Core processors are introduced. CPU operate in excess of 3000MHz.

This time period is dominated by Majdalani[6] and Flandro. Most of the work is centered on improving the standard stability prediction code. This includes adding several new correction factors. The transformation of the volume integrals to surface integrals and then into an acoustic form, makes it possible to avoid the difficulty of defining the rotational flow fields which can be uncertain in an arbitrary geometry. This makes the analysis applicable directly to any geometry. The current formulation of the stability algorithm will be used and these works will be discussed in detail in Chapter 3.

[6]The second professor to fill the H. H. Arnold Chair of Excellence at UTSI. His research is diverse in areas of theoretical and numerical modeling of injection and swirl-driven combustion chambers. The introduction of the Wentzel, Kramers, and Brillouin (WKB) and multiple-scale theories by Majdalani and van Moorhen (59) revealed much of the underlying physics of the CI problem.

A.3 Conclusions

The timeline not only highlights the growth in understanding of the problem of combustion instability but also the attitude of the SRM industry to the problem. Many of the original source documents upon which many articles are based are not available. Little collaboration is shown with most articles presented being highly theoretical that gives little practical insight.

Industry seemingly in many cases has chosen to ignore the problem and rely on "rules of thumb" acquired through experience. Since, it was in many cases easier to use *ad hoc* solutions when CI occurs. However, it has also been shown that ignoring this problem can have dire implications. Being able to adequately predict combustion instability will improve the quality of the final product.

It also shows that funding was not always available. There have been stagnant periods when few researchers published on the subject. Baum and Levine's work for instance was a direct response to a case of combustion instability. This work was possible presumably only due to the funds being made available.

The research has been dominated by a handful of researchers. Flandro and Culick have been publishing on the subject since the mid 1960's. Other researchers such Price, Beckstead and Vuillot have also contributed for sustained periods of time. It also can be seen that much time has been spent on refuting each other's ideas and methods. This may in some cases been detrimental to the understanding of combustion instability. This study will investigate these different approaches and attempt to answer these questions.

Appendix B

Current Experimental and Analytical Procedures

B.1 Testing Strategies

The current testing procedure that is followed was proposed by Blomshield emphet al., in (147),who set out to define a testing strategy. These were followed by programs in Canada, United Kingdom, and Australia. This study aims to replicate and improve this testing strategy while attempting to reduce costs. This strategy consists of:

1. Select a suitable baseline propellant. Criteria include easy manufacturing and good physical properties at high pressures. Such a propellant should therefore not exhibit exponent breaks or anomalous behaviour.

2. Perform T-Burner pressure coupled response testing on the baseline propellant over a broad range of frequencies and pressures. The T-Burner test will correspond to the operating pressure and the fundamental modes of the SRM to be pulse tested;

3. Perform laboratory pulser testing at high pressure to allow for accurate pulsing of motors;

4. Design and develop motor hardware which can safely and inexpensively be used at higher pressures;

5. Use the Standard Performance Prediction (SPP) and Standard Stability Prediction (SSP) codes;

6. Perform non-linear stability analysis with L/B non-linear code(Levine/Baum);

7. Facilitate the development of three-dimensional stability code coupled to a three-dimensional grain design and ballistic codes;

8. Perform pulsed motor firings that are instrumented with redundant high frequency pressure instrumentation. Parameters that should be varied include: pressure, geometry, pulsing, and propellant;

9. Perform extensive data analysis to determine the motors response to pulsing and compare results to the SPP, SSP and L/B code;

10. Distribute results to solid propulsion community.

This is an extremely expensive approach and is aimed to gain a universal code for SRM stability prediction. The codes mentioned above are not freely available. Thus the strategy employed here (cf.Figure 4.1) will be identical from steps 1-4 and 8 and 9 will be included upon evaluation of the feasibility of operating a T-Burner. It becomes clear that for a program to be successful, the capacity to analyse this data must be established. Secondly, a code needs to be produced that can aid in the prediction of a motor stability.

B.2 Determining Acoustic Modes

The acoustic modes of a SRM are a fundamental part of the quantification of combustion instability. It has been shown that the response of a propellant is strongly linked to the frequency. The expected frequency range is important and will determine the test matrix to obtain the admittance function. For tubular grains this is a relatively easy task. For a circular geometry the fundamental frequency in the longitudinal direction (assuming that it is a pipe with a closed end) is:

$$f = n\frac{a_0}{2L} \qquad n = 1, 2, 3..... \tag{B.2.1}$$

For the tangential mode in circular geometry:

$$f = \frac{a_0}{2\pi R}\beta_{m0} \tag{B.2.2}$$

Where β is the solution to the following well known Bessel function:

$$\frac{dJm(\beta)}{d\beta} = 0 \tag{B.2.3}$$

β refers to solutions of the Bessel functions and R to the radius of the conduit. The Bessel functions solutions can be found by using numerical programs or from tables. The order of the harmonics is determined by the integers m and n for tangential and radial, respectively.

The tangential and radial modes are solved for in a similar way except that in the case of the radial, the antinode occurs at the outer periphery and at the centre of the cylinder:

$$f = \frac{a_0}{2\pi R}\beta_{m,0} \tag{B.2.4}$$

There are two methods to determine the acoustic modes of complex geometries. The first method to obtain the modes is the use of finite element analysis of the motor cavity using software that is currently available. The second method has been used since the 1960s and is still recommended by Culick in 2000(2). This method consists of creating the grain out of wood, metal, or a plastic. The end of the motor is enclosed with a rigid boundary. At the head end a microphone and a speaker are mounted. The speaker provides acoustic waves that vary the frequency while keeping the amplitude constant. The longitudinal mode for even complex geometries can be determined using equation (B.2.1). The mode shape will be distorted but the frequency will be approximately the same.

At a particular frequency a steady wave system is formed that can be measured by the microphone. When the frequency is in the order of 1KHz or more, a response from the chamber is recorded by the microphone as shown in Figure B.1. The peaks represent the resonant or fundamental modes.

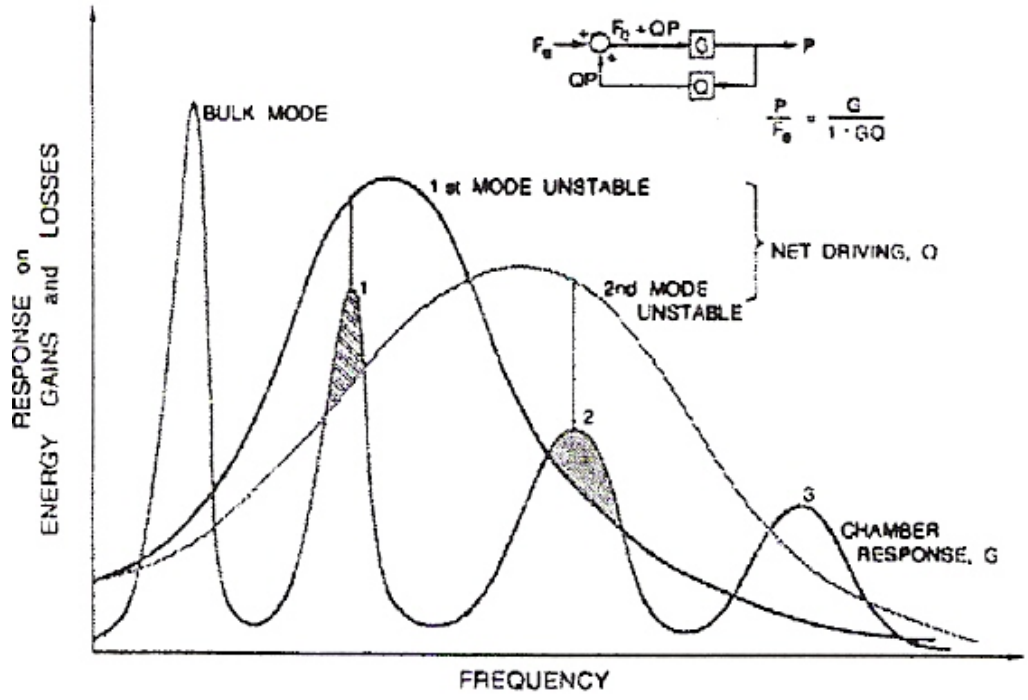

Figure B.1: Determination of Fundamental Modes [Culick (2)]

B.3 Experimental Devices

Measurement of combustion response is one of the largest areas of concern. Any prediction algorithm is only as good as the input data. Culick (2) shows that a great deal of research has been done on some new methods of measuring the response function. Most of these methods have not yielded much success. These include:

- Laser-Recoil devices;
- Ultrasonic Doppler;
- Magnetohydrodynamics/velocimetry;
- Microwave Doppler;
- Transient Device.

None of these methods are applicable to the problems encountered in motors due to one or more of the following deficiencies:

- Restrictive frequency ranges(<600-1000Hz);
- Restricted to low pressures;
- Inapplicable to metallised propellants;
- Large uncertainties in data,

There, however, exists a set of devices that have been used more extensively as measurement devices. The operating ranges and general comments on these can be viewed in Table B.1.

From this it is clear that the T-Burner is still the most recognized and established testing device. It is suggested by Flandro (105) that a combination of devices is to be used. However, for this program it seems that the T-Burner is the best device to obtain data that can be used with certainty. It is attempted to extend the basic principle of a T-Burner to pulsed motor firings in order to obtain an admittance function.

B.4 The T-Burner

A previous study has been performed for DENEL Munitions by J.H. Knoetze in 2000. A T-Burner was constructed without a surge tank. Since a design has been done and the hardware exists, this section will give a brief description of a typical T-Burner, reasons for various designs and the cost implications. The main focus is on the analysis of data.

It must be stressed that over time many improvements have been made on the way the data analysis is done (specifically concerning flow fields and the affect of acoustic boundary layers). Much of this analysis is still based on the analysis from the 1960s (especially the work of Coates and Horton). Vuillot in (177) for instance gives a comparison between Flandro's admittance correction and Culick's Flow turning correction. It must also be stated that information on the analysis is contained in many confidential company and government documents that are not available.

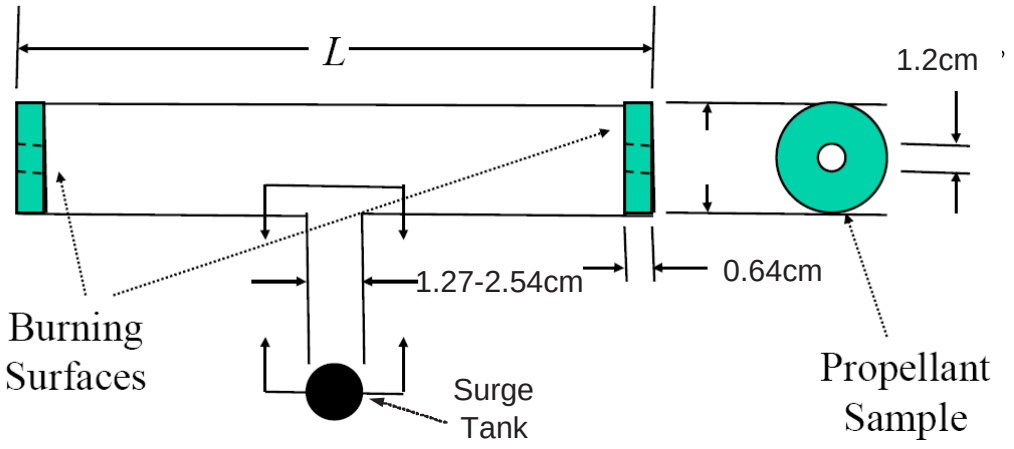

Figure B.2: Typical T-Burner Design Blomshield (36). Courtesy F. Blomshield, with permission.

The T-Burner is not only the most widely used, but also the oldest method. It was designed by Ed Price at China Lake, California. It has subsequently been used by nearly all rocket motor companies and government laboratories. The oldest working T-Burner in the U.S.A. is at China Lake and has performed over 24,000 tests. It is essentially a SRM designed in such a manner that the loss factors can easily be calculated and also has a simple flow field that has been well characterised. It is the standard against which all other methods must be evaluated. It, however, has some distinct disadvantages:

- Uses 25-150g of propellant per test;

Table B.1: Pressure Coupled Measurement Devices Flandro (100)

Method	Pulsed T-Burner	Variable Area T-Burner	Rotating Valve	Toothed Wheel	Laser Recoil	Impedance Tube	Microwave Burner	Magnetic Flow Meter
Frequency-Range-Hz	300-5000 up to 10 000 for slotted T-Burner	300-5000	0-800	0-100	0-200	0-2400	0-1000	2000
Maximum Pressure	29MPa	14MPa	10MPa	7MPa	1.4MPa	3.5MPa	7MPa	14MPa
Cost	High	Really High	Medium	Medium	Low	Low	Medium	Low
Comments	Measures Damping Difficult with metallised Propellants Subjective	Measures damping Subjective Has Complicated flow field	Does not measure damping	French Device Measures damping Simple Device	Measures phase Measures heat flux response. Requires transfer function to get pressure coupled response Bad data scatter	Measures damping Difficult to extend to higher pressures	Does not measure damping Capital costs higher than other methods	Does not measure damping French have had good success
Articles on devices	(12; 82; 112; 114; 121; 122; 124; 131; 139–141; 154; 176; 183–188)	(82)	(188)	(177)	(177)	(72)		(189; 190)
	Measures real part of the response only				Measures real & imaginary Parts(amplitude & Phase)			

- 15-30 tests at one pressure are needed to generate a response curve over a frequency range;
- Data interpretation can be subjective;
- Expensive to maintain and use.

Additionally, if several pressures are required due to the differing operating pressures of the SRM, the amount of propellant needed becomes large. More importantly, the amount of tests increase and correspondingly the amount of man hours required to operate it and thus the cost.

B.4.1 Specific Designs and Considerations

As stated earlier, the T-Burner is essentially a simplistic SRM. It consists of a pipe with two grains at the end, it is centre vented through a pipe preferably into a pressurised tank or surge tank. The Mach number of the steady flow field generated by the burning surface is minimal. The disks burn normal to their faces. Thus the only variable is the chamber length that can be calculated at any instant from the burn rate. This means that the mode shape is known at all times. The main mode of oscillation is the first axial mode. The general factors to consider are (34):

- Costs: A smaller diameter reduces the amount of propellant required. Reducing the size of the surge tank and other hardware also reduces costs. The time between tests can also be reduced. However, the smaller the burn area the smaller is the chance of spontaneous oscillations occurring, because the acoustic energy gained decreases with area.
- Geometry: The one-dimensional mode, an extended mode and a variable area mode should be considered. For smaller diameters the variable area testing allows shorter grain lengths for a given area ratio and thus causes less of a frequency shift. This minimizes the effects of velocity coupling and flow/acoustic interactions. An extended mode would cause an increase in frequency change and thus make data interpretation even more difficult.
- Wall Losses: Those can be considered negligible when compared to particle dampening. For propellants without particles these losses must be accounted for.
- Combustion efficiency: It has been seen that for small diameter T-Burners there is a marked decrease in burning rate due to heat loss to chamber walls. Larger test hardware seems to reduce data scatter and improve the combustion efficiency. There have been reports of increased efficiency when preheating the chamber walls.

The response of a propellant is a strong function of both frequency and pressure. To vary the frequency, a set of varying length T-Burners will be required. This can clearly be seen from the equation for the fundamental mode i.e. essentially the equation for a tube closed on both ends:

$$f = \frac{a_0}{2L} \tag{B.4.1}$$

Increasing the length will decrease the frequency and vice versa. The pressure can be altered by varying the nozzle diameter (without surge tank) or controlled by the surge tank. Decreasing the diameter will increase the T-Burner operating pressure. It should be noted that speed of sound is a weak function of pressure and is relatively constant for changes in pressure.

There are several different configurations for T-Burners. The primary goal of these design modifications is to ensure that instability occurs. When investigating the response of propellants without additives, the standard T-Burner design as in Figure B.2 is sufficient. However, in most modern propellants particle additives are used as a dampening agent to prevent combustion instability.

A variable area T-Burner achieves this by enlarging the burning surface (191). Thus the possible energy input to the T-burner is increased by making it possible to overcome dampening affects. This can have two adverse affects. In the case of enlarging the diameter of the T-Burner, it increases chamber volume and the amount of propellant. In the case of using an annular or cup shaped grain as shown in Figure B.3, the flow fields are complicated.

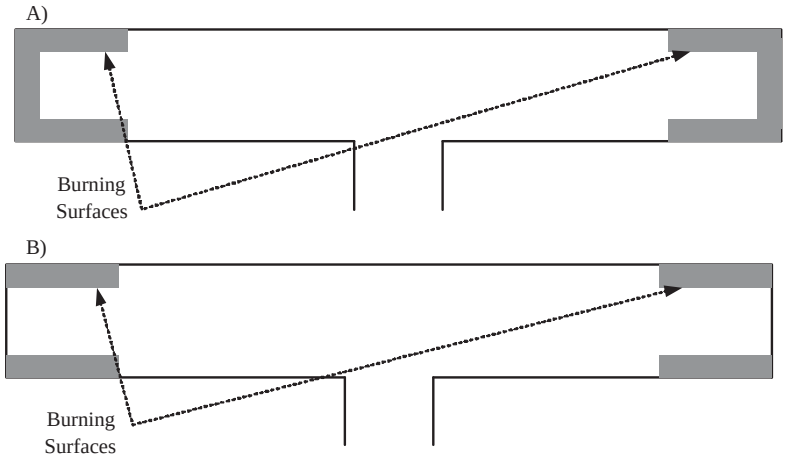

Figure B.3: Extended Area T-Burner: A) Cup and B) Annular Configurations [Redrawn French and Flandro (191)]

A pulsed T-Burner initiates a shock wave and introduces foreign matter into the T-Burner. The addition of free volume for the pulsers can add additional losses to the analysis that need to be accounted for. The quarter wave position is the suggested location for such a device.

Taking into consideration the above factors, the following design steps are taken when attempting to determine the response function for a specific SRM:

- Determine the resonant frequencies of the SRM;
- The particles added to the propellant will determine if a pulsed or extended area T-burner must be used;
- Choose T-Burners that will generate the required frequencies;
- Select the correct nozzle diameter or calculate the pre-firing pressure of the surge tank to match the SRM operating pressure.

B.4.2 Data Analysis

The T-Burner analysis is done in such a way that the response function can be found. The two-parameter solution which has been found by several different authors in the form first reported by (22):

$$\frac{r_b'/\bar{r}_b}{p'/p} = \frac{m'/\bar{m}}{p'/\bar{p}} = R_b = \frac{nAB}{\lambda + A/\lambda - (1+A) + AB} \approx \frac{1}{M_b}\left(\frac{A_b}{\gamma} + M_b\right)$$

$$where\ \lambda(\lambda - 1) = i\Omega = Dimentionless\ frequency\ parameter \tag{B.4.2}$$

$$\Omega = \frac{\kappa\omega}{\bar{r}_b^2}$$

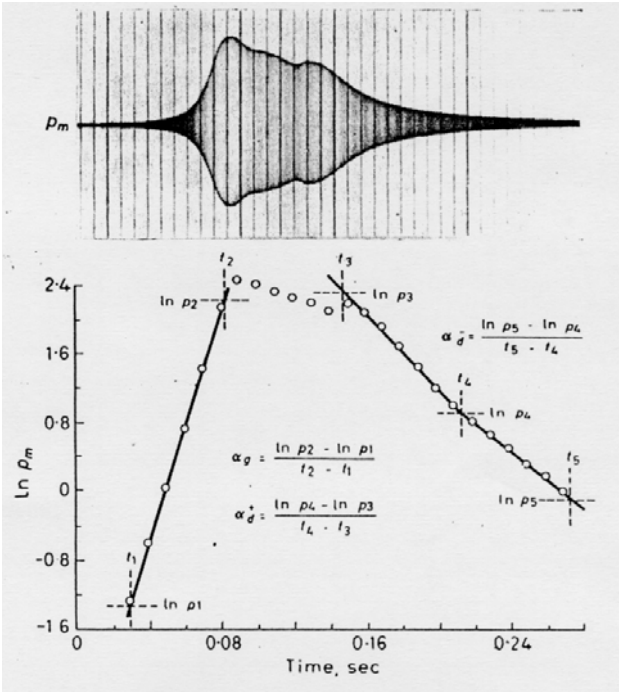

Figure B.4: Typical T-Burner Data with Surge Tank [Blomshield (36), Courtesy F. Blomshield with permission]

This two parameter fit has been obtained based on the QSHOD(Quasi-steady gas phase, one dimensional and homogeneous propellant), refer to appendix A) method by several researchers. The parameters A and B depend on the combustion model used and are listed in (23). A and B can be obtained relatively easily from the routinely measurable parameter in a steady burning test using the Z-N Model (Zeld'ovich and Novozhilov):

$$
\begin{aligned}
r &= \left(\frac{\partial \bar{T}_s}{\partial T_c}\right)_{\bar{p}} \\
k &= \left(\frac{\partial \ln \bar{r}}{\partial \bar{p}}\right)_{T_c} \left((\bar{T}_s - T_c\right) \\
A &= \frac{k}{r} \\
B &= \frac{1}{k}
\end{aligned}
\tag{B.4.3}
$$

However, it has long been known that the data from these models do not provide the data required for all operating conditions. However, it can serve as a good check for the validity of the T-Burner results. Thus, it is necessary to use the T-Burner data to generate a response function for unsteady operating conditions. Figure B.4 show typical data obtained from a T-Burner test. In general the acoustic pressure can be described by a cosine waveform:

$$p' = p_0 e^{\alpha t} \cos(\omega t) \tag{B.4.4}$$

For the first mode this is:

$$p \;=\; p_0 e^{\alpha t} sin(\frac{\pi x}{L}) sin(2\pi f t) \tag{B.4.5}$$

The oscillating pressure amplitude p_m:

$$p_m = p_0 e^{\alpha t} \tag{B.4.6}$$

The growth constant, α_g, obtained is in fact the sum of several constants. These components are:

- Energy gain from propellant combustion: α_b;
- The affect of the nozzle: α_n;
- The interaction with the burning surface: α_w;
- The dissipation of the combustion products: α_p.

$$\alpha = \alpha_b + \alpha_n + \alpha_w + \alpha_p \tag{B.4.7}$$

Taking the natural logarithm of equation(B.4.6):

$$\ln p_m = \ln p_0 + \alpha t \tag{B.4.8}$$

By taking the pressure peaks from the T-burner data and taking their natural logarithm, it is then possible to plot $\ln p_m$ versus time. The slope of the line is α. The intercept with the y-axis $\ln p_0$ is obtained as is illustrated in Figure B.5 or analytically:

$$\alpha = \frac{\ln p_{m1} - \ln p_{m2}}{t_2 - t_1} \tag{B.4.9}$$

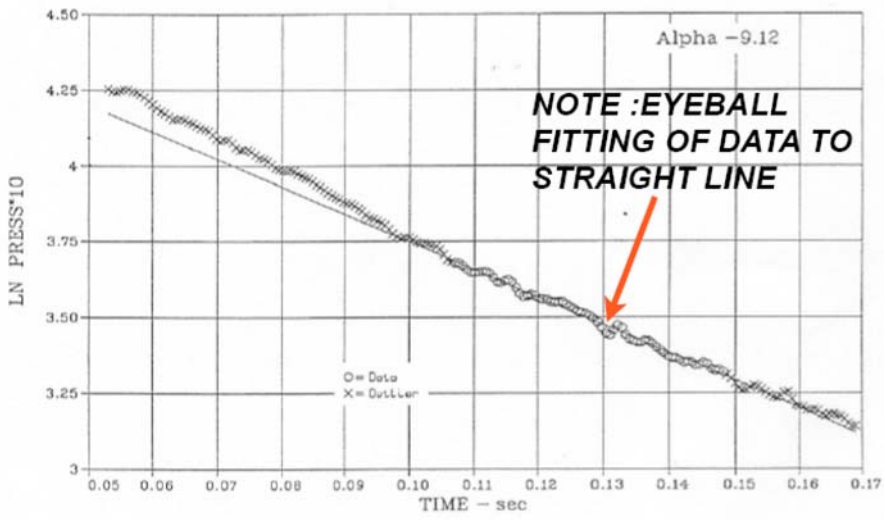

Figure B.5: Example of linear fit of T-Burner Data [Flandro (105). Courtesy G. Flandro, with permission]

However as is shown in Figure B.5 taking the log of the data does not linearise it enough to be able to fit a straight line.

If, however, it is assumed that the predominant non-linear loss is that of the shockwave losses as in (48), the linear gains and losses can be expressed as a function of the system amplitude, ε:

$$\begin{aligned} \frac{d\varepsilon}{dt} &= \alpha\varepsilon + \beta_{sw}\varepsilon^2 \\ \beta_{sw} &= -\frac{(\gamma+1)}{6\gamma}\frac{a_0}{L} \end{aligned} \tag{B.4.10}$$

By using this fit, a much better result is obtained as shown in Figure B.6 than that obtained in Figure B.5. The α obtained corresponds to the alpha previously mentioned. Instead of calculating β_{sw}, it can also be regarded as an unknown and the data fitted to the two parameters with β_{sw} representing non-linear losses (31). These parameters can be related simply by the following correlation:

$$\Pi = \frac{\alpha/f}{R_\infty/\bar{p}} = \beta_{sw}\frac{\bar{p}}{f} \tag{B.4.11}$$

R_∞ appears as the limit amplitude of the T-Burner. It was found that Π stays constant for many sets of data and is known as the Pi Theorem. Incorporating this technique into the analysis will greatly improve the accuracy of the admittance function obtained.

As shown earlier, the α is the sum of losses and gains. It is now necessary to determine the contribution of the burning surface. Two approaches can be used. Firstly, if a surge tank is used it can be assumed that the decay measured after burn out of the propellant is a measure of the dampening factors and is equal to the decay factors during the burn time. This assumption is based on the mean pressure staying constant. In light of more modern theory this may not be a valid assumption as illustrated in (177). There are other loss mechanisms at the burning surface that would not be accounted for. These will not be incorporated in this analysis but will be investigated in the future (pending new literature).

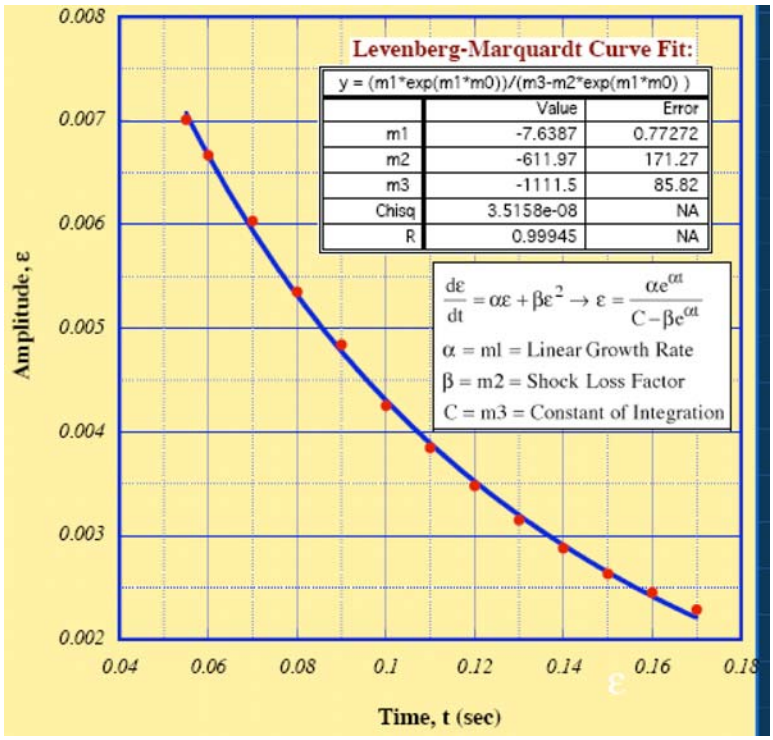

Figure B.6: Incorporating shock wave losses into analysis [Flandro (105). Courtesy G. Flandro, with permission]

Thus, for a T-Burner with a surge tank, and assuming that other loss mechanisms due to the combustion zone is negligible, the growth rate can be determined as:

$$\alpha_b = \alpha_g - \alpha_d \quad (for\ two\ sides) \tag{B.4.12}$$

In this equation g denotes the growth at the beginning and d denotes the decay at the end. The second method with a surge tank is also proposed. First a test is performed with propellant on both sides. The second test has only one side with propellant. It is assumed that the losses are equal in both tests and α_b is proportional to the burning surface. The result is:

$$\alpha_{b,T} = \alpha - \alpha_{1/2} \tag{B.4.13}$$

The second approach could possibly yield good results. However there are several complicating factors. The decrease in area may reduce the driving so that it cannot sustain an oscillation. If only one side is burning then it would be difficult to match the frequency shift. This method is also only applicable if a surge tank is connected to regulate the pressure. To ensure that the pressure remains the same, the nozzle would have to be changed that would make the assumption that loss factors are the same incorrect.

If, however, no surge tank is available, the decay factors must be calculated analytically or through approximations. Thus the burning surface growth rate can be calculated:

$$\alpha_b = \alpha - \alpha_w - \alpha_n - \alpha_p \tag{B.4.14}$$

The thermal and viscous losses at the walls are regarded as negligibly small. The wall losses according to (145) are:

$$\alpha_{w,n} = -\frac{12.99 f_n}{R} \tag{B.4.15}$$

In this equation R is the radius in meters and f is the frequency of the longitudinal oscillations. Equation is valid for an end burning configuration. The nozzle losses can be computed for longitudinal modes as:

$$\alpha_{n,l} = a_0 \frac{J}{L} \tag{B.4.16}$$

For tangential modes the attenuation is:

$$\alpha_{n,l} = a_0 \frac{J}{2L} \tag{B.4.17}$$

Particle dampening is an extremely useful tool as a suppressing agent of combustion instability. In modern tactical motors, that are required to be smokeless, ZrC and SiC particles have become the particles of choice. However, adding particles reduce the SRM performance (since more particles means less propellant). Thus, it is important to ascertain the particles dampening coefficient and thus minimize the required particle loading. The T-Burner allows for this to be evaluated easily. Several methods have been proposed:

Epstein and Caphart render reasonable results(163):

$$\alpha_p = -36\pi X \delta f \frac{(1+z)z^2}{16z^4 + 72\delta + 81\delta^2(2z^2+2z+1)} \qquad where\ z = (\pi f d^2/4\nu\delta)^{1/2} \tag{B.4.18}$$

According to Culick (64), the following has been shown to work for small particles and lower frequencies (Similar approach followed by Baum and Levine (75)):

$$\alpha_p = -\frac{1}{2}\left(\frac{\delta}{1+\delta}\right)\left[X_1 + (\bar{\gamma}-1)\frac{C}{\bar{C}_p}X_2\right]$$

$$Where:\ \bar{C}_v = \frac{C_v + \delta C}{1+\delta};\ \bar{C}_p = \frac{C_p + \delta C}{1+\delta};\ \bar{\gamma} = \frac{\bar{C}_p}{\bar{C}_v} \tag{B.4.19}$$

$$X_1 = (\omega_n \Omega_d)/(1+\Omega_d^2);\ X_2 = (\omega_n \Omega_t)/(1+\Omega_t^2)$$

This has been refined to(95):

$$\alpha_p = \frac{C_m}{(1+C_m)}\frac{\omega}{2}\frac{\omega\tau_D}{1+(\omega\tau_D)^2} \tag{B.4.20}$$

Where the particle relaxation time τ_D becomes:

$$\tau_D = \frac{\rho_p D^2}{18\mu} \tag{B.4.21}$$

If a T-Burner with a surge tank is used the particle dampening can be obtained from the results:

$$\alpha_p = \alpha - \alpha_b - \alpha_n - \alpha_w \tag{B.4.22}$$

As illustrated by Culick's analysis, the addition of particles changes the specific heats of the gas phase. This translates into a change in speed of sound within the medium. Since it is often the case that thermodynamic programs cannot correctly determine the shift in the speed of sound nor the specific heats of the gas particle mixture, it, would be of use if these properties can be measured. The speed of sound can be found in two ways. Firstly, the frequency of the mode can be determined using Fourier analysis and using equation (B.2.1). This is because the frequency observed is generally that of the first longitudinal mode. The second method is to have transducers on both ends of the T-Burner and to measure the time between two corresponding peaks. The distance travelled is known and thus the speed of sound can be calculated.

Having established how the growth rate constant for the burning surface can be found, it is now possible to return to the original problem of obtaining the response function and thus the admittance function to be used in the stability prediction. The first thing to realise is that the response and admittance function is in fact a complex quantity:

$$\begin{aligned} R_b &= R_b^{(r)} + R_b^{(i)} \\ A_b &= A_b^{(r)} + A_b^{(i)} \end{aligned} \tag{B.4.23}$$

From a T-Burner analysis the real part of the function is found. It has been well established that the real part of the response function can be obtained as (13):

$$R_b^{(r)} = \frac{\bar{p}}{4\rho_p \bar{r} a_b} \frac{(\alpha_g + \alpha_d)}{f} \tag{B.4.24}$$

However, for low frequencies there are several complicating factors that prohibit the direct application of equation (B.4.24):

- The acoustic losses are more dominant;
- The increased volume of the T-Burner;
- Oscillations tend to start before equilibrium within the chamber is reached.

Dehority *et al.* (141) gives a correction for non-uniform heat loss as:

$$R_b^{(r)} = \frac{\bar{p}}{4\rho_p \bar{r} a} \frac{(\alpha_g + \alpha_d)}{f} \left(\frac{a}{a_b} \right) \tag{B.4.25}$$

The response can now be plotted against the dimensionless frequency. The two parameter solution can now be fitted to the experimental data and the parameters A and B can be found for a particular propellant. This should be evaluated against the A and B parameters found in using the Z-N model or a similar model.

After rearranging Equation (B.4.2) , the admittance function is given as (12):

$$A_b^{(r)} = \gamma M_b \frac{\bar{a}}{\bar{a}_b} \left[R_b^{(r)} - \frac{1}{\gamma} \right] \tag{B.4.26}$$

Horton (185) derives the admittance function in terms of T-Burner length and the growth and decay measured:

$$A_b^{(r)} = -\left(\frac{L}{2\rho a_0^2} \right) (\alpha_g - \alpha_d) \tag{B.4.27}$$

If an extended area T-Burner is used, the flow turning effect must be factored into the analysis. The flow turning correction is introduced by Culick (63) and Flandro's "admittance correction"(167). Both were reviewed by Vuillot (177). The study by Vuillot indicates that Flandro's correction gives better results and will therefore be used in this study. For a cup shaped T-Burner the growth and decay can be expressed in terms of the extension ratio, e(L/(length of extended propellant)):

$$\alpha = \alpha_{end} + \alpha_{cup} - \alpha_d \tag{B.4.28}$$

Where:

$$\alpha_{end} = \frac{2a}{L}(M_b + A_{bN}^{(r)}) \tag{B.4.29}$$

and

$$\begin{aligned} &\alpha_{cup} = \frac{2a}{L}\left(M_b + A_{bN}^{(r)} + \Delta A^{(r)}\right)\left[e + \frac{\sin(2\pi e)}{2\pi}\right] \\ &where: \; A_b^{(r)} = A_{bN}^{(r)} + \Delta A^{(r)} \end{aligned} \tag{B.4.30}$$

It is shown that the driving force of the mean gas motion M_b is cancelled by the admittance correction $\Delta A_{(r)}$ for waves parallel to the burning surface. Thus for the first mode $n = 1$ and $M_b/\sqrt{Re^{-1}}$ 4:

$$\alpha_{cup} = \frac{2a}{L}\left(A_{bN}^{(r)}\right)\left[e + \frac{\sin(2\pi e)}{2\pi}\right] \tag{B.4.31}$$

This is a significant decrease in growth rate decrease. For any longitudinal mode integer and any value of $M_b/\sqrt{Re^{-1}} > 4$:

$$\begin{aligned} &\Delta\alpha_{cup} = -\frac{2a}{r}\left[e + \frac{\sin(2\pi e)}{2\pi}\right]\frac{1}{\left(\sqrt{Re^{-1}}\right)}\frac{n\pi b}{(a^2+b^2)} \\ &where\, a\, and\, b\, are\, defined: \\ &a^2 + b^2 + \left(M_b \Big/ \sqrt{Re^{-1}}\right) a = 0 \\ &2a + \left(M_b \Big/ \sqrt{Re^{-1}}\right) = k/b \end{aligned} \tag{B.4.32}$$

The acoustic Reynolds number is defined as:

$$Re = \frac{D_p}{2\nu_0 a_0} \tag{B.4.33}$$

Thus, the admittance for an extended area T-Burner can be found (167). By using the relationship from Equation (B.4.2) the response function can also be found. The data analysis shown here is still based primarily on work done in the 1960-1975. There have definitely been some improvements, but little has been published in recent times.

B.5 Conclusions

Blomshield's test regime is out of reach for the average motor designer. This program has yielded high quality data that has contributed significantly to the understanding of combustion instability. All result from the proposed analysis will have to be measured against the results obtained by Blomshield and his co-workers. Most peripheral data such as frequency analysis and particle dampening are well in hand. These values can easily be obtained analytically and experimentally. New test apparatuses that have been developed are limited and require much improvement. The T-Burner is the industry standard. T-Burners are expensive to both operate and maintain due mainly to the number of tests (15-30 at a specific pressure) required to completely evaluate a propellant at all pressures and frequencies. It is also limited and does not provide any information about triggering. It gives the admittance of an unstable propellant and as such can only provide information on the limiting amplitude. Difficulties arise due to the effective lengthening of the chamber causing the frequency to change continuously. It is also a very subjective analysis making the results dependent on the skill level of the operator.

It also has several advantages. The addition of a T-Burner with a surge tank not only allows the response function to be determined more easily, but also the particle dampening to be obtained. The variation in propellant composition (excluding particles) to minimize the propellant response is unrealistic at this time. Thus, the only realistic tool is that of using particle dampening. Though there are currently several models to predict this dampening, it will be important to evaluate these against practical results. The goal is to reduce the amount of particulate matter and keep the SRM performance as close as possible to the maximum possible performance.

It will also allow the evaluation of thermodynamic properties of the gas/particle mixture in terms of the speed of sound in the motor. Thermodynamic predictive tools do not always predict the thermodynamic properties such as heat capacities and thus the speed of sound of a mixture accurately. Thus any model for particle dampening based on such predictions, will be in error.

Appendix C

Pulsers

C.1 Sample calculation of Burst Pressure

The following example shows the calculation for a 3.66mm orifice diameter and a 0.05mm orifice plate. Firstly, the pressure curves up to the point of rupture are plotted as shown in Figure C.1.The next step is to fit the 5^{th} order polynomials.

Having obtained all the polynomials, these curves can now be used in(2.1.15). Setting these equations equal to each other in, Excel solver can now be used to solve for $P_{y,atm}$ and Δt.

For this configuration a maximum deviation of 1.47 is found and the average is 19.23 MPa. Thus, by using these values in the program, results will be obtained in the $\pm$ 1.5 MPa error range.

C.2 Pulser Pressure Curves

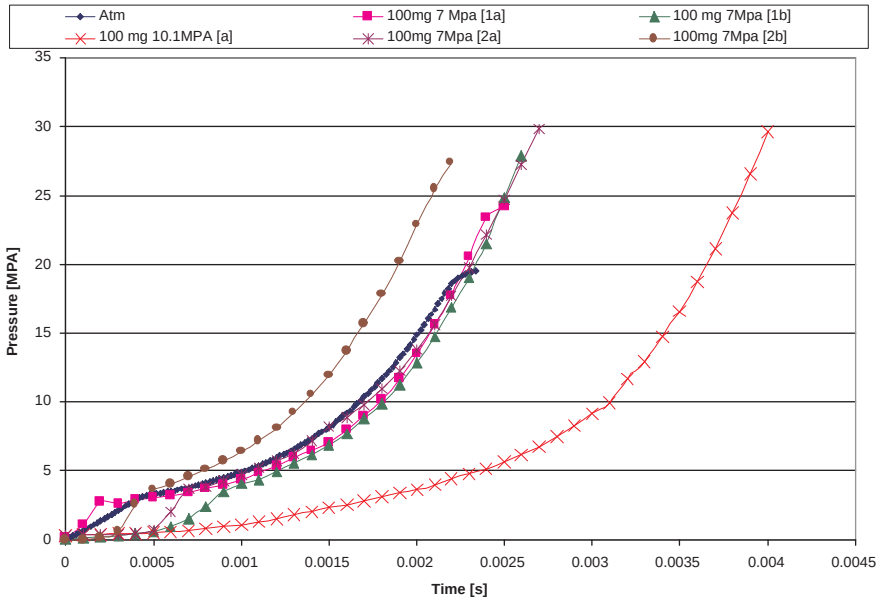

Figure C.1: Pressure Curves Orifice diameter 3.36mm and 0.05mm Burst diagram

Table C.1: Calculations Orifice Diameter 3.66mm and burst Plate 0.05mm

No	Test	Formula	R^2	P_c	t_f	**Equation** (2.1.15)
1	**Atmospheric**	P = -1513855970050050x^5 + 7215519470896x^4 - 8434612925x^3 + 37629x^2 + 7653x - 0.0247	0.9992	0.1	0.00234	19.75419
2	**100 mg 10.1MPa [a]**	P = 24310304368128x^5 + 178126562126x^4 - 1407410015x^3 + 3431599x^2 - 1469x + 0.45642	0.9997	10.19	0.004	18.9026
3	**100 mg 7.4MPa [1b]**	P = -725594536755200x^5 + 6290111456912x^4 - 16835580740x^3 + 20295173x^2 - 5722x + 0.36	1.00	7.45	0.0026	19.75419
4	**100 mg 7MPa [2a]**	P = -1621125821011970x^5 + 11724224811216x^4 – 28405925444x^3 + 29859914x^2 - 7302x + 0.5245	0.9990	7	0.0027	22.24662
5	**100 Mg 6.6MPa [1a]**	P = -512017536296960x^5 + 2234246052272x^4 + 715925297.9375x^3 - 7379929x^2 + 8885.5346x + 0.4218	0.9970	6.6	0.0025	17.78843
6	**100 mg 7MPa [2b]**	P = -5104440117673980x^5 + 27528140293184x^4 - 48974694265x^3 + 35637551x^2 - 2396x - 0.1096	0.9990	7.035	0.0022	19.95191
				AVE(1,2,3,5,6)		19.23027
		Δt = $2.33E^{-05}$			**STDEV**	1.472278

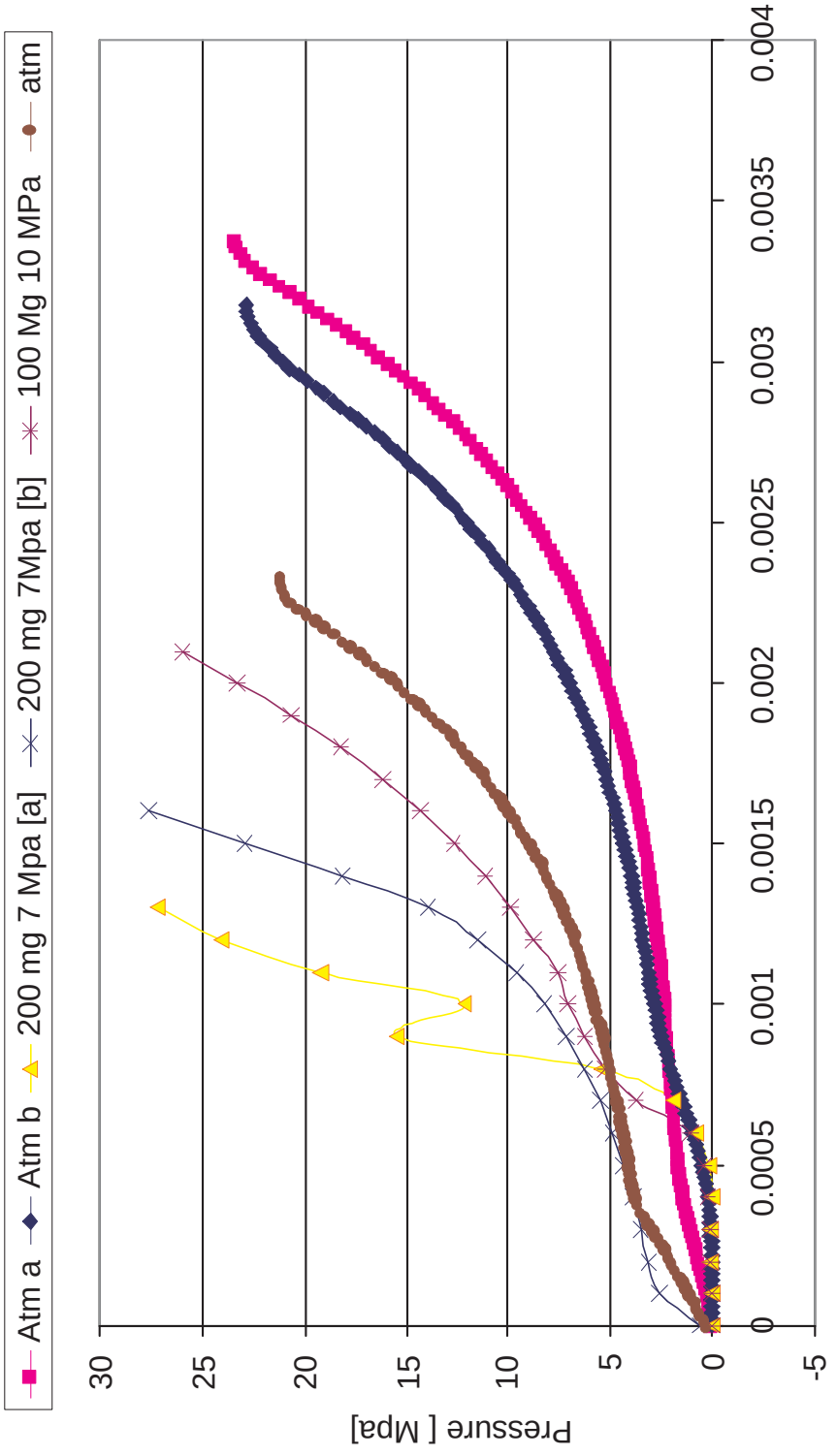

Figure C.2: Pressure Curves Orifice Diameter 5.05mm and Burst plate 0.1mm

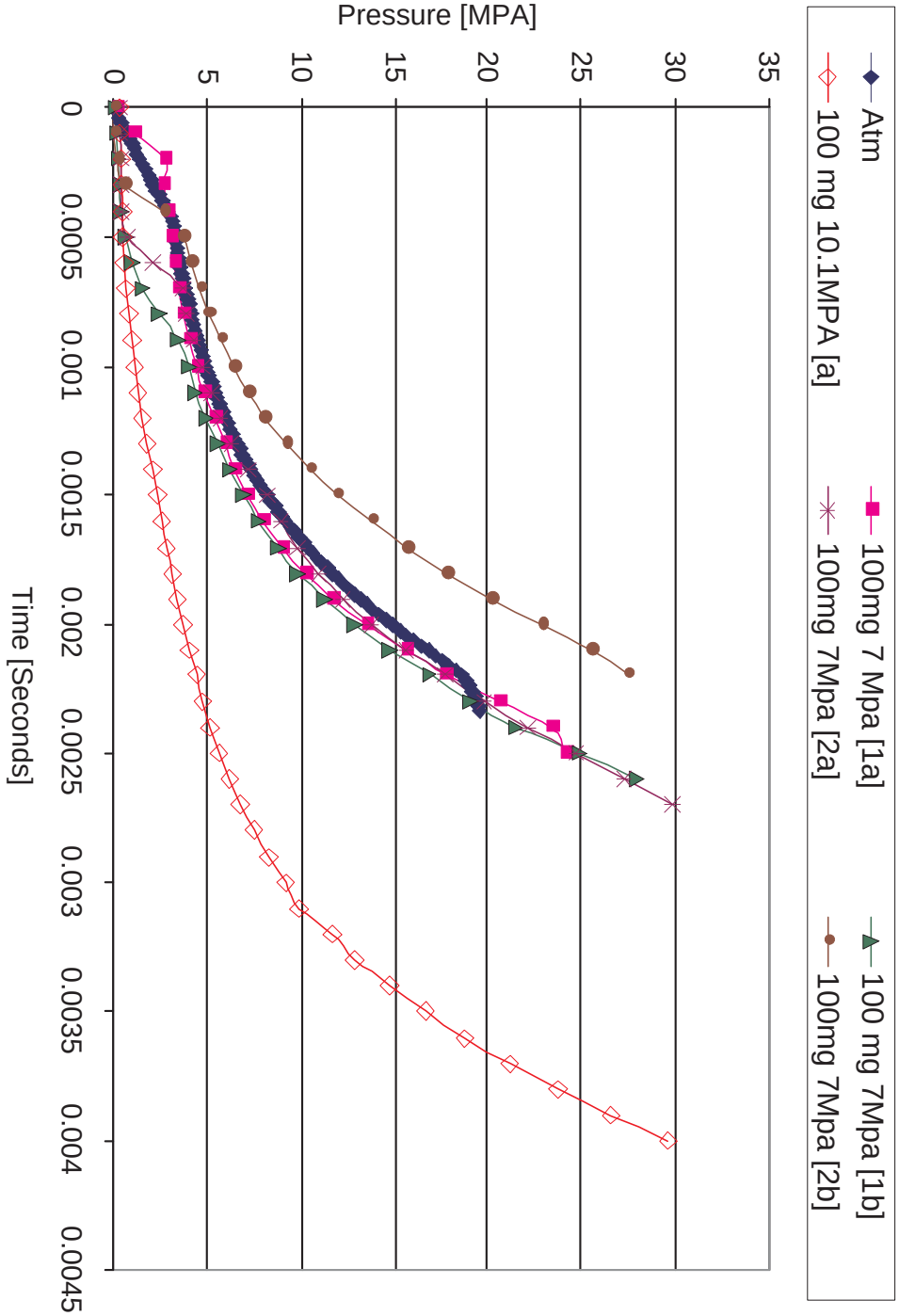

Figure C.3: Pressure Curves 3.66 mm Orifice Diameter and Burst Plate 0.05mm

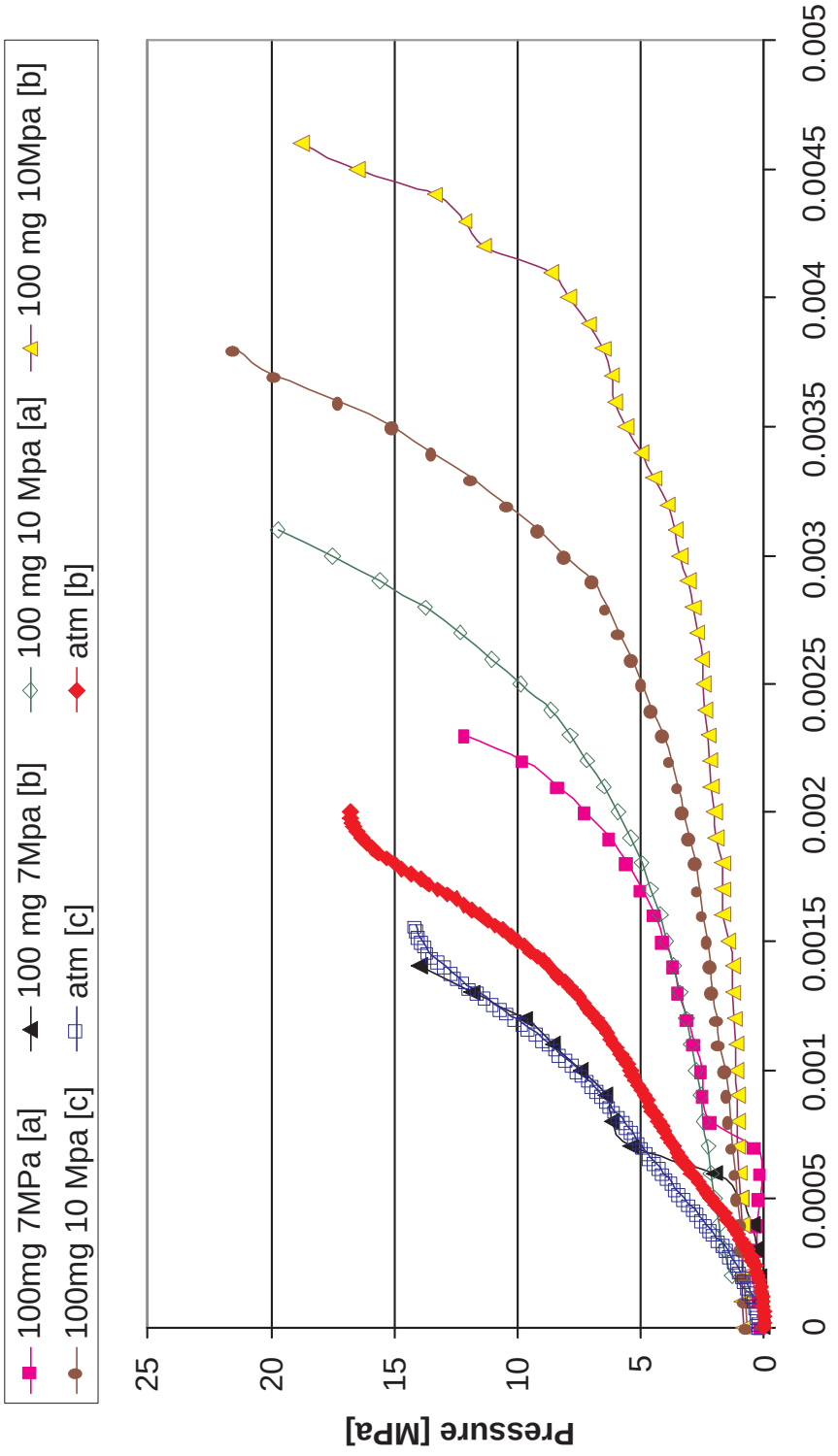

Figure C.4: Pressure Curves 5.05mm and Burst Plate 0.05mm

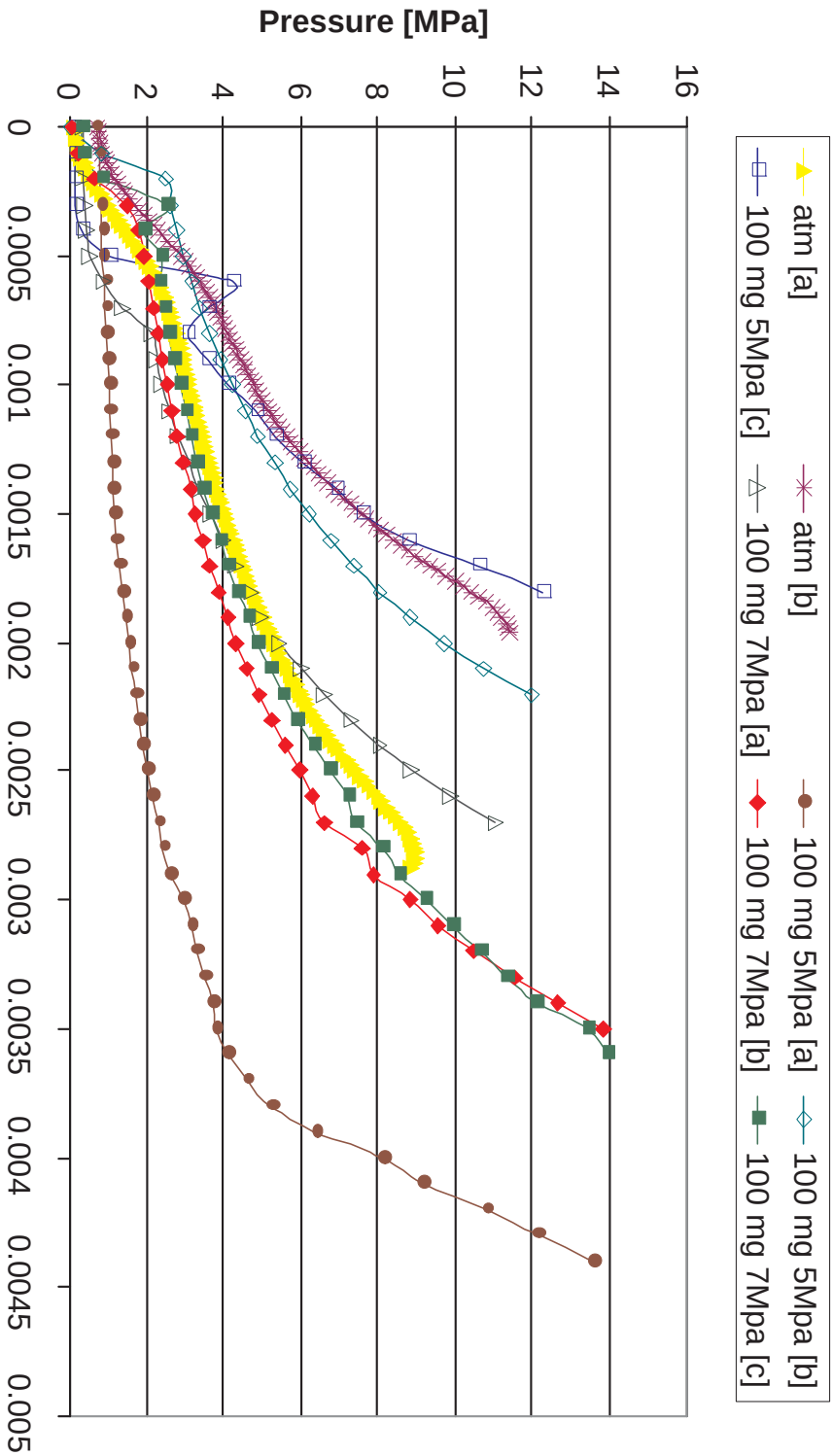

Figure C.5: Pressure Curves Orifice diameter 9.02mm and Burst plate 0.1mm

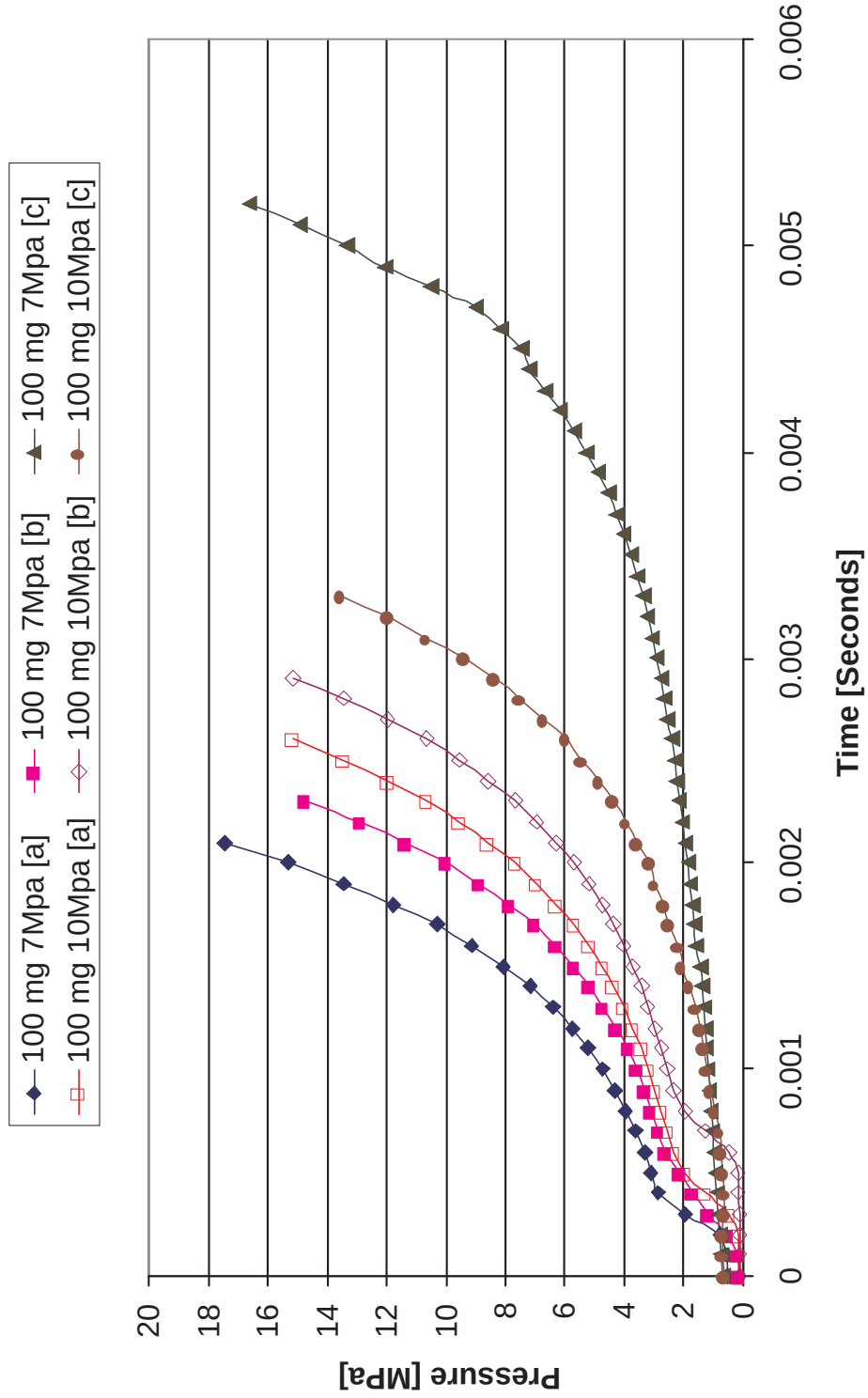

Figure C.6: Pressure Curves Orifice diameter 7.49mm and Burst plate 0.1mm

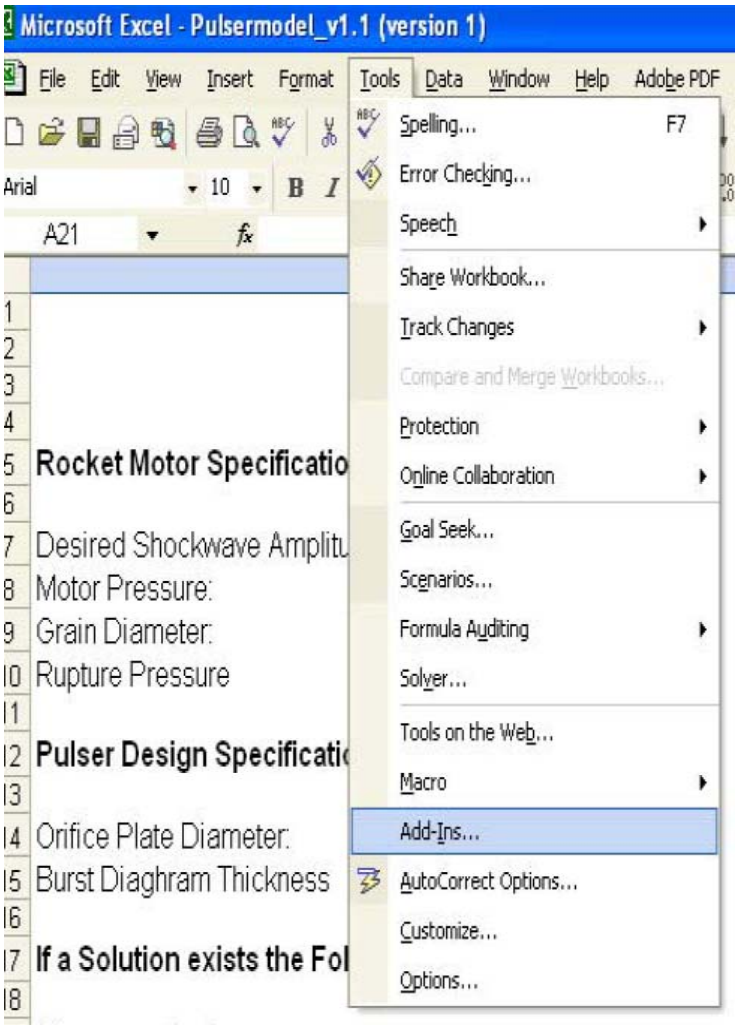

Figure C.7: Add-In Solver Step 1

C.3 Computer Program Users Manual

Installation

Copy the excel File Pulsermodel_v1.1.xls onto computer hard drive at desired location. The program is a excel program and can be run immediately. It is also necessary to add Solver if it is not already installed (Figure C.7).

Next, open the Tools drop-down menu and select Add-Ins.

The screen as shown in Figure C.8 will appear. Select the solver add-inn and click OK.

Startup

When starting up the program the following error message may be displayed (Figure C.9).

Click OK:

Select tools, Go to Macro, and then select security Figure C.10.

The Figure C.11 is displayed. Set the security levels to low, close the program and then open the program again. The macros within the program will now be allowed to run.

Figure C.8: Add-In Solver Step 2

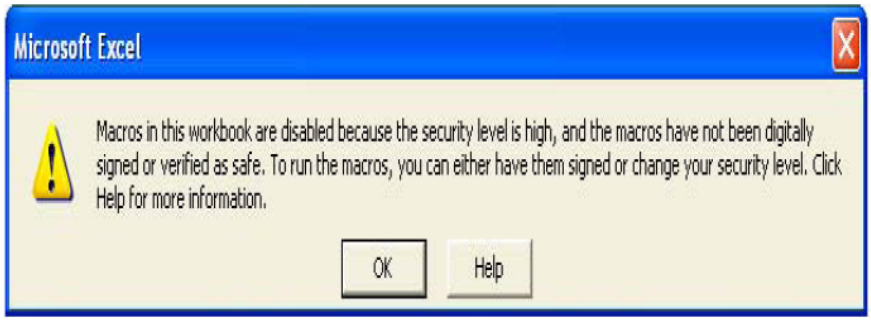

Figure C.9: Security alert Macros

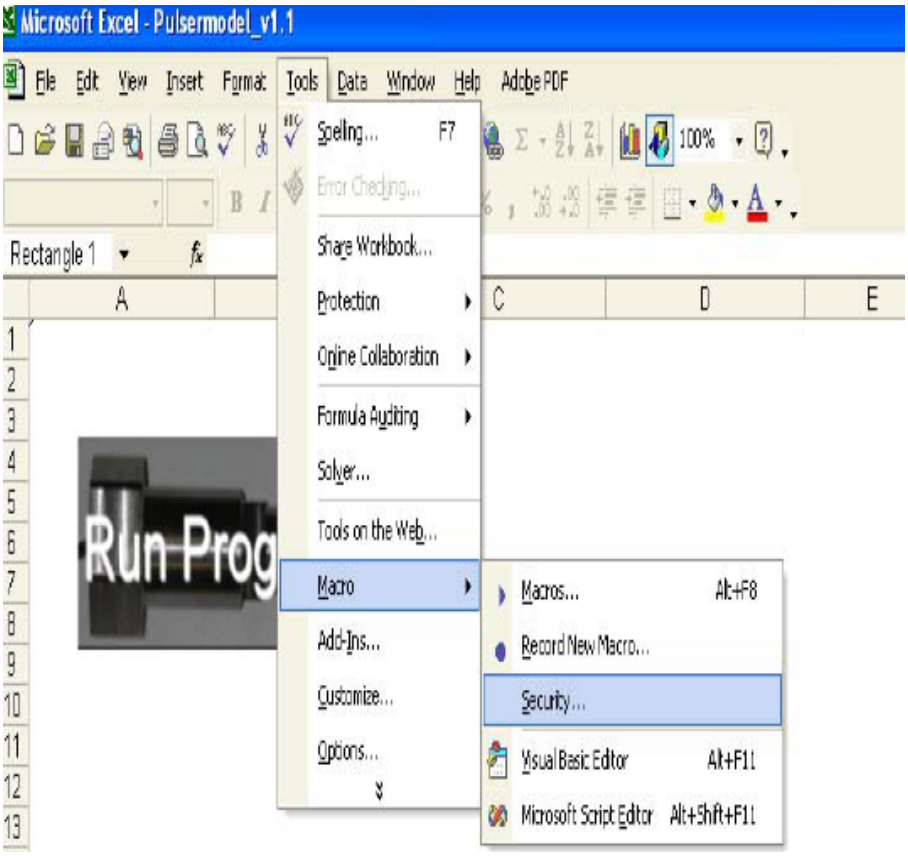

Figure C.10: Accessing Macro Security

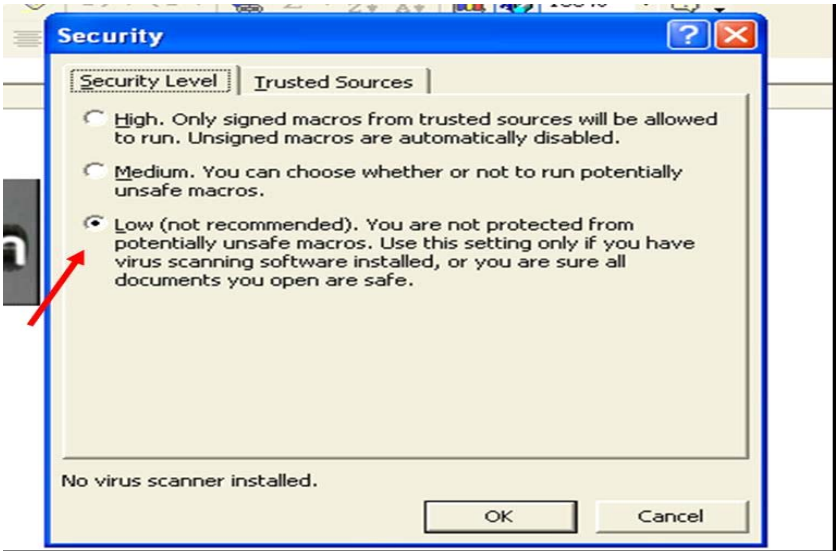

Figure C.11: Enabling Macros

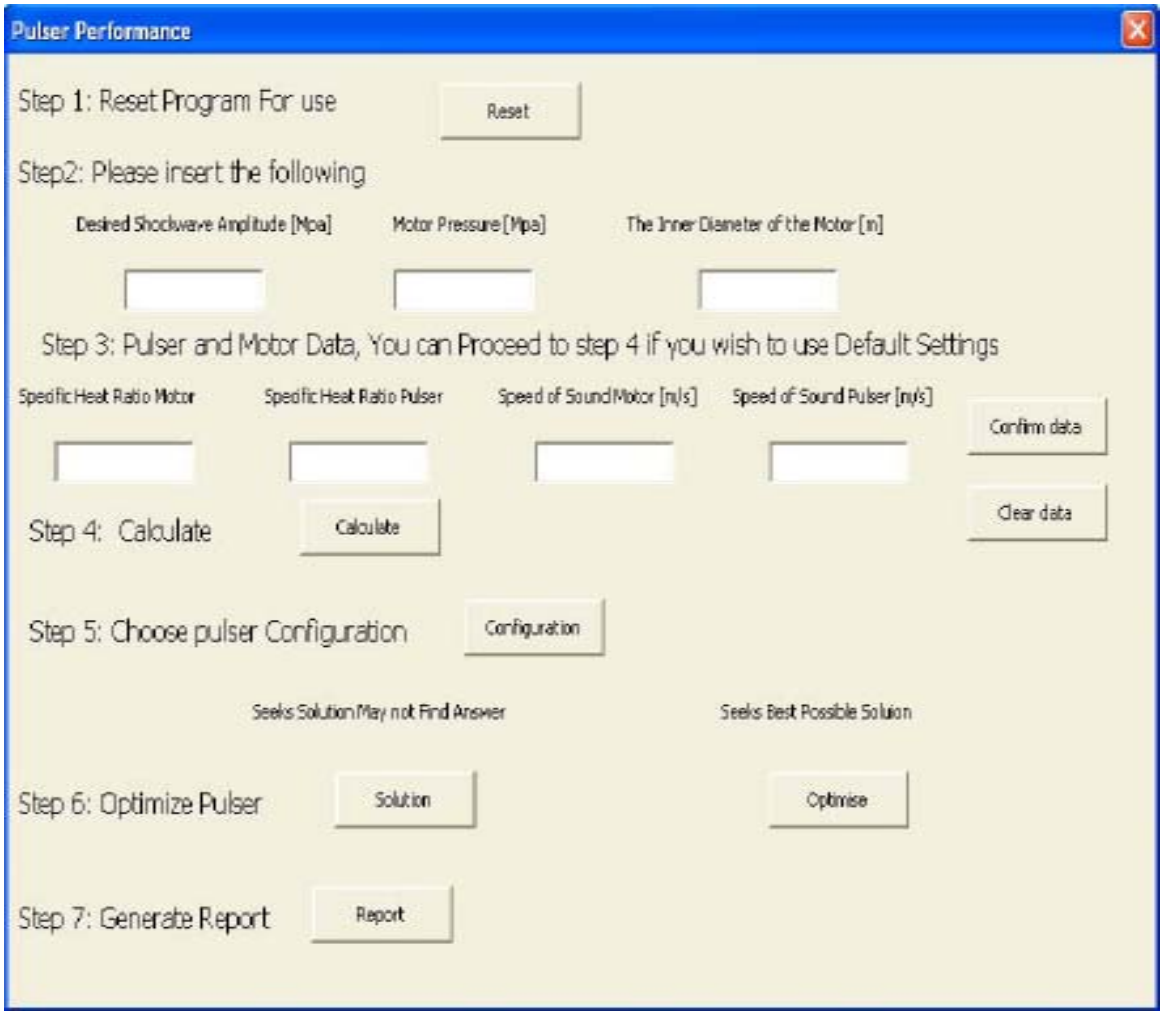

Figure C.12: Main Program

This, however, sets Excel security on low. If the Excel version automatically gives the option to enable the macros this will also work.

When opening the program the following screen will appear Figure C.12:

Using Program

Step 1: Reset

Reset sets the values of the pressure time curves is set equal to zero. It is important to do this before proceeding since Solver may not find a valid solution otherwise. The following window appears to remind the user to export results of the previous run since all previous data will be lost (Figure C.13).

Step 2: Please input following values

In this step the desired Pulse amplitude and the motor pressure is entered in MPa. The inner diameter of the rocket motor grain needs to be given in meters. These values are used to calculate the required rupture pressure.

Step 3: Pulser and Motor Data

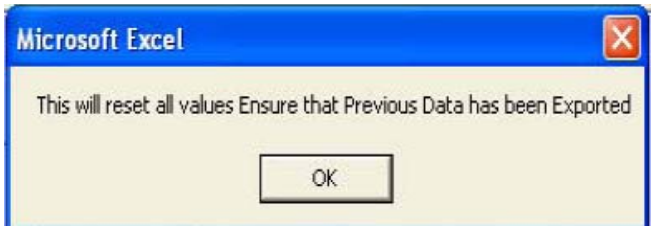

Figure C.13: Reminder to Export Report

Figure C.14: Default Settings

Step three is only required if the thermodynamic data does not match the default settings for the following:

1. Ratio of specific heats of Rocket Motor: Default 1.66
2. Speed of sound in Motor: Default 1014 [m/s]
3. Ratio of specific heats Pulser: Default 1.193 [m/s]
4. Speed of sound in pulser: 955 [m/s]

Once these values have been entered, click on Confirm data. This will replace the default settings in the calculations. If you wish to use another set of data, click on Clear data and put in new values.

Step 4: Calculate

This step calculates the required rupture pressure from the input data. The following window will appear to confirm that you wish to use the default settings, it will not appear if the data has been updated (Figure C.14).

Click OK and the screen will appear as shown in Figure C.15 upon successful calculation.

Click OK.

Step 5: Configuration

This will select a pulser configuration from the experimental database that will give the best result. If a valid configuration exists, the following message box will appear (Figure C.16).

Click OK.

Step 6: Optimization

Figure C.15: Calculation Complete

Figure C.16: Verification of Pulser

Solution: This button seeks an exact solution. Since we are dealing with experimental data it may not exist due to the physical limits of the pulsers. When the program is run one of two windows will appear. In both cases click OK:

One possible window will show that a solution has been found(Figure C.17):

Another possible window (Figure C.18) shows that no solution was found.

Optimization: Since there may not be an exact solution it may be necessary to optimize the solution. What this does is to find the pulser that will give the closest value to that which is required.

Step 6: Report

This generates a report on which all the relevant information is given for the manufacture of the pulser. It is possible to create a PDF, create a Word document or print the report. It is important for the user to note that the next time the program is run, the report will be regenerated and thus all values will be lost. It is thus suggested that a PDF be created as a digital copy of the report if it is desired to manufacture the pulser.

Interpreting Report

The first section in the report shows the specifications given by the user as well as the required rupture pressure to achieve the required pulse amplitude. The next section gives the configuration of the pulsers.

The next two sections both give the optimization results. It gives both the amount of gun powder to be added and the time from ignition to rupture of the burst diaphragm. The user will have to use discretion when interpreting the results. There are three possible cases:

- That the optimization result and the exact solution match. This is the ideal case the two results verify each other.
- The exact solution gives an error message as in Figure C.18, but on the graph it appears to give a better solution than the optimization result. This can be attributed to the solver having too high precision for convergence. This can be altered by changing the settings within solver:

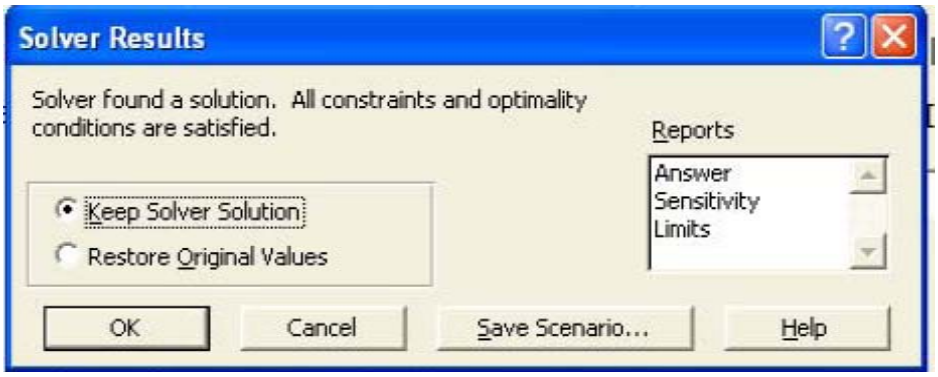

Figure C.17: Solver valid solution Message

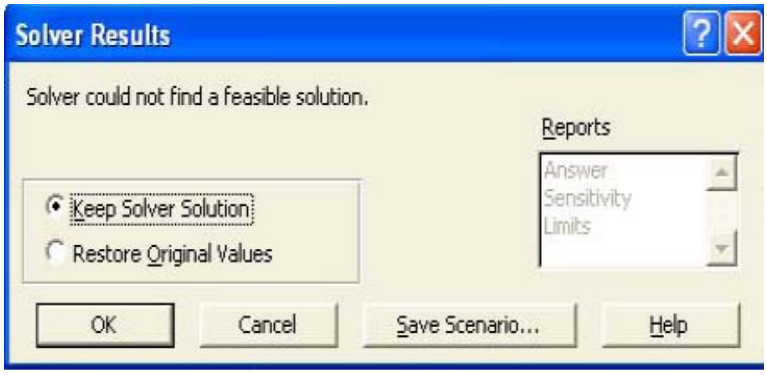

Figure C.18: Solver Error Message

Select the Pulser Data worksheet. Go to the Tools drop-down menu and select Solver (Figure C.19).

Set Precision to 0.0001 (Figure C.20). Run the program again to see if a valid solution is obtained.

The final possibility is that, an exact solution may not exist. The optimization result must then be used.

Figure C.21 and C.22 show a typical report.

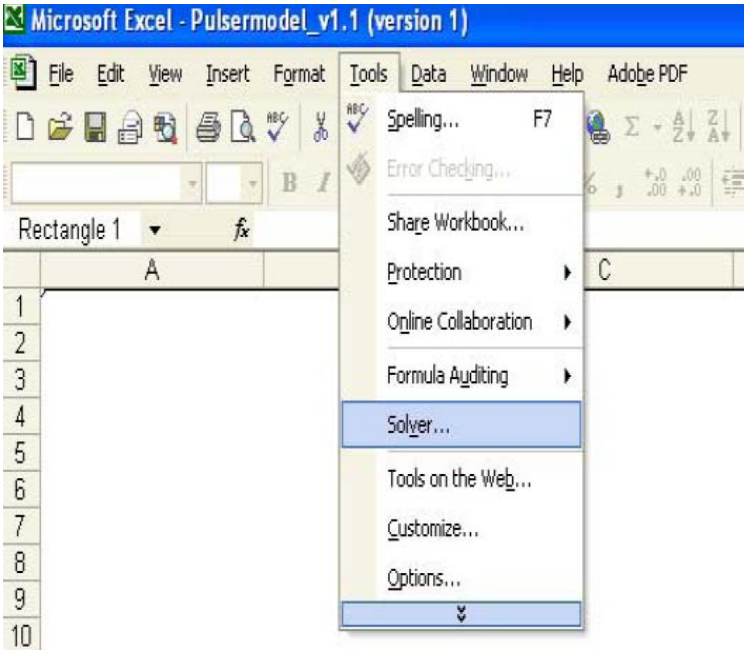

Figure C.19: Select Solver

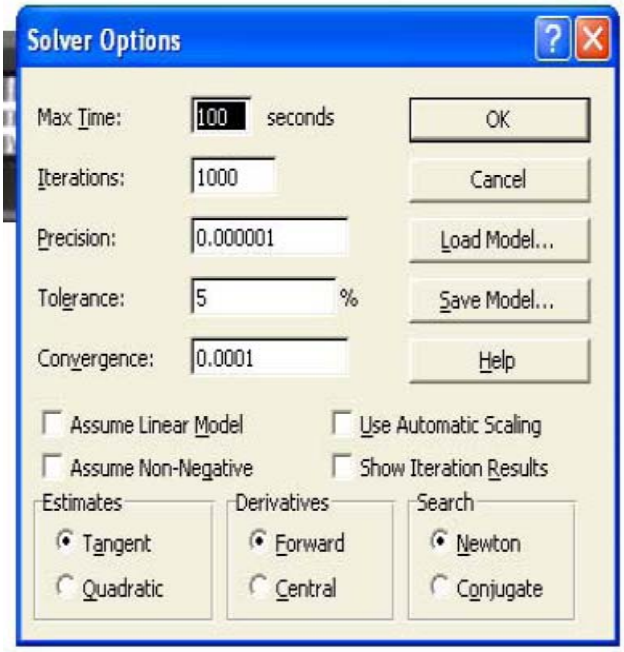

Figure C.20: Solver Options

Design Of Pulser

Rocket Motor Specifications:

Desired Shockwave Amplitude:	0.7	MPA
Motor Pressure:	7	MPA
Grain Diameter:	0.1	m
Rupture Pressure	25.6025	MPA

Pulser Design Specifications are:

Orifice Plate Diameter:	5.05	mm
Burst Diaghram Thickness	0.1	mm

If a Solution exists the Following is Valid:

Charge required:	121.209	mg
Time From Ignition to Rupture	0.00344	s
Rupture Pressure	25.6025	MPA

If the minimum error Solution is valid:

Charge required:	121.209	mg
Time From Ignition to Rupture	0.00344	s
Rupture Pressure	25.6025	MPA

These Solutions are based on experimental results, and should be verified by cold flow tests before proceeding to live rocket Motors. A variance of 2MPA is to be expected

Figure C.21: Example of Report Page 1

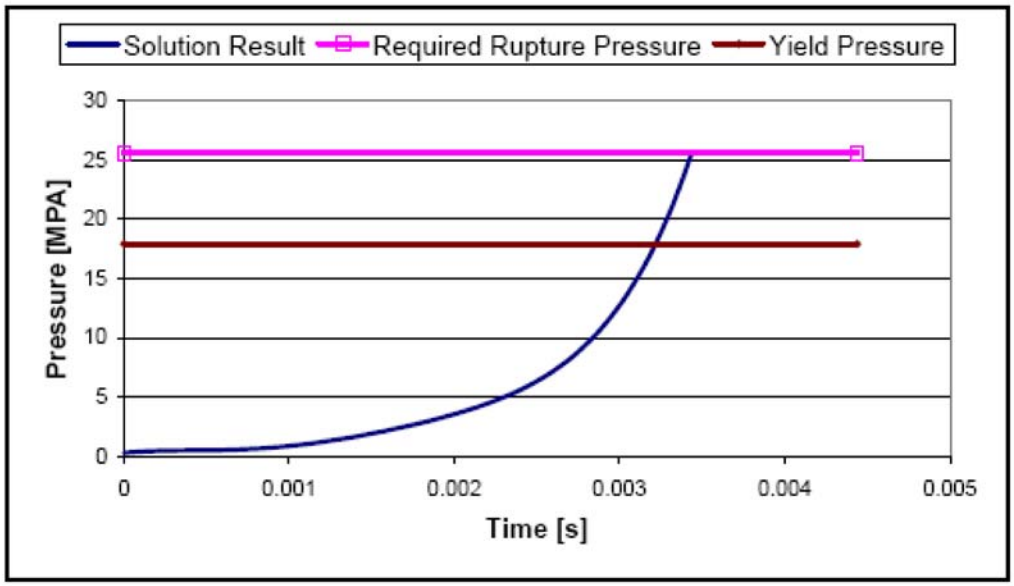

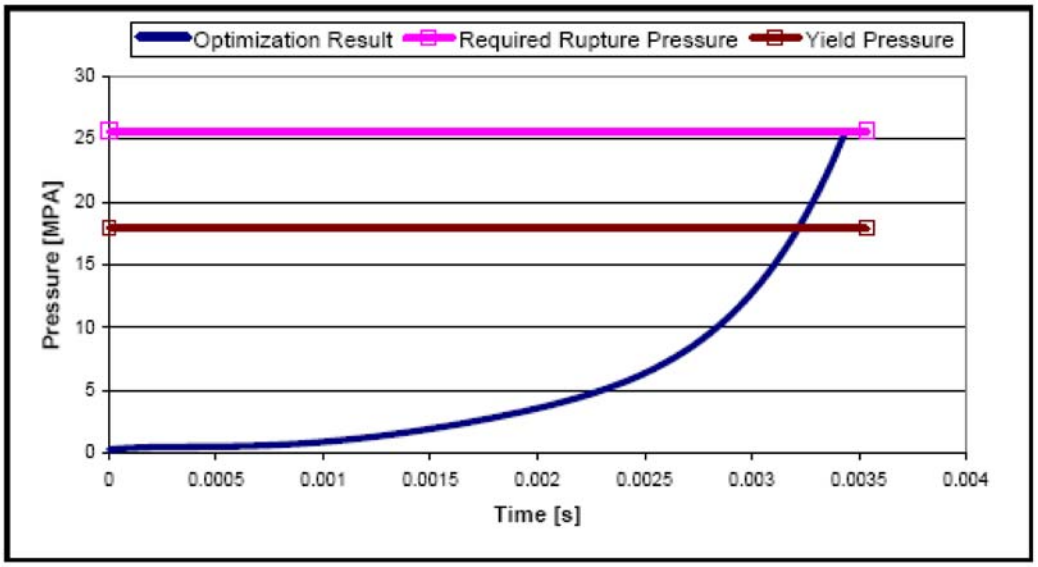

Figure C.22: Example of Report Page 1

References

[1] Blomshield, F. S., "Historical Perspective of Combustion Instability in Motors: Case Studies," *37th AIAA/ASME/SAE/ASEE Joint Propulsion Conference and Exhibit*, AIAA, Salt Lake City, Utah, 2001, pp. 1–13.

[2] Culick, F. E. C., "Combustion Instabilities: Mating Dance of Chemical, Combustion, and Combustor Dynamics," *36th AIAA/ASM/SAE/ASEE Joint Propulsion Conference and Exhibit*, AIAA, 2000.

[3] King, M. K., "Examination of Chemical Approaches to Establish Composite - Propellant Combustion," *Journal of Propulsion and Power*, Vol. 12, No. 3, 1996, pp. 554–563.

[4] Hart, R. W. and McClure, F. T., "Theory of acoustic Instability in Solid-Propellant Rocket combustion," *Tenth Symposium (International) on Combustion*, The Combustion Institute, 1965, pp. 1047–1065.

[5] Flandro, G. A., Perry, E. H., and French, J. C., "Nonlinear Rocket Motor Stability Computations: Understanding the Brownlee-Marble Observations," *44th AIAA Aerospace Sciences Meeting and Exhibit*, No. AIAA-2006-539, AIAA, Reno, Nevada, 2006, pp. 6538–6558.

[6] Tang, K. C. and Brewster, M. Q., "Nonlinear Dynamic Combustion in Sold Rockets: L* Effects," *Journal of Propulsion and Power*, Vol. 17, No. 4, 2001, pp. 909–918.

[7] Schöyer, H. F. R., "Results of Experimental Investigations of the L* Phenomena," *Journal of Spacecraft and Rockets*, Vol. 17, No. 3, 1980, pp. 200–207.

[8] Schöyer, H. F. R., "L* Oscillations and Pressure Frequency Correlation for Solid Rocket Propellants," *AIAA Journal*, Vol. 15, No. 9, 1977, pp. 1347–1348.

[9] Schöyer, H. F. R. and de Boer, R. S., "Experimental Investigation into L* Instability of Double Base Rocket Propellants," *Propellants and Explosives*, Vol. 3, 1978, pp. 88–96.

[10] Sehgal, R. and Strand, L., "A Theory of Low-Frequency Combustion Instability in Solid Rocket Motors," *AIAA Journal*, Vol. 2, No. 4, 1964, pp. 696–702.

[11] Coates, R. L., Cohen, N. S., and Harvil, L. R., "An Interpretation of L* Combustion Instability in Terms of Acoustic Instability Theory," *AIAA Journal*, Vol. 5, No. 6, 1967, pp. 1097–1102.

[12] Beckstead, M. W., Mathes, H. B., Price, E. W., and Culick, F. E. C., "Combustion Instability of Solid Propellants," *Sixteenth Symposium (International) on Combustion*, The Combustion Institute, Massachussets Institute of Technology, 1976, pp. 203–211.

[13] Beckstead, M. W. and Culick, F. E. C., "A Comparison of Analysis and Experiments for Solid Propellant Combustion Instability," *AIAA Journal*, Vol. 9, No. 1, 1971, pp. 147–154.

[14] Inami, Y. H. and Shanfield, H., "Nonacoustic Combustion Pulsations of Ammonium Perchlorate Containing Aluminium," *AIAA Journal*, Vol. 2, No. 7, 1964, pp. 1314–1318.

[15] Kubota, N. and Kimura, J., "Oscillatory Burning of High-Pressure Exponent Double-Base Propellants," *AIAA Journal*, Vol. 15, No. 1, 1977, pp. 126–127.

[16] Jahnke, C. C. and Culick, F. E. C., "Application of Dynamic Systems Theory of Nonlinear Combustion Instabilities," *Journal of Propulsion and Power*, Vol. 10, No. 4, 1994, pp. 508–517.

[17] Burnley, V. S., Culick, F. E. C., and Swenson, G., "Pulsed Instabilities in Solid-Propellant Rockets," *Journal of Propulsion and Power*, Vol. 11, No. 4, July-August 1996, pp. 657–665.

[18] Isella, G. C. and Culick, F. E. C., "Modeling the effects of velocity coupling on the global dynamics of combustion chambers," *AIAA/ASME/SAE/ASEE Joint Propulsion Conference and Exhibit*, No. AIAA-2000-3187, AIAA, Huntsville, AL„ July 16-19 2000.

[19] Ananthkrishnan, N., Deoy, S., and Culick, F. E. C., "Reduced-order Modelling and Dynamics of Non-Linear Acoustic waves in a Combustion Chamber," *Combustion Science and Technology*, Vol. 177, 2005, pp. 1–27.

[20] Flandro, G. A., "Irregular Burning: On the Origin of the DC Shift," *43rd AIAA/ASME/SAE/ASEE Joint Propulsion Conference and Exhibit*, AIAA, AIAA, 2007.

[21] Flandro G.A., F. S., "Effects of Parallel Wave Incidence on Combustion Instability Driving Mechanisms," *43rd AIAA/ASME/SAE/ASEE Joint Propulsion Conference & Exhibit*, No. AIAA 2007-5807, Cincinnati, OH, AIAA, 8 - 11 July 2007 2007.

[22] Denison, M. R. and Baum, E., "A Simplified Model of Unstable Burning in Solid Propellants," *ARS Journal*, 1961, pp. 1112–1122.

[23] Culick, F. E. C., "Acoustic Oscillations in Solid Propellant Rocket Motors," *Acta Astronautica*, Vol. 12, No. 2, 1966, pp. 113–126.

[24] Culick, F. E. C., "The Stability of One Dimensional Motions in a Rocket Motor," *Combustion Science and Technology*, Vol. 7, 1973, pp. 165–175.

[25] Flandro, G. A. and Majdalani, J., "Aeroacoustic Instability in Rockets," *AIAA Journal*, Vol. 41, No. 3, 2003, pp. 485–497.

[26] Majdalani, J., Flandro, G. A., and Fischbach, S. R., "Some Rotational Corrections To The Acoustic Energy Equation In Injection-Driven Enclosures," *Physics of Fluids*, Vol. 17, 2005, pp. 074102–1–074102–20.

[27] Chibli, H. A., Majdalani, J., and Flandro, G. A., "Fundamental Growth Rate Corrections in Rocket Motor Stability Calculations," *38TH AIAA/ASME/SAE/ASEE Joint Propulsion Conference and Exhibit*, No. AIAA-2002-3610, AIAA, Indianapolis, Indiana, 2002.

[28] Fischbach, S. R., Flandro, G. A., and Majdalani, J., "Volume-to-Surface Transformations of Rocket Stability Integrals," *40th AIAA/ASME/SAE/ASEE Joint Propulsion Conference and Exhibit*, No. AIAA-2004-4053, AIAA, Fort Lauderdale, Florida, 2004.

[29] Fischbach, S., Majdalani, J., Flandro, G., and French, J., "Verification and Validation of Rocket Stability Integral Transformations," *41st AIAA/ASE/SAE/ASEE Joint Propulsion Conference and Exhibit*, , No. AIAA-2005-4001, 2005.

[30] Culick, F., *Unsteady Motions in Combustion Chambers for Propulsion Systems*, No. RTO-AG-AVT-039, Research and Technology Organization North Atlantic Treaty Organization, 2006.

[31] Flandro, G. A., Majdalani, J., and French, J. C., "Incorperation of Nonlinear Capabilities in the Stability Prediction Program," *40th AIAA/ASME/SAE/ASEE Joint Propulsion Conference and Exhibit*, No. AIAA-2004-4182, AIAA, Fort Lauderdale, Florida, 2004.

[32] van Moorhem, W. K., "Flow Turning in Solid-Propellant Rocket Combustion Stability Analysis," *AIAA Journal*, Vol. 20, No. 10, 1982, pp. 1420–1425.

[33] Solanki, N., *Effect of External Pulse on Solid Propellant Rocket Internal Ballistics*, Masters in applied sciences, University of Toronto, 2000.

[34] Knoetze, J. H., "Design Criteria for an Experimental Set-Up for Combustion Instability," Tech. rep., DENEL Land Systems Western Cape, 2000.

[35] Rousseau, C. W., "Pulsers: First Step to testing for the exictence of Combustion Instability in Solid Rocket Motors," Final year project, University of Stellenbosch, 2005.

[36] Blomshield, F. S., "Solid Propellant Combustion Instability," AIAA Advanced Solid Rocket Course.

[37] Blomshield, F. S., Mathes, H. B., Crump, J. A., and Beckstead, M. W., "Nonlinear Stability Testing and Pulsing of Full Scale Tactical Motors," *27th AIAA/ASME/SAE/ASEE Joint Propulsion Conference and Exhibit*, AIAA, Sacremento, CA, 1991.

[38] Blomshield, F. S., Crump, J. A., Mathes, H. B., and Beckstead, M. W., "Stability Testing of Full Scale Tactical Motors," *27th AIAA/ASME/SAE/ASEE Joint Propulsion Conference and Exhibit*, AIAA, Sacremento, CA, 1991.

[39] Blomshield, F. S., Crump, J. A., Mathes, H. B., and Beckstead, M. W., "Stability Testing of Full Scale Tactical Motors," *Journal of Propulsion and Power*, Vol. 13 no.3, 1997, pp. 349–355.

[40] Blomshield, F. S., Mathes, H. B., Crump, J. A., and Bieter, C. A., "Nonlinear Stability Testing of Full-Scale Tactical Motors," *Journal of Propulsion and Power*, Vol. 13, No. 3, 1997, pp. 356–366.

[41] Lovine, R. L., Baum, J. D., and Levine, J. N., "Ejecta Pulsing of Subscale Solid Propellant Rocket Motors," *AIAA Journal*, Vol. 23, No. 3, 1985, pp. 416–423.

[42] Brownlee, W. G., "Nonlinear Axial Combustion Instability in Solid Proplellant Motors," *AIAA Journal*, Vol. 2, No. 2, 1964, pp. 275–284.

[43] Dickinson, L. A., "Command Initiation of Finite Wave Axial Combustion Instability in Solid Propellant Rocket Engines," *ARS Journal*, Vol. 32, 1962, pp. 643–644.

[44] Fischbach, S. R., Majdalani, J., and Flandro, G. A., "Acoustic Instability of the Slab Rocket Motor," *40th AIAA/ASME/SAE/ASEE Joint Propulsion Conference and Exhibit*, AIAA, Fort Lauderdale, FL, 2004.

[45] French, J. C., "Non-Linear Combustion Instability Predicition of SRMS using SPP/SSP," *39th AIAA/ASME/SAE/ASEE Joint Propulsion Conference*, No. AIAA-2003-4668, von Baun Center, 2003.

[46] Malhortha, S., *On Combustion Instability in Solid Rocket Motors*, Doctor of philosophy, California Institute of Technology, 2004.

[47] Flandro, G. A., Fischbach, S. R., and Majdalani, J., "Nonlinear Rocket Stability Prediction: Limit Amplitude, Triggering, and Mean Pressure Shift," *40th AIAA/ASME/SAE/ASEE Joint Propulsion Conference and Exhibit*, No. AIAA-2004-4054, AIAA, Fort Lauderdale, Florida, 2004.

[48] Flandro, G. A., "Approximate Analysis of Nonlinear Instability with Shock Waves," *18th AIAA/SAE/ASME Joint Propulsion Conference*, No. AIAA-82-1220, AIAA, Cleveland, Ohio, 1982.

[49] Flandro, G. A., "Energy Balance Analysis of Nonlinear Combustion Instability with Shock Waves," *Journal of Propulsion and Power*, Vol. 1, No. 3, 1985, pp. 210–221.

[50] Culick, F. E. C., "Some Recent Advances for Nonlinear Acoustics in Combustion Chambers," *AIAA Journal*, Vol. 32, No. 1, 1994, pp. 146–169.

[51] French, J. C., "A Comparison of Nonlinear Combustion Instability Methods," *42nd AIAA/ASME/SAE/ASEE Joint Propulsion Conference*, No. AIAA-2006-4422, 2006.

[52] Culick, F. E. C., "Rotational Axisymetric Mean Flow and Dampening of Acoustic Waves in a Solid Propellant Rocket," *AIAA Journal*, Vol. 4, No. 8, 1966, pp. 1462–1464.

[53] Culick, F. E. C., "Stability of Longitudinal Oscillations with Pressure and Velocity Couplng in a Solid Propellant Rocket," *Combustion Science and Technology*, Vol. 2, 1970, pp. 179–201.

[54] Culick, F. E. C., "Stability of Three-Dimensional Motions in a Combustion Chamber," *Combustion Science and Technology*, Vol. 10, No. 3-4, 1975, pp. 97–187.

[55] Flandro, G. A., "Effects of Vorticity on Rocket Combustion Stability," *Journal of Propultion and Power*, Vol. 11, No. 4, 1995, pp. 607–625.

[56] Flandro, G. A., "On Flow Turning," *31st AIAA, ASME, SAE, and ASEE Joint Propulsion Conference and Exhibit*, No. AIAA-1995-2730, 1995.

[57] Brown, R. S., Blackner, A. M., Dunlap, R., and Willoughby, P. G., "Vortex Shedding as a Source of Acoustic Energy in Segmented Rockets," *Journal of Spacecraft and Rockets*, Vol. 18, No. 4, 1981, pp. 312–319.

[58] Avalon, G. and Comas, P., "Simulative Study Of Of The Unsteady Flow Inside A Solid Rocket Motor," *27th AIAA/ASME/SAE/ASEE Joint Propulsion Conference*, 1991.

[59] Majdalani, J. and van Moorhem, W. K., "Multiple Scales Solution to Acoustic Boundary Layer in Solid Rocket Motors," *Journal of Propultion and Power*, Vol. 13, No. 2, 1997, pp. 186–193.

[60] Majdalani, J., "The Boundary Layer Structure In Cylindrical Rocket Motors," *AIAA Journal*, Vol. 36, 1998, pp. 241.

[61] Fischbach, S. R., Majdalani, J., and Flandro, G. A., "Acoustic Instability of the Slab Rocket Motor," *Journal of Propulsion and Power*, Vol. 23, No. 1, 2007, pp. 146–157.

[62] Flandro, G. A., Malhortha, S., and Gazra, D. M., "Nonlinear Combustion Instability Data Reduction," *AIAA/ASME/SAE/ASEE Joint Propulsion Conference*, No. AIAA-96-3251, AIAA, Lake Beuna Vista, FL, 1996.

[63] Culick, F. E. C., "Nonlinear Behaviour of Acoustic Waves in Combustion Chambers-I," *Acta Astronautica*, Vol. 3, 1976, pp. 715–734.

[64] Culick, F. E. C., "Nonlinear Behaviour of Acoustic Waves in Combustion Chambers-II," *Acta Astronautica*, Vol. 3, 1976, pp. 735–575.

[65] Paprizos, L. G. and Culick, F. E. C., "The Two-Mode Approximation to Non-linear Acoustics in Combustion Chambers," *Combustion Science and Technology*, Vol. 65, 1989, pp. 39–65.

[66] Awad, E. and Culick, F. E. C., "On the Existence and Stability of Limit Cycles for Longitudinal Acostic Modes in a Combustion Chamber," *Combustion Science and Technology*, Vol. 46, 1986, pp. 195–222.

[67] Burnley, V. S., *Nonlinear Combustion Instabilities and Stochastic Sources*, Ph.D. thesis, California Institute of Technology, 1996.

[68] Hart, R. W., Bird, J. F., and McClure, F. T., *The Influence of Erosive Burning on Acoustic Instablility in Solid Propellant Rockets*, Vol. Vol. 1 of *Solid Propellant Rocket Research*, Academic Press, 1960.

[69] Levine, J. N. and Baum, J. D., "A Numerical Study of Nonlinear Instability Phenomena in Solid Rocket Motors," *AIAA Journal*, Vol. 21, No. 4, 1983.

[70] Ma, Y., van Moorhem, W. K., and Shorthill, R. W., "Experimental Investigation of Velocity Coupling in Combustion Instability," *Journal of Propulsion and Power*, Vol. 7, 1991, pp. 692–699.

[71] Ananthkrishnan, N., Deoy, S., and Culick, F. E. C., "Modeling and Dynamics of Nonlinear Acoustic Waves in a Combustion Chamber," *38th AIAA/ASME/SAE/ASEE Joint Propulsion Conference and Exhibit,*, No. AIAA-2002-3592, AIAA, Indianapolis, Indiana,, Huly 2002.

[72] Baum, J. D., Daniel, B. R., and Zinn, B. T., "Determination of Aluminized Solid Propellant Admittances by the Impedance Tube Method," *AIAA Journal*, Vol. 20, No. 3, 1982, pp. 417–421.

[73] Baum, J. D. and Levine, J. N., "A Critical Study for the solution of Nonlinear Hyperbolic Equations for Resonance Systems," *Journal of Computational Physics*, Vol. 58, No. 1, 1985.

[74] Baum, J. D. and Levine, J. N., "Numerical Investigation of Acoustic Refraction," *AIAA Journal*, Vol. 25, No. 12, 1987, pp. 1577–1586.

[75] Baum, J. D. and Levine, J. N., "Modeling of Nonlinear Longitudinal Instability in Solid Rocket Motors," *AIAA Journal*, Vol. 13, No. 6/7, 1986, pp. 339–348.

[76] Guery, J., Ballereau, S., Godfroy, F., Gallier, S., Orlandi, O., Pieta, P., and Robert, E., "Thrust Oscillations in Solid Rocket Motors," *44th AIAA/ASME/SAE/ASEE Joint Propulsion Conference & Exhibit*, Hartford, Ct, 2008.

[77] Vuillot, F. and Avalon, G., "Acoustic Boundry Layers in Solid Propellant Rocket Motors using Navier-Stokes Equations," *Journal of Propulsion and Power*, Vol. 7, No. 2, 1991, pp. 231–239.

[78] Vuillot, F., "Vortex-Shedding Phenomenon in Solid Rocket Motors," *Journal of Propulsion and Power*, Vol. 11, No. 4, 1995, pp. 626–639.

[79] Anthoine, J., Mettenleiter, M., Repellin, O., Buchlin, J. M., and Candel, S., "Influence of Adaptive Control on Vortex-Driven Instabilities in a Scaled Model of Solid Propellant Motors," *Journal of Sound and Vibration*, Vol. 262, 2003, pp. 1009–1046.

[80] Dupays, J., "Two-phase unsteady flow in solid rocket motors," *Aerospace Science and Technology*, Vol. 6, 2002, pp. 413–422.

[81] Fabignon, Y., Dupays, J., Avalonand, G., Vuillot, F., Lupoglazoff, N., Casalis, G., and Prévost, M., "Instabilities and pressure oscillations in solid rocket motors," *Aerospace Science and Technology*, Vol. 7, 2003, pp. 191–200.

[82] French, J. C. and Coats, D. E., "Automated 3-D Solid Rocket Combustion Stability Analysis," *35th AIAA / ASME / SAE / ASEE Joint Propulsion Conference and Exhibit*, AIAA, Los Angeles, CA, 1999.

[83] French, J., "Three Dimensional Combustion Stability Modeling For Solid Rocket Motors," *34th AIAA / ASME / SAE / ASEE Joint Propulsion Conference and Exhibit*, AIAA, Cleavland, Ohio, 1998.

[84] French, J. C. and Dang, A. L., "Analytic Combustion Stability Analysis Of Non-Axi-Symmetric Motor Cavity, Including Non-Axial Acoustic Modes: A Status Report," *35th JANNAF Combustion Subcommittee*, Tucson, AZ, 1998.

[85] French, J. C. and Flandro, G. A., "Linked Solid Rocket Motor Combustion Stability and Internal Ballistic Analysis," *41th AIAA/ASME/SAE/ASEE Joint Propulsion Conference*, No. AIAA-2005-3998, AIAA, AIAA, Tucson, Arizona, 2005.

[86] French, J. C., "Analytical Evaluation of a Tangential Mode Instability in Solid Rocket Motors," *36th AIAA/ASM/SAE/ASEE Joint Propulsion Conference and Exhibit*, No. AIAA 20003698, AIAA, 2000.

[87] French, J. C., "Tangential Mode Instability of SRMs with Even and Odd Numbers of Slots," *38th AIAA / ASME / SAE / ASEE Joint Propulsion Conference*, AIAA, AIAA, Huntsville, AL, 2002.

[88] French, J. C. and Dunn, S. S., "New Capabilities in Solid Rocket Motor Grain Design Modeling (SPP02)," *38th JANNAF Combustion Subcommittee*, AIAA, AIAA, Destin, FL, 2002.

[89] French, J. and Tullos, J., "Solid Rocket Grid Generation and CFD Internal Ballisitc Analysis," *41th AIAA/ASME/SAE/ASEE Joint Propulsion Conference*, 2005.

[90] Culick, F. E. C., "Non-Linear Growth and Limiting Amplitude of Acoustic Oscillations in Combustion Chambers," *Combustion Science and Technology*, Vol. 3, 1971, pp. 1–16.

[91] Levine, J. N. and Culick, F. E. C., "Numerical Analysis of Longitudinal Combustion Instability in Metallized Solid Rocket Motors," Tech. Rep. AFRPL-TR-72-88, Ultrasystems, Inc, 1972.

[92] Levine, J. N. and Culick, F. E. C., "Nonlinear Analysis of Solid Rocket Combustion Chambers," Tech. Rep. AFRPL-TR-74-45, Air Force Rocket Propulsion Labratory, 1974.

[93] French, J. C. and Flandro, G., "Nonlinear Combustion Stability Prediction With SPP/SSP," *39th JANNAF Combustion Subcommittee*, AIAA, AIAA, Colorado Springs, CO, 2003.

[94] Rousseau, C. W. and Knoetze, J. H., "Calculating an Admittance Function from Pulsed Tubular Grain Motor Tests," *Journal of Propulsion and Power*, Vol. 26, No. AIAA-40286-119, September-October 2010, pp. 998–1005.

[95] Blomshield, F. S., Stalnaker, R. A., and Beckstead, M. W., "Combustion Instability Additive Investigation," *35th AIAA/ASME/SAE/ASEE Joint Propulsion Conference and Exhibit*, , No. AIAA-1999-2226, 1999.

[96] Blomshield, F. S., "Solid Propellant Response Function," *8th International Symposium on Chemical Propulsion*, 2009.

[97] Majdalani, J., Fishbach, S. R., and Flandro, G. A., "Improved energy Normalization function in rocket motor Stability calculations," *Aerospace Science and Technology*, Vol. 10, 2006, pp. 495–500.

[98] Chibli, H., Majdalani, J., and Flandro, G., "Improved Energy Normalization Function in Rocket Motor Stability Calculations," 2003.

[99] Evans, G. I. and Smith, P. K., "The Suppression of Combustion Instability by Particulate Dampening in Solid Rocket Motors," *AGRAD Conference and Proceedings No. 259: Solid Rocket Motor Technology*, NATO, NATO, 1979.

[100] McBride, B. I., Reno, M. A., and Gordon, S., *CET93 and CETPC: An Interim Updated Version of the NASA Lewis Computer Program for Calculating Complex Chemical Equilibria With Applications*, NASA, Cleveland: NASA Glenn Research Center,, nasa technical memorandum 4557 ed., 1994.

[101] Baum, J. D., Levine, J. N., and Lovine, R. L., "Pulsed Instability in Rocket Motors: A Comparison Between Predictions and Experiments," *Journal of Propulsion and Power*, Vol. 4, No. 4, 1988, pp. 308–316.

[102] Davenas, A., *Solid Rocket Propulsion Technology*, Pergamon, Oxford, England, 1993.

[103] Lamberty, J. T., "A Report on the Grain Design and Internal Ballistic Module of the Improved Solids Performance Program," *AIAA 19th Aerospace Sciences Meeting*, Vol. AIAA-81-0034, 1981.

[104] Isella, G. C., *Modeling and Simulation of Combustion Chamber and Propellant Dynamics and Issues in Active Control of Combustion Instabilities*, Ph.D. thesis, California Institute of Technology, 2001.

[105] Flandro, G. A., "Course Notes Combustion Instability," http://flandro.utsi.edu/CI.htm, July 11, 2005.

[106] Hart, R. W. and McClure, F. T., "Combustion instability: Acoustic Interaction with a Burning Propellant Surface," *The Journal of Chemical Physics*, Vol. 30, No. 6, 1959, pp. 1501–1514.

[107] Hart, R. W. and Cantrell, R. H., "Amplification And Attenuation of Sound by Burning Propellants," *AIAA Journal*, Vol. 1, No. 2, 1963, pp. 398–404.

[108] Cantrell, R. H. and Hart, R. W., "Interact on Between Sound and Flow in Acoustic Cavities: Mass, Momentum and Energy Considerations," *The Journal of the Acoustical Society of America*, Vol. 36, No. 4, 1964, pp. 697–706.

[109] Cantrell, R. H., Hart, R. W., and McClure, F. T., "Linear Acoustic Gains and Losses in Solid Propellant Rocket Motors," *AIAA Journal*, Vol. 2, No. 6, 1964, pp. 1100–1105.

[110] Capener, E. L., Dickinson, L. A., and Kier, R. J., "Driving Processes of finite-Amplitude Axial Mode Instability in Solid-Propellant Rockets," *AIAA Journal*, Vol. 5, No. 5, 1967, pp. 938–945.

[111] Friedly, J. C. and Petersen, E. E., "Influence of Combustion Parameters on Instability in Solid Propellant Motors: Part I. Develpoment of Model and linear Anlalysis," *AIAA Journal*, Vol. 4, No. 9, 1966, pp. 1604–1610.

[112] Swithembank, J., "Combustion Instability In Solid Propellant Rocket Motors," Tech. rep., Department of Fuel Technology and Chemical Engineering, 1969.

[113] Unknown, "Theoretical Analysis of Combustion Instability," 1970.

[114] Dickinson, L. A., Capener., E. L., and Kier, R. J., "Research on Unstable Combustion in Solid Propellant Rockets," Tech. rep., Advanced Research Project Agency, 1964.

[115] McClure, F. T., Angelus, T. A., Cheng, S., Cheung, H., Jr, L. G., Hart, R. W., Price, E. W., Ryan, N. W., Summerfield, M., Torda, T., and Watermeier, L., "Solid Propellant Combustion Instability," *Eighth Symposium Inaternaitonal on Combustion*, Vol. 904-932, Williams and Wilkins, Baltimore, 1962.

[116] Horton, M. D., "Acoustic Admitance of a Burning Solid Propellant Surface," *ARS Journal*, 1962, pp. 644–645.

[117] Deters, O. J., "Effects of Gas phase and Solid phase dampening on Instability of Low frequency Modes in Solid Propellant Rockets," *ARS Journal*, 1962, pp. 378–384.

[118] T'ien, J. S., "Oscillatory Burning of Solid Propellants including GAs Phase Time Lag," *Combustion Science and Technology*, Vol. 5, No. 2, 1972, pp. 47–54.

[119] Ryazantsev, Y. S. and Tulskih, V. E., "Calculation of Acoustic Admittance at a Burning Surface," *Acta Astronautica*, Vol. 3, 1976, pp. 171–185.

[120] Blair, D. W., Erikson, E., and Berge, G. K., "Acoustic Absorbtion Coefficients of Combustion Gases," *AIAA Journal*, Vol. 2, No. 2, 1964, pp. 392–393.

[121] Price, E. W., "Experimantal Research in Solid Rocket Combustion Instability," *Tenth Symposium (International) on Combustion*, The Combustion Institute, 1965, pp. 1067–1082.

[122] Eisel, J. L., Horton, M. D., Price, E. W., and Rice, D. W., "Preferred Frequency Oscillatory Combustion of Solid Propellants," *AIAA Journal*, Vol. 2, 1964, pp. 1319–1323.

[123] Hackett, R. M., "Three-Dimentional Finite Element Combustion Instability Analysis," Tech. rep., Propulsion Directorate, 1980.

[124] Culick, F. E. C., "A Review of Calculations for Unsteady Burning of Solid Propellants," *AIAA Journal*, Vol. 6, No. 12, 1968, pp. 2241–2255.

[125] Hart, R. W. and Bird, J. F., "Scaling Problems Associated with Unstable Burning in Solid Propellant Rockets," *Modeling Principles*, 1961, pp. 993–1004.

[126] Hart, R. W., Bird, J. F., Cantrell, R. H., and McClure, F. T., "Nonlinear effects in Instability of Solid Propellant Rocket Motors," *AIAA Journal*, Vol. 2, No. 7, 1964, pp. 1270–1273.

[127] McClure, F. T., Hart, R. W., and Cantrell, R. H., "Interaction Between Sound and Flow: Stability of T-Burners," *AIAA Journal*, 1963, pp. 586–587.

[128] Bird, J. F., Haar, L., Hart, R. W., and McClure, F. T., "Effect of solid Propellant Compressibility on Combustion Instability," *The Journal of Chemical Physics*, Vol. 32, No. 5, 1960, pp. 1423–1429.

[129] Cantrell, R. H., McClure, F. T., and Hart, R. W., "Acoustic Dampening in Cavities with Mean Velocity and Thermal Boundary Layers," *The Journal of the Acoustical Society of America*, Vol. 35, No. 4, 1963, pp. 500–509.

[130] Sirigano, W. A., "A theory of Axial-Mode Shock-Wave Oscillations in a Solid-Rocket Combuster," *Sixteenth Symposium (International) on Combustion*, The Combustion Institute, Massachusetts Institute of Combustion, 1976, pp. 129–136.

[131] Barrere, M. and Williams, F., "Comparisons of Combustion instabilities found in Various Types of Combustion Chambers," *Sixteenth Symposium (International) on Combustion*, The Combustion Institute, Massachusetts Institute of Technology, 1976, pp. 169–181.

[132] DeLuca, L., Silvestro, R. D., and Cozzi, F., "Intrinsic Combustion Instability of Solid Energetic Materials," *Journal of Propultion and Power*, Vol. 11, No. 4, 1995, pp. 804–815.

[133] Cohen, N. S. and Bowyer, J. M., "Combustion Response Modeling for Composite Solid Propellants," Tech. rep., California Institute of Technology, 1978.

[134] Hackett, R. M., "Three-Dimensional Finite-Element Acoustic Analysis of Solid Rocket Motor Cavities," *Journal of Spacecraft and Rockets*, Vol. 13, No. 10, 1976, pp. 585–588.

[135] Son, S. F. and Brewster, M. Q., "Linear Burning Rate Dynamics of Solids Subjected to Pressure or External Radiant Heat Flux Oscillations," *Journal of Propulsion and Power*, Vol. 9, No. 2, 1993, pp. 222–232.

[136] Roberts, A. K. and Brownlee, W. G., "Nonliniear Longitudinal Combustion Instability: Influence of Propellant Composition," *AIAA Journal*, Vol. 9, No. 1, 1971, pp. 140–146.

[137] Baum, J. D., Levine, J. N., and Lovine, R. L., "Pulse-Triggered Instability in Solid Rocket Motors," *AIAA Journal*, Vol. 22, No. 10, 1984, pp. 1413–1419.

[138] Baum, J. D., Lovine, R. L., and Levine, J. N., "Pulsing Techniques for Solid-Propellant Rocket Motors: Modeling and Cold-Flow Testing," *Journal of Propultion and Power*, Vol. 20, No. 2, 1983, pp. 150–157.

[139] Coates, R. L. and Horton, M. D., "Further Considerations o the Interaction of Sound and Flow in Rocket Motors and T-Burners," *Combustion Science and Technology*, Vol. 9, 1974, pp. 95–102.

[140] Oberg, C. L., Ryan, N. W., and Baer, A. D., "A Study of T-Burner Behavior," *AIAA Journal*, Vol. 6, No. 6, 1968, pp. 1131–1137.

[141] Dehority, G. L. and Mathes, H. B., "Acoustic Response Function Equation for a T-Burner with High Heat Loss," *AIAA Journal*, Vol. 6, No. 4, 1968, pp. 741–742.

[142] Culick, F. E. C., "Research on Combustion Instability and Application to Solid Propellant Rocket Motors- II," *AIAA/SAE Joint Propulsion Specialist Conference*, AIAA, New Orleans, Loisiana, 1972.

[143] Janardan, B. A. and Zinn, T., "Rocket Nozzle Damping Characterisitcs Measured Using Different Experimental Techniques," *AIAA Journal*, Vol. 15, No. 3, 1977, pp. 442–444.

[144] Matta, L. M. and Zinn, B. T., "Study of the flow Turning Loss in A Simulated Solid Rocket Motor," *Journal of Propulsion and Power*, Vol. 11, No. 2, 1995, pp. 278–284.

[145] Coates, R. L. and Horton, M. D., "Design Considerations Combustion Instability," *ICRPG/AIAA 3rd Solid Propulsion Conference*, AIAA, Atalantic City, New Jersey, 1968.

[146] Harris, P. G., de Champlain, A., and Bourque, C., "Pulse Triggered nonlinear Instability in Solid Rocket Motors - An experimental Study," *AIAA/ASME/SAE/ASEE Joint Propulsion Conference and Exhibit 33rd*, AIAA, Seatle, 1997, pp. 1–21.

[147] Blomshield, F. S., Bicker, C. J., and Stalnaker, R. A., "High Pressure Pulsed Motor Firing Combustion Instability Investigations," *33rd AIAA/ASME/SAE/ASEE Joint Propulsion Conference and Exhibit*, AIAA, Seattle WA, 1997.

[148] Harris, P. G. and de Champlain, A., "Experimantal Database Describing Pulse triggered Nonlinear Instability in Solid Rocket Motors," *Journal of Propulsion and Power*, Vol. 14, No. 4, 1998, pp. 429–439.

[149] Marxman, G. A. and Wooldridge, C. E., "Finite Amplitude Axial Instability in Solid-Rocket Combustion," *Sixteenth Symposium (international) on Combustion*, The Combustion Institute, Massachusetts Institute of Technology, 1976, pp. 115–126.

[150] Coates, R. L., "Comment on Stability of Longitudidinal Oscillations with Pressure and Velocity Coupling in a Solid Propellant Rocket," *Combustion Science and Technology*, Vol. 3, 1971, pp. 153.

[151] Buffum, F. G., Dehority, G. L., Slates, R. O., and Price, E. W., "Acoustic Attenuation Experiments on Subscale, Cold-Flow Rocket Motors," *AIAA Journal*, Vol. 5, No. 2, 1967, pp. 272–280.

[152] Vuillot, F., "Acoustic Mode Determination in Solid Rocket Motor Stability Analysis," *AIAA Journal*, Vol. 3, No. 4, 1987, pp. 381–384.

[153] Kirkopuru, K., Kassow, D. R., and Zhao, Q., "Unsteady Vorticity Generation and Evolution in a Model of Solid Rocket Motor," *Journal of Propulsion and Power*, Vol. 12, No. 3, 1996, pp. 646–654.

[154] Gould, R. D., "Combustion Instability Studies with Plastic Propellent," *Acta Astronautica*, Vol. 9, No. 4, 1971, pp. 560–564.

[155] Fletcher, E. A. and Foley, J., "Amplification of Pressure Oscillations in Solid-Propellant Combustion," *Thirteenth Symposium (International) on Combustion*, The Combustion Institute, Pittsburg, Pensylvania, 1971, pp. 541–550.

[156] Culick, F. E. C., "Calculation of the Admittance Function for a Burning Surface," *Acta Astronautica*, Vol. 13, No. 3, 1967, pp. 221–238.

[157] Liou, T.-M. and Lien, W.-Y., "Numerical Simulation of Injection -Driven Flows in a Two-Dimensional Nozzleless Solid-Rocket Motor," *Journal of Propulsion and Power*, Vol. 11, No. 4, 1995, pp. 600–606.

[158] Joulin, G. and Champion, M., "Stretch Effects and Solid Propellant Burning," *Combustion and Flame*, Vol. 69, 1987, pp. 263–261.

[159] Majdalani, J., Flandro, G. A., and Roh, T. S., "Implications of Unsteady Analytical Flowfields On Rocket Combustion Stability," *34th AIAA/ASME/SAE/ASEE Joint Propulsion Conference & Exhibit*, AIAA, Cleveland, Ohio, 1998.

[160] Roh, T. S., Tseng, I.-S., and Yang, V., "Effects of Acoustic Oscillations on Flame Dynamics of Homogeneous Propellants in Rocket Motors," *Journal of Propulsion and Power*, Vol. 11, No. 4, 1995, pp. 640–650.

[161] Brown, R. S., Blackner, A. M., Willoughby, P. G., and Dunlap, R., "Coupling Between Acoustic Velocity and Oscillations and Solid Propellant Combustion," *Journal of Propulsion and Power*, Vol. 2, No. 5, 1986, pp. 428–437.

[162] Beddini, R. A. and Roberts, T. A., "Response of Propellant Combustion to a Turbulent Acoustic Boundry Layer," *Journal of Propulsion and Power*, Vol. 8, No. 2, 1992, pp. 290–296.

[163] Horton, M. D., Eisel, J. L., and Price, E. W., "Low Frequency Acoustic Oscillator Combustion," *AIAA Journal*, Vol. 1, No. 11, 1963, pp. 2652–2654.

[164] Dobbins, R. A. and Temkin, S., "Measurement of Particulate Acoustic Attenuation," *AIAA Journal*, Vol. 2, No. 6, 1964, pp. 1106–1111.

[165] Temkin, S. and Dobbins, R. A., "Attenuation and Dispersion of Sound by Particulate-Relaxation Processes," *The Journal of the Acoustical Society of America*, Vol. 40, No. 2, 1966, pp. 317–324.

[166] Povinelli, L. A., "Particulate Dampening in Solid-Propellant Combustion Instability," *AIAA Journal*, Vol. 5, No. 10, 1967, pp. 1791–1796.

[167] Flandro, G. A., "Solid Propellant Acoustic Admittance Corrections," *Journal of Sound and Vibration*, Vol. 36, No. 3, 1974, pp. 297–312.

[168] Pamanabhan, M. S. and Powell, E. A., "On the Applicability of the method of averaging in Solid Rocket Stability Analysis," *Combustion Science and Technology*, Vol. 20, 1979, pp. 170–184.

[169] Unknown, "Combustion Instability in Solid Propellant Motors," *Performance predicition for Solid Propellant*, 1986, pp. 97–105.

[170] Wicker, M., Green, W. D., Kim, S., and Yang, V., "Triggering of Longitudinal Combustion Instabilities in Rocket Motors: Nonlinear Combustion Response," *Journal of Propulsion and Power*, Vol. 12, No. 6, 1996, pp. 1148–1158.

[171] Yang, V., Sinha, A., and Tih, F. Y., "State-Feedback Control of Longitudinal Combustion Instabilities," *Journal of Propultion and Power*, Vol. 8, No. 1, 1992, pp. 66–73.

[172] Coats, D. E. and Dunn, S. S., "Improved Motor Stability Predictions for 3-D Grains Using the SPP Code," *33rd AIAA / ASME / SAE / ASEE Joint Propulsion Conference and Exhibit*, AIAA, Seattle, WA, 1997.

[173] Price, E. W., "Velocity Coupling in Oscillatory Combustion of Solid Propellants," *AIAA Journal*, Vol. 17, No. 7, 1979, pp. 799–800.

[174] Sirignano, W. A. and Crocco, L., "A Shock Wave Model For Unstable Rocket Combustors," *AIAA Journal*, Vol. 2, No. 7, 1964, pp. 1285–1296.

[175] Baum, J. D. and Levine, J. N., "Numerical Techniques for Solving Non-linear instability Problems in Solid Rocket Motors," *AIAA Journal*, Vol. 20, No. 7, 1982, pp. 955–961.

[176] Beck, W. H. and Jolley, W. H., "Harmonic Analysis of the Piston and Pyrotechnic Pulsers for T-Burners," *Journal of Propulsion and Power*, Vol. 4, No. 3, 1988, pp. 283–285.

[177] Vuillot, F. and Kuentzmann, P., "Flow Turning and Admittance Correction: An Experimental Comparison," *Journal of Propulsion and Power*, Vol. 2, No. 4, 1986, pp. 345–353.

[178] Flandro, G. A., "Vortex Driving Mechanism in Oscillatory Rocket Flows," *Journal of Propulsion and Power*, Vol. 2, No. 3, 1986, pp. 206–214.

[179] Swithebank, J. and Sotter, G., "Vortices in Solid Propellant Rocket Motors," *AIAA Journal*, Vol. 1, No. 7, 1963, pp. 1682–1684.

[180] Swithembank, J. and Sotter, G., "Vortex Generation in Solid Propellant Rockets," *AIAA Journal*, Vol. 2, No. 7, 1964, pp. 1297–1302.

[181] Sotter, G. and Flandro, G. A., "Resonant Combustion In Rockets," *Scientific America*, 1968, pp. 95–107.

[182] Malhortha, S. and Flandro, G. A., "On Nonlinear Combustion Instability," *33rd AIAA/ASME/SAE/ASEE Joint Propulsion Conference and Exhibit*, AIAA, Seattle, WA, 1997.

[183] Coates, R., Horton, M. D., and Ryan, N. W., "T-Burner Method of Determining the Acoustic admittance of Burning Propellants," *AIAA Journal*, Vol. 2, No. 6, 1964, pp. 1119–1122.

[184] Foner, S. N., Hudson, R. L., and Nall, B. H., "Admittance Measurement of Solid Propellants by an acoustic Oscillator Technique," *AIAA Journal*, Vol. 2, No. 6, 1966, pp. 1123–1129.

[185] Horton, M. D., "Testing the Dynamic Stability of Solid Propellants Techniques and Data," Tech. rep., NAVWEPS, 1964.

[186] Ryan, N. W. and Coates, R. L., "Acoustic Instability: Influence of and on the Solid Phase," *AIAA Journal*, Vol. 2, No. 6, 1964, pp. 1130–1134.

[187] Price, E. W., Mathes, H. B., Madden, O. H., and Brown, B. G., "Pulsed T-Burner Testing of Combustion Dynamics of Aluminized Solid Propellants," *Astonautics and Aeronautics*, 1972, pp. 65–67.

[188] Kuentzmann, P. and Nadaud, L., "Response of Solid Propellants to Pressure and Velocity Oscillations," *Combustion Science and Technology*, Vol. 11, No. 3, 1975, pp. 85–163.

[189] Cauty, F., Comas, P., and Vuillot, F., "Magnetic Flow Meter Measurement of Solid Proplellant Pressure - Coupled Responses using an Acoustic Analysis," *Journal of Propulsion and Power*, Vol. 12, No. 2, 1995, pp. 436–438.

[190] Wilson, J. R. and Micci, M. M., "Direct Measurement of High Frequency Solid Propellant Pressure-Coupled Admittances," *Journal of Propulsion and Power*, Vol. 12, No. 2, 1987, pp. 296–392.

[191] French, J. C. and Flandro, G. A., "Mode Shape Distortion in Extended Area T-Burners," *36th JANNAF Combustion Subcommittee*, Cocoa Beach, FL, 1999.